TESIS DE LA UNIVERSIDAD DE ZARAGOZA

2024 217

Pablo Armañac Julián

Cardiovascular Signal Processing Oriented to Long-Term Monitoring

Director/es
Gil Herrando Eduardo
Bailón Luesma, Raquel

ISSN 2254-7606

Prensas de la Universidad
Universidad Zaragoza

Universidad de Zaragoza
Servicio de Publicaciones

ISSN 2254-7606

Universidad Zaragoza
1542

Tesis Doctoral

CARDIOVASCULAR SIGNAL PROCESSING ORIENTED TO LONG-TERM MONITORING

Autor

Pablo Armañac Julián

Director/es

Gil Herrando Eduardo
Bailón Luesma, Raquel

UNIVERSIDAD DE ZARAGOZA
Escuela de Doctorado

Programa de Doctorado en Ingeniería Biomédica

2024

instituto de investigación en ingeniería de Aragón

BSICoS
Biomedical Signal Interpretation & Computational Simulation

Cardiovascular Signal Processing Oriented to Long-Term Monitoring

Author
Pablo Armañac-Julián

Supervisors
Raquel Bailón and Eduardo Gil

PhD in Biomedical Engineering
Universidad de Zaragoza
2023

Cardiovascular Signal Processing Oriented to Long-Term Monitoring

Pablo ARMAÑAC JULIÁN, 2023
Cardiovascular Signal Processing Oriented to Long-Term Monitoring.
Date of current version: January 31st, 2024 (available online in *bsicos.i3a.es*; submitted in December 2023; defense in March 2024)

This Ph.D. thesis in Biomedical Engineering has been developed within the Department of Electronic Engineering and Communications and the Aragón Institute for Engineering Research (I3A) at the University of Zaragoza (Zaragoza, Spain).
The research presented in this thesis was supported by a personal grant to Pablo ARMAÑAC JULIÁN by Gobierno de Aragón (Spain) and the projects supported by Ministerio de Ciencia, Innovación y Universidades and European Regional Development Fund (FEDER) under project PID2021-126734OB-C21, by CIBER - Consorcio Centro de Investigación Biomédica en Red through Instituto de Salud Carlos III, TED2021-131106B-I00, and by Gobierno de Aragón (Reference Group BSICoS T39-23R).

This thesis was printed thanks to the financial support of BSICoS Group at University of Zaragoza.

ABSTRACT

Through this thesis, I investigate the use of noninvasive analysis of cardiac, respiratory, and photoplethysmography (PPG) signals to assess autonomic nervous system (ANS) activity across clinical and non-clinical settings. The work is methodically structured into five main parts, each focusing on different aspects of cardiovascular status assessment, with the particularity of the analysis in long-term monitoring setups. The thesis combines extensive physiological research with innovative methodologies and practical applications, utilizing signal processing techniques for comprehensive cardiovascular health evaluation.

Part I (Chapters 1, 2, and 3) establishes the foundational context of the thesis, encompassing physiological and methodological aspects necessary for subsequent investigations. Chapter 1 delves into the physiology and functioning of the ANS, cardiac, cardiovascular and respiratory systems, providing an in-depth look at the biosignals under study and offering insights into the pathophysiology, diagnosis, and treatment of various health conditions. Chapter 2 outlines the specific disorders and applications targeted in the thesis, including weaning readiness from mechanical ventilation in intensive care units (ICU), obstructive sleep apnea in pediatric populations, and the potential biomarkers that can be extracted from PPG sensors to be included into wearables. Chapter 3 introduces the developed methodologies, detailing Heart Rate Variability (HRV) and respiratory signals analysis, and presents approaches for cardiopulmonary coupling (CPC) and respiration-guided HRV analysis, along with methodologies to obtain biomarkers from PPG devices.

Part II (Chapters 4, 5, and 6) centers on the process of weaning patients from mechanical ventilation in ICUs. Chapter 5 investigates Baroreflex Sensitivity (BRS) and HRV in predicting successful weaning outcomes, by monitoring these during the last hour prior to the spontaneous breathing trial (SBT). A novel finding is that BRS, particularly measured through Bivariate Phase Rectified Signal Average (BPRSA), shows significant potential with predictive value, since in 9 successfully weaned patients (S-group) and 6 unsuccessfully weaned (F-group), the capacity to change in BRS, showed clear distinctions between the groups. Conversely, temporal HRV indices, while different, did not show statistically significant difference between patients ready to be weaned and patients that failed SBT. Chapter 6 extends this

analysis by assessing Cardiopulmonary Coupling (CPC) as new potential estimates for weaning readiness, too. However, this analysis is performed not only in the hour prior to the SBT, but expands the monitoring to the 24 hours before the SBT. Notably, traditional variables such as heart rate and respiratory frequency did not show any significant differences between patients with successful and failed weaning. However, the study uncovered significant statistical differences in CPC parameters across the two groups throughout the entire recording period. Particularly at night, these significant differences were more pronounced, likely due to increased respiratory episodes in patients with failed weaning.

Part III (Chapters 7, 8, 9, and 10) starts with Chapter 7, where the datasets and participant groups for the study of obstructive sleep apnea (OSA) in pediatric patients are outlined. Chapter 8 provides a novel perspective by comparing HRV measures during apnea and normal breathing episodes, revealing significant differences. This challenges previous interpretations of HRV metrics during apnea and highlights the need for comprehensive HRV analysis. Chapter 9 employs CPC, specifically time-frequency coherence (TFC), between respiratory effort and HRV, to assess OSA severity. Interestingly, the study finds that TFC in the low-frequency band increases with OSA severity, offering a new method for severity assessment. Chapter 10 investigates the potential causal relationship between OSA and metabolic syndrome (MetS) in prepubertal children. A notable aspect of this chapter is the introduction and preliminary validation of a MetS score, designed as a new tool to assess cardiometabolic health in pediatric patients. This MetS score, while still in the early stages of validation, represents a promising step towards a better understanding of cardiovascular risks in childhood associated with OSA. Additionally, the chapter employs causal mediation analysis to find the causal role of OSA in influencing cardiovascular health. These findings contribute to the growing body of research exploring the complex interactions between sleep disorders and metabolic health in pediatric populations.

Part IV (Chapters 11, 12, 13, and 14) delves into the potential of PPG in wearable devices. It begins with Chapter 11, detailing databases and experimental setups for PPG studies in wearable devices. Chapter 12 focuses on quantifying the coverage of PPG sensors under various conditions, reveal-

ing how sensor location and stress conditions affect the estimation of vital metrics like Pulse Rate (PR) and Pulse Arrival Time (PAT). Surprisingly, coverage rates varied significantly based on the sensor location and the fiducial point chosen for PPG delineation. Chapter 13 assesses the pulse transit time difference (PTTD) as a marker for acute mental stress, finding that its standard deviation effectively distinguishes between stress and relaxation states, and a visible lowered trend of PTTD during stress, that could be attributed to vasoconstriction, as compared to relax. Chapter 14 investigates the use of PPG-derived pulse wave velocity (PWV) surrogates, including Pulse Arrival Time (PAT) and Pulse Transit Time Difference (PTTD), to assess vascular reactivity under heat stress. The study reveals that while PAT and Pulse Wave Decomposition Analysis (PDA) show a significant decrease correlating with heart rate changes under stress, PTTD exhibits an abrupt change that remains constant while stress is present, suggesting its superior reliability as an indicator of vasoconstriction and vascular reactivity.

Conclusions: The thesis concludes by synthesizing the extensive findings, emphasizing the significant role of noninvasive signal analysis in healthcare advancement. It discusses the potential of these methods in improving clinical decision-making and patient monitoring, with a focus on cardiovascular and respiratory health. Future research directions, particularly the growing importance of wearable technologies and their role in personalized healthcare, are also highlighted. Overall, this thesis presents a detailed study of noninvasive monitoring techniques, bridging theoretical knowledge with practical applications and contributing significantly to biomedical engineering and healthcare technology.

RESUMEN Y CONCLUSIONES

Esta tesis trata sobre el análisis no invasivo de señales cardíacas, respiratorias y de fotopletismografía (PPG) para evaluar la actividad del sistema nervioso autónomo (SNA) en contextos clínicos y no clínicos. El trabajo está estructurado metódicamente en cinco partes principales, cada una enfocada en diferentes aspectos de la evaluación del estado cardiovascular, con la particularidad de análisis en configuraciones de monitorización a largo plazo. La tesis combina una extensa investigación fisiológica con metodologías innovadoras y aplicaciones prácticas, utilizando técnicas de procesamiento de señales para una evaluación integral de la salud cardiovascular.

La Parte I (Capítulos 1, 2 y 3) establece el contexto fundamental de la tesis, abarcando aspectos fisiológicos y metodológicos necesarios para las investigaciones subsiguientes. El Capítulo 1 profundiza en la fisiología y funcionamiento del SNA, los sistemas cardiaco, cardiovascular y respiratorio, proporcionando una visión detallada de las bioseñales bajo estudio y ofreciendo perspectivas sobre la patofisiología, diagnóstico y tratamiento de diversas condiciones de salud. El Capítulo 2 describe los trastornos específicos y aplicaciones objetivo de la tesis, incluyendo la preparación para el destete de la ventilación mecánica (o también llamada extubación), en unidades de cuidados intensivos (UCI); la apnea obstructiva del sueño en poblaciones pediátricas; y los biomarcadores potenciales que pueden extraerse de los sensores PPG para ser incluidos en dispositivos portátiles. El Capítulo 3 introduce las metodologías desarrolladas, detallando el análisis de la Variabilidad de la Frecuencia Cardíaca (HRV) y las señales respiratorias, y presenta enfoques para el acoplamiento cardiopulmonar (CPC) y el análisis de HRV guiado por la respiración, junto con metodologías para obtener biomarcadores de dispositivos PPG.

La Parte II (Capítulos 4, 5 y 6) se centra en el proceso de destete de pacientes de la ventilación mecánica en UCI. El Capítulo 5 investiga la Sensibilidad del Barorreflejo (BRS) y la HRV para predecir resultados exitosos de destete, monitorizando estos durante la última hora antes de la prueba de respiración espontánea (SBT). Un hallazgo novedoso es que la BRS, especialmente medida a través del Promedio de Señal Rectificada de Fase Bivariante (BPRSA), muestra un potencial significativo con valor predictivo, ya que en 9 pacientes exitosamente destetados (grupo S) y 6 no destetados

(grupo F), la capacidad de cambio en BRS mostró distinciones claras entre los grupos. Por el contrario, los índices temporales de HRV, aunque diferentes, no mostraron una diferencia estadísticamente significativa entre pacientes listos para ser destetados y pacientes que fallaron en el SBT. El Capítulo 6 amplía este análisis evaluando el Acoplamiento Cardiopulmonar (CPC) como nuevas estimaciones potenciales para la preparación para el destete. Sin embargo, este análisis se realiza no solo en la hora previa al SBT, sino que amplía el monitoreo a las 24 horas antes del SBT. Notablemente, variables tradicionales como la frecuencia cardíaca y respiratoria no mostraron diferencias significativas entre pacientes con destete exitoso y fallido. Sin embargo, el estudio descubrió diferencias estadísticas significativas en los parámetros de CPC a través de los dos grupos durante todo el período de grabación. Particularmente en la noche, estas diferencias significativas fueron más pronunciadas, probablemente debido a episodios respiratorios aumentados en pacientes con destete fallido.

La Parte III (Capítulos 7, 8, 9 y 10) comienza con el Capítulo 7, donde se describen los conjuntos de datos y los grupos de participantes para el estudio de la apnea obstructiva del sueño (OSA) en pacientes pediátricos. El Capítulo 8 ofrece una perspectiva novedosa al comparar las medidas de HRV durante la apnea y episodios de respiración normal, revelando diferencias significativas. Esto desafía las interpretaciones anteriores de las métricas de HRV durante la apnea y destaca la necesidad de un análisis completo de HRV. El Capítulo 9 emplea CPC, específicamente la coherencia tiempo-frecuencia (TFC), entre el esfuerzo respiratorio y HRV, para evaluar la gravedad de la OSA. Curiosamente, el estudio encuentra que la TFC en la banda de baja frecuencia aumenta con la gravedad de la OSA, ofreciendo un nuevo método para la evaluación de la gravedad. El Capítulo 10 investiga la posible relación causal entre OSA y síndrome metabólico (MetS) en niños prepuberales. Un aspecto notable de este capítulo es la introducción y validación preliminar de un puntaje de MetS, diseñado como una nueva herramienta para evaluar la salud cardiometabólica en pacientes pediátricos. Este puntaje de MetS, aunque aún en las primeras etapas de validación, representa un paso prometedor hacia una mejor comprensión de los riesgos cardiovasculares en la infancia asociados con la OSA. Además, el capítulo emplea análisis de mediación causal para encontrar el papel causal de la

OSA en la influencia de la salud cardiovascular. Estos hallazgos contribuyen a la creciente investigación que explora las interacciones complejas entre los trastornos del sueño y la salud metabólica en poblaciones pediátricas.

La Parte IV (Capítulos 11, 12, 13 y 14) se adentra en el potencial de los dispositivos PPG en dispositivos portátiles. Comienza con el Capítulo 11, detallando bases de datos y configuraciones experimentales para estudios PPG en dispositivos portátiles. El Capítulo 12 se enfoca en cuantificar la cobertura de los sensores PPG bajo varias condiciones, revelando cómo la ubicación del sensor y las condiciones de estrés afectan la estimación de métricas vitales como la Tasa de Pulso (PR) y el Tiempo de Llegada del Pulso (PAT). Sorprendentemente, las tasas de cobertura variaron significativamente según la ubicación del sensor y el punto fiducial elegido para la delineación PPG. El Capítulo 13 evalúa la diferencia de tiempo de tránsito del pulso (PTTD) como un marcador de estrés mental agudo, encontrando que su desviación estándar distingue eficazmente entre estados de estrés y relajación, y una tendencia visiblemente reducida de PTTD durante el estrés, que podría atribuirse a la vasoconstricción, en comparación con el relax. El Capítulo 14 investiga el uso de surogados de la velocidad de la onda de pulso (PWV) derivados de PPG, incluyendo el Tiempo de Llegada del Pulso (PAT) y la Diferencia de Tiempo de Tránsito del Pulso (PTTD), para evaluar la reactividad vascular bajo estrés térmico. El estudio revela que mientras PAT y el Análisis de Descomposición de la Onda de Pulso (PDA) muestran una disminución significativa correlacionada con cambios en la frecuencia cardíaca bajo estrés, PTTD exhibe un cambio abrupto que se mantiene constante mientras el estrés está presente, sugiriendo su superior fiabilidad como indicador de vasoconstricción y reactividad vascular.

En general, esta tesis explora técnicas de monitoreo no invasivas, uniendo teoría y práctica en ingeniería biomédica y tecnología de atención médica. La sección final resume los hallazgos, destacando el papel crucial del análisis de señales no invasivo en mejorar la atención médica, especialmente en salud cardiovascular y respiratoria. Discute cómo estos métodos potencian la toma de decisiones clínicas y el monitoreo de pacientes, enfocándose en las futuras direcciones de investigación, incluyendo la relevancia de los wearables en la atención médica personalizada.

Unas palabras ...

Llevo postergando escribir estos agradecimientos porque no sé ni cómo siquiera empezar a juntar todos mis pensamientos y todo lo que he vivido, y menos aún de manera clara y ordenada. Este camino hasta terminar mi tesis doctoral no solo ha sido un desafío académico, sino también una aventura de crecimiento personal y profesional, enriquecida y soportada por muchas personas maravillosas. Me sorprendo a mí mismo cuando echo la mirada atrás, y pienso en toda la gente tan especial que he conocido y querido, y todo en muy buena parte a la oportunidad que me ha dado el doctorado de hacer y vivir todo aquello que he querido y como he querido (aunque poder hacer eso es gracias a mis directores que son lo mejor).

Pues la verdad es que primero de todo me lo quiero agradecer a mí mismo por haber llegado y aguantado hasta aquí. En este momento me siento hasta orgulloso de lo que he hecho, del camino, y de las cosas que he podido hacer. Gracias a esta experiencia del doctorado, ya que durante mi estancia, en un día cualquiera, me escribiste María para quedar en Bruselas, y de ahí empezar a conocernos. Qué inconcebible es haberte encontrado, el amor de mi vida, *mis sentimientos no caben en esta pluma.* Que me hagas sentir vulnerable, que me quieras tanto, y que siga enamorado después de tanto tiempo de todo lo que eres y de todo lo feliz que me haces, hacen que contigo haya siempre color donde nunca antes hubo. Y a Bea que, aunque no entiendas nada, haces que yo tampoco siga sin saber ni entender si eres causa o efecto o ambas de todo lo que soy y lo que hago, y a mis animales Gordito, Chispas y Piparra el demonio y Matías, también a Olga y Luis. Papá y mamá y abuelas y abuelos y tíos y prima, sé que estáis orgullosos de mí, pero yo más de vosotros por todo lo que sois y hacéis y sois capaces de soportar. Me gusta ser mayor para haberme dado cuenta de la risa que damos todos juntos vistos desde fuera. A mis amigos por nuestra intimidad, Vicen por querernos tanto y bueno a todos por seguir dándonos muchos abrazos y besos y seguir soltando veneno y barbaridades (y por esa cena pec que nos vamos a meter juntos en cuanto presente), y a las amigas de María que sois lo más y os quiero mucho también, me encanta no tener tiempo si es para irnos de viaje y estar con vosotras.

Necesito dejar por escrito y expresar mi más sincero agradecimiento a mis directores, Raquel y Edu. Vuestra guía, apoyo y valiosos consejos no solo

han dado forma a esta investigación, sino que también me habéis cambiado como investigador y como persona. Aunque no es algo de lo que podáis ser siquiera conscientes, me habéis motivado y ayudado a crecer, entender y conocer. No pongo fotos porque me daría mucha vergüenza, pero solo viendo cómo ha cambiado mi pelo y mi cara en estos 5 años es la muestra más simple de todo lo que he crecido y madurado. Además, gracias por enseñarme lo que es la ciencia, y darme la oportunidad de trabajar en algo que honestamente me parece útil y bonito. Sé que no cualquiera puede enseñar y transmitir lo que vosotros me habéis dado en estos años, y mucho menos con esta manera peculiar que tenemos en bsicos. De ti Edu me quedo con cómo tratas de conectar con nosotros, y cómo hay que preocuparse de aquellos que están a cargo de ti. Si trabajar es una angustia, contigo como compañero eso se vuelve en una tarea entretenida, que hasta me gusta hacer, y en la que entregarme día a día, paso a paso. De ti Raquel también cada día me sorprendes más y más. Podría decir que me llevo tu espíritu crítico, tu ocurrencia ideas, y el sonido de tus tacones antes de entrar al laboratorio. Pero vaya, que lo que más admiro de ti es tu entrega y dedicación por hacer que todo salga muy bien.

También cómo no, Pablo gracias por tus comentarios, siempre cuando menos y de lo que menos me espero. Ya lo sabes y todos te lo decimos, nos haces crecer un montón. La gente de fuera ve que eres y has sido un gran investigador, pero no saben lo que eres de verdad y es una muestra de lo que hay que hacer y ser, una persona honesta, sincera y entregada en aquello que sea que estés haciendo. Me sorprende verte todavía manchándote las manos con todos nosotros estudiantes de doctorado, como si fuésemos tus primeros estudiantes a los que diriges. Me hace gracia seguir viendo cómo te desesperas cada vez que no entiendes algo que alguien está tratando de explicar, para así mirar a Cris y reírnos por lo bajini porque esta vez no estamos siendo nosotros las víctimas. A todos mis compañeros que ha habido y que habrá muchas gracias, ya que creo que cada uno de nosotros hace que tengamos un ambiente tan acogedor. Ya la he mencionado, pero un gracias especial a Cris y también a Diego, gracias por escucharme y tenernos entre nosotros para ayudarnos y trabajar juntos. Por todos los nuevos y nuevas que habéis aparecido, y a Andrés y Rodrigo, que es un gusto trabajar con vosotros. También como no a Spyros que, aunque hace ya tiempo que

no estás por aquí, sabes que te llevo conmigo. Y vaya, que a todo el resto también, no me voy a poner a decir nombres porque ya no cabemos ni en cafetería. Para aquellos y aquellas que venís, mi consejo es que confiéis en el proceso. El día a día de esto la verdad que es duro y poco reconfortante. Hasta que al final de tu tesis no ves el tocho bien escrito y bien organizadito no eres consciente de todo lo que has hecho y mejor aún, sido capaz de hacer.

A María y Tere, mis amigas en Lovaina. Cómo os puedo llevar tan en lo profundo de mi corazón, ojalá vernos. A mis compañeros y compañeras del grupo de Lovaina, y sobre todo a Carolina, porque no se puede ser más buena persona y profesora como lo fuiste. Da gusto irse de estancia a sitios en los que te cuidan tan bien, en momentos en los que te sientes inseguro. Y hablando de sitios en los que me han cuidado bien, al grupo de Valladolid, porque vuestra acogida y amistad fue toda una sorpresa para mí. Gonzalo, eres otro ejemplo claro de admiración y de lo que hay que ser. Y a ti Adrián, que jamás me podía imaginar hacer un amigo como tú por casualidad, porque nos mandaron 1 mes a cada uno de intercambio como en el cole. Dales un abrazo a todos, porque a ti ya te lo daré pronto con muchas ganas.

Gracias de corazón a todos y cada uno de vosotros por ser parte de este significativo capítulo de mi vida.

De Pablo para quien lo lea

Table of Contents

List of Acronyms

AI	Apnea Index
AHI	Apnea-Hypopnea Index
ANS	Autonomic Nervous System
AV	Atrioventricular Node
BP	Blood Pressure
BR	Breathing Rate
BRS	Baroreflex Sensitivity
BPRSA	Bivariate Phase Rectified Signal Averaging
CHAT	Childhood Adenotonsillectomy Trial
CMA	Causal Mediation Analysis
CO	Cardiac Output
CPAP	Continuous Positive Airway Pressure
CPC	Cardiopulmonary Coupling
CVD	Cardiovascular Disease
CVR	Cardiovascular Risk
DBP	Diastolic Blood Pressure
eAT	early Adenotonsillectomy
ECG	Electrocardiography
FP	Fiducial Point
HF	High Frequency Band
HI	Hypopnea Index
HR	Heart Rate
HRV	Heart Rate Variability
ICU	Intensive Care Unit
IPFM	Integral Pulse Frequency Modulation Model
ID	Information Dynamics
LF	Low Frequency Band
LPD	Low Pass Derivative
MAD	Median Absolute Deviation
MetS	Metabolic Syndrome
mHR	mean Heart Rate
MV	Mechanical Ventilation
NN	Normal-to-Normal Interval
NREM	Non REM sleep
OB	Obesity
OSA	Obstructive Sleep Apnea
OSP	Orthogonal Subspace Projection
PAV	Pulse Amplitude Variability
PAT	Pulse Arrival Time
PDA	Pulse Decomposition Analysis
PEP	Pre-Ejection Period

PNS Parasympathetic Nervous System

PPG Pulse Photoplethysmography

PR Pulse Rate

PRV Pulse Rate Variability

PSD Power Spectral Density

PSG Polysomnography

PSV Pressure Support Ventilation

PTT Pulse Transit Time

PTTD Pulse Transit Time Difference

PWV Pulse Wave Velocity

REM Rapid Eye Movement sleep

RR R-wave to R-wave interval

RSA Respiratory Sinus Arrhythmia

PWV Pulse Wave Velocity

SA Sinoatrial Node

SBP Systolic Blood Pressure

SBT Spontaneous Breathing Trial

SDNN Standard Deviation of NN Intervals

SNS Sympathetic Nervous System

SpO2 Blood Oxygen Saturation

SV Stroke Volume

RMSSD Root Mean Square of Successive Differences

TFC Time-Frequency Coherence

TF Time-Frequency

TPR Total Peripheral Resistance

TTT Tilt-table stress test

TV Tidal Volume

TVIPFM Time Varying IPFM model

VCV Volume Controlled Ventilation

VLF Very-Low Frequency Band

WWSC Watchful Waiting with Supportive Care

Part I

Physiology, Target Disorders and Signal Processing Methods

Chapter 1

Introduction and Physiology

1.1 Introduction to the Thesis

1.1.1 Context and Motivation

Biomedical signals offer a window into the human body's function and health status [1]. The analysis of these signals provides valuable and vital information about underlying biological systems and helps characterize various pathological conditions [1]. While the information within these signals isn't typically discernible visually, biomedical signal processing methods are crucial for uncovering hidden medical information that is not obvious through

simple observation [2]. Modern signal processing techniques are now paving the way for automated analyses, holding potential for diagnosis, treatment, and monitoring a wide range of diseases [2].

By delving into cardiovascular signals and potential biomarkers, my goal is to uncover and elucidate the mechanisms and patterns within these signals. This exploration employs modern signal processing techniques to yield findings that are not only scientifically relevant but also practically applicable for healthcare professionals.

The fusion of novel data processing techniques, analysis, and acquisition systems has been transformative across numerous sectors, notably beyond medicine and health sciences. Signal processing, particularly when applied to human biological functions, has spurred extensive research and deepened our understanding of human physiology and pathophysiology, while developing innovative diagnostic and monitoring systems. Yet, the synergy between technology and medicine requires more than mere data analytics. New analytical tools should be grounded in a thorough understanding of human anatomy and physiology to ensure that findings are both meaningful and practical for the implementation of new diagnosis techniques.

My thesis focuses on non-invasive biological signal processing, particularly in assessing Autonomic Nervous System (ANS) activity. This assessment includes analyzing Heart Rate Variability (HRV), respiratory signals, and Cardiopulmonary Coupling (CPC) across various clinical and non-clinical scenarios. The non-invasive evaluation of ANS imbalances is crucial, offering insights into the physiological mechanisms behind lots of medical conditions. While HRV analysis forms the core of my research, other biosignals like the Electrocardiography (ECG), Pulse Photoplethysmography (PPG), and Blood Pressure (BP) have also been integral to my studies.

Advancements in technology and the adoption of non-invasive methodologies have significantly propelled personalized medicine. During my thesis, I have focused on employing signal processing techniques to address ANS imbalances in various clinical scenarios. For instance, in Mechanical Ventilation (MV) in the Intensive Care Unit (ICU), these techniques are crucial for non-invasively assessing a patient's autonomic stability and respiratory control, essential for determining weaning readiness, and spontaneous breathing. In the case of Obstructive Sleep Apnea (OSA), signal processing allows for

the analysis of sleep patterns and heart and respiratory rhythms, revealing underlying ANS dysregulation, which is vital for accurate diagnosis and effective monitoring. This approach not only enhances diagnostic accuracy and patient comfort but also contributes significantly to our understanding of pathophysiology, aiding in the development of targeted treatment strategies and marking a substantial stride in predictive medicine. Similarly, in wearable technology applications, real-time monitoring of ANS-related parameters like Heart Rate (HR), HRV and respiratory patterns enables the characterization of autonomic regulation, useful, e.g., for screening of cardiovascular diseases, and assessment of stress and overall well-being in daily life.

1.1.2 Structure

To offer clarity on the multifaceted subjects addressed in the next chapters, an overview of the physiological fundamentals of the human systems, biological signals, and contexts pertinent to this dissertation are elaborated in the next sections. In general, the present thesis dissertation has five main parts, and is structured as follows:

- **Part I. Physiology, target disorders, and methodologies**: In this first part of the thesis, the ANS and the most relevant biological signals used in this thesis are introduced. Moreover, a physiological background of all the scenarios considered throughout the next chapters, and the explanation of the methodologies are provided.
- **Part II. Cardiovascular signal processing in critical care medicine**. In this Part II, I delve into cardiovascular signal processing methodologies with a specific focus on enhancing the analysis and monitoring of patients admitted to ICU. Owing to their compromised health, they rely on MV to sustain respiratory function. My research is focused on improving the determination and assessment of weaning readiness. The research described in this chapter generated the following publications:
  - **P. Armañac-Julián**, D. Hernando, J. Lazaro, C. de Haro, R. Magrans, L. Sarlabous, J. López-Aguilar, P. Laguna, E. Gil, L. Blanch, R. Bailón (2020) Baroreflex Sensitivity Evolution before Weaning from Mechanical Ventilation, Proceedings of the XLVII

International Conference on Computing in Cardiology. Rimini, Italy, doi:10.22489/CinC.2020.235.

- JF. Morales-Tellez, J. Moeyersons, **P. Armañac-Julián**, M. Orini, L. Faes, S. Overeem, M. Van Gilst, J. Van Dijk, SV. Huffel, R. Bailon, C. Varon (2021) Model-Based Evaluation of Methods for Respiratory Sinus Arrhythmia Estimation. IEEE Trans Biomed Eng. vol. 68, n. 6.
- **P. Armañac-Julián**, D. Hernando, J. Lazaro, C. de Haro, R. Magrans, J. Morales, J. Moeyersons, L. Sarlabous, J. Lopez-Aguilar, C. Subira, R. Fernandez, M. Orini, P. Laguna, C. Varon, E. Gil, R. Bailon, and L. Blanch (2021) Cardiopulmonary Coupling Indices to Assess Weaning Readiness from Mechanical Ventilation. Scientific Reports. 11, 16014.

- **Part III. Cardiovascular signal processing in sleep apnea patients**. Here I explore different cardiovascular signal processing methodologies and data analysis for the stratification, characterization, and assessment of OSA severity in pediatric patients. The research described in this chapter generated these publications:

  - **P. Armañac-Julián**, A. Martín-Montero, J. Lázaro, S. Kontaxis, D. Álvarez, D. Gozal, R. Hornero, P. Laguna, G. Gutiérrez-Tobal, R. Bailón and E. Gil (2022) Changes in HRV metrics during sleep apnea episodes in children, European Study Group on Cardiovascular Oscillations (ESGCO), Štrbské Pleso (Slovakia). *2nd best poster award*
  - A. Martín-Montero, **P. Armañac-Julián**, E. Gil, L. Kheirandish-Gozal, D. Álvarez, J. Lázaro, R. Bailón, D. Gozal, P. Laguna, R. Hornero, GC. Gutiérrez-Tobal (2023) Pediatric sleep apnea: Characterization of apneic events and sleep stages using heart rate variability. Computers in Biology and Medicine, 154, 106549.
  - S. Hietakoste,**P. Armañac-Julián**, T. Karhu, R. Bailón, S. Sillanmäki, J. Töyräs, T. Leppanen, S. Myllymaa, S. Kainulainen (2023). Acute cardiorespiratory coupling impairment in worsening sleep apnea-related intermittent hypoxemia. IEEE Transactions on Biomedical Engineering.
  - **P. Armañac-Julián**, A. Martín-Montero, J. Lázaro, R. Hornero,

P. Laguna, L. Kheirandish-Gozal, D. Gozal, E Gil, R. Bailón, G. Gutiérrez-Tobal (2023) Characterization of the Cardiopulmonary Coupling in pediatric sleep apnea. Computing in Cardiology, Atlanta (Georgia).

– **P. Armañac-Julián**, A. Martín-Montero, J. Lázaro, R. Hornero, P. Laguna, L. Kheirandish-Gozal, D. Gozal, E. Gil, R. Bailón, G. Gutiérrez-Tobal (2023) Persistent Sleep Disordered Breathing Independently Contributes to Metabolic Syndrome in Prepubertal Children. Pediatric Pulmonology.

- **Part IV. Cardiovascular signal processing oriented to wearable devices**. This final part of the thesis is focused on identifying and analyzing different parameters derived from PPG signals. I further delve into the physiological origins of these biomarkers that can be obtained. The data for this study was collected in a laboratory environment. The goal is to lay the groundwork for understanding and interpreting the parameters that wearable devices, like wristbands, can measure in real-world settings. This analysis led to the following publications:

  – **P. Armañac-Julián**, S. Kontaxis, A. Rapalis, V. Marozas, P. Laguna, R. Bailón, E. Gil, J. Lázaro (2022) Reliability of Pulse Photoplethysmography Sensors: Coverage Using Different Setups and Body Locations, Front. Electron. 3:906324.

  – **P. Armañac-Julián**, S. Kontaxis, J. Lazaro, P. Laguna, R. Bailón, E. Gil (2019) Cardiovascular Changes Induced by Acute Emotional Stress Estimated from the Pulse Transit Time Difference. Proceedings of the XLVI International Conference on Computing in Cardiology. Singapore.

  – **P. Armañac-Julián**, S. Kontaxis, A. Rapalis, V. Marozas, P. Laguna, R. Bailón, E. Gil, J. Lázaro (2023) Vascular Reactivity Characterized by PPG-derived Pulse Wave Velocity. Under Review: BSPC.

- **Part V. Conclusions and future work**: This last part contains the main conclusions of the research presented in this thesis, as well as a proposal of future research lines.

1.2 Cardiovascular System

This section will provide a comprehensive explanation regarding the key concepts related to the cardiovascular system, heart function, cardiovascular regulation, and the baroreflex. The fact of understanding all these concepts is crucial for conducting research in the field of biomedical engineering, particularly when it pertains to the evaluation of cardiovascular health.

The cardiovascular activity is regulated and coordinated by the functioning of the heart and blood vessels. It involves the pumping of blood by the heart, which plays a central role in cardiovascular activity, the circulation of blood through the blood vessels, and the regulation of blood pressure.

1.2.1 Heart and Cardiac Activity

The heart, the main organ of the cardiovascular system, is primarily composed of four chambers: two atria and two ventricles, with one of each on each side of the heart. The right side receives deoxygenated blood from the body and pumps it to the lungs for oxygenation while respiration. The oxygenated blood then returns to the left side of the heart, which pumps it out to the rest of the body. This continuous circulation of blood is essential for the metabolism and the delivery of oxygen and nutrients to all body's cells, tissues and organs.

The heart consists of specialized cardiac muscle cells, namely cardiomyocytes, which have intrinsic and specific electrical properties. The origin of the electric cardiac cycle begins with the generation of an electrical impulse in the Sinoatrial Node (SA) node, located in the upper part of the right atrium (see Fig 1.1).

The SA node acts as the natural pacemaker of the heart, which spontaneously generates rhythmic electrical signals that set the pace for the heartbeat [2]. From the SA node, the electrical impulse spreads across the atria, causing them to contract and push blood into the ventricles. The electrical signals then pass through the Atrioventricular Node (AV) node, located between the atria and the ventricles. The AV node acts as a gatekeeper, and briefly delays their transmission, allowing the atria to fully contract and fill the ventricles with blood before ventricular contraction begins (see Fig 1.1).

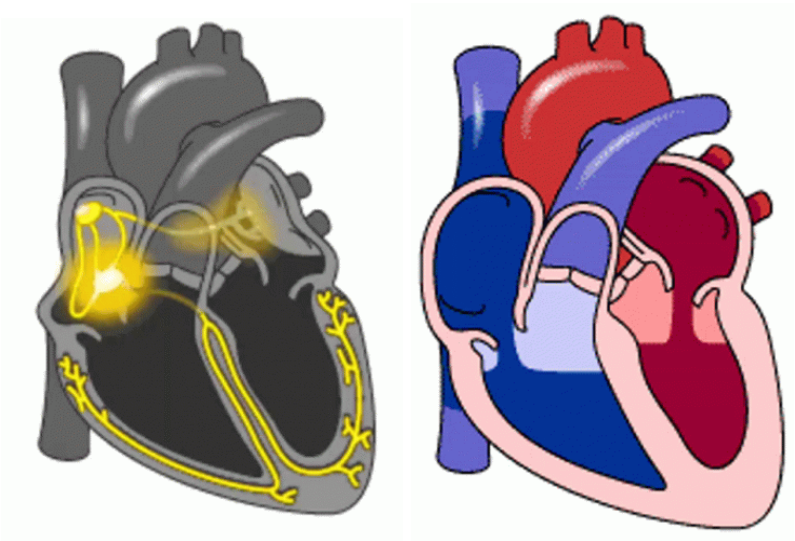

(a) (b)

Figure 1.1: Animated GIF showing cardiac activity: (a) Electrical Conduction; (b) Mechanical Activity.

Once the electrical impulse passes through the AV node, it travels rapidly along specialized conducting pathways called bundle branches and Purkinje fibers, which distribute the electrical signal to the ventricular muscle cells (see Fig 1.1). This coordinated electrical activation leads to the forceful contraction of the ventricles, pumping blood out of the heart to the lungs (right ventricle), and the rest of the body (left ventricle).

Electrocardiography

The ECG is the tool used to record and analyze the electrical activity of the heart non-invasively, providing essential information about the timing, duration, and morphology of the cardiac cycle [2]. To capture the ECG, electrodes are placed on the skin in a specific configuration, and connected to a electronic instrumentation device capable of detecting the small electrical signals generated by the cardiomyocytes within the heart. These electrodes record bipolar potential differences between different body locations, ultimately creating a visual representation of the heart's electrical activity. It's crucial to pay attention to the relative positions of these electrodes, as they lead to variations in the recorded waveform (see Fig. 1.2).

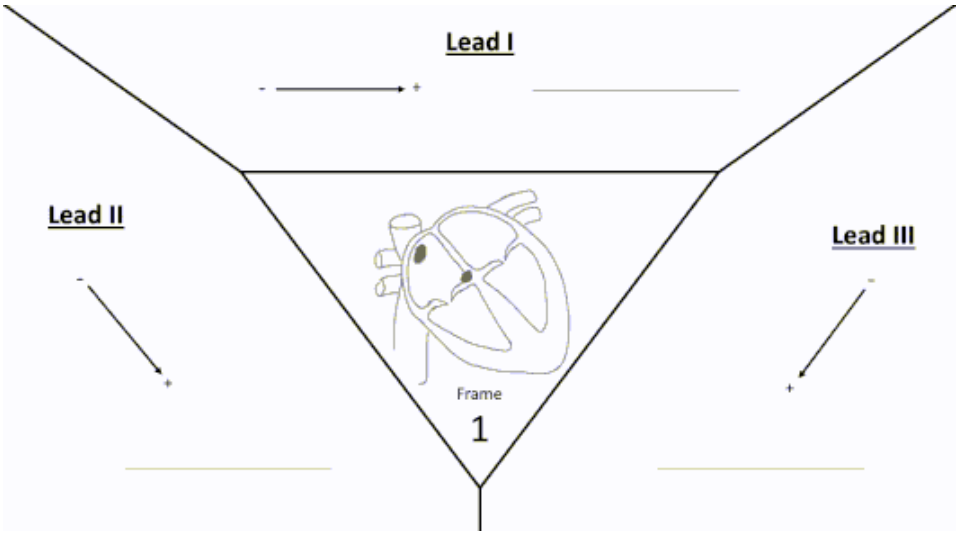

Figure 1.2: Animated GIF showing limb leads and electrical conduction through the heart.

The normal ECG waveform comprises several distinctive waves and intervals, with the overall ECG representation resulting from the cumulative action potentials of all cardiomyocytes (see Fig. 1.3). The P-wave represents the electrical depolarization and contraction of the atria, while the QRS complex corresponds to the depolarization and contraction of the ventricles. The T-wave represents the repolarization or recovery phase of the ventricles. The duration and shape of these waves provide valuable and non-invasive diagnostic information about the integrity and functioning of the cardiac electrical system, aiding in the detection and management of various cardiac conditions.

The number and placement of electrodes on the body's surface for ECG recording are determined by the specific clinical information required, since different electrode configurations offer insights into particular spatio-temporal variations in the cardiac electrical field. The widely used clinical configuration is the standard 12-lead ECG, which consists of 3 bipolar limb leads (I, II, III), 3 augmented unipolar limb leads (aVR, aVL, aVF), and 6 unipolar precordial leads (V1, V2, V3, V4, V5, V6). These electrode placements enable the characterization of cardiac electrical activity from various angles in the frontal and horizontal planes (see Fig. 1.4). For example, in the horizontal plane, leads V1 and V2 primarily capture the right ventricular activity,

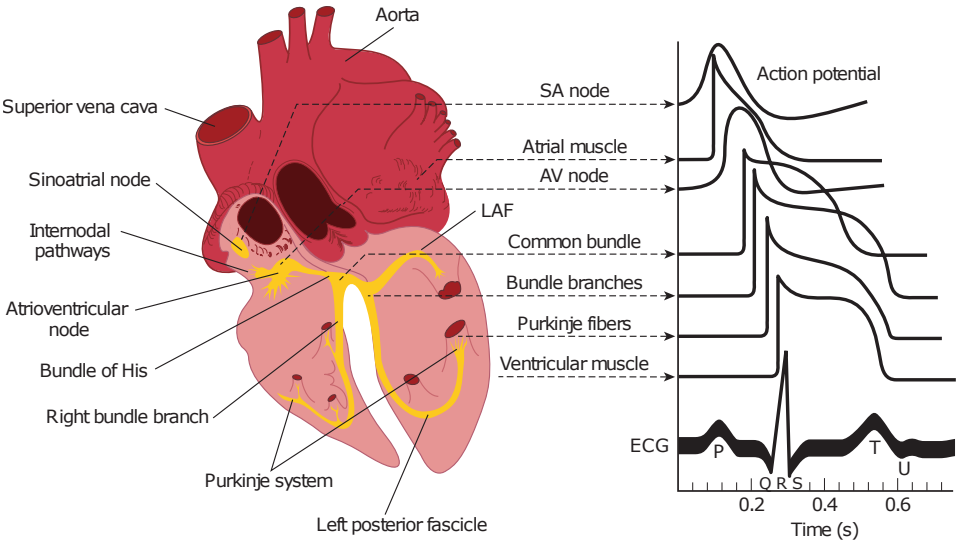

Figure 1.3: Conducting system of the heart. Left: Anatomic depiction of the human heart with additional focus on areas of the conduction system. Right: Typical transmembrane action potentials for the SA and AV nodes, other parts of the conduction system, and the atrial and ventricular muscles are shown along with the correlation to the ECG. LAF, left anterior fascicle. Adapted from [3].

while the remaining precordial leads depict the left ventricle's activity. An alternative lead system that allows examination of electrical activity in the three perpendicular directions (X, Y, and Z) is the orthogonal or Frank lead system [2], which facilitates a 3D representation of the electric field through the heart.

By analyzing the ECG, healthcare professionals can assess the rhythms and regularity of the heartbeat, in order to detect abnormalities in the conduction system, identify arrhythmia, and evaluate the overall health of the heart. Changes in the ECG pattern can be indicative of various cardiac conditions, such as myocardial infarction, heart rhythm disorders, and electrolyte imbalances [2].

Note that an extra electrode is essential for measuring the three bipolar limb leads of the ECG (see Fig. 1.5). The Driven Right Leg circuit is crucial in setups aquiring biolectrical signals, effectively reducing common-mode noise [4]. It operates by measuring the common-mode signal, typically the average of the signals at the positive input electrodes, and feeding a compensating signal back into the body through the right leg electrode. This process effectively reduces the potential difference between the patient

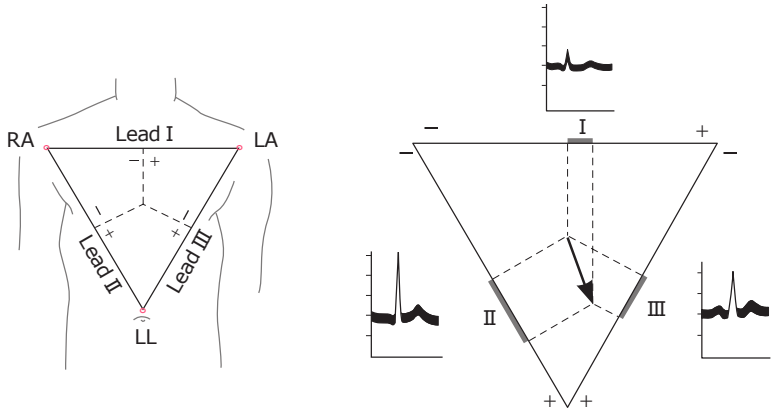

Figure 1.4: Cardiac vector. Left: Einthoven triangle. Perpendiculars dropped from the midpoints of the sides of the equilateral triangle intersect at the center of electrical activity. RA, right arm electrode; LA, left arm electrode; LL, left leg electrode. Right: Calculation of mean QRS vector. In each lead, distances equal to the height of the R wave minus the height of the largest negative deflection in the QRS complex are measured off from the midpoint of the side of the triangle representing that lead. An arrow drawn from the center of electrical activity to the point of intersection of perpendiculars extended from the distances measured off on the sides represents the magnitude and direction of the mean QRS vector. Adapted from [3].

and the recording equipment, diminishing the noise and artifacts that can obscure the true ECG signal. Notably, wearables like the AppleWatch or SamsungWatch, which measure lead I of the ECG, require three electrodes for accurate signal capture (see Fig. 1.6).

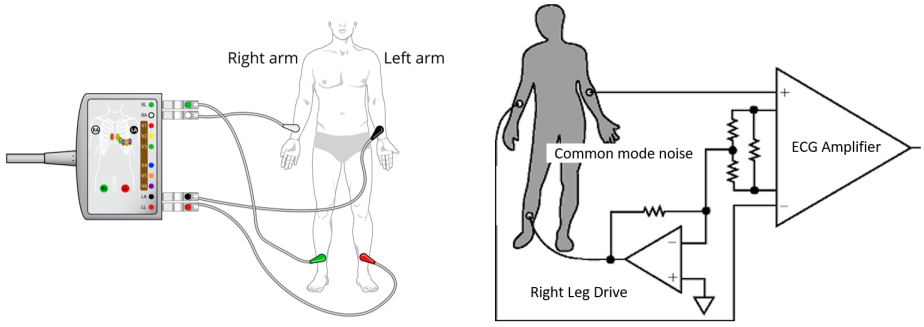

Figure 1.5: ECG setup with Driven Right Leg circuit. On the left, electrode placement for standard ECG recording is illustrated. On the right, the circuitry shows how common mode noise is reduced, improving the signal quality captured by the ECG amplifier.

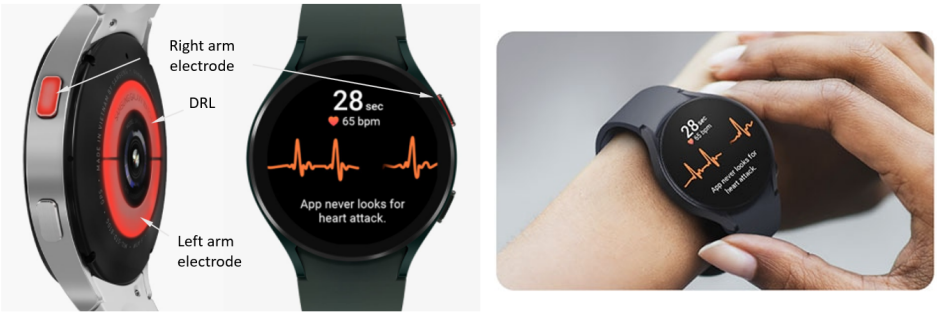

Figure 1.6: Illustration of a smartwatch equipped with ECG functionality (model, Samsung Watch 5). The left image highlights the contact points for the right and left arm electrodes, including the integration of a driven right leg circuit system for noise reduction. The right image shows the smartwatch in use, providing real-time ECG monitoring on the wearer's wrist.

The Electro-Mechanical View of the Heartbeat

The mechanical contraction of cardiomyocytes is the response to the electrical activation explained in the previous section. This process begins with the release of calcium ions from the sarcoplasmic reticulum within the cardiomyocyte, triggered by the electrical activation during the action potential. The influx of calcium ions into the cytoplasm then initiates the interaction between actin and myosin—the essential contractile machinery— within cardiac cells to facilitate contraction [5].

This synchronized and sequenced mechanical contraction across all cardiomyocytes, mediated by the specific electrical wavefront through the conduction system of the heart, generates an effective contraction of the ventricles to propel blood out to the body. In these terms, the Wiggers diagram provides a graphical representation of this coordinated electromechanical cardiac cycle and associated hemodynamic events [5], including left ventricular pressure, aortic pressure, ECG, and blood flow (see Fig. 1.7).

The electro-mechanical process of the heart's contraction involves several distinct phases, starting with ventricular diastole. During this phase, the ventricles are relaxed, allowing blood to fill the chambers after atrial contraction. This ventricular diastole phase is characterized by a decrease in left ventricular pressure and aortic pressure. The ECG waveform displays the P wave, indicating atrial depolarization and subsequent ventricular filling.

The next phase is ventricular depolarization, marked by the QRS complex

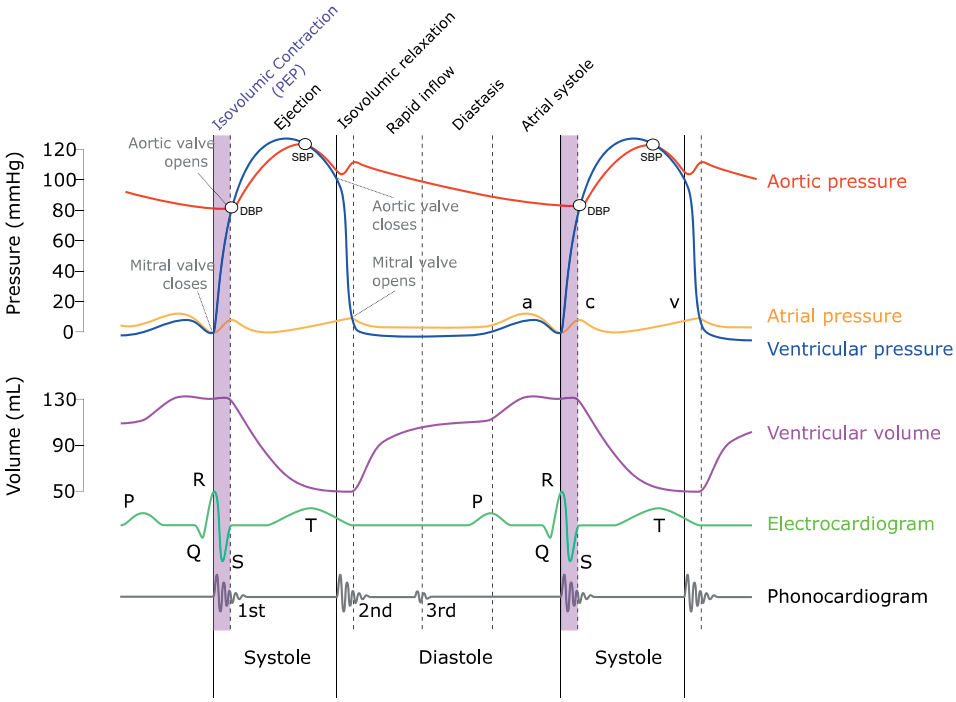

Figure 1.7: Wiggers diagram illustrating the coordinated electro-mechanical cardiac cycle and associated hemodynamic events. The left ventricular pressure waveform shows the changes in pressure within the left ventricle, reflecting diastole, isovolumetric contraction, ejection, and isovolumetric relaxation phases. Aortic pressure indicates the pressure in the aorta, with a sharp rise during ejection, until reaching Systolic Blood Pressure (SBP), followed by a gradual decline until the next blood filling of the ventricles, reaching Diastolic Blood Pressure (DBP). The ECG waveform corresponds to the electrical events in the heart, including atrial and ventricular depolarization and repolarization. Adapted and reproduced from [5].

on the ECG, leading to ventricular systole after a short refractory period of electromechanical delay. As the ventricles contract, the left ventricular pressure increases, initiating the isovolumic contraction or also known as Pre-Ejection Period (PEP). When this rise in ventricular pressure surpasses the aortic pressure, the aortic valve opens, allowing blood to be ejected into the systemic circulation. This phase corresponds to the QRS complex on the ECG, reflecting ventricular depolarization. The aortic pressure waveform exhibits a sharp increase followed by a gradual decline.

Following ventricular ejection, there is a brief period of isovolumetric relaxation, during which both aortic and ventricular pressures decrease. This relaxation phase is represented by the T wave on the ECG. Finally, the

ventricles enter the diastolic filling phase again, and the entire cycle repeats.

Pulse Photoplethysmography

PPG is a non-invasive technique for assessing cardiovascular activity [6], [7]. It captures variations in blood volume and blood flow within peripheral blood vessels following each heartbeat, triggered by the electrical depolarization of the heart. This is achieved using a light source and a photodetector.

The fundamental principle underlying PPG is the absorption of light by blood. As blood flows after a heartbeat, the amount of absorbed light changes (see Fig. 1.8). The PPG sensor emits light into the skin–at many possible wavelengths including red (670nm), infrared (940nm), and green light (530nm)–and a photodetector that measures the intensity of the transmitted or reflected light. By analyzing these changes in light absorption, PPG provides valuable information about HR, pulse waveform, and peripheral perfusion across various applications [8].

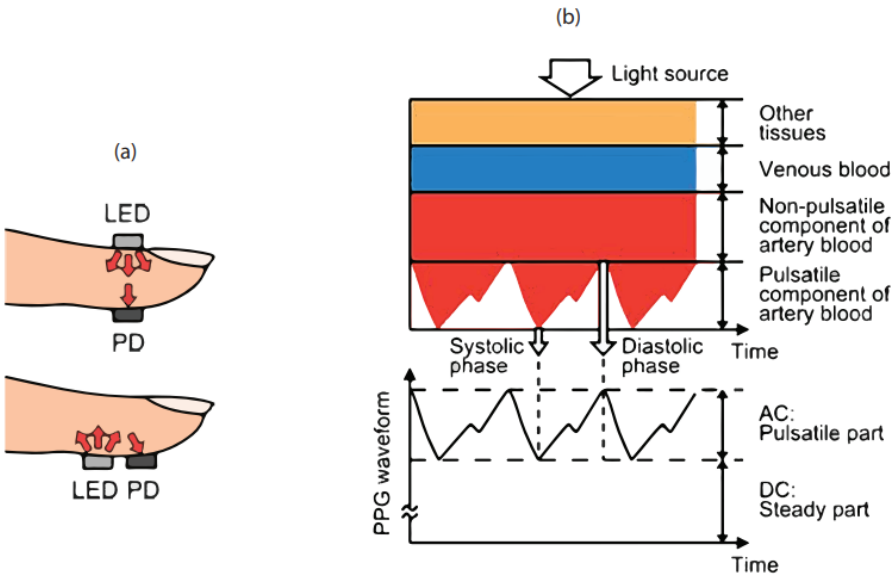

Figure 1.8: PPG. (a) Modes of PPG, transmission (top) and reflectance (bottom), and (b) characteristic PPG waveform that arise from light attenuation by tissues. LED, light-emitting diode; PD, photodetector. Reproduced and modified from [9].

Its applications extend to assessing cardiovascular function, monitoring HRV, and detecting cardiac abnormalities like arrhythmia, due to its similar-

ities with ECG. The widespread integration of PPG into wearable devices [6], such as fitness trackers and smartwatches, enables real-time monitoring of cardiovascular parameters without the need for expensive or uncomfortable equipment measuring ECG.

The ECG provides detailed information about the heart's electrical functioning, including rhythm, heart rate, and the presence of any electrical abnormalities, and the PPG describes the blood flow dynamics and vascularity related to each heartbeat (see Fig. 1.9).

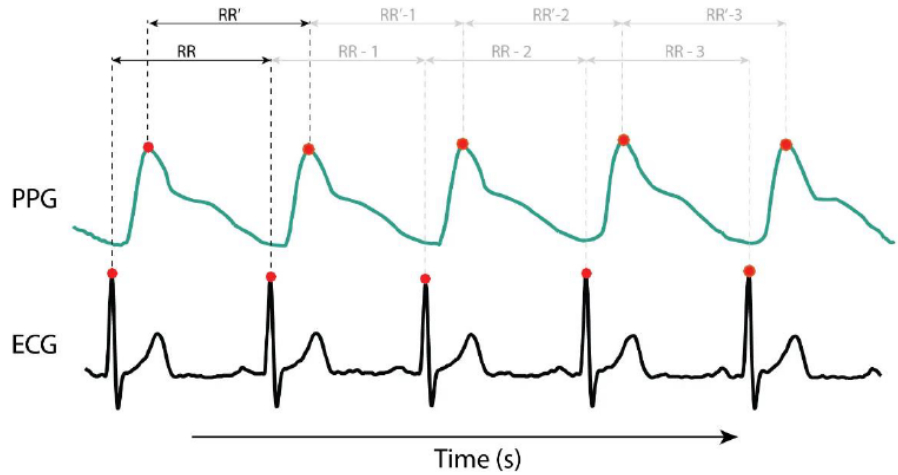

Figure 1.9: Comparative illustration of PPG and ECG signals, highlighting the synchronization of the heart's electrical activation with peripheral pulse propagation and the transit time of the pulse wave following ECG depolarization. The relationship between the R-wave to R-wave interval (RR) and the Pulse to Pulse interval (PP) is also shown.

1.2.2 Cardiovascular Control and Regulation

The intrinsic regulation of the heart has been explained and detailed in the previous section, regarding the mechanisms and processes that occur within the heart itself to regulate its activity without direct influence from external factors, such as neural and hormonal mechanisms. Key components of this self-regulatory system include the SA node, AV node, and Purkinje fibers in the cardiac conduction system. Auto-regulation allows the heart to adjust contraction force based on factors like venous return, ensuring optimal Stroke Volume (SV).

While intrinsic factors play a crucial role, external factors, such as ANS, Baroreflex Sensitivity (BRS), and hormonal regulation, modulate and fine-tune the heart's activity in response to different conditions [10]. Although survival is possible without ANS, the ability to adapt to environmental stressors and other challenges would be severely compromised.

Autonomic Nervous System

The ANS is a division of the peripheral nervous system that regulates the involuntary functions of the body. It operates without conscious control and is responsible for maintaining internal balance and responding to changes in the external environment. Therefore, the ANS plays a crucial role in controlling various physiological processes such as HR, blood pressure, digestion, respiration, body temperature, and glandular secretion.

This system consists of three main branches: the Sympathetic Nervous System (SNS), the Parasympathetic Nervous System (PNS), and the enteric nervous system. It must be noted that SNS and PNS divisions typically work in opposition to each other in order to maintain balance and adapt to different situations. A schematic of ANS anatomy is depicted in Fig. 1.10.

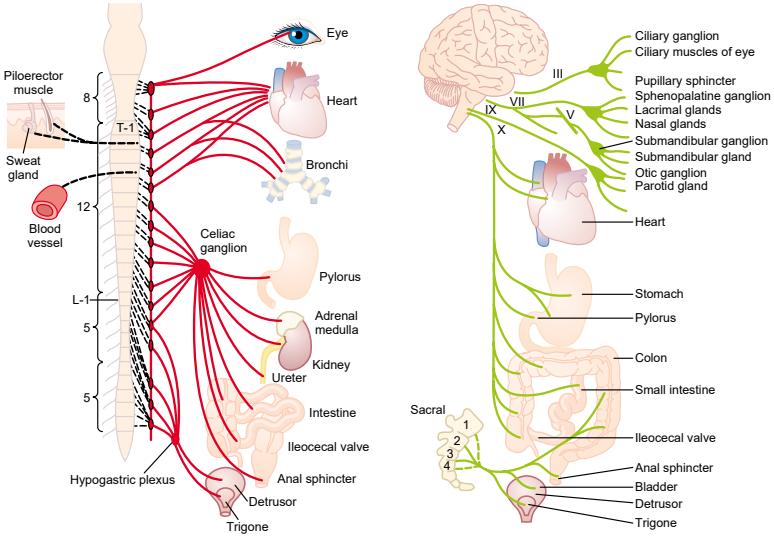

(a) (b)

Figure 1.10: Autonomic Nervous System: (a) Sympathetic branch. (b) Parasympathetic branch. Figure reproduced from [11].

The SNS is responsible for the "fight or flight" response. Activation of the sympathetic system leads to the release of the neurotransmitter nor adrenaline, which binds to adrenergic receptors in the heart and blood vessels. Nor adrenaline promotes increased HR, increased blood pressure, dilation of the airways, mobilization of energy reserves, and heightened mental alertness. It prepares the body for action in response to stressful stimuli or danger. In contrast, the PNS is associated with the "rest and digest" state. It releases the neurotransmitter acetylcholine, which binds to muscarinic receptors, promoting the contrary effect of SNS; decreased HR, reduced vasoconstriction, increased digestive activity, constriction of the airways, and stimulation of glandular secretions. All of this induces relaxation, conserves energy, and allows the body to recover and repair, while facilitating digestion, nutrient absorption, and overall bodily maintenance.

Overall, the ANS functions as a complex and finely regulated system that maintains internal balance, i.e., homeostasis, and responds to changes in the environment. Its intricate control over vital functions ensures the proper functioning of various organ systems and adaptation to different physiological and environmental demands.

Heart Rate Variability

Then, the regulation of cardiac activity is strongly influenced by the ANS, since the SA node has innervation from the PNS, primarily via the vagus nerve. Whereas the morphology of the ECG provides a comprehensive view of the heart's electrical activity, HRV offers insight into the small timing variations of consecutive heartbeats, and the regulatory mechanisms behind them. For this reason, HRV has gained significant attention in clinical research and practice due to its potential as a non-invasive marker of various health conditions.

The HR is not a perfectly regular rhythm; but there is natural variation in the time intervals between heartbeats. Rather than simply calculating an average HR over a period of time, HRV looks at the precise variations in length between successive heartbeats' intervals, which can be milliseconds apart. HRV is a key indicator of the dynamic changes in HR, reflecting the continuous interplay between the sympathetic and parasympathetic branches of ANS, that modulate the intrinsic pacemaker of the heart, the SA node.

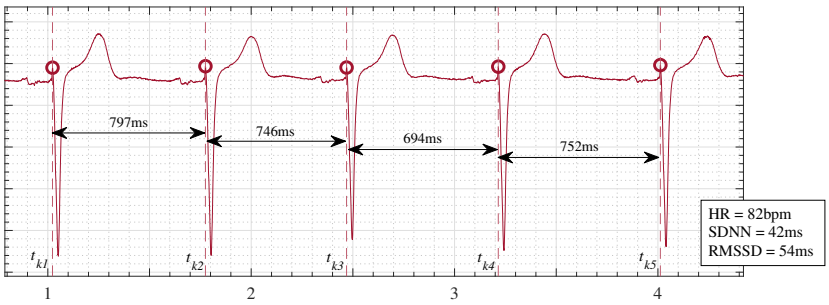

Figure 1.11: Consecutive R-R intervals. The standard deviation of the intervals (SDNN) of the displayed segment is calculated and showed in the textbox, as one common measure of HRV. The presented ECG signal was obtained using the orthogonal system, particularly the lead X. The R-wave of each heart beat is represented with a circle.

The temporal occurrence of heartbeats in sinus rhythm is typically defined based on the timing of the P waves, as the cardiac muscle depolarization initiates at the SA node. However, the P wave often has a very low amplitude and can be entirely absent in some heartbeats. Given the relatively consistent interval between the P and R waves, R-to-R (RR) intervals are commonly used to characterize the time between successive heartbeats [2], whose dynamics are known as HRV.

In the forthcoming Section 3.3, a detailed description is provided regarding the biomarkers from HRV, encompassing both time and frequency domain analyses. Time-domain analysis, such as Standard Deviation of NN Intervals (SDNN) and Root Mean Square of Successive Differences (RMSSD), evaluates overall and short-term HRV variations, respectively. Frequency-domain analysis decomposes the HRV signal into spectral bands, notably Low Frequency Band (LF) (0.04-0.15 Hz) and High Frequency Band (HF) (0.15-0.4 Hz). LF band represents mixed sympathetic and parasympathetic activity, while HF band indicates parasympathetic modulation. The normalized LF frequency (LFn = LF / (LF+HF)) ratio offers insights into the sympathovagal balance. See Fig. 1.12 to see the change of HRV spectra, for frequency domain analysis. During resting conditions, HF power is high, whereas during stress stimulation, HF power decreases and LF power increases, as response to the increase in sympathetic activity.

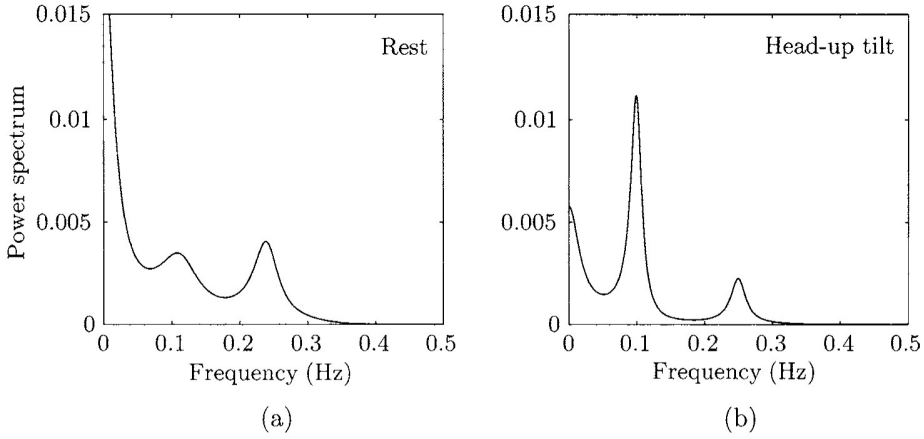

Figure 1.12: Frequency-domain analysis of the HRV signal acquired from a normal subject during (a) resting conditions and (b) a 90^{o} head-up tilt. The head-up tilt increases sympathetic activity as reflected by the increased peak at 0.1 Hz. Adapted and reproduced from [2].

Implications and Clinical Relevance of HRV

HRV is recognized as an important indicator of cardiac health, autonomic function, and overall well-being. Reduced HRV has been associated with a spectrum of pathological conditions, including cardiac arrhythmia, myocardial infarction, hypertension, diabetic neuropathy, and psychological disorders like anxiety and depression [12], [13]. On the other hand, higher HRV reflects a robust, adaptable cardiovascular system and greater physiological flexibility.

HRV also serves as a prognostic tool, with reduced levels indicating an increased risk of mortality and adverse cardiovascular outcomes across various patient groups. This makes HRV a valuable asset in risk stratification, informing treatment choices, and tracking the progression of disease states [14], [15].

Beyond its traditional use in cardiovascular monitoring, HRV has found applications in diverse areas due to the advent of wearable technologies. Devices such as Holter monitors and sports performance trackers have sparked interest in leveraging HRV for insights into stress management, mental health, athletic performance, and general wellness. HRV biofeedback techniques, in particular, are being used to teach individuals how to regulate their autonomic functions, which can enhance stress coping mechanisms and

improve emotional health [16], [17].

1.2.3 Baroreflex System and Blood Pressure Regulation

As explained, the influence of SNS and PNS activity on the heart is regulated by higher brain centers using the feedback received from various receptors located in the body [3]. The baroreflex mechanism, a key component of cardiovascular homeostasis, operates as a negative feedback loop, primarily involving baroreceptors located in the carotid sinus and aortic arch. These receptors sense BP changes and send signals to the brain's medulla oblongata, the cardiovascular control center.

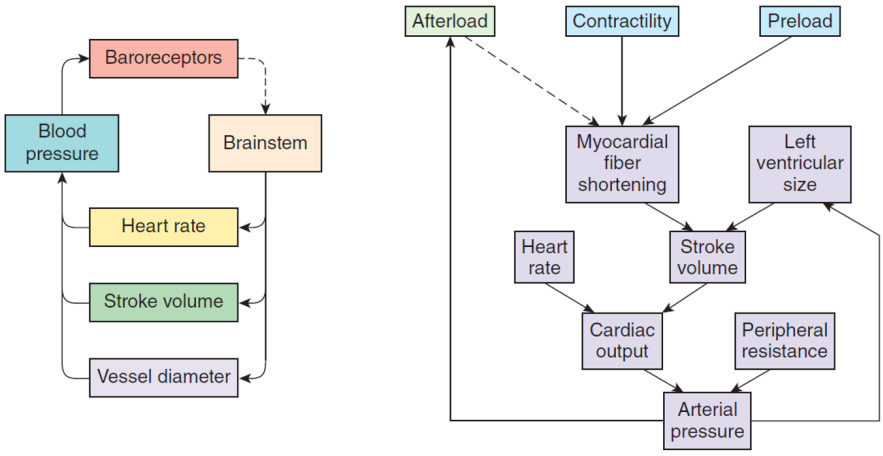

Figure 1.13: Feedback control of blood pressure. (left) Brainstem excitatory input to sympathetic nerves to the heart and vasculature increases HR and SV and reduces vessel diameter. Together these increase blood pressure, which activates the baroreceptor reflex to reduce the activity in the brainstem. (right) Interactions between the components that regulate Cardiac Output (CO) and arterial pressure. Adapted from [3].

Blood pressure is a vital sign, indicative of the force exerted by circulating blood against vessel walls, and fluctuates due to factors like CO, peripheral resistance, and systolic blood volume [3]. Baroreceptors respond to BP elevations by transmitting signals that decrease sympathetic outflow and increase parasympathetic activity, resulting in a decrease in vasoconstriction, reduced HR, and decreased cardiac contractility. Conversely, a drop in BP triggers opposite effects to elevate BP.

Arterial system mechanics, including wave reflection and arterial stiffness, also contribute to BP regulation. Changes in arterial state, like vasoconstriction or vasodilation, and physiological aging impact central pressure waveform morphology. Peripheral resistance, predominantly at arteriole level, is a major determinant of wave reflection.

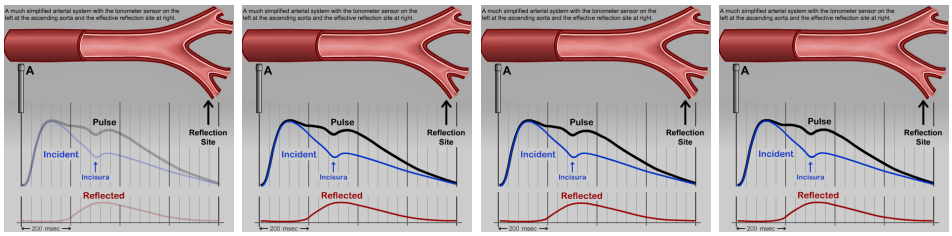

(a) (b) (c) (d)

Figure 1.14: Animated GIFs showing pressure waveforms under various arterial conditions: (a) normal, (b) vasoconstricted, (c) vasodilated, and (d) stiff aorta. These animations demonstrate the effect of arterial changes on the incident and reflected waves. Source: [18]

Sympathetic activation increases BP through vasoconstriction, elevated venous return and CO, and HR acceleration. These effects are encapsulated in the formula:

$$BP = CO * TPR, \tag{1.1}$$

where the acronyms stand for CO, and Total Peripheral Resistance (TPR). This equation highlights the interaction between cardiac function and vascular resistance in determining blood pressure.

1.3 Respiratory Activity and Regulation

Breathing, essential for life, involves inhaling oxygen and exhaling carbon dioxide. This process, regulated by the respiratory center in the medulla oblongata, is coordinated through rhythmic signals from inspiratory and expiratory neurons [19]. Central chemoreceptors in the brain monitor carbon dioxide levels in cerebrospinal fluid, while peripheral chemoreceptors in the carotid and aortic bodies respond to changes in Blood Oxygen Saturation (SpO2), carbon dioxide, and pH levels [20]. These receptors work together to maintain optimal blood gas composition.

Respiratory function is crucial for maintaining overall health, with disorders such as Chronic Obstructive Pulmonary Disease [21], infections, cystic fibrosis, and asthma significantly affecting both respiratory and cardiovascular systems [22], [23]. These conditions can impair oxygen delivery and immune response.

Spirometry is an important tool for quantifying lung function, measuring air volume displacement during breathing. Figure 1.15 illustrates typical lung volumes and capacities. Tidal Volume (TV), the air volume inhaled or exhaled during normal breathing, usually ranges from 500–750 mL. Assessing these parameters provides insight into respiratory dynamics, aiding in the diagnosis and management of lung function. Additionally, Breathing Rate (BR) and its frequency range (bandwidth) are critical for evaluating respiratory health [24], [25].

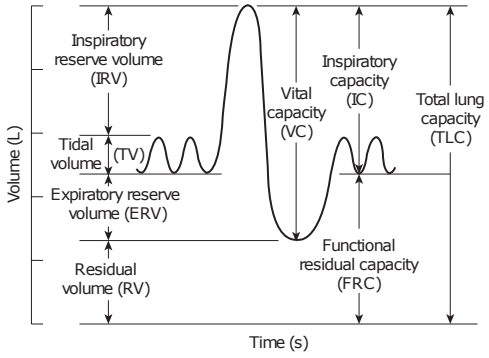

Figure 1.15: Spirometry showing lung volumes and capacities. The figure depicts TV during normal breathing. Adapted from [11].

1.4 Cardio-Pulmonary Interactions

The regulation of breathing is intricately interconnected with cardiac and cardiovascular activity (Fig. 1.16). Whereas exhalation aids in cardiac chamber blood emptying, inhalation, facilitated by diaphragmatic contraction, creates a negative pressure in the chest, drawing air into the lungs. This action simultaneously increases thoracic volume, and enhances venous return to the right atrium, elevating preload, SV, and CO [26], [27].

A well-known CPC mechanism involves this mechanical effect of respiration on the ECG and HRV (see Fig. 1.17). The ECG signal exhibits

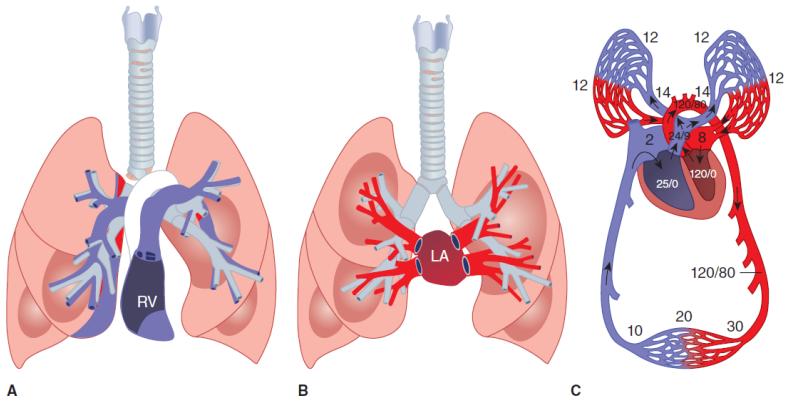

Figure 1.16: Schematic representation of pulmonary circulation, illustrating the relationship between respiratory and cardiac functions. Reproduced from [3].

inspiration-related alterations, such as a slight P-wave amplitude decrease and an R-wave amplitude increase, portraying amplitude-modulated cardiac activity signals with respiration as the carrier [28].

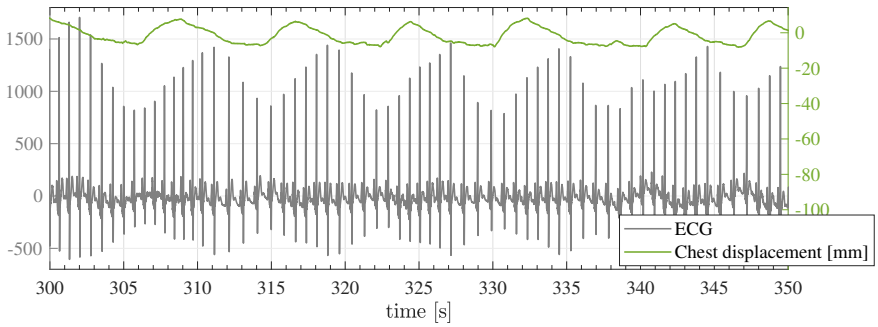

Figure 1.17: Amplitude modulation of respiration in an illustrative ECG signal.

1.4.1 Respiratory Sinus Arrhythmia

Respiratory Sinus Arrhythmia (RSA) represents a physiological phenomenon where the instantaneous HR synchronizes with the respiratory cycle, a process modulated by the ANS [29]. This modulation results in sympathetic activation that increases HR during inspiration, and parasympathetic activity that decelerates HR during expiration (see Fig. 1.18).

The SNS specifically enhances HR during inspiration to pump more deoxygenated blood into the lungs, optimizing gas exchange [30], ventilation,

and perfusion [31]–[34]. Consequently, this synergy plays a pivotal role in efficient oxygen and carbon dioxide exchange in the lungs.

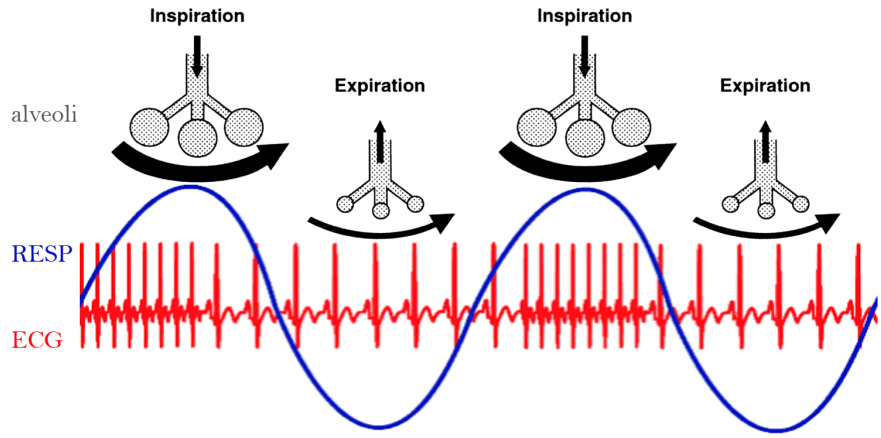

Figure 1.18: RSA illustration depicting two cycles of respiration in blue, and the corresponding filling of alveoli. In red, the frequency modulation of the ECG sinus rhythm mediated by respiration is shown. The observed variation in HR synchronized with the respiratory cycles, known as RSA, highlights the influence of the respiratory system on cardiac autonomic modulation.

In relaxed, healthy individuals, this interaction creates a distinct cyclic pattern, where HR accelerates with inspiration and decelerates with exhalation. This results in the frequency modulation of HR by respiration, which is observable in the cyclic variations of HR aligned with the breathing pattern (see Fig. 1.19).

RSA has been extensively studied and is considered a physiological phenomenon associated with healthy cardiovascular function. RSA is more prominent during restful conditions and becomes less evident during exercise or stress, and it is also influenced by factors such as age, gender, and BR [35]–[38]. However, RSA can be affected by various physiological and pathological conditions [39]–[41]. For example, reduced RSA is observed in individuals with cardiovascular diseases, autonomic dysfunction, and certain psychiatric disorders [42]. Some studies have reported the occurrence of CPC in various conditions such as periods of rest, controlled breathing, or anesthesia [34], [43], [44]. For these reasons, CPC is being one of the main subjects of study in the present thesis. Then, CPC provides insights into autonomic function, cardiorespiratory health, sleep quality, and the impact

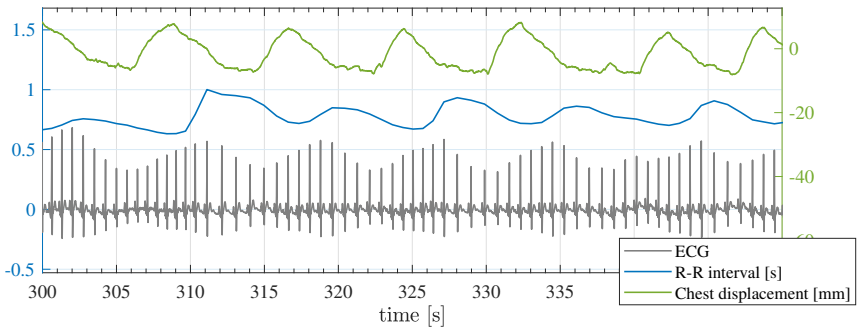

Figure 1.19: Real illustrative example of RSA, showcasing the frequency modulation of respiration on the ECG signal. The respiratory movement of the chest is represented by the green trace, indicating chest displacement, while the blue trace depicts the RR interval derived from the ECG. Note that this ECG signal is the same as the one used in Fig. 1.17.

of interventions [36]–[38], [43]. These measures can be used to assess the ANS, identify abnormalities in both cardiovascular and respiratory regulation, and guide treatment strategies in various health conditions.

The baroreflex plays also a crucial role in mediating respiratory and cardiovascular interactions [39]–[41]. Changes in intrathoracic pressure during respiration stimulate baroreceptors and stretch receptors, which respond by adjusting sympathetic and parasympathetic activities, affecting HR and vascular tone. During inspiration, the increase in venous return and subsequent stretching of the baroreceptors result in an enhanced baroreceptor firing rate. This leads to increased parasympathetic activity (vagal tone) and decreased sympathetic activity, resulting in a decrease in HR and vasodilation. Conversely, during expiration, the reduced venous return and decreased baroreceptor firing rate lead to a decrease in parasympathetic activity and an increase in sympathetic activity, causing an increase in HR and vasoconstriction.

The changes in intrathoracic pressure and lung inflation during respiration activate the baroreceptors located in the walls of major blood vessels, particularly in the aortic arch and carotid sinus. The baroreceptors sense changes in blood pressure and transmit signals to the cardiovascular control centers in the brain.

1.4.2 Inclusion of Respiration in HRV Analysis

Several medical conditions can elevate the demand for ventilation. These include respiratory diseases causing airway obstructions, cardiovascular diseases affecting oxygenated blood flow, or metabolic acidosis increasing blood acidity. Abnormal respiratory rates, either elevated or decreased and deviating from the normal range of 12 to 18 breaths per minute, are crucial biomarkers for identifying potential clinical risks, particularly in elderly and critically ill patients. The brainstem's respiratory center modulates the strength and rhythmicity of breathing, influenced by chemical, mechanical, and cortical inputs.

HRV research has gained attention as a non-invasive marker of cardiac vagal tone, reflecting the PNS's influence on cardiac regulation [45]–[47]. However, variations in respiratory parameters like breathing rate and tidal volume can affect the interpretation of RSA and cardiac vagal tone [48], [49]. To mitigate respiratory influences on RSA, some studies have subjects breathe at a constant rate [47]. However, this method may remove important variability linked to neural control of cardiac vagal tone [45]. Therefore, including BR information in HRV analysis during spontaneous breathing can enhance ANS assessment [50]. Additionally, mathematical tools are available to separate respiratory influences from HRV analysis, emphasizing the importance of considering respiration when evaluating ANS biomarkers related to HRV [51]. Besides, respiratory parameters, which play a key role in autonomic regulation, can be indirectly estimated from ECG and PPG signals, eliminating the need for additional sensors [52], [53].

1.4.3 Effect of Respiration on the PPG

Respiratory modulation extends its influence to PPG signals, too [54], [55]. The modulation affects the amplitude of PPG systolic waves and pulse rate variability, showcasing the broad impact of respiration on physiological parameters (Fig. 1.20).

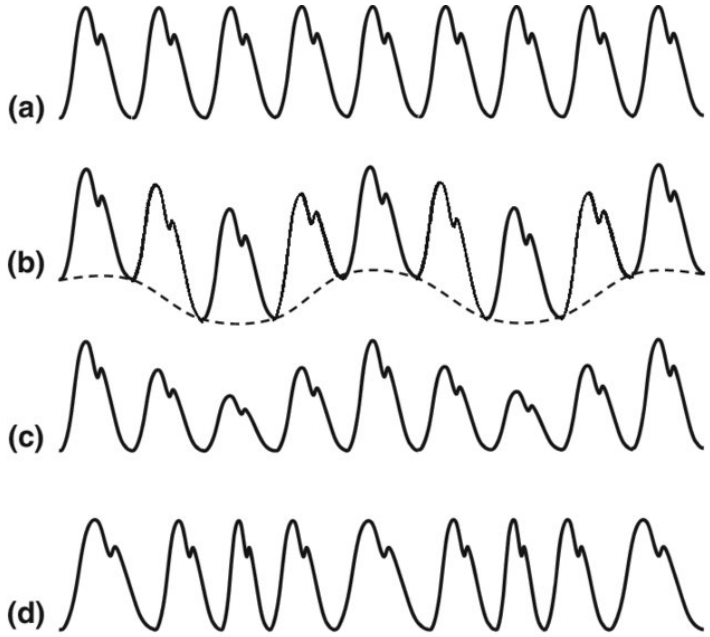

Figure 1.20: Modulations of the PPG due to respiration (modulation through two complete respiratory cycles shown). (a) PPG showing unmodulated cardiac pulse waveforms. (b) Baseline modulation (cardiac pulses riding on top of baseline shown dashed). (c) Amplitude modulation (cardiac pulses amplitudes varying over respiratory cycle). (d) RSA (pulse period varying over respiratory cycle). Adapted and reproduced from [56].

Chapter 2

Target Disorders and Applications

In this chapter, I offer a comprehensive overview of the various disorders and applications where I will apply non-invasive biomarkers. Specifically, I will delve into the topic of weaning of patients from MV in Section 2.1, an in-depth analysis of OSA and its clinical implications in Section 2.2, and discuss the key concepts related to the analysis of PPG oriented to wearable

devices in Section 2.3. Concluding each section, I will outline and justify the specific signal processing methodologies I propose for each target disorder and application, elucidating how these approaches effectively meet the set objectives.

2.1 Mechanical Ventilation and Weaning in the ICU

Mechanical ventilation is a crucial intervention used in ICUs to assist patients with respiratory failure or compromised lung function in breathing. It involves the use of a ventilator, a machine that delivers air to the lungs and helps both remove carbon dioxide and supply oxygen, when critical patients are struggling to do this vital function. The air gets to the lungs through the endotracheal tube, which has to be placed with sedation into the trachea.

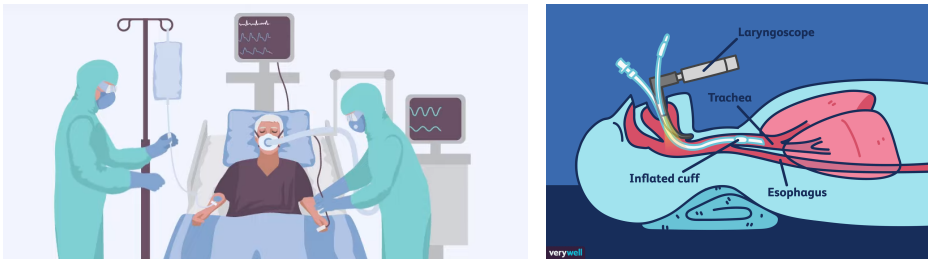

(a) (b)

Figure 2.1: (a) The context of ICU patients: connected to many different monitoring systems and assisted with mechanical ventilation. (b) The endotracheal tube, placed into the trachea, necessary for mechanical ventilation.

2.1.1 Weaning Process and Extubation

Weaning refers to the process of gradually reducing and eventually discontinuing MV once the patient's condition improves [57], [58]. It is important to liberate patients from ventilator support as soon as possible to minimize complications associated with prolonged ventilation, such as infection or lung injury [59]. Weaning protocols involve assessments of the patient's readiness for Spontaneous Breathing Trial (SBT), where they breathe without ventila-

tor support for a specific duration. Successful SBTs indicate readiness for extubation.

Therefore, before withdrawing MV, a mechanically ventilated patient must pass a criteria for weaning readiness, but must perform and pass also the SBT afterwards. Extubation is the removal of the endotracheal tube used for MV, after successful SBT. It is typically performed if the patient demonstrates stable respiratory function, adequate oxygenation, and is able to protect the airway effectively. Extubation success relies on factors such as the patient's underlying condition, strength of respiratory muscles, and ability to clear secretions. In some cases, extubation may be followed by non-invasive ventilation to provide additional support as the patient transitions to spontaneous breathing.

However, weaning failure and reintubation after a premature weaning is really critical and around 20% of patients that passed SBT have to be reintubated [60]–[62]. This reintubation leads to a significant increased risk of severe respiratory complications such as pneumonia, lung injury, or diaphragmatic dysfunction [59]. Of note, weaning failure increases the risk of mortality in the range from 25 to 50% [60], [63], [64]. For a more detailed exploration of weaning predictors, criteria, procedures, and the assessment of extubation in mechanically ventilated patients, I suggest the reader consulting the comprehensive review provided in [65], [66].

2.1.2 Spontaneous Breathing Trial

The SBT is essentially a "test drive" where the patient's ability to breathe without the assistance of a ventilator is evaluated. During this trial, the level of ventilatory support is minimized or completely withdrawn, allowing clinicians to monitor how the patient copes under such circumstances [59], [67]–[69]. There are two primary methods of conducting an SBT [67]–[69]:

- **Low-level Pressure Support Ventilation**: In this technique, the patient breathes through the MV circuit, but with minimal levels of Pressure Support Ventilation (PSV). This method allows for a gradual reduction in support while closely monitoring the patient's ability to manage without full ventilatory assistance.
- **T-piece Circuit**: Alternatively, SBT can be performed by disconnecting the patient from the ventilator and employing a straightforward

circuit, as depicted in Figure 2.2. A source of O2 is delivered to the patient at a high flow rate (higher than the patient's inspiratory flow rate). This setup ensures efficient oxygen delivery and actively aids in expelling exhaled CO2, thereby avoiding CO2 rebreathing. Because this circuit employs a T-shaped adapter, it is popularly known as a T-piece circuit.

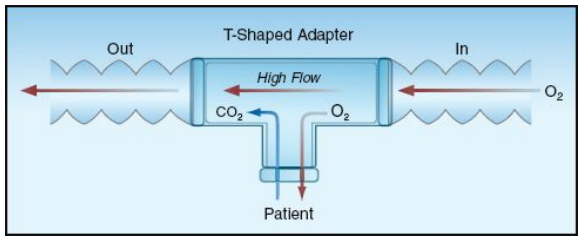

Figure 2.2: T-piece breathing circuit for SBT, after removing the mechanical ventilation support.

There is no clinically proven advantage with either method of SBT ([70]–[72]). Regardless of the method chosen, rapid breathing during SBT can be detrimental in several ways, including the promotion of hyperinflation, intrinsic Positive End-Expiratory Pressure (known as PEEP), reduced CO, increased dead space ventilation, decreased lung compliance, and diaphragm dysfunction. Rapid breathing also reduces ventilation in diseased lung regions (where time constants for alveolar ventilation are prolonged), and this promotes alveolar collapse and hypoxemia. Additionally, rapid breathing elevates whole-body oxygen consumption, placing added burden on systemic oxygen transport. These considerations underscore the importance of carefully managing a patient's respiratory status during SBT and finely choose those presumably ready to perform the SBT [73], [74].

2.1.3 Ventilation Modes

In the context of patients under MV, it is crucial to understand the various modes of ventilation and the types of breaths that can be administered. MV breaths can be categorized as controlled, assisted, or supported. Additionally, there are two primary methods of breath delivery: volume-based and pressure-based.

1. Controlled Ventilation: In this mode, the ventilator completely controls

the breathing process. Patients under controlled ventilation do not exert any effort; the ventilator is responsible for all aspects of breathing.

2. Assisted Ventilation: Here, the ventilator responds to the patient's initial effort to breathe. When a patient attempts to initiate a breath, the ventilator detects this effort and delivers a full mechanical breath. The patient must generate a change in pressure or flow to trigger the ventilator.
3. Supported (Spontaneous) Ventilation: Similar to assisted ventilation, supported breaths are also initiated by the patient. However, once triggered, the ventilator provides partial support, unlike the full support offered in assisted ventilation.

Regarding the methods of breath delivery:

(a) Volume-based Ventilation: The ventilator delivers a predetermined volume of air into the lungs and then extracts it. This method focuses on controlling the amount of air the patient receives per breath.

(b) Pressure-based Ventilation: In this approach, the ventilator inflates the lungs to a specific pressure level and then releases. The ventilator is programmed to maintain this pressure for each breath.

Combining these types and methods leads to various ventilation modes, each tailored to specific patient requirements. Common modes include:

- Assist-Control Ventilation (ACV): Provides a set number of breaths per minute, which can be either controlled by the ventilator or assisted based on the patient's breathing effort.
- Pressure Support Ventilation (PSV): Assists the patient's spontaneous breaths by providing a preset level of pressure support, enhancing patient-initiated breaths (see Fig. 2.3).
- Synchronized Intermittent Mandatory Ventilation (SIMV): A hybrid mode combining controlled and spontaneous breaths, allowing more autonomy for the patient in the breathing process.
- Volume Controlled Ventilation (Volume Controlled Ventilation (VCV)): Delivers a consistent and pre-set volume of air to the patient, with each ventilator-initiated breath, ensuring stable ventilation regardless of changes in lung compliance or airway resistance (see Fig. 2.4).

The choice of ventilation mode and method depends on various factors, including the patient's respiratory condition and the clinical objectives of the ventilation therapy.

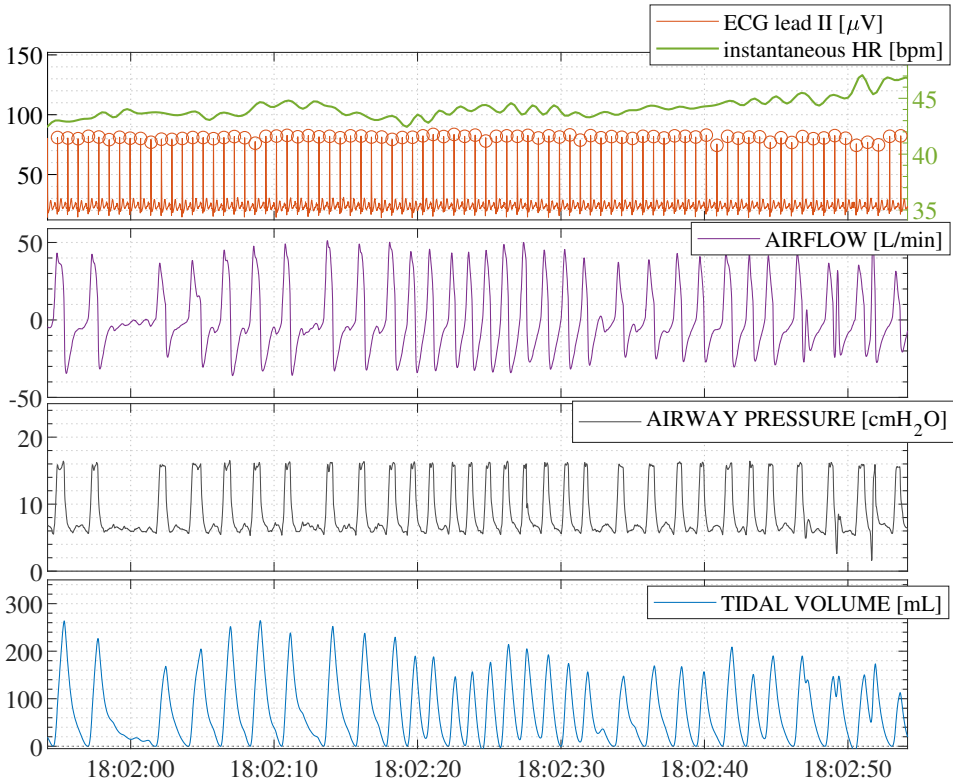

Figure 2.3: PSV patterns, and example of ineffective efforts (IE), e.g., around 18:02:00, where airway pressure (PAW) did not pass the threshold to activate an inspiration.

2.1.4 Mortality and Pathophysiology

As the reader may have noticed, MV, while life-saving, presents lots of risks and complications. Ventilator-associated pneumonia (VAP) is one of the most common and severe complications, leading to increased morbidity and mortality [75]–[77]. Other complications include barotrauma (lung injury due to high pressure), ventilator-induced lung injury (VILI), and ventilator-associated lung injury (VALI) [78]. These injuries can result from excessive tidal volumes, high inspiratory pressures, or repetitive alveolar collapse and expansion [79]. In fact, one new risk parameter has been found by De Haro et al. [80], where they identify asynchronies between MV and the patient. This is called double cycling and its occurrence originates VILI and VALI due to asynchronies that lead to, e.g., doubling the amount of air volume that the patient needed (Fig. 2.4), or ineffective efforts (Fig. 2.3).

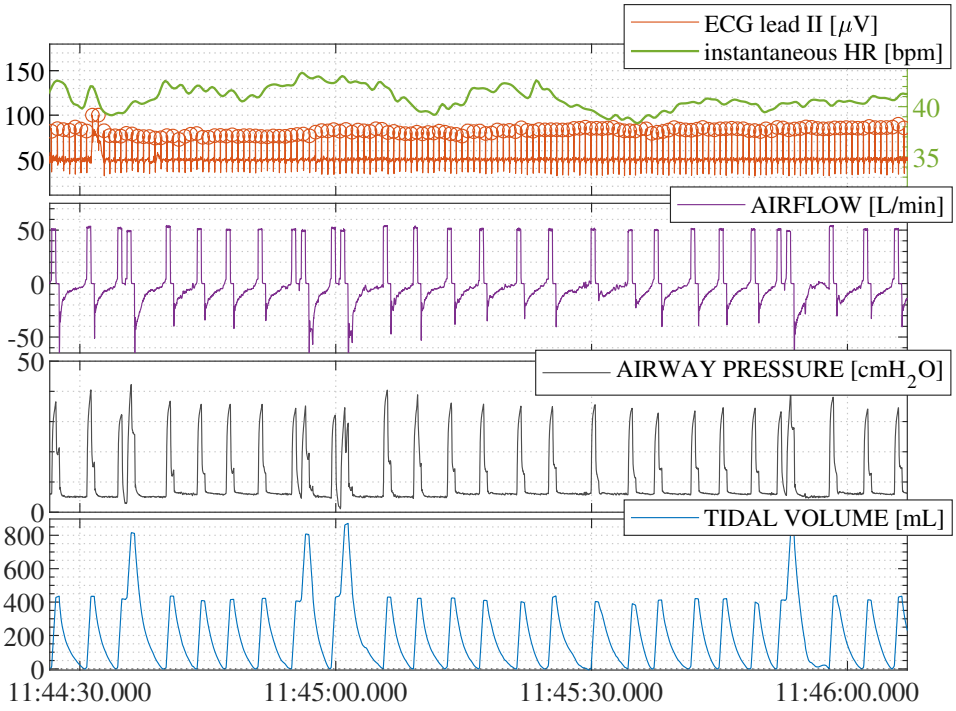

Figure 2.4: VCV mode and some visible Double Cycling asynchronies.

The pathophysiology underlying ventilator-associated lung injury involves several mechanisms, including inflammation, oxidative stress, and impaired gas exchange [81], [82]. High-pressure ventilation can trigger an inflammatory response, leading to the release of pro-inflammatory cytokines, recruitment of inflammatory cells, and subsequent lung damage. VALI can also occur due to overdistention of alveoli or shear stress during cyclic opening and closing of collapsed lung units [83].

To mitigate these risks, lung-protective ventilation strategies are employed, including the use of low tidal volumes and limited inspiratory pressures [84]. Additionally, strategies to prevent VAP, such as elevation of the head of the bed, regular oral care, and appropriate sedation management, are implemented [85], [86].

2.1.5 Objectives of Part II

As mentioned, MV is a cornerstone in the management of respiratory failure within ICUs. The custom ventilation modes and adherence to weaning

protocols are critical for safely guiding patients from mechanical support to spontaneous breathing. Despite existing protocols and criteria, determining the optimal timing for weaning remains a complex challenge, with significant room for improvement in the assessment of readiness for weaning. To address these challenges, Part II comprises two studies focusing on signal processing methodologies to enhance the criteria for weaning readiness and to decrease unsuccessful weaning attempts.

Study One: Baroreflex Sensitivity and Weaning Readiness

The first study, detailed in Chapter 5, involves the estimation of BRS through the analysis of blood pressure signals and HRV. The goal is to evaluate BRS during the last hour preceding a SBT and to investigate whether BRS, as an ANS marker, can contribute additional insights to enhance the prediction of weaning outcomes. This study is motivated by the observed diminished baroreflex control in various cardiac and cardiovascular conditions where ANS is impaired, as documented in the literature.

Detailed in Section 3.6, two distinct non-invasive techniques are employed to measure BRS. These include the spectral analysis of HRV and SBP to compute the established α index, and a proposed alternative method, called Bivariate Phase Rectified Signal Averaging (BPRSA), which constructs an averaged HRV profile reflecting the cardiac response to SBP fluctuations.

Study Two: Cardiopulmonary Interactions and Weaning Readiness

The second study, presented in Chapter 6, expands analysis to include a set of biomarkers derived from respiration, HRV, and CPC for the assessment of weaning readiness. On the contrary to the first study, this analysis utilizes data from the 24-hour prior to SBT, and not limited to the final hour. This approach allows for a broader evaluation of patient readiness for weaning. Moreover, the first study's scope was more limited regarding the patient cohort size, constrained by the availability of high-quality invasive BP recordings.

This second study introduces an innovative exploration of heart-lung interactions and the evaluation of CPC indices in a prospective design, while ensuring the analysis remains blind to the SBT outcome. This approach aims

to improve the assessment of patients' readiness for weaning from mechanical ventilation, potentially leading to more accurate and effective clinical decision-making. Methodologies for estimating respiratory signals and HRV are explained in Section 3.1 and 3.3.3, respectively, with a subsequent detailed exploration of the three main methods for CPC quantification in Section 3.4. The CPC estimation methods include Time-Frequency Coherence (TFC) in Section 3.4.1, information dynamics (ID) in Section 3.4.2, to estimate the cross entropy, and Orthogonal Subspace Projections (OSP) in Section 3.4.3, to decompose the HRV signal into a component related to respiration and a residual component. Furthermore, this study two examines the timing of assessment throughout the day before SBT and its potential correlation with SBT outcomes.

2.2 Obstructive Sleep Apnea

After delving into the main concepts of MV and weaning, we transition to another vital aspect of respiratory health [87], [88]. Sleep is a fundamental physiological process, during which the body recovers. While the exact reasons and purposes for sleep remain unknown, this state, which occupies a third of our lives, is undeniably vital. However, sleep can be disrupted by respiratory-related disorders, going from primary snoring, to the most severe and common: OSA.

Hypnograms provide a visual depiction of sleep architecture, detailing the transitions between different sleep stages over the course of a night [87], [88]. The hypnogram displayed in Fig. 2.5 reveals a normal sleep pattern, that begins with wakefulness, followed by a descent into non-rapid eye movement (NREM) sleep, progressing from the lightest stage (Stage 1) to the deepest (Stage 4), and then ascending to the rapid eye movement (REM) stage, characterized by vivid dreaming and increased brain activity. This cycle, which recurs roughly every 90 to 110 minutes, typically features more extended periods of deep sleep during the initial cycles and increasingly longer REM periods towards the morning.

OSA is characterized by repetitive interruptions in breathing during sleep, due to upper airway obstruction [89], [90]. These interruptions alter the normal sleep cycle (Fig. 2.5), the hypnogram of a person with OSA may

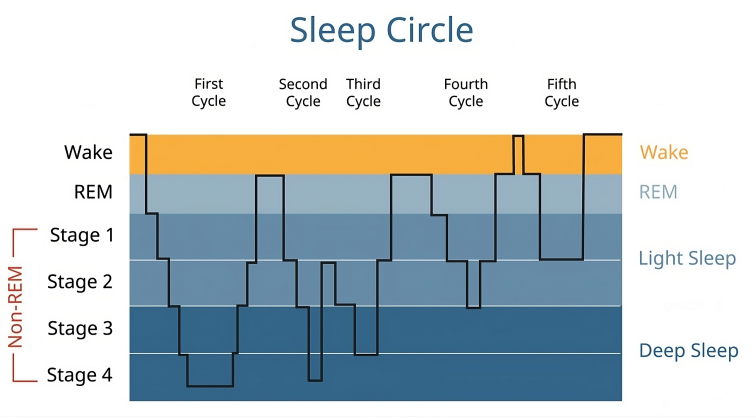

Figure 2.5: Normal Sleep Architecture Hypnogram. This chart traces the typical progression through wakefulness, NREM stages 1 to 4, and REM sleep over five sleep cycles. The cyclical nature of sleep stages and the increasing predominance of REM sleep in successive cycles are evident. OSA can disrupt this pattern, leading to a hypnogram characterized by increased awakenings and diminished deep sleep.

show a fragmented pattern with more frequent transitions to wakefulness and reduced or absent deep sleep stages. This prevents individuals with OSA from achieving deep, restorative sleep, and the resultant poor sleep quality may lead to daytime fatigue and drowsiness, but end up in serious health implications, including cardiovascular, metabolic, and neurocognitive diseases [91].

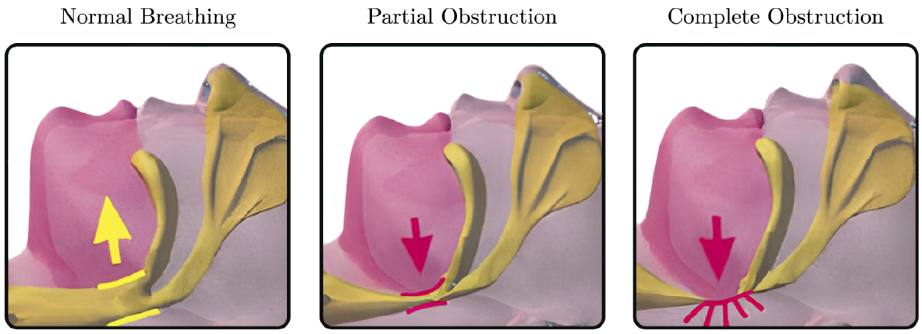

Figure 2.6: Representation of normal breathing, partial, and complete obstruction. Adapted and reproduced from [92].

As shown in Fig. 2.6 and 2.7, OSA is originated by a total (apneas) or partial (hypopneas) occlusion of the upper airways [89], [90], which blocks the airflow while the respiratory effort persists. If this blockage is sustained,

i.e., more than 10s in adults, it may lead to oxygen desaturation [93], visible in the SpO2 signal (see Fig. 2.7). During critical developmental stages in pediatric population, sleep disruptions can significantly impact children's motivation and behavior.

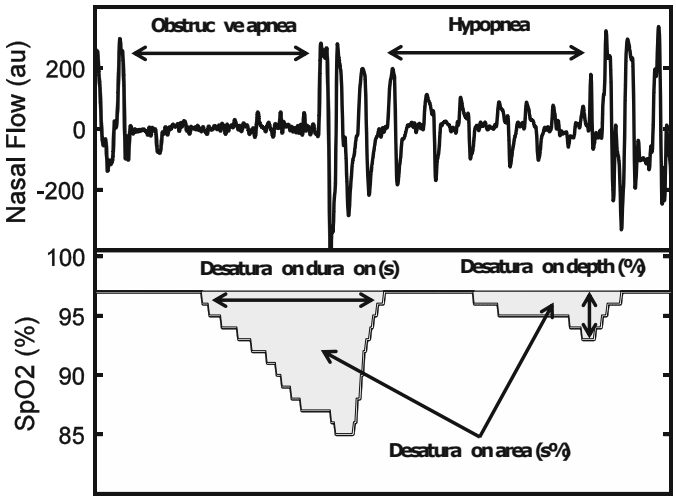

Figure 2.7: Example of the duration (s), area (s%), and depth (%) of desaturation events following obstructive apnea and hypopnea. Adapted and reproduced from [94].

However, while the breathing cessations are obstructive more often, these can also be central [90] (Fig. 2.8). The main difference between them relies on the fact that in the case of central apneas, the brain stops sending stimulus for breathing impulse, leading to cessation of both oronasal airflow and inspiratory effort movement.

OSA has emerged as a major public health issue. Epidemiological studies suggest that OSA is now prevalent in approximately 5.7% of the pediatric demographic [95], [96]. A multicenter study involving 4,191 pediatric participants revealed that, of children referred to specialized sleep laboratories due to clinical suspicion of OSA, 43.3% were diagnosed with mild OSA, 12.8% with moderate, and 16.8% with severe OSA [97]. Data from the *Subdirección General de Información Sanitaria Española* as of March 2021 further indicates a 9.56% prevalence rate for pediatric OSA in Spain, distinguishing 10.83% of the affected as boys and 8.20% as girls below 15 years. In the adult demographic, OSA prevalence can reach up to 49% [98]. Despite this alarming increase in prevalence, the condition remains largely underdiagnosed, as emphasized by [99], and other research findings [98].

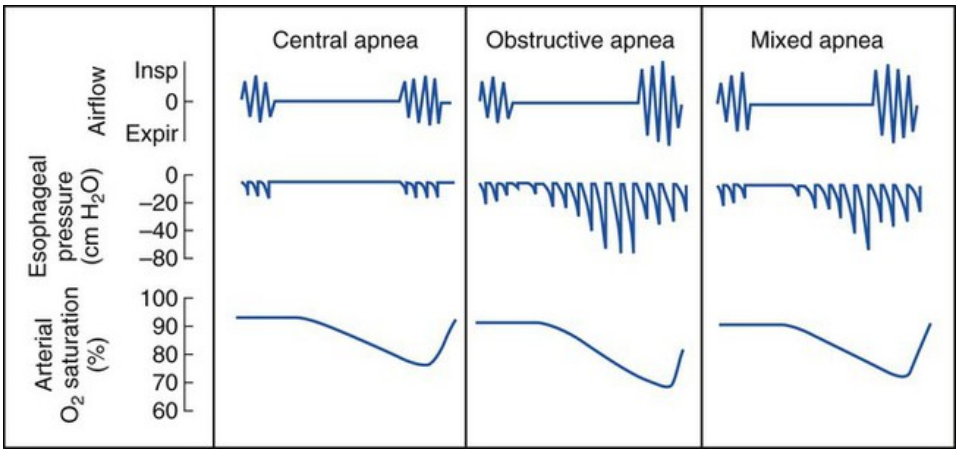

Figure 2.8: Patterns of airflow, respiratory efforts (reflected through the esophageal pressure), and arterial oxygen saturation produced by central, obstructive, and mixed apneas.

2.2.1 Diagnosis

Polysomnography (PSG) conducted in a sleep laboratory is the standard method for diagnosing OSA, as it records the essential physiological signals [95]. Despite PSG being the gold standard, it's a tedious and expensive method requiring the measurement of numerous physiological variables and the expertise of sleep specialists [100], [101]. Given its cost, complexity, and the limitations in the availability of sleep centers, many OSA cases remain undetected.

Due to its significance as a cardiovascular morbidity factor and the availability of effective treatments, there have been efforts to simplify diagnostic studies to reduce costs and assist more patients [95], [102]. For example, overnight oximetry, which monitors SpO2 using a pulse-oximeter, is particularly child-friendly [103], and the automated analysis of the SpO2 signal has proven good diagnostic efficacy for OSA screening [103].

2.2.2 Etiology and Consequences of OSA

The pharyngeal collapse and cessation of airflow occur during inspiration, resulting from the negative intraluminal pressure generated by diaphragm contraction. The obstruction is aggravated by sleep-induced flaccidity and hypotonia of the pharyngeal muscles [105]. During normal inspiration, the

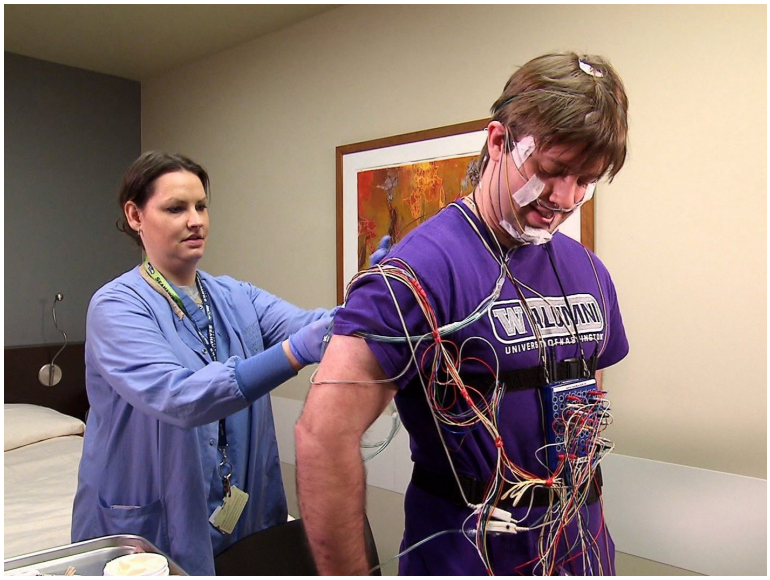

Figure 2.9: Sensor Configuration for a Standard Clinical Polysomnography.

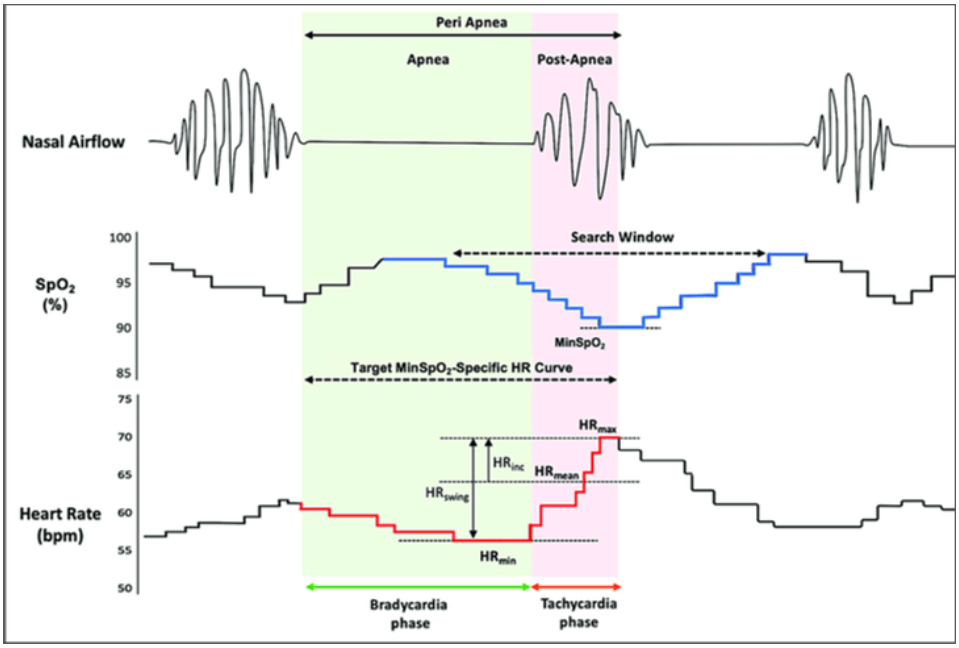

Figure 2.10: Bradycardia-Tachycardia pattern following an apnea/hypopnea event. Adapted and reproduced from [104].

contraction of respiratory muscles, especially the diaphragm, creates negative intrathoracic pressure, inducing airflow to the lungs [105], [106]. Sleep, especially in its REM phase and deep non-REM phases, favors the loss of

coordination, due to relaxation, between respiratory and pharyngeal muscles. As a result, the upper airway tends to collapse, increasing resistance to airflow and, eventually, resulting in apnea or hypopnea episodes (see Fig. 2.11).

This interruption in respiratory flow during an apnea event leads to a drop in SpO2 levels and intensified respiratory efforts. If these efforts are insufficient and hypercapnia levels become dangerous, a subconscious "arousal" or awakening is triggered. This arousal serves as an instinctive, protective mechanism, causing the person to adjust their position, often unconsciously, which reopens the airway and restores normal breathing. Such episodes can occur hundreds of times in a single night, posing serious health implications.

In patients with OSA, the heart responds to respiratory events with progressive bradycardia followed by abrupt tachycardia, although such patterns can be highly variable depending on the duration and severity of each of the respiratory events [108]–[111]. These characteristics patterns are the basis for the study of the treatment effects on HRV trends. For example, Isaiah et al. [112], and Martin-Montero et al. [113] analyzed changes in HRV related to pediatric OSA treatment employing the CHAT database to conduct a Causal Mediation Analysis (CMA). They found that OSA treatment affects HRV activity in terms of change in severity and disease resolution, and demonstrated the potential utility of HRV as biomarker of OSA resolution [113].

Repeated subconscious arousals due to apneas result in sleep fragmentation, preventing deep, restorative sleep. This disrupted sleep structure causes neuropsychiatric manifestations like excessive daytime sleepiness and leads to behavioral issues. OSA can also induce significant alterations in intrapulmonary gas exchange, causing chemical and structural damage at the cellular level in the central nervous system, leading to dysfunctions in the brain's prefrontal cortex regions [107], [108]. These alterations in gas exchange increase the risk of cardiovascular and cerebrovascular diseases [114], [115]. Similarly, these patients also have a higher incidence of cardiac arrhythmia and sudden nocturnal death. Morning headaches, also quite frequent in OSA patients, result from cerebral vasodilation caused by the hypercapnia accompanying the apneas.

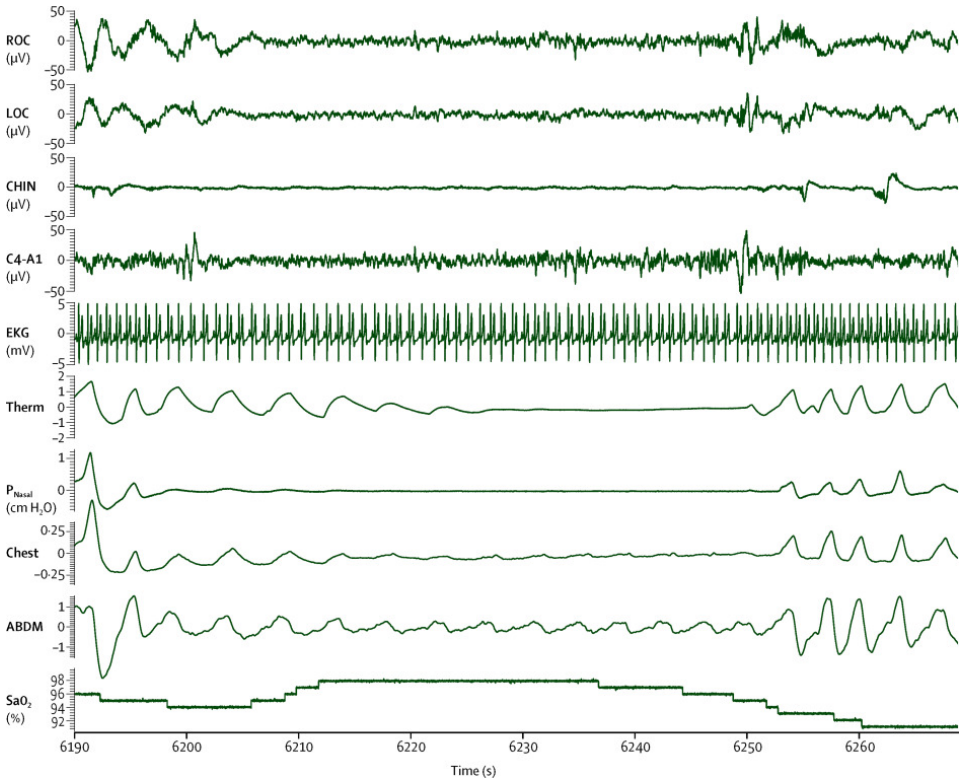

Figure 2.11: An example of the signals recorded during overnight polysomnography. Shows an obstructive apnea with cessation of airflow for more than 10 s despite persistent respiratory efforts shown on the chest and abdominal respiratory bands. The apnea is associated with arterial oxygen desaturation and is terminated by arousal from sleep. C4-A1=electroencephalogram. LOC=left electro-oculogram. ROC=right electro-oculogram. CHIN=chin electromyogram. CHEST=respiratory inductance plethysmography bands placed around the thorax. ABDM=respiratory inductance plethysmography bands placed around the abdomen. PNasal=airflow monitoring by nasal air pressure. Therm=airflow monitoring by thermal air sensor. SaO2=arterial oxygen saturation. EKG=electrocardiogram. Adapted and reproduced from [107]

2.2.3 Definition of Apneic Events in Children

The American Academy of Sleep Medicine (AASM) characterizes apnea in children as either a complete absence or a reduction of airflow by $\geq$90% for at least 2 breaths [90]. Hypopnea is defined as a reduction in airflow ranging from 30% to 90% for a minimum of 2 breaths, coupled with a $\geq$3% SpO2 desaturation or an arousal [90]. It's important to highlight that these criteria differ between children and adults, with the AASM stipulating a minimum duration of 2 respiratory cycles (around 6 seconds) for children

and 10 seconds for adults [90], [116].

2.2.4 Objectives of Part III

The gold standard for the diagnosis of OSA typically relies on overnight PSG, despite being time-consuming, expensive and requiring specialized personnel. Given these challenges, there is a clear need for more accessible and convenient diagnostic tools to simplify the process. Part III of the thesis is structured into three main studies. All have in common to explore various cardiovascular signal processing methodologies and data analysis techniques to improve the stratification and severity assessment of OSA, as well as the associated cardiovascular risk (CVR) in pediatric patients.

Study One: Heart Rate Variability During Apneic and Normal Breathing

Regarding Chapter 8, I examine the differences of HRV values during apnea episodes and compares it with HRV during normal sleep. In this chapter I study whether the sympathetic activation observed in OSA patients is persistent throughout the night or it is just primarily a reaction to apneic events, being that literature suggests that sympathetic activation during apneic events is more pronounced in patients with severe OSA.

This study will contrast HRV metrics across apnea episodes, normal breathing periods, and entire night recordings in a pediatric cohort. The differentiation of HRV in these contexts seeks to discern if the sympathetic dominance is episodic or sustained, aiming to better understand the underlying ANS response to OSA.

Due to the non-stationary nature of overnight PSG recordings, the frequency domain parameters are calculated using a Time-Frequency (TF) distribution belonging to the Cohen's class [117], that will be extensively detailed in Sec. 3.3.4.

Study Two: Cardiopulmonary Coupling as a Diagnostic Tool in Pediatric OSA

In Chapter 9, the research delves into CPC and its utility in the context of pediatric OSA. By utilizing TFC analysis, the study aims to characterize

CPC across different sleep stages and groups categorized by OSA severity. This exploration is grounded in the hypothesis that higher CPC levels may be indicative of better sleep health, and overall cardiovascular health in children with OSA.

Considering the role of CPC in reflecting the interplay between cardiac and respiratory rhythms, and its implications for pulmonary gas exchange and cardiovascular efficiency, this study aims to extend the understanding of CPC in the pediatric OSA population, an area where adult research suggests potential but remains underexplored.

Given the non-stationary nature of overnight PSG recordings, CPC estimation is approached using TFC. The methodology for estimating CPC via TFC is an essential methodology of this thesis, and is thoroughly explained in Sec. 3.4.1.

Study Three: MetS as CVR Index in Children

After having obtained and characterized HRV, CPC and respiratory values from pediatric OSA patients, the next step was to compare those values to levels of cardiovascular risk (CVR) in this population of pediatric patients. However, after a intensive review of the literature, the definition of CVR has never been proposed in children before.

Chapter 10 seeks to establish and validate a measure of CVR among children with OSA by evaluating the applicability of Metabolic Syndrome (MetS). The study investigates whether MetS can serve as a reliable indicator of OSA severity and the efficacy of OSA treatment in the pediatric population—a novel approach not previously explored.

The relationship between OSA and MetS is particularly pertinent given the documented association between OSA and increased risks of obesity, insulin resistance, and systemic inflammation both in children and adults. This work will employ a CMA to probe the mediating factors of OSA treatment outcomes, positioning MetS, obesity, and C-reactive protein levels as potential biomarkers for CVR. This could potentially lead to the recommendation of MetS screening in children diagnosed with OSA.

Whereas OSA in children does not affect critically the cardiovascular function, OSA does result in serious neurocognitive consequences, regarding behavioral and learning disorders, making timely diagnosis and treatment

crucial. If OSA persists through childhood, it can firmly establish CVR for adulthood, thereby underscoring the necessity for prompt diagnosis and intervention of worsened cardiovascular health.

2.3 Analysis of PPG Oriented to Wearable Devices

Many users of wearables may not be aware that these devices, including fitness bands and smartwatches like the Garmin, Samsung Watch, or Apple Watch, routinely monitor the cardiovascular health by capturing the PPG signal. This optical measurement of the arterial pulse wave reflects heart activity and vascular condition. This section aims to summarize the basics of wearable PPG, and its fundamentals.

Figure 2.12: Examples of wearable devices measuring PPG signals. The top images show the devices, and the bottom images display the sensor sides. Adapted from [118].

The increasing popularity of wearables equipped with PPG sensors has opened new avenues for real-time cardiovascular monitoring [6], [119]. PPG's implementation in pulse oximeters for SpO2 assessment marks its significant impact on clinical care. Beyond SpO2, PPG provides insights into cardiac, vascular, respiratory, and autonomic functions. Advanced signal

processing techniques are being developed to extract novel information from PPG signals, transforming the landscape of cardiovascular disease (CVD) assessment. In fact, as wearables gain popularity [120]–[122], their potential in democratizing cardiovascular health becomes apparent.

2.3.1 Physical Fundamentals of PPG

PPG is a non-invasive method that measures blood flow changes by detecting variations in light absorption, linked to the cyclic changes in blood volume during the cardiac cycle. The principle behind PPG is the differential absorption of light by tissues, affected by the concentration of oxyhemoglobin and deoxyhemoglobin.

PPG devices employ a light source, such as an LED, and a photodetector to detect volumetric changes in blood in microvascular tissue beds at various sites, like the fingertip, earlobe, or wrist. The resulting PPG waveform is characterized by pulsatile fluctuations corresponding to the cardiac cycle, superimposed on a slowly varying baseline that reflects respiratory activity. Although PPG is tipically captured with specialized devices, Fig. 2.13 illustrates that a phone's camera and flash LED can suffice to detect changes in light absorption due to pulsating blood vessels, enabling an smartphone app to monitor PPG.

The choice of light wavelength is crucial, as it affects penetration depth, signal quality, and applicability to different skin types [124]. Wavelengths in the red and near-IR band penetrate the skin the most and are commonly used for measuring oxygen levels. Visible light wavelengths, particularly in the green spectrum, are used to detect blood flow.

After capturing the PPG signal, various features can be extracted, such as blood volume dynamics, rise time, systolic amplitude, diastolic amplitude, and pulse area. These parameters provide information about vascular elasticity, peripheral resistance, and physiological changes. Additionally, pulse-to-pulse interval is often analyzed as a surrogate for HRV, known as Pulse Rate Variability (PRV).

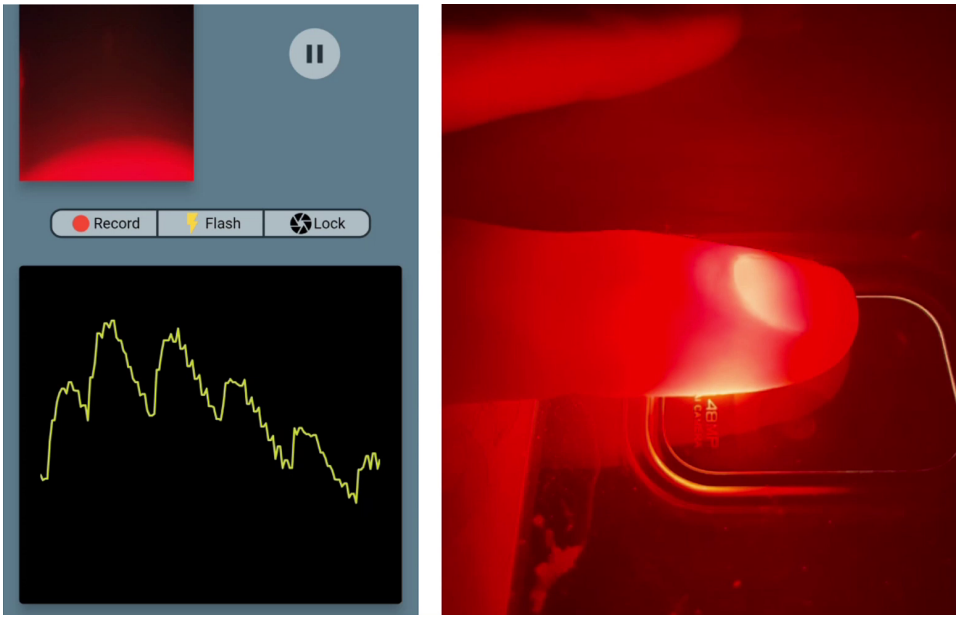

Figure 2.13: Animated GIF demonstrating PPG signal acquisition, using a smartphone application developed by [123]. The top-left panel shows the smartphone's camera view of the fingertip in place. Below, the app's interface translates changes in flash LED light detected from the camera into a reflective PPG waveform. The right panel offers a synchronized video, illustrating the blood flow's effect on light transmission, which is then analyzed by the app to track PPG signals.

2.3.2 PPG Measurement Sites

PPG signal morphology varies depending on the measurement site [7]. The fingertip, often used in pulse oximeters, provides a standard PPG waveform, primarily influenced by blood flow in digital arteries, with a high signal-to-noise ratio. The wrist, popular for wearable devices, may experience more motion artifacts [118]. Earlobe and forehead sites might offer more stable signals with reduced motion impact in certain scenarios, even though the morphology of the PPG signals changes.

The attachment method of wearable PPG sensors influences signal quality [8]. Consistent skin contact and optimal contact pressure are key for accurate measurements, with flexible and adhesive sensors showing promise for improved data quality.

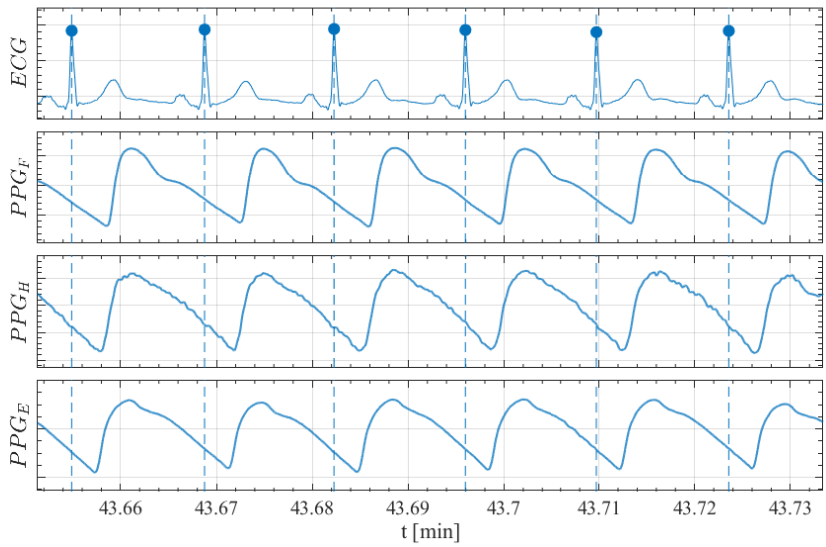

Figure 2.14: Illustration of ECG and PPG signals synchronously recorded. Three PPG signals are at Forehead (PPG_H), at Earlobe (PPG_E) and at Finger (PPG_F), respectively. Both red PPG (R-PPG, in red) and infrared PPG (IR-PPG, in gray) lights, are also illustrated. Refer to [125], [126], for more information on the morphology of PPG in different body locations.

2.3.3 PPG in Clinical Practice

PPG's clinical applications have expanded since its inception in the 1930s. Its use in pulse oximeters from the 1980s revolutionized continuous SpO2 monitoring [127]. Today, pulse oximeters are essential in various medical settings, from neonatal care to critical care, aiding in early detection of clinical deterioration and respiratory diseases. Beyond pulse oximetry, PPG shows potential for broader clinical applications in cardiovascular monitoring.

2.3.4 Objectives of Part IV

Part IV of the thesis is dedicated to the analysis and interpretation of parameters derived from PPG signals, with a focus on their physiological significance for application in wearable devices. This research aims to lay the groundwork for understanding parameters that could be obtained using wearables, like wristbands, in real-world scenarios. I explore novel PPG-derived parameters offering deeper cardiovascular insights than the commonly measured pulse frequency in wearables.

Recognizing the high cost associated with traditional data recording, wearables have value as sources of accessible and easy-to-gather data. Despite the common challenge of signal quality due to motion artifacts in wearable PPG technology, this section will also investigate methodologies for artifact and pulse detection, signal quality assessment, and biomarker extraction in different scenarios.

Study One: Coverage of PPG

PPG signals are well-known to be very susceptible to motion artifacts, which can severely compromise signal quality during active periods in daily life. Chapter 12 explores the concept of 'coverage' in PPG signals—the proportion of time physiological parameters can be reliably estimated by the sensor. Coverage is highly dependent on sensor configuration of the PPG, including transmission/reflection modes, sensor location, and the stability of sensor-body contact.

Coverage rates for raw PPG signals have been reported in prior studies; this research extends this by analyzing the coverage of series dependent on PPG, such as pulse rate, Pulse Arrival Time (PAT), and Pulse Amplitude Variability (PAV), across various body locations and under different stress conditions. The methodologies for estimating these PPG indices are detailed in Sec. 3.5.4.

Study Two: PPG-Derived PWV to Assess Mental Stress

Presented in Chapter 13, this study investigates the vascular response to mental stress by examining Pulse Transit Time Difference (PTTD), an alternative to pulse wave velocity (PWV) that is independent of PEP variability.

The aim is to determine PTTD's potential as a stress biomarker, given its association with cardiovascular data and blood pressure. To accurately estimate PTTD, two PPG sensors are placed at different body locations, requiring thorough signal artifact removal and pulse delineation. Investigating PTTD alterations during acute mental stress will evaluate its potential as a stress biomarker, considering its theoretical correlation with PWV and relevance to cardiovascular information and blood pressure estimation. The study also establishes normal physiological ranges for PTTD and PAT, with

a comprehensive methodology for PPG signal analysis to obtain PTTD outlined in Sec. 3.5.4.

Study Three: Vascular Reactivity and PPG-Derived PWV

Due to the limited amount of good quality signals to firmly characterize PTTD, Chapter 14 broadens the scope to include a complete vascular reactivity analysis. Fifteen subjects underwent a heat stress test—a passive stressor suitable for characterizing PPG-derived PWV biomarkers, with no mental or physical activity required.

Initially focused on PTTD, the study expanded to assess vascular reactivity using various non-invasive techniques, including PAT, PTTD, and Pulse Decomposition Analysis (PDA). This investigation assesses the cardiovascular response to heat stress and the potential of novel PWV surrogates for evaluating cardiovascular changes induced by such stressors, biomarkers that cannot be obtained using only ECG sensors and HRV indices. Methodologies for calculating PAT, PTTD, and PDA are explained in Sec. 3.5.4.

Chapter 3

Contextualized Signal Processing Methodologies

In the previous chapters, the needs and basics of HRV and CPC analysis have been explained, along with the target disorders and applications under study in the present thesis. In this section, I will delve into the main aspects of all the different methodologies and algorithms that I needed to implement to extract the specific features for each of the target disorders I have been studying.

To summarize, from the respiratory signals, we can use the signal itself, but also the BR. From the ECG we can detect the heartbeats to afterwards estimate the HR and HRV. At this moment, the analysis of CPC can be done, by estimating the changes in HRV associated to respiration, for which different methods exist that can be applied. Finally, from the PPG signal, we can obtain similar characteristics as those from the ECG, but also some measurements related to vasculature that cannot be measured using only the ECG.

3.1 Analysis of Respiratory Signals

During this research, I've worked with various respiratory signals to extract features from respiration. These signals encompassed respiratory effort measurements using stretch sensors, placed for the assessment of thoracic and abdominal effort; impedance pneumography, collected alongside ECG data, involving a high-frequency impedance signal (e.g., at 120Hz); oronasal pressure signals obtained to define obstructive events in OSA by measuring airflow with a thermistor; airflow and esophageal pressure signals, invasively recorded during mechanical ventilation; and ECG-derived respiration signals [52], [128].

The distinct nature of each signal needs specific pre-processing methods to derive some possible respiratory features, including the instantaneous BR, the bandwidth as a measure of the smoothness and regularity of respiration, and calculating the tidal volume from the airflow signal. In the subsequent sections, a method to estimate the tidal volume from the airflow signal is elaborated upon. Additionally, a methodology for estimating and tracking the BR in long-term recordings is detailed.

3.1.1 Tidal Volume Estimation

A tidal volume signal, $r(t)$, can be obtained integrating the instantaneous airflow signal followed by baseline subtraction. The baseline is estimated by modified Akima piecewise cubic Hermite interpolation at the delineated onsets of inspiration (see Fig. 3.1 (b)). This interpolation methodology is chosen since it was designed to reduce the overshoots and undershoots in regions with rapidly changing gradients. Similar to pchip interpolation, this results in a smoother curve that still respects the local data structure without introducing excessive wiggles, ensuring that each tidal volume breath begins and ends with zero liters, as depicted in Fig. 3.1 (c).

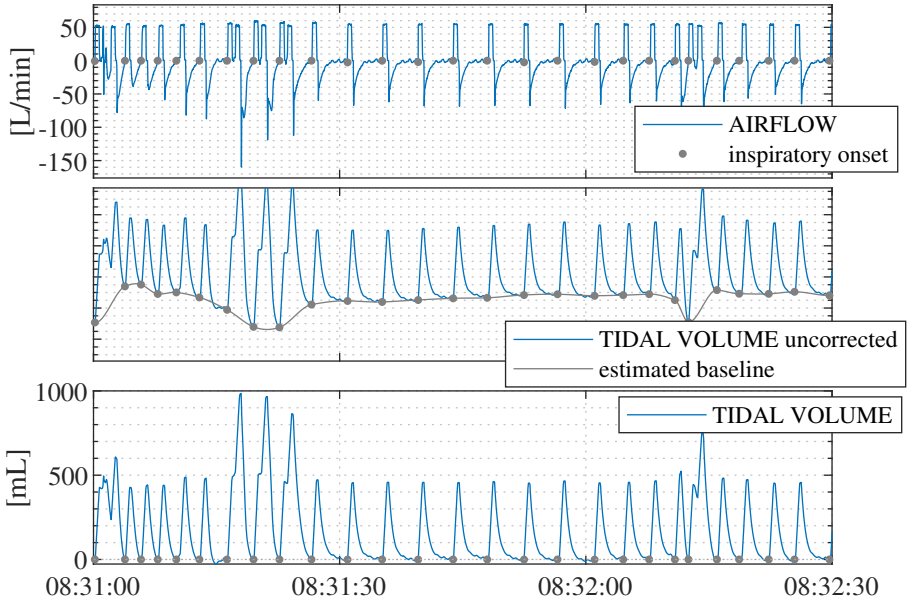

Figure 3.1: Illustration of tidal volume estimation. (a) Airflow signal showing the breathing pattern in VCV mode, with units in L/min. (b) Integrated airflow leading to an uncorrected tidal volume curve; the estimated baseline correction is indicated by a gray line. (c) Final corrected tidal volume signal in mL, with each respiratory cycle starting and ending at zero liters, reflecting the baseline and amplitude adjustments.

3.1.2 Breathing Rate Estimation

BR is calculated from the timing of each breath's initiation, referred to as the inspiration onset, denoted as o_i. The instantaneous breathing rate $\hat{f}_r(t)$

is derived by measuring the time interval between successive inspirations:

$$\hat{f}_r(t) = \int \frac{60}{o_i - o_{i-1}} \delta(t - o_i) dt, \tag{3.1}$$

in units of respiratory cycles per minute ([r.p.m]).

The signals for tidal volume, $r(t)$, and the estimated BR, $\hat{f}_r(t)$, are then uniformly sampled at 4 Hz. This results in two corresponding signals: the tidal volume, $r(n)$, and the discrete BR, $\hat{f}_r(n)$.

However, when the inspiration onset marks are not available, an estimate $\hat{f}_r(t)$ of the BR can be directly obtained using spectral peakedness, a measure of spectral concentration (see Fig. 3.2). The concept of "peakedness" was first introduced by Bailón et al. [129] in the context of robust BR estimation, and it was later exploited by Lázaro et al. [130], Hernando et al. [50], and Kontaxis et al. [52] for PPG-based BR estimation, stress assessment, and ECG-derived respiration, respectively.

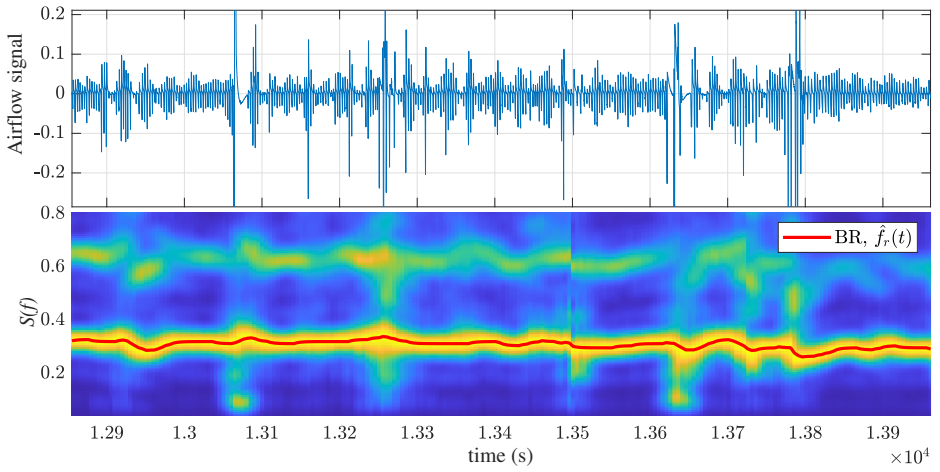

Figure 3.2: BR estimation using the airflow signal, from a patient with OSA. (a) Airflow signal of patient with obstructive episodes. (b) Corresponding Time–frequency spectrum obtained from the airflow signal. The estimated BR, $\hat{f}_r(t)$, is displayed with a red line. Refer to [52] for further information on the method.

Essentially, the peakedness, $\wp$, represents a measurement of how the power of a given frequency band is concentrated around a frequency of

interest, and it can be expressed mathematically as:

$$\wp = \frac{\int_{\Omega_1} \hat{S}_r(f)\, df}{\int_{\Omega_2} \hat{S}_r(f)\, df}, \tag{3.2}$$

where Ω_1 is a frequency band centered in the frequency of interest for BR estimation, Ω_2 is the whole frequency range considered, and $S_r(f)$ is the spectrum to be analyzed. According to Eq. 3.2, $\wp$ will range from 0 to 1, being 0 when there is no power in Ω_1 and 1 when all the power in Ω_1 is also contained in Ω_2. At this point, it is clear that the main challenge in the definition of $\wp$ is the selection of appropriate frequency bands, which should be guided by physiology and application. Further details on the methodology and parameter selection can be found in [52].

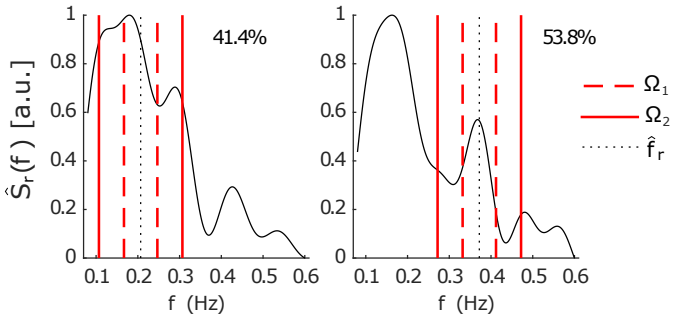

Figure 3.3: Examples of spectral peakedness computed using Eq. 3.2. Spectrum analysis showing a large percentage of $\hat{S}_r(f)$ power concentrated: (left) outside Ω_2, indicating most power outside the band of interest for BR estimation; (right) within $\Omega_2(k)$. Adapted and reproduced from [17].

3.2 Single-lead ECG Delineation

The detection process of heartbeats involves identifying the occurrence, whereas delineation focuses on establishing the precise instant when each ECG wave appears within a heartbeat. Once heartbeats are delineated accurately at the R-waves, one can estimate the HRV signal, representing the non-invasive assessment of ANS. This is commonly achieved by capturing the timing of the R-wave and analyzing the variability in intervals between consecutive R-waves.

In this study, single-lead ECG delineation is done using a wavelet trans-

form based method [131]. This QRS detector decomposes the ECG signal using basis functions derived from wavelets. This method can be seen as the derivative of a low-pass filter, with its cutoff frequency varying according to the wavelet's specific parameters. It is thus very useful to analyze the slopes of the ECG waves in the different scales. Notably, the QRS complex, due to its unique frequency profile, is treated distinctly from P and T waves. The delineation process starts by identifying the QRS complex's center of mass, followed by separate delineation of the Q, R, and S waves.

3.3 HRV Estimation

After delineating the R-wave in each heartbeat, HRV analysis assesses the influence of the ANS on the SA node's activity during sinus rhythm. Analyzing the continuous fluctuations in HR allows to non-invasively measure the ANS's impact on the SA node, and the relative balance between sympathetic and parasympathetic activity. The vagus nerve, a key component of the PNS, shares the role of regulating HRV and respiration.

Converting the RR interval series into indices reflecting this interaction is a translation challenge extensively addressed in engineering, which has been recently reviewed in [132]. The simplest HRV approach involves computing uni-variate statistical measures of the RR interval series, such as average and standard deviation. However, spectral analysis, introduced early in HRV history [14], [133], has recently become the preferred approach in clinical studies, due to its closer interpretation in terms of SNS and PNS. Given the irregular sampling of RR intervals, equidistant resampling is often required to allow proper interpretation of the power spectrum, for which different methods exist with different implications and resulting HRV series estimated. For a complete and detailed explanation of the HRV estimation methodologies, refer to [2] and [132].

3.3.1 Integral Pulse Frequency Modulation model

For frequency domain analysis, a HRV signal has to be estimated first, this representing the functioning of the SA node, modulated by the ANS. The output of the SA node can be modeled as a series of event times, t_k at which

the node fires off an electrical impulse,

$$t_0, t_1, ..., t_M. \tag{3.3}$$

Alternatively, a frequently used heart rhythm representation is the interval tachogram $d_{\mathrm{IT}}(k)$ in which the events, occurring at $t_0, t_1, ..., t_M$, are transformed into a discrete-time signal consisting of the successive intervals, i.e., the RR intervals,

$$d_{\mathrm{IT}}(k) = t_k - t_{k-1}, \quad k = 1, 2, \ldots, M \tag{3.4}$$

(see Fig. 1.11). Hence, the interval tachogram is the heart rhythm representation upon which the simple time domain measures rest, and it has been extensively used in the literature on HRV analysis.

A major drawback when using $d_{\mathrm{IT}}(k)$ is that both these signals are indexed by an interval number rather than by a sample number as is commonly the case with the discrete-time signal, evenly sampled in time [2], [132]. Consequently, power spectral analysis of these two signals cannot be expressed in units of "cycles per second" (Hertz).

To solve this, the Integral Pulse Frequency Modulation Model (IPFM) is by far the most popular model for generating an event series, explained by its simplicity and yet physiological relevance, [132], [134]. The input signal, consisting in $m(t)$ —assumed to carry ANS modulation of SA— superimposed to a DC level, is integrated until the threshold, T —which represents the inverse of mean Heart Rate (mHR)— is reached. Then, a beat occurs and the integration process is reset. The first integrator output, $y(t)$, corresponds to charging of the membrane potential of a SA pacemaker cell.

A major limitation of the IPFM model is that a fixed T implies a constant HR. Since this is unrealistic in long-term applications where the HR changes over time, e.g., during exercise, stress testing, sleep apnea, and general overnight ECG recordings, the Time Varying IPFM model (TVIPFM), needs to be considered [134], meaning that $T \to T(t)$.

Then, the relationship between the modulating signal $m(t)$ and the beat occurrence time series t_k , $\forall k$, is given by,

$$k = \int_0^{t_k} \frac{1 + m(t)}{T(t)} dt = \int_0^{t_k} d_{\mathrm{HR}}(t) dt \tag{3.5}$$

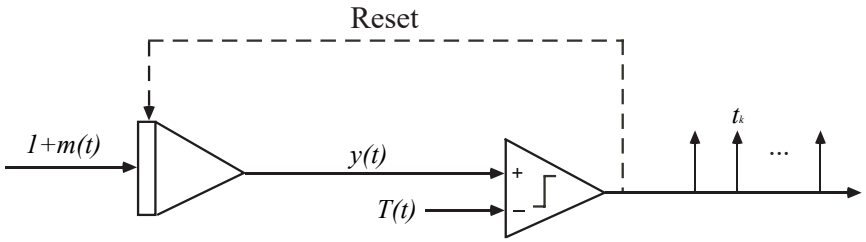

Figure 3.4: The TVIPFM model, with the input function $1 + m(t)$ that modulates the variability of inter-event intervals, resulting in the event series $t_0, t_1, \ldots, t_k$. Adapted and reproduced from [135]. he generation of an event series, i.e., t_k, from a continuous-time modulating signal $m(t)$ when the time-varying threshold $T(t)$ is reached.

where $d_{\mathrm{HR}}(t)$ refers to the instantaneous HR that is composed by rapid variations, $m(t)/T(t)$, superposed to a slow-changing mean HR, $d_{\mathrm{mHR}}(t) = 1/T(t)$. In physiological terms, $m(t)$ determines the variability in HR as modulated by autonomic activity on the sinoatrial node.

Thus, $m(t)$ is derived from,

$$m(t) = \frac{d_{\mathrm{HR}}(t) - d_{\mathrm{mHR}}(t)}{d_{\mathrm{mHR}}(t)} \tag{3.6}$$

where $d_{\mathrm{mHR}}(t)$ can be estimated by low-pass filtering $d_{\mathrm{HR}}(t)$ at 0.04Hz (see Fig. 3.5), assuming that $T(t)$ varies slower than $m(t)$. Note that $m(t)$ is dimensionless [1]. It should be taken into account that the TVIPFM model accounts for the presence of gaps in the beat occurrence time series, created by deleting ectopic and wrong detections [136]. Finally, a discrete-time version of the modulating signal, $m(n)$, is obtained by resampling $m(t)$ at 4 Hz.

Time-domain indices will be computed based on the tachogram, $d_{\mathrm{IT}}(k)$, while frequency-domain indices will be computed from the modulating signal $m(n)$. For example, the HRV signal displayed in Fig. 3.5 (b), is the modulating signal, $m(t)$, which was estimated using the TVIPFM model. The upper plot represents the instantaneous HR, $d_{\mathrm{HR}}(t)$, and the gray line is the mean HR, $d_{\mathrm{mHR}}(t)$ signal, representing the slow rhythmic changes of HR (slower than 0.04Hz), like circadian rhythms.

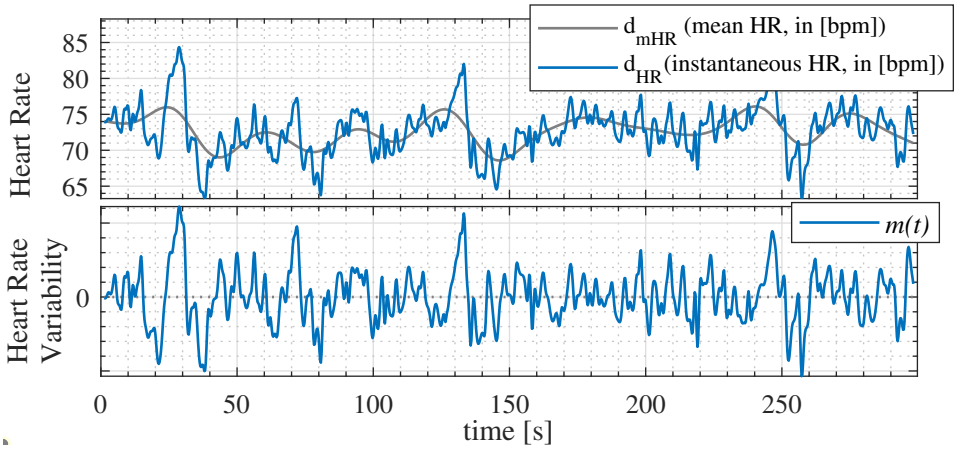

Figure 3.5: Estimation of Heart Rate (HR) and HRV using the IPFM model. The upper panel illustrates the instantaneous HR (in bpm), showing beat-to-beat fluctuations with the mean HR depicted in gray to highlight slower rhythmic changes (slower than 0.04Hz). The lower panel shows the modulating signal, $m(t)$, which can be derived by calculating the difference between the instantaneous HR and the mean HR over time.

3.3.2 Correction of Ectopic Beats

For HRV analysis, it is crucial to ensure the accuracy of RR intervals used. Incorrect detections, or missed beats, which can arise from low-amplitude QRS complexes or signal artifacts, yield invalid RR intervals. Additionally, the RR interval can exhibit abnormal changes due to impulses generated outside the SA node [136]. Such beats, whether of supra-ventricular or ventricular origin, are termed ectopic beats. Since ectopic beats do not represent ANS influence on the SA node's depolarization, the RR intervals associated with ectopic or miss-detected beats aren't suitable for HRV evaluation.

The exclusion of non-normal RR intervals, which do not represent the ANS function, results in the Normal-to-Normal Interval (NN) series [2]. For the HRV analysis of this thesis, the simplified correction based on the heart timing signal has been applied. Ectopic beats are identified and rectified by setting a threshold for maximum allowable deviation linked with sinus rhythm, as detailed in [132], [136].

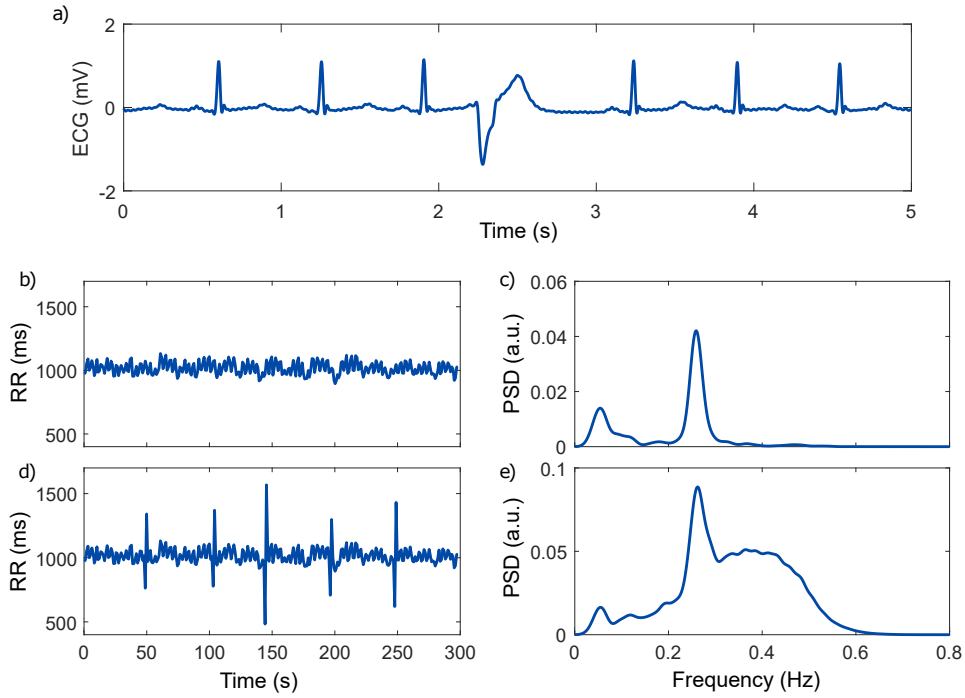

Figure 3.6: The effect of ectopic beats on HRV. (a) Demonstrates a real premature ventricular contraction, a type of ectopic beat, as seen in the ECG signal. Panels (b) and (c) depict an example of an original tachogram and its spectra. However, in panel (d) ectopic beats were artificially introduced into the R-wave to R-wave interval (RR) series shown in (b). The distortion of the Power Spectral Density (PSD) in the HRV spectra (e), caused by the increasing number of ectopic beats is evident, highlighting the impact such beats have on the accuracy of HRV analysis. Adapted and reproduced from [137].

3.3.3 Respiration-Guided HRV Biomarkers

HRV biomarkers can be broadly categorized into time-domain and frequency-domain measures. Time-domain measures include metrics directly derived from NN intervals or their differences. Key time-domain HRV measures are:

- Mean Heart Rate (mHR) for a given period, expressed in beats per minute (bpm).
- Standard Deviation of NN intervals (SDNN). SDNN reflects overall HRV over a 24-hour period, and it is considered a gold standard for cardiac risk stratification [14].
- Root Mean Square of Successive Differences (RMSSD), highlighting short-term, vagally mediated HRV variations.

Frequency-domain indices are derived from the PSD, $S_m(f)$, of the

modulating signal, $m(n)$, estimated using the IPFM model [134], as explained in Sec. 3.3.1. This analysis provides insights into the ANS functioning by analyzing specific frequency bands. From the total power, $\mathrm{P_{TOT}}$, in the HRV's spectrum, the power within different frequency bands, mainly Very-Low Frequency Band (VLF), LF, and HF, reflect different physiological states:

- LF power, $\mathrm{P_{LF}}$, is the power within the LF band, $\Omega_{\mathrm{LF}} = (0.04, 0.15]$ Hz. $\mathrm{P_{LF}} = \mathrm{P}(\Omega_{\mathrm{LF}})$ indicates both parasympathetic and sympathetic influences.
- HF power, $\mathrm{P_{HF}}$, is the power within the HF band, $\Omega_{\mathrm{HF}} = (0.15, 0.4]$ Hz. $\mathrm{P_{HF}} = \mathrm{P}(\Omega_{\mathrm{HF}})$ mainly represents efferent vagal activity, particularly associated with RSA.

The PSD within the classical HF band (0.15–0.4 Hz) predominantly reflects vagal activity influenced by respiratory activity. However, using a fixed HF band becomes problematic in scenarios where respiratory frequencies vary significantly [132]. In Sec. 1.4.2, the reasons to perform a HRV analysis guided by respiration have been extensively explained. Then, the HF band needs to be redefined to be centered at the BR:

$$\Omega^r_{\mathrm{HF}} = [\hat{f}_r - 0.125, \hat{f}_r + 0.125] \text{ Hz}. \tag{3.7}$$

From now on, in this thesis, $\mathrm{P_{HF}}$, will always be referred to, as the power within this band centered on BR, Ω^r_{HF}. For instance, the use of the modified HF band is specifically encouraged by the increased BR observed in some mechanically ventilated patients, and also in children, since I observed during my research that they both usually have BR higher than 24 rpm, i.e., 0.4 Hz. Therefore, the need to center the HF band to the BR is crucial to perform a proper and more powerful interpretation of the results in the frequency domain, in order to avoid an underestimation of the HF power using the classical HF band, as shown in Fig. 3.7.

Of note, Ω^r_{HF} can also be defined time-varying, $\Omega^r_{\mathrm{HF}}(t)$, in the case that there is available an instantaneous estimation of the BR, $\hat{f}_r(t)$:

$$\Omega^r_{\mathrm{HF}}(t) = [\hat{f}_r(t) - 0.125, \hat{f}_r(t) + 0.125] \text{ Hz}. \tag{3.8}$$

Then, the LF/HF power ratio, $P_{\mathrm{LF}}/P_{\mathrm{HF}}$, is often proposed as the non-

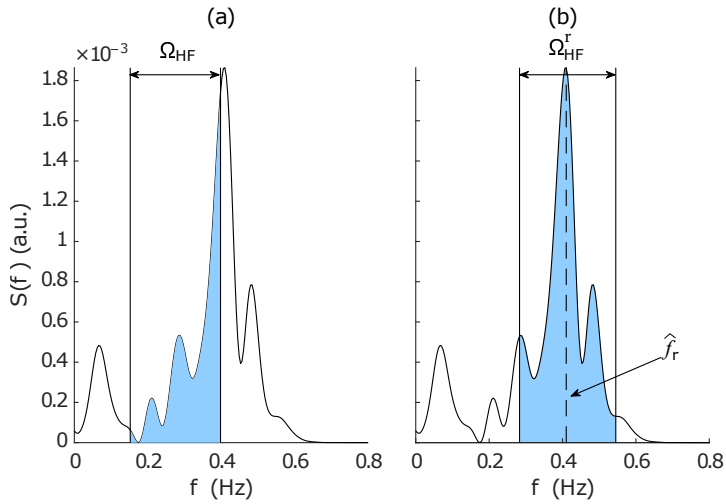

Figure 3.7: Definition of the HF band. For the same spectrum, (a) the classical HF band, Ω_{HF}, and (b) the HF band centered around the mean BR f_{r} with bandwidth of 0.125 Hz, $\Omega^{\mathrm{r}}_{\mathrm{HF}}$. Adapted and reproduced from [17].

invasive biomarker of sympathovagal balance [14]. However, normalized LF power ($P^n_{\mathrm{LF}} = P_{\mathrm{LF}}/(P_{\mathrm{LF}} + P_{\mathrm{HF}})$) is preferred to mitigate total power impact on LF components [132] (see Fig. 3.8).

In addition, VLF power, $\mathrm{P}_{\mathrm{VLF}}$, is the power within the VLF band, $\Omega_{\mathrm{VLF}} = (0, 0.04]$ Hz. $\mathrm{P}_{\mathrm{VLF}}$ =$\mathrm{P}(\Omega_{\mathrm{VLF}})$ reflects long-term regulatory mechanisms like thermoregulation and circadian rhythm [15]. Note that using $d_{\mathrm{mHR}}(t)$ signal is necessary to correctly estimate $\mathrm{P}_{\mathrm{VLF}}$, whereas $m(t)$ was used to estimate P_{LF} and P_{HF}.

Finally, note that appropriate HRV analysis necessitates a minimum sampling rate of 500Hz for the ECG signal [14]. In instances where the ECG signal is sampled at a rate lower than 1000Hz, it is advisable to upsample the signal to 1000 Hz using cubic spline interpolation. Subsequently, the detection of QRS-complexes can be carried out employing the wavelet-based method detailed in Sec. 3.2.

Traditional spectral analysis typically operates under the assumption of stationary recordings, estimating PSD of HRV using 5-minute length segments. Techniques such as Welch's periodogram, and autoregressive models are employed for estimation of $m(n)$ [2], [132]. Using Welch periodogram, the PSD of $m(n)$, $\hat{S}_{\mathrm{m}}(f)$, is typically estimated using a Hamming window of 50 seconds, and 50% overlap [14].

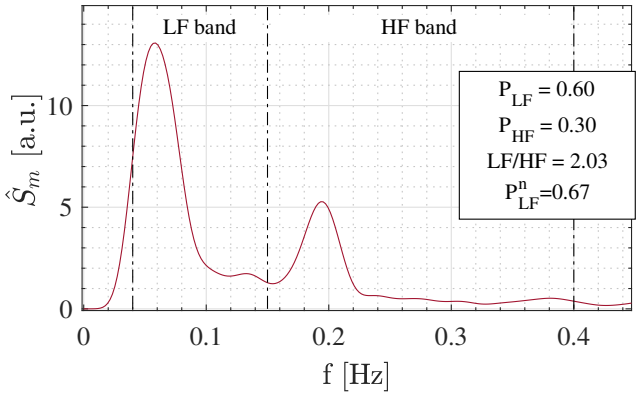

Figure 3.8: Frequency-domain analysis of HRV in the 5-min segment plotted in Fig. 3.5. For example, the peak at 0.25 Hz can be attributed to respiration as controlled by parasympathetic activity.

3.3.4 Time-Frequency Evolution of HRV

However, this dependence on stationarity to obtain a PSD estimation of HRV limits its applicability in various scenarios, including exercise stress testing, tilt-table assessments, overnight HRV monitoring in OSA, and ICU settings. Alternatively, TF techniques can be utilized to account for the non-stationarity nature of the data and to monitor the evolution of HRV in long-term recordings. With the increasing adoption of non-stationary analysis in cardiovascular studies, previous research has already explored the different TF techniques and their effectiveness for HRV monitoring [117].

Cohen's Class Wigner Ville Distribution

Specifically, the TF spectrum of HRV, $\hat{S}_{\mathrm{m}}(t,f)$, can be estimated using a TF distribution from Cohen's class [117]:

$$\hat{S}_{\mathrm{m}}(t,f) = \iint_{-\infty}^{\infty} A_{\mathrm{m}}(\nu,\tau)\Phi(v,\tau)e^{j2\pi(t\nu-f\tau)}d\nu d\tau \tag{3.9}$$

where $A_{\mathrm{m}}(\nu,\tau)$, represents the ambiguity function [117]. It is derived from the analytical signal representation of the modulating signal, $m(t)$. These analytical representations are typically obtained using the Hilbert transform. Moreover, $\Phi(\nu,\tau)$ acts as a smoothing function within the ambiguity domain, which aids in reducing quadratic terms, and it is a simplified version

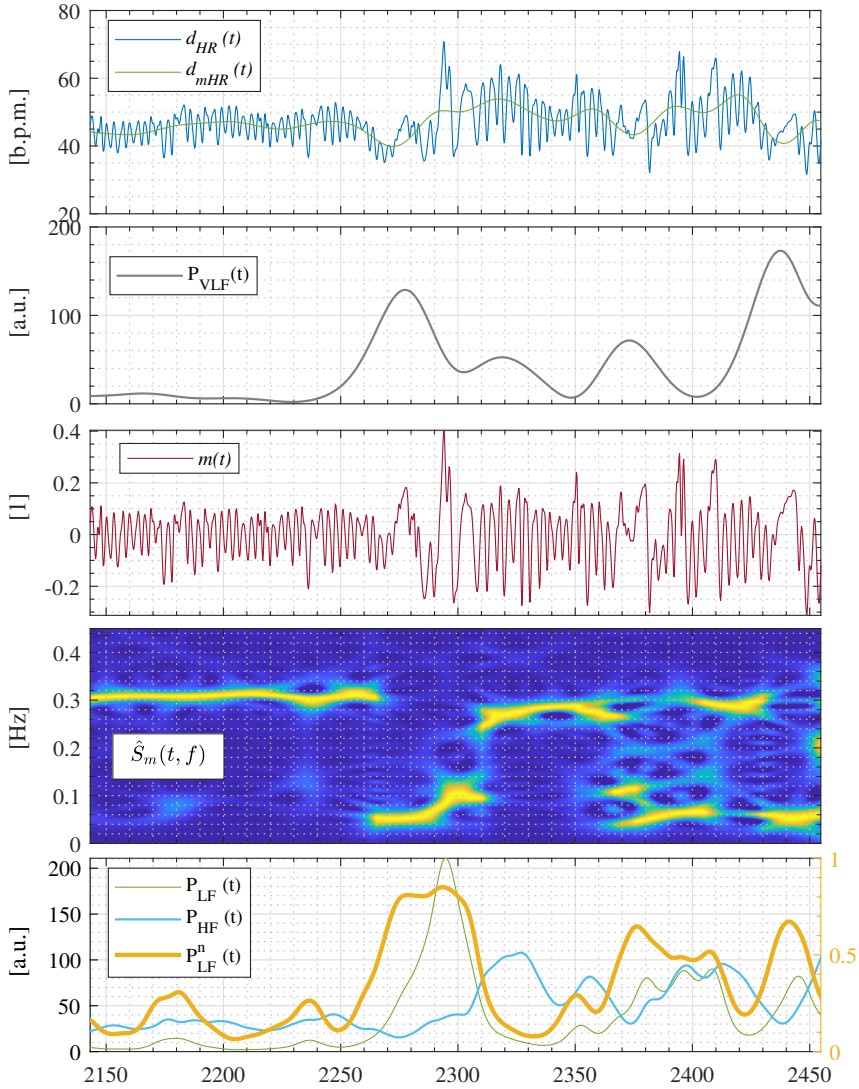

Figure 3.9: Illustration of TF Analysis for a HRV Signal. Using the TVIPFM model, three key components are derived: instantaneous heart rate ($d_{\mathrm{HR}}(t)$), mean heart rate ($d_{\mathrm{mHR}}(t)$), and the modulating signal ($m(t)$). The TF map of $d_{\mathrm{mHR}}(t)$ allows for the estimation of VLF power, $\mathrm{P}_{\mathrm{VLF}}(t)$. Similarly, the TF map of $m(t)$, $\hat{S}_m(t,f)$, facilitates the computation of LF, $\mathrm{P}_{\mathrm{LF}}(t)$, and HF power, $\mathrm{P}_{\mathrm{HF}}(t)$. On the right, with yellow color, the normalized LF power ($\mathrm{P}^n_{\mathrm{LF}}(t)$) represents the sympatho-vagal balance, illustrating the continuous power dynamics derived from the HRV signal.

of the multiform-tiltable exponential kernel [117]. In this dissertation, an elliptic exponential kernel was chosen for this purpose [117]. Their respective mathematical formulations are:

$$A_{\mathrm{m}}(\nu,\tau)=\int_{-\infty}^{\infty} x_{\mathrm{m}}\left(t+\frac{\tau}{2}\right)x_{\mathrm{m}}^{*}\left(t-\frac{\tau}{2}\right)e^{-j2\pi\nu t}dt, \tag{3.10}$$

$$\Phi(\nu,\tau)=e^{-\pi\left[\left(\frac{\nu}{\nu_0}\right)^2+\left(\frac{\tau}{\tau_0}\right)^2\right]\lambda}. \tag{3.11}$$

This approach offers an excellent temporal resolution, making it particularly effective for tracking transient variations in HRV. The resolution of $\hat{S}_{\mathrm{m}}(t,f)$ in both time and frequency can be fine-tuned by adjusting the shape of the smoothing kernel from Eq. 3.11 via the parameters ν_0 and τ_0, respectively. Furthermore, the roll-off factor of this kernel is modifiable through λ. The parameters of $\Phi(\nu,\tau)$ are set to $\nu_0=0.045$, $\tau_0=0.05$, and $\lambda=0.3$, leading to a time and frequency resolution of 11.25 s and 0.039 Hz, respectively. These values effectively suppress interference terms, as supported by [117]. Fig. 3.9 shows the evolution of the LF and HF power of HRV, using this TF technique.

3.4 Cardiopulmonary Coupling Estimation

As mentioned earlier, there is an intrinsic connection between HRV and respiration, with RSA playing a significant role in the rapid fluctuations of HR. Consequently, any interpretation of HRV analysis should always consider its interplay with respiratory activity. However, incorporating respiratory information into HRV analysis, as presented in Sec. 3.3.3, is not the sole approach for addressing the impact of respiration on HRV.

Until very recently, there has been a lack of consensus on the optimal method for measuring CPC, with a range of techniques suggested in existing literature. Techniques range from Granger causality and entropy measurements, to phase synchronization analysis and nonlinear prediction methods. Morales et al. [138] conducted an extensive evaluation of these varied methodologies using both real and simulated HRV and respiration signals. The findings underscored the superior performance of TFC for CPC estimation, detailed in Sec. 3.4.1. However, the methods described in Sec-

tions 3.4.2, and 3.4.3 also exhibited a very accurate estimation of CPC under different conditions.

3.4.1 Time-Frequency Coherence

The TFC distribution can be expressed based on the spectral coherence:

$$\hat{\gamma}(t,f) = \frac{\left|\hat{S}_{r,m}(t,f)\right|}{\sqrt{\hat{S}_r(t,f)\hat{S}_m(t,f)}}, \tag{3.12}$$

where $\hat{S}_{\mathrm{m}}(t,f)$ and $\hat{S}_{\mathrm{r}}(t,f)$ denote the TF spectra for the modulating and respiratory signals, respectively, as described in Eq. 3.9. The TF cross-spectrum, $\hat{S}_{\mathrm{m,r}}(t,f)$, can be estimated by substituting $\hat{S}_{\mathrm{m}}(t,f) \rightarrow \hat{S}_{\mathrm{m,r}}(t,f)$ in Eq. 3.9, considering:

$$A_{\mathrm{m,r}}(\nu,\tau) = \int_{-\infty}^{\infty} x_{\mathrm{m}}\left(t+\frac{\tau}{2}\right) x_{\mathrm{r}}^{*}\left(t-\frac{\tau}{2}\right) e^{-j2\pi\nu t} dt. \tag{3.13}$$

From the resulting $\hat{\gamma}(t,f)$ distribution, various metrics can be derived, which likely reflect the extent of CPC. For this purpose, a significant coherence level between HRV and respiration must be first established by a threshold, denoted as $\gamma_{\mathrm{TH}}(t,f;\alpha)$. This significant coherence threshold is determined through surrogate data analysis, with $\alpha = 1\%$ risk that two signals are coupled when real coupling does not exist $\gamma_{\mathrm{TH}}(t,f;0.01) = \gamma_0$.

To derive γ_0, spectral coherence $\hat{\gamma}(t,f)$ is computed for two 5-minute white Gaussian noise signals, which are expected to be uncorrelated by definition. This process is repeated iteratively 1000 times, and the 99^{th} percentile of $\hat{\gamma}(t,f)$ is established as the threshold for significant spectral coherence, i.e., $\gamma_0 = 0.8860$.

Note that this threshold for significant spectral coherence, γ_0, is very dependent on the parameters ν_0, τ_0, and λ, used for calculating the smoothing function $\Phi(\nu,\tau)$. An illustrative example of the TF spectral coherence, along with the zones above the significant spectral coherence, γ_0, is provided in Fig. 3.10.

The region $\Omega_{\mathrm{HF}}^{r,c}(t,f)$, from which the coherence is estimated, is identified within the HF band centered at the BR, $\Omega_{\mathrm{HF}}^{r}(t)$, with the purpose of

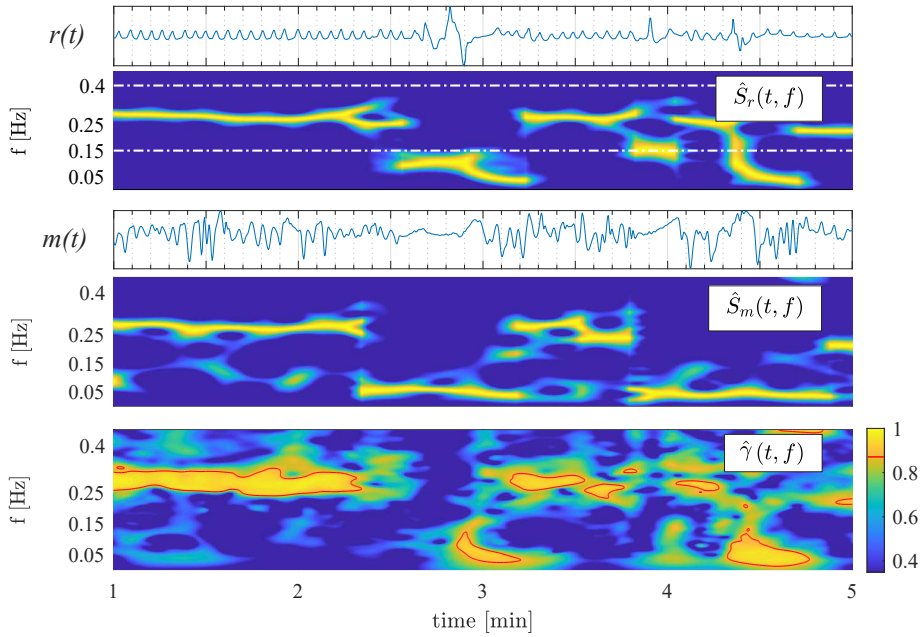

Figure 3.10: TFC for CPC estimation. From respiratory signal, $r(t)$, and HRV signal, $m(t)$, TF spectra $S_r(t,f)$ and $S_m(t,f)$ are calculated, respectively. Spectral coherence $\gamma(t,f)$ is used to obtain the coherence between respiration and HRV. Significant spectral coherence, $\hat{\gamma}(t,f) > \gamma_0$, is outlined in red.

determining the area in the HF band where the TFC is significant:

$$\Omega^{r,c}_{\mathrm{HF}}(t,f) = \left\{(t,f) \in (\mathbb{R}^+ \times \Omega^{r}_{\mathrm{HF}}(t)) \mid \hat{\gamma}(t,f) > \gamma_0\right\}. \tag{3.14}$$

To characterize the temporal evolution of the local coupling between the spectral components of the signals, the index $\mathcal{C}_{\mathrm{HF}}(t)$ is introduced, which is defined as:

$$\mathcal{C}_{\mathrm{HF}}(t) = \int_{\Omega^{r,c}_{\mathrm{HF}}} \hat{\gamma}(t,f)df \Big/ \int_{\Omega^{r,c}_{\mathrm{HF}}} 1 \; df. \tag{3.15}$$

This index captures the magnitude of local coupling, averaged over the HF band. Averaging the significant coherence, $\mathcal{C}_{\mathrm{HF}}(t)$, over a specific time period results in:

$$\mathscr{C}_{\mathrm{HF}} = \int \mathcal{C}_{\mathrm{HF}}(t)dt \Big/ \int 1 \; dt. \tag{3.16}$$

Finally, for all the time course, the existence of significant coupling at

any frequency in the whole band $\Omega^r_{\text{HF}}(t)$ is identified as:

$$\mathcal{T}_{\text{HF}}(t) = \begin{cases} 1, & \text{if } \Omega^{r,c}_{\text{HF}}(t,f) \neq \emptyset \\ 0, & \text{if } \Omega^{r,c}_{\text{HF}}(t,f) = \emptyset \end{cases} \tag{3.17}$$

Once the "mask" $\mathcal{T}_{\text{HF}}(t)$ is defined, the percentage where TFC is significant in a period of time, $\mathscr{T}_{\text{HF}}$, can be defined as:

$$\mathscr{T}_{\text{HF}} = \int \mathcal{T}_{\text{HF}}(t)dt \Big/ \int 1 \; dt. \tag{3.18}$$

Within this framework, the index I'm proposing for the assessment of CPC is derived using Eqs. 3.16 and 3.18. This index, denoted as $\mathscr{C}^{\mathcal{T}}_{\text{HF}}$, incorporates the mean significant coherence averaged over time, $\mathscr{C}_{\text{HF}}$, and the percentage of time where TFC is significant in that period, $\mathscr{T}_{\text{HF}}$:

$$\mathscr{C}^{\mathcal{T}}_{\text{HF}} = \mathscr{C}_{\text{HF}} \cdot \mathscr{T}_{\text{HF}}. \tag{3.19}$$

3.4.2 Dynamic Mutual Information

It is known that the RSA defines a causal relationship from respiration to HRV, since respiration drives acceleration/deceleration in the HR. This relationship implies that the uncertainty about HRV, can be resolved not only by knowing itself, but also by taking into account the information transferred from respiration. This resolution of entropy, or uncertainty, can be quantified using measures of predictive information [139].

Let's denote r_n and m_n as the scalar random values obtained by sampling the process $r(n)$ and $m(n)$, respectively, at the present time, n. The vectors $\mathbf{r}^- = [r(n-1), ..., r(n-M)]^T$, and $\mathbf{m}^- = [m(n-1), ..., m(n-M)]^T$, are defined to describe the whole past of each process, with M the model order. If the information carried by the HRV is split into components related to respiration and others, the predictive information leads to the definition of the Cross Entropy term, $\mathscr{CE}_{\text{r}\leftrightarrow\text{m}}$. This term quantifies the amount of information shared at a certain time, n, between the present value of HRV, m_n, and the past of respiration, $\mathbf{r}^-$:

$$\mathscr{CE}_{\text{r}\leftrightarrow\text{m}} = I\left(m_n; \mathbf{r}^-\right) = H\left(m_n\right) - H\left(m_n|\mathbf{r}^-\right), \tag{3.20}$$

where $I(\cdot;\cdot)$ quantifies the *mutual information*, $H(m_n)$ expresses the amount of information carried by the process in terms of the average uncertainty about m_n, the so-called *Shannon entropy*. $H(m_n|\mathbf{r}^-)$ denotes the *conditional entropy* and it quantifies the average uncertainty that remains about m_n when $\mathbf{r}^-$ is known [139].

The computation of $\mathscr{CE}_{\mathrm{r}\leftrightarrow\mathrm{m}}$ is done using the approach presented in [139], using the link between information theory and predictability. It is possible to describe the dynamics of the system using a linear vector autoregressive model. The model order, M, is defined as the minimum amount of delays obtained using both the Minimum Description Length principle and the Akaike Information Criterion. The maximum possible delay is set to 10 seconds in order to avoid over-fitting. The minimum possible delay is set to the period equivalent to the lowest frequency of the respiration bandwidth in order to avoid a too-simple model [138].

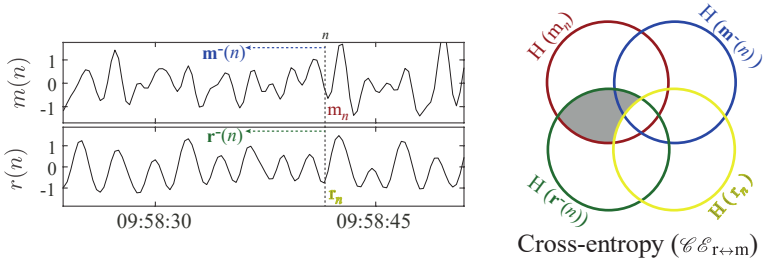

Figure 3.11: Cross Entropy decomposition using Information Dynamics. The two left-side plots are the time evolution of the modulating signal, $m(n)$ and the respiratory signal, $r(n)$. The right-side is an illustration of the entropy decomposition using information dynamics. The shaded area corresponds to the information retrieved by $\mathscr{CE}_{\mathrm{r}\leftrightarrow\mathrm{m}}$. The $\mathscr{CE}_{\mathrm{r}\leftrightarrow\mathrm{m}}$ term quantifies the amount of information shared, in a certain sample n, between HRV, m_n in red, and the past of respiration, $r^-(n)$ in green. For further information, see [139].

3.4.3 HRV Decomposition

By using subspace projections, the HRV can be decomposed into two different components [51]. First, the component describing all variations of HRV linearly related to respiration is derived. After that, the remainder, namely residual component, describes all dynamics modulated by other mechanisms different from respiration, such as the sympathetic modulations or other vagal

modulators unrelated to respiration, plus the possible non-linear influences of respiration.

Given are the respiratory signal, $r(n)$, and the HRV estimated from the modulating signal, $m(n)$. The vectors $\mathbf{r} = [r(0), r(1), ..., r(N-M+1)]^T$ and $\mathbf{m} = [m(0), m(1), ..., m(N-M+1)]^T$ are defined to construct a respiratory subspace, with N the number of samples in a computational period and M the number of delays. The model order, M, is the same used for the $\mathscr{CE}_{\mathrm{r}\leftrightarrow\mathrm{m}}$ computation (see previous section). The OSP projects $\mathbf{m}$ onto the subspace $\mathbb{V}$, which is the subspace defined by all variations in $\mathbf{r}$. The matrix $\mathbf{V}$ spans the subspace $\mathbb{V}$, and it is constructed as a time-delay embedding of $\mathbf{r}$, using M delays. Once the matrix $\mathbf{V}$ is constructed, the HRV can be projected onto the respiratory subspace $\mathbb{V}$, by means of the projection matrix $\mathbf{P}$:

$$\mathbf{m}_{\mathrm{r}} \;=\; \mathbf{P}\;\mathbf{m}, \tag{3.21}$$

with the projection matrix, $\mathbf{P}$, obtained from the respiratory subspace as:

$$\mathbf{P} = \mathbf{V}\left(\mathbf{V}^T\mathbf{V}\right)^{-1}\mathbf{V}^T. \tag{3.22}$$

As a result, all dynamics of HRV linearly related to respiration are described in $\mathbf{m}_{\mathrm{r}}$. The orthogonal component, $\mathbf{m}_{\perp}$, computed as the residual, $\mathbf{m}_{\perp} = \mathbf{m} - \mathbf{m}_{\mathrm{r}}$, is explained by all other HR modulators not linearly related to respiration. An example of the HRV decomposition can be seen in Fig. 3.12. After decomposing the HRV, the relative power of the respiratory component, $\mathscr{P}_{\mathrm{m_r}}$, is computed as an estimate of the CPC [51]:

$$\mathscr{P}_{\mathrm{m_r}} \;=\; \frac{\mathbf{m}_{\mathrm{r}}^T\;\mathbf{m}_{\mathrm{r}}}{\mathbf{m}^T\;\mathbf{m}}. \tag{3.23}$$

3.5 Analysis of Pulsatile Signals

Now, the focus shifts to the analysis of pulsatile signals. The objective is to apply signal processing algorithms to extract vital cardiovascular features from both PPG and BP signals.

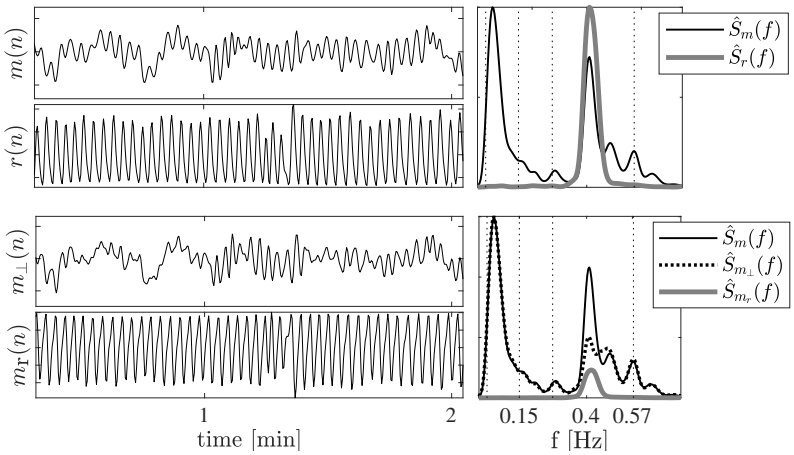

Figure 3.12: Illustrative example of the OSP decomposition using the HRV and Respiratory signals. The three upper plots are the time evolution of the modulating signal, $m(n)$, the respiratory signal, $r(n)$, and their respective spectra on the upper-right side, $\hat{S}_m(f)$ for $m(n)$ and $\hat{S}_r(f)$ for $r(n)$. The three plots below represent the OSP decomposition. The respiratory component of HRV, $m_r(n)$, is obtained projecting $m(n)$ onto the respiratory subspace. The modulators of HRV unrelated to respiration are represented in the term $m_\perp(n)$. Their corresponding spectra are on the lower-right side. $\hat{S}_{m_\perp}(f)$ corresponds to the spectra of $m_\perp(n)$, and $\hat{S}_{m_r}(f)$ to the spectra of $m_r(n)$. For further information, see [51].

3.5.1 Signal Preprocessing

First, pulsatile signals should be band-pass filtered between 0.3 and 15 Hz with a 4-th order Chebyshev type II filter, in order to eliminate the baseline contamination and high frequency noise. The selection of this filtering was studied and analyzed in [140]. Forward-backward zero-phase filtering is applied for preserving signal morphology. Then, after filtering, removing artifacts, and conditioning the signals, pulse detection and delineation can be done.

3.5.2 Data Cleansing and Artifact Detection

Due to the physical principle used to obtain pulsatile signals, based on plethysmography, these are susceptible to various artifacts that can distort their morphology. Among these, motion artifacts are the most common and are typically caused by the relative movement of individuals and sensors during signal recording. Other sources of artifacts may include external light

interference in the case of PPG, and bad sensor placement. It is crucial to ensure that the recordings are free from these artifacts for a reliable analysis and interpretation.

Energy-Based Artifact Detection

Then, before delineating, e.g., a PPG signal, $x_{\text{PPG}}(n)$, it is crucial to address motion artifacts. Various artifact detection methods are available in the literature, but I have developed an energy-based approach to accurately eliminate significant artifacts characterized by higher energy levels compared to clean segments of pulsatile signal [141].

The energy-based artifact detection process comprises the following steps —notation is for PPG signals:

1. Initially, a PPG signal, $x_{\text{PPG}}(n)$, is squared to accentuate high-energy artifacts, $x^2_{\text{PPG}}(n)$.
2. A moving variance signal, $\sigma^2(x^2_{\text{PPG}}(n))$, is calculated using a 5-second window.
3. The moving median signal, denoted as $med(n)$, of $x^2_{\text{PPG}}(n)$ is determined with a 5-minute window.
4. A decision criterion is established, where a PPG sample at index "n" is classified as an artifact if $\sigma^2(x^2_{\text{PPG}}(n))$ exceeds or is equal to 20 times $med(n)$. In such cases, this deviation from the PPG median is denoted as an artifact.

The selection of the two window lengths and the scalar for the decision criteria are set empirically. Once the segments containing artifacts are detected, they are removed from the original data for further analysis (see Fig. 3.13).

3.5.3 Pulse Delineation

The delineation of pulsatile signals requires essentially, three main steps:

1. **Signal accommodation for pulse detection**: The initial phase involves a linear filtering transformation of the signal, to facilitate posterior pulse detection.
2. **Pulse Detection**: The next step involves detecting pulses, each of which corresponds to a heartbeat within the signal. For this, differ-

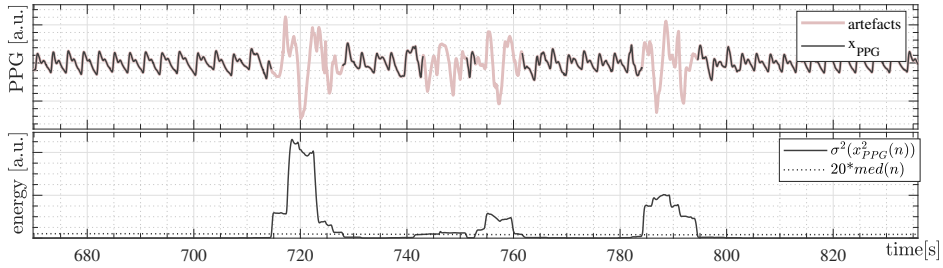

Figure 3.13: Energy-based artifact detection in a PPG signal. Detected segments containing artifacts are in red at the top. The estimated energy, $\sigma^2(x^2_{\text{PPG}}(n))$, and the decision criterion, $20 * med(n)$, are plotted at the bottom.

ent dynamic, time-varying thresholds can be calculated. Here, I'm presenting two different methods.

3. **Pulse Delineation**: a process to define various Fiducial Point (FP)s, each representing distinct physiological instants.

Subsequent subsections provide in-depth explanations for each of these steps.

Signal Accommodation for Pulse Detection

The initial step involves a linear filtering transformation, using a Low Pass Derivative (LPD). The LPD filter is constructed using a least squares linear-phase FIR technique. It encompasses a transition band ranging from 7.7 Hz to 8 Hz, chosen to account for the fact that the upslopes of PPG and BP pulses predominantly occur within these frequency ranges [142]. Fig. 3.14 illustrates the impulse response and transfer function of this filter.

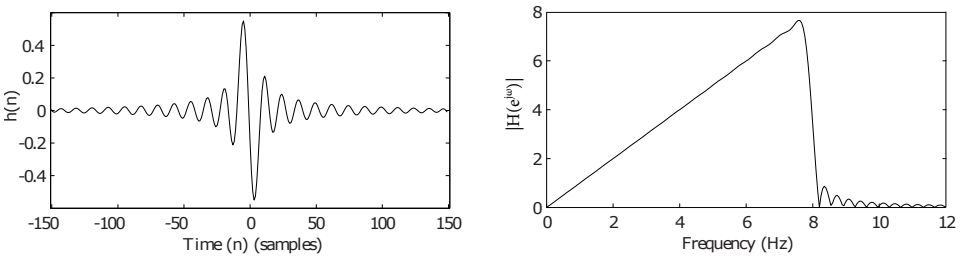

Figure 3.14: Implemented LPD filter. (a) impulse response of the LPD filter designed, and (b) transfer function.

This transformation is specifically designed to emphasize the abrupt upslopes observed in PPG and BP pulses, as opposed to the relatively smoother ones found in the dicrotic notch. Fig. 3.15 is an example of PPG signal fil-

tering using the LPD. As already mentioned, this filtering transformation clearly facilitates pulse detection.

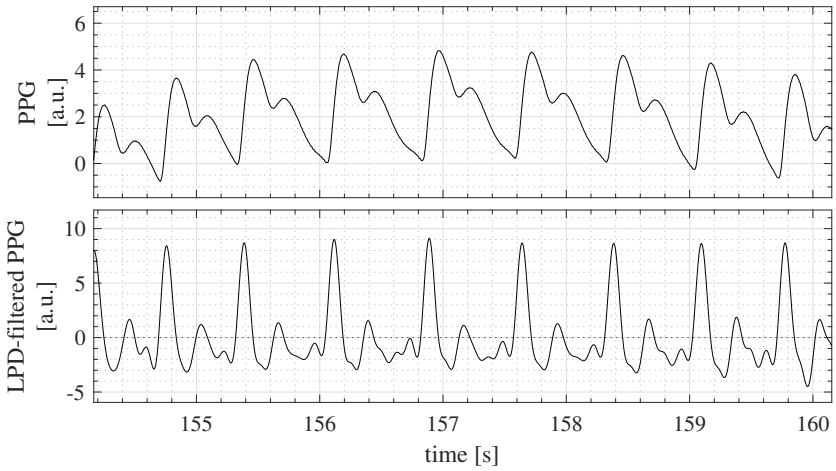

Figure 3.15: LPD filter applied over an illustrative PPG signal. (a) original PPG signal. (b) LPD-filtered PPG signal.

Pulse Detection using Adaptive Thresholding

The first approach for detecting peaks, n_{D_i}, in the filtered signal, is based on a time-varying threshold $\gamma(n)$ that gradually decreases between detected peaks (see Fig. 3.16). This threshold maintains the value of the previously detected peak [142], denoted as $\gamma(n) = y(n_{D_{i-1}})$, during a refractory period equivalent to 300 ms (i.e., $N_r = 0.3f_s$). Following this refractory period, the threshold starts to decrease linearly. In the event that no new detection occurs after a specified time period $\hat{m}_{A_i}$, the threshold would have diminished to a fraction $\alpha < 1$ of $y(n_{D_{i-1}})$. From this moment onward, the threshold retains its value. For further information on the method, refer to [142].

This detection methodology was initially designed to identify peaks within the PPG signal in the context of sleep apnea [142]. Significantly, during episodes of obstructive sleep apnea, the amplitude of PPG signals decreases, warranting the implementation of a linear threshold decrease and a refractory period [142]. Comparative assessments of this methodology have demonstrated the highest accuracy in pulse detection during sinus rhythm [143], but also a high performance in different use cases [144].

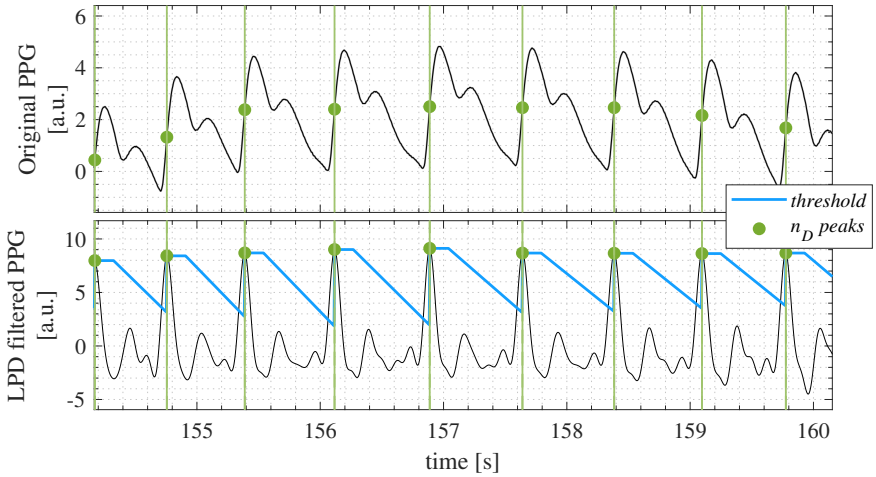

Figure 3.16: Example of adaptive threshold detector: (a) shows the raw PPG signal, and (b) shows the LPD-filtered PPG signal, and the resulting time varying threshold (slashed blue line).

Pulse Detection using Envelope Thresholding

The second approach for detecting peaks in pulsatile signals is based on envelope thresholding, previously designed and implemented for QRS detection in the ECG [36], [145]. This envelope-based procedure was employed to enhance the QRS complexes while flattening the rest of the ECG. This approach is used in combination with an adapted version of the Pan–Tompkins algorithm, and combines the simplicity of an envelope-based procedure with the accuracy of more elaborate methods.

Regarding pulsatile signals, the upper (U) and lower (L) envelopes have to be firstly computed from the LPD-filtered pulsatile signal using the secant method. This method selects the segment with the steepest positive and negative slopes within a defined window length. Once U and L are obtained, a flattened, positive version of the signal (F) is derived as $F = U - L$. Subtracting L from U eliminates the baseline, leaving only a positive signal, F.

The pulse locations are identified by detecting the peaks in the flattened version, F. This complete peak detection procedure is detailed in [145], which fundamentally find peaks in the flattened version, F, a modified version of the Pan–Tompkins algorithm is employed to determine the peaks correlating with the maximum upslope instants of the pulses. A graphical depiction of

the process can be seen in Fig. 3.17.

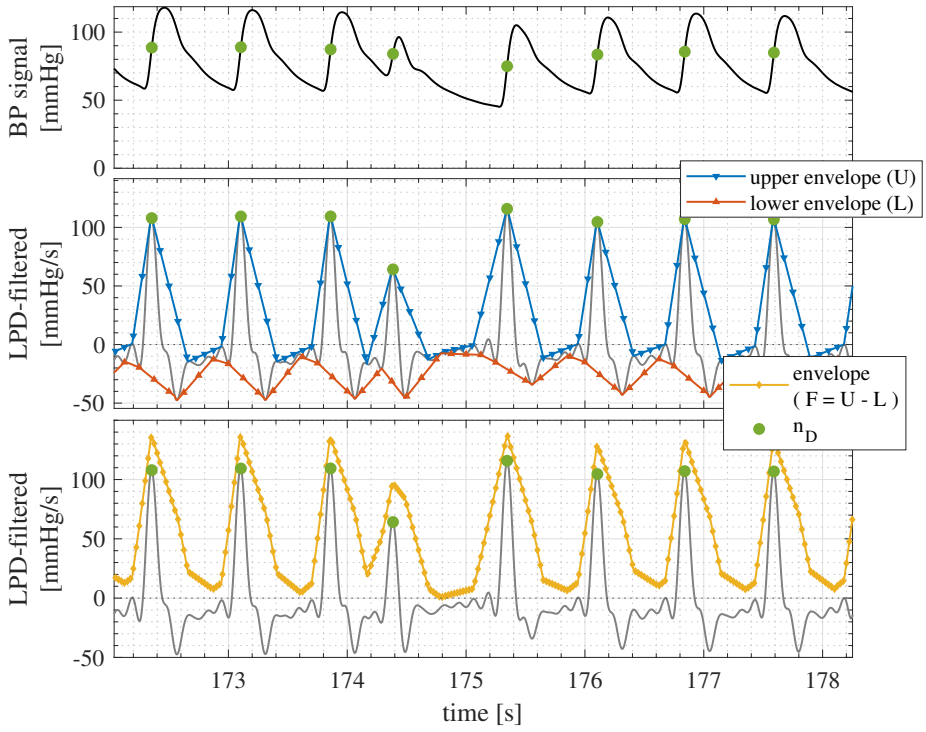

Figure 3.17: Envelope threshold detection. (a) shows an illustrative BP signal; (b) and (c) shows its LPD filtered version (solid gray line), $x'_{\mathrm{BP}}(n)$. The upper and lower envelope o the signal are displayed in (b), in blue and red dotted lines, respectively. The flattened-positive envelope, $x_{\mathrm{F}}(n)$, of $x'_{\mathrm{BP}}(n)$ is represented with the yellow dotted line, obtained by subtracting the upper and the lower envelope. From $x_{\mathrm{F}}(n)$, the location of the pulses, n_{D_i}, can be identified.

An exploratory analysis was conducted for the detection of pulses in the invasive BP signal. This envelope-based algorithm seemed better at handling and detecting also ectopic beats, and BP pulses with lower systolic upslope. Nevertheless, a future, thorough comparative study is required to evaluate the two methodologies for PPG peaks detection I've introduced. The comparison should consider their performance on both PPG and BP signals, under conditions like normal subjects, patients with cardiac conditions causing ectopic beats, and in noisy environments.

Pulse Delineation and Fiducial Points

Following pulse detection, where apex of the first derivative PPG signal are identified (n_D), many other FPs can be computed and compared (see Fig. 3.18), including apex (n_A), middle-amplitude (n_M), and basal (n_B) instant of a PPG pulse, and intersection point (n_T) of the tangent to the PPG waveform between n_D and n_B [146].

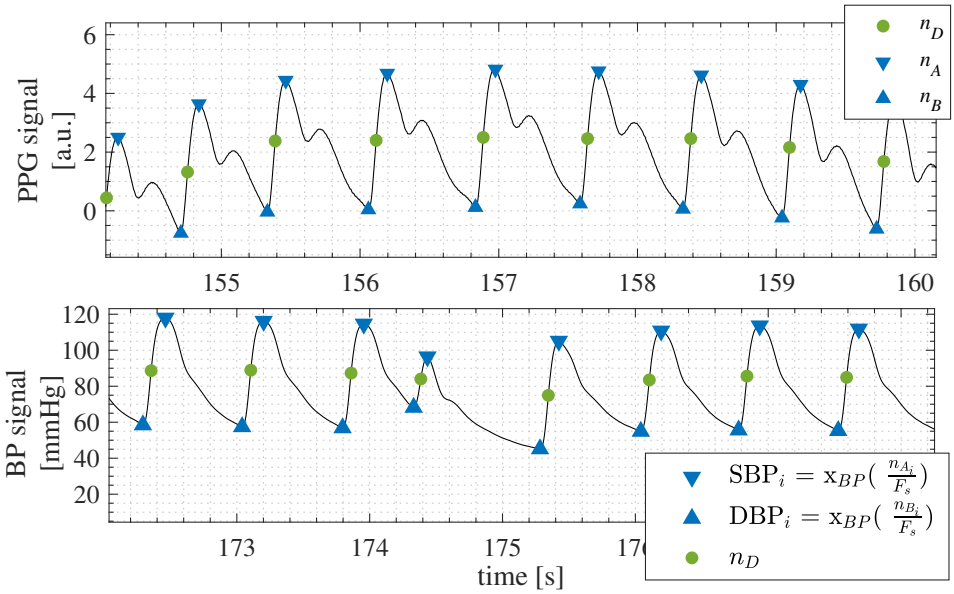

Figure 3.18: Illustrative example of pulse delineation in (a) a signal of PPG at fingertip, and (b) a signal of BP. Some FPs delineated on the PPG signals, shown in the figure, are: n_{D} for the maximum up-slope instant, n_{A} for the apex point and n_{B} for the basal point.

For example, in the case of PPG signals, n_D represents the instant of maximum velocity of blood flow through the arteries and arterioles; n_B represents the systolic onset; and n_A represents the end of the systolic phase in the pulse. On the other hand, the delineation in BP signals, $x_{\mathrm{BP}}(n)$, has a well known physiological meaning, since the values at the apex, n_A , and at the basal, n_B, correspond to the SBP and DBP values, respectively.

Then, once the locations of the pulses, n_{D_i}, are identified, the BP signal, $x_{\mathrm{BP}}(n)$, is used to obtain, at the maximum of each pulse, n_{A_i}, the corresponding SBP value, $x_{\mathrm{BP}}(n_{\mathrm{A}_i})$. An illustration of the procedure is in Fig. 3.18. Furthermore, for the analysis of SBP, incorrectly detected SBP

values should been manually adjusted. Many different tools exist, but the R-DECO GUI is recommended for this purpose [145].

3.5.4 Biomarkers from the PPG

PR Estimation

A PPG signal, $x_{\mathrm{PPG}}(n)$, offers various biomarkers for cardiovascular assessment. The most commonly extracted feature is the Pulse Rate (PR), a surrogate of HR suitable for wearable environments:

$$d^{u}_{\mathrm{PR}}(n) \;=\; \sum_{i} \left[n_{\mathrm{FP}_i} - n_{\mathrm{FP}_{i-1}}\right] \cdot \delta(n - n_{\mathrm{FP}_i}), \quad \mathrm{FP} \in \{n_A, n_B, n_D\}. \tag{3.24}$$

Additionally, PRV can be derived as a surrogate of HRV, though its accuracy may be affected by the presence of PEP, since PEP uncorrelates HRV and PRV.

Beyond this standard and well established parameters, the PPG signal allows for the extraction of more advanced markers, which are not commonly used. Pulse Wave Velocity (PWV), an indicator of arterial stiffness and endothelial dysfunction, reflects the velocity of the blood pressure wave along the arterial tree and is linked to increased cardiovascular risks [147]–[149]. While PWV assessment traditionally required invasive methods [150], recent advances have enabled non-invasive approaches using ECG and PPG [151].

PAT Estimation

PAT, the time interval between the ECG R-wave and a peripheral PPG pulse (see Fig. 3.19), the inverse of the PWV serves as a non-invasive surrogate for PWV, since it measures the time a BP wave takes to travel from the heart to peripheral arteries. However, its inclusion of the PEP period limits also its accuracy for non-invasive BP estimation [152]. PAT can be defined for various locations, including the finger(F), forehead (H), and earlobe(E) [153]:

$$d^{u}_{\mathrm{PAT,L}}(n) \;=\; \sum_{i} \left[n_{\mathrm{B}_i,L} - n_{\mathrm{R}_i}\right] \cdot \delta(n - n_{\mathrm{R}_i}), \quad \mathrm{L} \in \{F, H, E\}. \tag{3.25}$$

The evenly sampled series, $d_{\mathrm{PAT,L}}(n)$ can be obtained by interpolating $d^{u}_{\mathrm{PAT,L}}(n)$ with cubic spline interpolation at 4Hz. For illustrative purposes,

$d^u_{\mathrm{PAT,L}}(n)$ series has been defined using n_{B} as FP, but it can be obtained using any of the FP available, like n_{D} and n_{A}.

PTTD Estimation

PTTD can be used as non-invasive surrogate of the Pulse Transit Time (PTT) (see Fig. 3.19), and it offers an alternative to PAT by measuring the time difference between two PPG pulses at different arterial sites [154], therefore unaffected by PEP. With signals from the finger, forehead, and earlobe, three PTTD signals can be computed, potentially offering more precise insights into vascular reactivity [155], [156].

PTTD calculates the time difference between the arrival of PPG pulses at different arterial sites. With three PPG signals at finger (F), forehead (H), and earlobe (E), we can thus calculate three PTTD signals denoted: $d^u_{\mathrm{PTTD,EF}}(n)$, $d^u_{\mathrm{PTTD,HF}}(n)$ and $d^u_{\mathrm{PTTD,EH}}(n)$, as follows:

$$\begin{aligned} d^u_{\mathrm{PTTD,EF}}(n) &= \sum_i [n^{\mathrm{F}}_{\mathrm{B}_i} - n^{\mathrm{E}}_{\mathrm{B}_i}] \cdot \delta(n - n^{\mathrm{F}}_{\mathrm{B}_i}) \\ d^u_{\mathrm{PTTD,HF}}(n) &= \sum_i [n^{\mathrm{F}}_{\mathrm{B}_i} - n^{\mathrm{H}}_{\mathrm{B}_i}] \cdot \delta(n - n^{\mathrm{F}}_{\mathrm{B}_i}) \\ d^u_{\mathrm{PTTD,EH}}(n) &= \sum_i [n^{\mathrm{H}}_{\mathrm{B}_i} - n^{\mathrm{E}}_{\mathrm{B}_i}] \cdot \delta(n - n^{\mathrm{H}}_{\mathrm{B}_i}) \end{aligned} \tag{3.26}$$

The evenly sampled series, $d_{\mathrm{PTTD,EF}}(n)$, $d_{\mathrm{PTTD,HF}}(n)$, and $d_{\mathrm{PTTD,EH}}(n)$ can be obtained by interpolating with cubic spline interpolation at 4Hz.

As for $d^u_{\mathrm{PAT,L}}(n)$, any of the FP available can be used to obtain each PTTD series. Note that, in order to have mostly positive time interval series, the time reference for each PTTD series is defined at finger for $d^u_{\mathrm{PTTD,EF}}(n)$ and $d^u_{\mathrm{PTTD,HF}}(n)$, and at forehead for $d^u_{\mathrm{PTTD,EH}}(n)$.

PAV Estimation

PAV quantifies the amplitude variation in the PPG signal (see Fig. 3.20, providing insights into arterial compliance and blood volume changes [157]:

$$d^u_{\mathrm{PAV}}(n) = \sum_i [x_{\mathrm{PPG}}(n_{\mathrm{A}_i}) - x_{\mathrm{PPG}}(n_{\mathrm{B}_i})] \cdot \delta(n - n_{\mathrm{B}_i}), \tag{3.27}$$

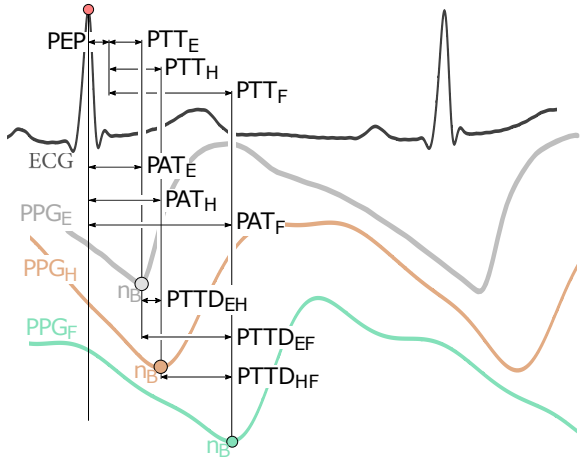

Figure 3.19: Illustration of PAT, PTTD and PDA definition. The ECG, earlobe ($\mathrm{PPG_E}$), forehead ($\mathrm{PPG_H}$) and finger ($\mathrm{PPG_F}$) PPG signals with the corresponding definitions of $\mathrm{PAT_E}$ (earlobe), $\mathrm{PAT_H}$ (head), $\mathrm{PAT_F}$ (finger) and $\mathrm{PTTD_{E\mathit{H}}}$ (earlobe-head), $\mathrm{PTTD_{E\mathit{F}}}$ (earlobe-finger), $\mathrm{PTTD_{H\mathit{F}}}$ (head-finger). Pulse Transit Time (PTT) refers to the time interval from the end of the Pre-Ejection Period (PEP) following a heartbeat to the arrival of the pulse wave at a peripheral site. The PEP interval shown is merely illustrative.

Again, the evenly sampled series, $d_{\mathrm{PAV}}(n)$ can be obtained by interpolating $d^{u}_{\mathrm{PAV}}(n)$ with cubic spline interpolation at 4Hz.

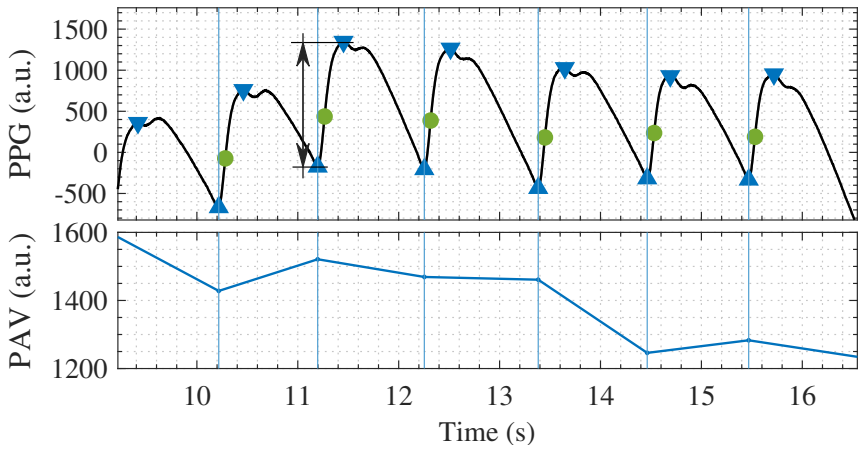

Figure 3.20: Pulse Amplitude Variability from a PPG signal and the FP delineated. In the bottom panel, the evolution of $d^{u}_{\mathrm{PAV}}(n)$ is shown with the blue line.

Pulse Decomposition

Finally, PDA is a signal processing technique to derive morphology indices from the PPG waveform [156]. Finger PPG pulses are decomposed into three wave components, a main wave and two reflected waves (see Fig. 3.21). From this analysis, we can derive the pulse waveform characteristics surrogates ($\mathscr{S}$) including main wave pulse width (W_1) and relative time delay between the main wave and the first reflected wave (T_{12}), which is used to derive the stiffness index [158], [159]. These are proposed in the present context as PWV surrogates, $\mathscr{S} \in \{W_1, T_{12}\}$.

$$d^u_{\mathscr{S}}(n) \;=\; \sum_i \mathscr{S}_i \cdot \delta(n - n^{\mathrm{F}}_{\mathrm{B}_i}), \quad \mathscr{S} \in \{W_1, T_{12}\}. \tag{3.28}$$

The evenly sampled series of $d^u_{\mathrm{W1}}(n)$, and $d^u_{\mathrm{T12}}(n)$ are obtained using cubic spline interpolation at 4Hz.

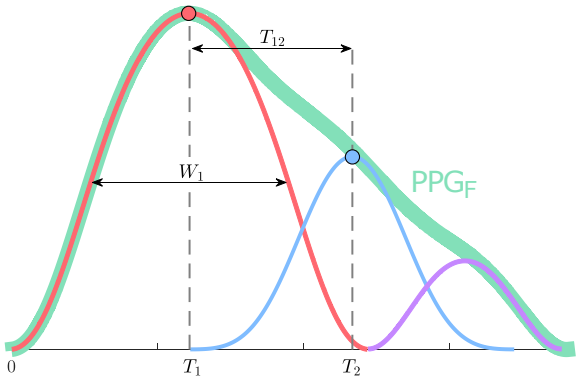

Figure 3.21: Pulse waveform characteristics of a PPG pulse at finger with PDA. Morphological features derived from width (W_1) and time (T_{12}) values of the first and second inner waves.

Outlier Rejection

Estimated values out-of-physiological range should be excluded from further analysis. This step must be performed before cubic spline interpolation to obtain the evenly sampled series (see Fig. 3.22). Then, an empirical range is first established for valid values of PAT, PTTD and PDA:

- $d^u_{\mathrm{PAT}}(n)$ values out of the $[50, 600]$ ms range.
- $d^u_{\mathrm{PTTD}}(n)$ values out of the $[-50, 175]$ ms range.

- From PDA, the features of a pulse are rejected if either [156]: (a) the pulse is decomposed in less than 3 waves; (b) the amplitude of the main wave is not the largest of the three waves; (c) the second wave is located at the end of the pulse interval; (d) the third wave occurs before 35% from pulse onset.

The physiological ranges were determined empirically following an exploratory analysis. These ranges correspond to values below the 1st percentile and above the 99th percentile of all PAT and PTTD intervals obtained in the dataset under study.

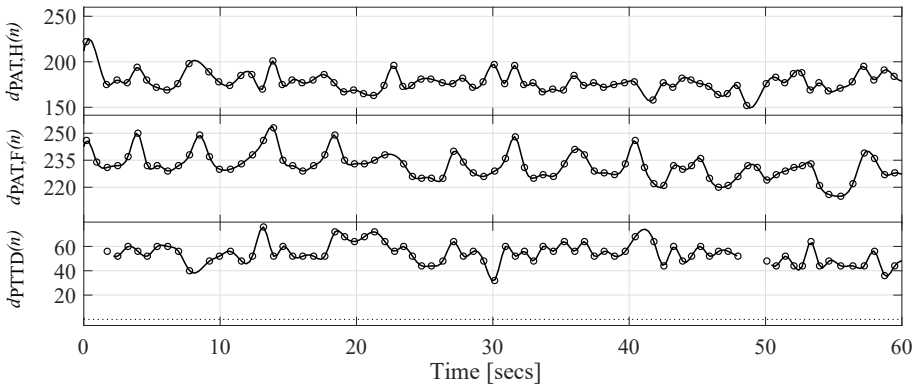

Figure 3.22: Example of $d^u_{\mathrm{PAT,H}}(n)$ on top, $d^u_{\mathrm{PAT,F}}(n)$ in the medium, and $d^u_{\mathrm{PTTD,HF}}(n)$ at bottom. Continuous lines represent the evenly sampled versions. Units are [msecs].

Afterwards, a Median Absolute Deviation (MAD) outlier rejection rule is applied [129], to complement suppression of spurious values from all the derived PWV surrogate series (see Fig. 3.23). The spurious pulses are eliminated by means of an outlier detector with the parameters adjusted empirically [160], $N_e = 10$ and $C = 2.75$. Outliers in PAV are also identified and removed based on MAD, as described.

3.6 Baroreflex Sensitivity Estimation

Various methodologies are more often employed to assess BRS using the BP signal, $x_{\mathrm{BP}}(t)$, focusing on spontaneous, beat-to-beat variations. Traditional techniques include the sequence method and spectral analysis of SBP and

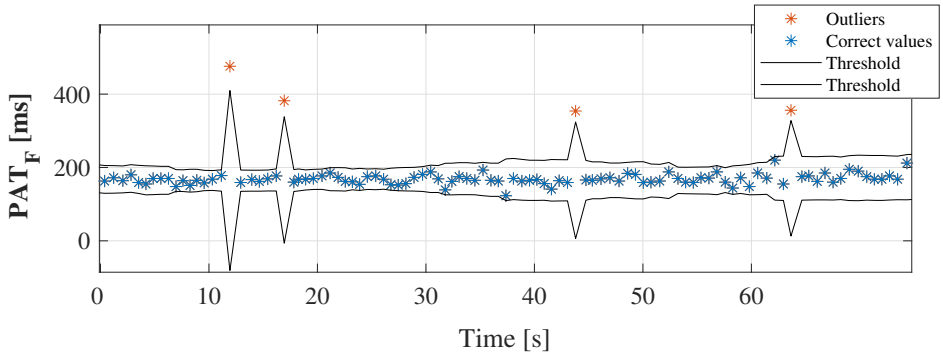

Figure 3.23: Outlier detection using the MAD method, from an illustrative PAT signal. The graphic shows how deviations from the median pulse time are identified, with outliers marked in contrast to the typical data range.

RR interval series, offering insights into the dynamic interplay between HR and BP [161].

To adress the nonstationary nature of cardiovascular signals, advanced methods like wavelet transform and TFC have emerged [117], [162], [163]. These approaches, like the TFC framework by Orini et al. [117], analyze the coupling strength and direction between HRV and SBP variability. Chen et al.'s closed-loop model within a point process framework represents another innovative direction for dynamic BRS assessment [164]. Pinna et al.'s review highlights the clinical value of spontaneous BRS in prognostic predictions across various cardiovascular conditions, despite challenges in standardization and measurability [165]–[167].

In line with recent advancements, this thesis presents two non-invasive techniques for BRS measurement. The first is spectral analysis of HRV and SBP to calculate the α index, a well-established metric. The second, BPRSA, offers an innovative method to construct an averaged HRV profile that reflects the heart's response to SBP changes. Notably, diminished control has been observed in conditions like coronary artery disease and hypertension, underscoring the importance of BRS evaluation in a clinical context [161], [165].

3.6.1 SBP Estimation

To delineate the BP signal, $x_{\mathrm{BP}}(t)$, the algorithm explained in Sec. 3.5.3 is used. Once the maximum of each pulse, n_{A_i}, and the corresponding SBP

value, $x_{\mathrm{BP}}(n_{\mathrm{A}_i})$ are detected, erroneous SBP detections need to be manually corrected using R-DECO [145].

Now, the SBP signal, $d^u_{\mathrm{SBP}}(n)$, can be estimated as:

$$d^u_{\mathrm{SBP}}(t) = \int x_{\mathrm{BP}}\left(\frac{n_{A_i}}{F_s}\right)\delta\left(t - \frac{n_{A_i}}{F_s}\right)dt, \tag{3.29}$$

where $\delta(\cdot)$ denotes the Kronecker delta function,, F_s is the sampling frequency, and the superscript "u" denotes that the signal is unevenly sampled, since heartbeats occur unevenly in time. The discrete evenly-sampled version, $d_{\mathrm{SBP}}(n)$, can be obtained with cubic spline interpolation at $F_s = 4$ Hz.

At this point, the BRS indices based on the α index can be calculated from the spectral analysis of HRV and SBP:

$$\alpha_{\mathrm{B}}(t) = \sqrt{\frac{\int_{\Omega_{\mathrm{B}}} \hat{S}_{\mathrm{m}}(t,f)\ df}{\int_{\Omega_{\mathrm{B}}} \hat{S}_{\mathrm{p}}(t,f)\ df}},\ B \in \{LF, HF\}, \tag{3.30}$$

where $\hat{S}_{\mathrm{m}}(t,f)$ and $\hat{S}_{\mathrm{p}}(t,f)$ are the time-varying power spectral densities of $m(t)$, and $d_{\mathrm{SBP}}(t)$, respectively, calculated by means of the Cohen's Class Wigner Ville Distribution (see sec. 3.3.4)

3.6.2 BPRSA Analysis

An alternative method to analyse BRS function has been proposed based on BPRSA [168]. Essentially, an averaged HRV profile is obtained of the overall heart response to SBP increases. For this, anchor points (AP) must be identified firstly in the $d_{\mathrm{SBP}}(n)$ series. Usually, AP's are defined in samples where the average of their T prior samples is greater than the average of their T subsequent samples [168]:

$$\frac{1}{T}\sum_{i=0}^{T-1} d_{\mathrm{SBP}}(n+i) > \frac{1}{T}\sum_{i=1}^{T} d_{\mathrm{SBP}}(n-i) \tag{3.31}$$

However, in this work, AP's are considered only if they are also local maxima in the corresponding series of Eq. (3.31). With this approach, only one AP is defined for each upslope. Now, windows of length $2L$ are segmented around each AP over the HRV series. Finally, the BPRSA curve is obtained by averaging all segmented windows in the HRV. In this study, L is set

to $10^{*}F_s$. T sets an upper frequency limit for the periodicity that can be detected by BPRSA [168]. For each patient, T is adjusted with their mean BR, $T \approx F_s/(2.5 \cdot \overline{f_r})$. An illustrative example of the methodology is shown in Fig. 3.24.

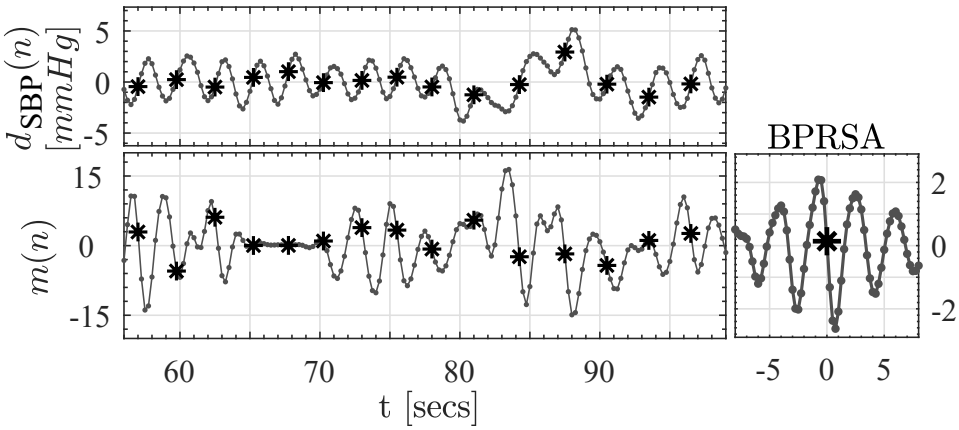

Figure 3.24: Estimation of the BPRSA curve for a patient. In top-left, the SBP signal, $d_{\mathrm{SBP}}(n)$, as driver mechanism, in which AP's (asterisks) are defined. In bottom-left, HRV signal, $m(n)$. Around each AP, segments of $2L$ length are extracted from the HRV signal. In bottom-right, the BPRSA curve, obtained averaging all segments of HRV.

The BRS, estimated from the BPRSA curve, is quantified with the capacity term, C [169]:

$$C = \frac{1}{2s}\sum_{i=1}^{s}\mathrm{BPRSA}(L+i) - \frac{1}{2s}\sum_{i=0}^{s-1}\mathrm{BPRSA}(L-i). \tag{3.32}$$

The index C is based on the Haar wavelet, but evaluated at a scale s and location $(L+1)$, in the center of the curve. Then, C can be either positive or negative. The scale, s, selects the oscillations in the BPRSA curve that most affect C. Of note, if s is taken to be equal to T, we avoids the need of optimization [169].

Bibliography of Part I

[1] J. D. Bronzino,
Biomedical engineering handbook.
CRC press, 1999,
Vol. 2.

[2] L. Sörnmo and P. Laguna,
Bioelectrical signal processing in cardiac and neurological applications.
Academic Press, 2005,
Vol. 8.

[3] K. E. Barrett, S. M. Barman, S. Boitano, and H. L. Brooks,
Ganong's Review of Medical Physiology, 25e.
New York, NY: McGraw-Hill Education, 2018.
[Online]. Available: `accessmedicine.mhmedical.com/content.aspx?aid=1115593202`.

[4] B. B. Winter and J. G. Webster, "Driven-right-leg circuit design",
IEEE Transactions on biomedical engineering, no. 1, pp. 62–66, 1983.

[5] J. R. Mitchell and J.-J. Wang, "Expanding application of the wiggers diagram to teach cardiovascular physiology",
Advances in physiology education, vol. 38, no. 2, pp. 170–175, 2014.

[6] P. H. Charlton, P. A. Kyriacou, J. Mant, V. Marozas, P. Chowienczyk, and J. Alastruey, "Wearable photoplethysmography for cardiovascular monitoring",
Proceedings of the IEEE, vol. 110, no. 3, 2022.

[7] J. Allen, "Photoplethysmography and its application in clinical physiological measurement",
Physiological measurement, vol. 28, no. 3, R1, 2007.

[8] P. H. Charlton, J. Allen, R. Bailon, S. Baker, J. A. Behar, F. Chen, G. D. Clifford, D. A. Clifton, H. J. Davies, C. Ding, *et al.*, "The 2023 wearable photoplethysmography roadmap",
Physiological Measurement, 2023.

[9] T. Tamura, Y. Maeda, M. Sekine, and M. Yoshida, "Wearable photoplethysmographic sensors—past and present",
Electronics, vol. 3, no. 2, pp. 282–302, 2014.

[10] J. J. Feher,
Quantitative human physiology: an introduction.
Academic press, 2017.

[11] A. C. Guyton, J. Hall, *et al.*, "Textbook of medical physiology. philadelphia",
PA: WB Saunders Company, 2006.

[12] J. F. Thayer, S. Yamamoto, and J. F. Brosschot, "The relationship of autonomic imbalance, heart rate variability and cardiovascular disease risk factors",
International Journal of Cardiology, vol. 141, no. 2, pp. 122–131, 2010.

[13] S. Vrijkotte, A. M. Roest, O. M. Laceulle, J. Ormel, and A. J. Oldehinkel, "Cardiac autonomic nervous system activation and metabolic profile in young children: The abcd study",
PLoS ONE, vol. 10, no. 9, e0138302, 2015.

[14] M. Malik, J. T. Bigger, A. J. Camm, R. E. Kleiger, A. Malliani, A. J. Moss, and P. J. Schwartz, "Heart rate variability: Standards of measurement, physiological interpretation, and clinical use. task force of the european society of cardiology and the north american society of pacing and electrophysiology",
Circulation, vol. 93, no. 5, 1996.

[15] F. Shaffer and J. Ginsberg, "An overview of heart rate variability metrics and norms",
Frontiers in public health, vol. 5, p. 258, 2017.

[16] P. M. Lehrer and R. Gevirtz, "Heart rate variability biofeedback: How and why does it work?",
Frontiers in psychology, p. 756, 2014.

[17] S. Kontaxis,
"Autonomic nervous system biomarkers from multi-modal and model-based signal processing in mental health and illness",
PhD in Biomedical Engineering,
Ph.D. dissertation, University of Zaragoza, 2020.
[Online]. Available: zaguan.unizar.es/record/100753.

[18] *Wave reflections animations*,
https://atcormedical.com/wavereflections-animations/,
Accessed: 2023-04-30,
2023.

[19] S. R. Braun, "Respiratory rate and pattern",
Clinical Methods: The History, Physical, and Laboratory Examinations. 3rd edition, 1990.

[20] P. Kumar and N. R. Prabhakar, "Peripheral chemoreceptors: Function and plasticity of the carotid body",
Comprehensive Physiology, vol. 2, no. 1, pp. 141–219, 2012.

[21] W. T. McNicholas, D. Hansson, S. Schiza, and L. Grote, "Sleep in chronic respiratory disease: Copd and hypoventilation disorders",
European respiratory review, vol. 28, no. 153, 2019.

[22] C. F. Vogelmeier, G. J. Criner, F. J. Martinez, A. Anzueto, P. J. Barnes, *et al.*, "Global strategy for the diagnosis, management, and prevention of chronic obstructive lung disease 2017 report: Gold executive summary",
European Respiratory Journal, vol. 49, no. 3, pp. 17–00 326, 2017.

[23] P. G. Gibson and H. Powell, "Written action plans for asthma: An evidence-based review of the key components",
Thorax, vol. 59, no. 2, pp. 94–99, 2004.

[24] R. Courtney, "The functions of breathing and its dysfunctions and their relationship to breathing therapy",
International Journal of Osteopathic Medicine, vol. 12, no. 3, pp. 78–85, 2009.

[25] J. L. Feldman and C. A. Del Negro, "Looking for inspiration: New perspectives on respiratory rhythm",

Nature Reviews Neuroscience, vol. 7, no. 3, pp. 232–242, 2006.

[26] R. M. Schwartzstein and M. J. Parker,
Respiratory Physiology: A Clinical Approach.
Lippincott Williams and Wilkins, 2006.

[27] M. R. Pinsky, "Cardiovascular issues in respiratory care",
Chest, vol. 128, no. 5, 592S–597S, 2005.

[28] J. S. Steingrub, M. Tidswell, and T. L. Higgins, "Hemodynamic consequences of heart-lung interactions",
Journal of Intensive Care Medicine, vol. 18, no. 2, pp. 92–99, 2003.

[29] G. G. Berntson, J. T. Cacioppo, and K. S. Quigley, "Respiratory sinus arrhythmia: Autonomic origins, physiological mechanisms, and psychophysiological implications",
Psychophysiology, vol. 30, no. 2, pp. 183–196, 1993.

[30] N. D. Giardino, R. W. Glenny, S. Borson, and L. Chan, "Respiratory sinus arrhythmia is associated with efficiency of pulmonary gas exchange in healthy humans",
American Journal of Physiology-Heart and Circulatory Physiology, vol. 284, no. 5, H1585–H1591, 2003.

[31] A. Ben-Tal, S. Shamailov, and J. Paton, "Evaluating the physiological significance of respiratory sinus arrhythmia: Looking beyond ventilation–perfusion efficiency",
The Journal of physiology, vol. 590, no. 8, pp. 1989–2008, 2012.

[32] F. Yasuma and J.-i. Hayano, "Respiratory sinus arrhythmia: Why does the heartbeat synchronize with respiratory rhythm?",
Chest, vol. 125, no. 2, pp. 683–690, 2004.

[33] G. E. Billman, "The lf/hf ratio does not accurately measure cardiac sympatho-vagal balance",
Frontiers in Physiology, vol. 4, p. 26, 2013.

[34] T. E. Dick, Y.-H. Hsieh, R. R. Dhingra, D. M. Baekey, R. F. Galán, E. Wehrwein, and K. F. Morris,
"Cardiorespiratory coupling: Common rhythms in cardiac, sympathetic, and respiratory activities",
In *Progress in brain research*,

Vol. 209,
Elsevier, 2014,
Pp. 191–205.

[35] R. J. Thomas, C. Wood, and M. T. Bianchi, "Cardiopulmonary coupling spectrogram as an ambulatory clinical biomarker of sleep stability and quality in health, sleep apnea, and insomnia",
Sleep, vol. 41, no. 2, zsx196, 2018.

[36] C. Varon, A. Caicedo, D. Testelmans, B. Buyse, and S. Van Huffel, "A novel algorithm for the automatic detection of sleep apnea from single-lead ECG",
IEEE Transactions on Biomedical Engineering, vol. 62, no. 9, pp. 2269–2278, 2015.

[37] Q.-M. Sun, L. Xing, C. Wang, and W. Liang, "Cardiopulmonary coupling analysis predicts early treatment response in depressed patients: A pilot study",
Psychiatry research, vol. 276, pp. 6–11, 2019.

[38] J. Milagro, M. Deviaene, E. Gil, J. Lázaro, B. Buyse, D. Testelmans, P. Borzée, R. Willems, S. Van Huffel, R. Bailón, *et al.*, "Autonomic dysfunction increases cardiovascular risk in the presence of sleep apnea",
Frontiers in Physiology, vol. 10, p. 620, 2019.

[39] D. L. Eckberg, "Point: Counterpoint: Respiratory sinus arrhythmia is due to a central mechanism vs. respiratory sinus arrhythmia is due to the baroreflex mechanism",
Journal of applied physiology, 2009.

[40] J. M. Karemaker, "Counterpoint: Respiratory sinus arrhythmia is due to the baroreflex mechanism",
Journal of applied physiology, vol. 106, no. 5, pp. 1742–1743, 2009.

[41] C. Julien, M. J. Parkes, S. Y. Tzeng, P. Y. Sin, P. N. Ainslie, P. Van De Borne, J.-O. Fortrat, M.-A. Custaud, C. Gharib, A. Porta, *et al.*, "Comments on point: Counterpoint: Respiratory sinus arrhythmia is due to a central mechanism vs. respiratory sinus arrhythmia is due to the baroreflex mechanism",
Journal of Applied Physiology, vol. 106, no. 5, pp. 1745–1749, 2009.

[42] A. Schäfer and J. Vagedes, "How accurate is pulse rate variability as an estimate of heart rate variability?: A review on studies comparing photoplethysmographic technology with an electrocardiogram", *International journal of cardiology*, vol. 166, no. 1, pp. 15–29, 2013.

[43] M. Riedl, A. Müller, J. F. Kraemer, T. Penzel, J. Kurths, and N. Wessel, "Cardio-respiratory coordination increases during sleep apnea", *PloS one*, vol. 9, no. 4, e93866, 2014.

[44] T. Stankovski, S. Petkoski, J. Raeder, A. F. Smith, P. V. McClintock, and A. Stefanovska, "Alterations in the coupling functions between cortical and cardio-respiratory oscillations due to anaesthesia with propofol and sevoflurane", *Philosophical Transactions of the Royal Society A: Mathematical, Physical and Engineering Sciences*, vol. 374, no. 2067, p. 20 150 186, 2016.

[45] S. Laborde, E. Mosley, and J. F. Thayer, "Heart rate variability and cardiac vagal tone in psychophysiological research–recommendations for experiment planning, data analysis, and data reporting", *Frontiers in psychology*, vol. 8, p. 213, 2017.

[46] G. E. Billman, H. V. Huikuri, J. Sacha, and K. Trimmel, *An introduction to heart rate variability: Methodological considerations and clinical applications*, 2015.

[47] P. Larsen, Y. Tzeng, P. Sin, and D. Galletly, "Respiratory sinus arrhythmia in conscious humans during spontaneous respiration", *Respiratory physiology and neurobiology*, vol. 174, no. 1-2, pp. 111–118, 2010.

[48] P. Grossman and E. W. Taylor, "Toward understanding respiratory sinus arrhythmia: Relations to cardiac vagal tone, evolution and biobehavioral functions", *Biological psychology*, vol. 74, no. 2, pp. 263–285, 2007.

[49] T. Ritz, M. Thöns, and B. Dahme, "Modulation of respiratory sinus arrhythmia by respiration rate and volume: Stability across posture and volume variations", *Psychophysiology*, vol. 38, no. 5, pp. 858–862, 2001.

[50] A. Hernando, J. Lázaro, E. Gil, A. Arza, J. M. Garzón, R. López-Antón, C. de la Cámara, P. Laguna, J. Aguiló, and R. Bailón, "Inclusion of respiratory frequency information in heart rate variability analysis for stress assessment",
IEEE journal of biomedical and health informatics, vol. 20, no. 4, pp. 1016–1025, 2016.

[51] C. Varon, J. Lázaro, J. Bolea, A. Hernando, J. Aguiló, E. Gil, S. Van Huffel, and R. Bailón, "Unconstrained estimation of HRV indices after removing respiratory influences from heart rate",
IEEE journal of biomedical and health informatics, vol. 23, no. 6, pp. 2386–2397, 2018.

[52] S. Kontaxis, J. Lázaro, V. D. Corino, F. Sandberg, R. Bailón, P. Laguna, and L. Sörnmo, "Ecg-derived respiratory rate in atrial fibrillation",
IEEE Transactions on Biomedical Engineering, vol. 67, no. 3, pp. 905–914, 2019.

[53] J. Lázaro, E. Gil, R. Bailón, A. Mincholé, and P. Laguna, "Deriving respiration from photoplethysmographic pulse width",
Medical and biological engineering and computing, vol. 51, no. 1, 2013.

[54] P. S. Addison, "Wavelet transforms and the ecg: A review",
Physiological Measurement, vol. 26, no. 5, R155, 2006.

[55] M. Elgendi, "On the analysis of fingertip photoplethysmogram signals",
Current Cardiology Reviews, vol. 8, no. 1, pp. 14–25, 2012.

[56] P. S. Addison, J. N. Watson, M. L. Mestek, and R. S. Mecca, "Developing an algorithm for pulse oximetry derived respiratory rate (rroxi): A healthy volunteer study",
Journal of clinical monitoring and computing, vol. 26, no. 1, pp. 45–51, 2012.

[57] N. R. MacIntyre *et al.*, "Evidence-based guidelines for weaning and discontinuing ventilatory support",
Chest, vol. 120, no. 6, 2001.

[58] R. D. Branson, "The ventilator circuit and ventilator-associated pneumonia",
Respiratory Care, vol. 50, no. 7, pp. 774–787, 2005.

[59] J.-M. Boles, J. Bion, A. Connors, M. Herridge, B. Marsh, C. Melot, R. Pearl, H. Silverman, M. Stanchina, A. Vieillard-Baron, *et al.*, "Weaning from mechanical ventilation",
European Respiratory Journal, vol. 29, no. 5, 2007.

[60] G. Béduneau, T. Pham, F. Schortgen, L. Piquilloud, E. Zogheib, M. Jonas, F. Grelon, I. Runge, N. Terzi, S. Grangé, *et al.*, "Epidemiology of weaning outcome according to a new definition. the WIND study",
American journal of respiratory and critical care medicine, vol. 195, no. 6, pp. 772–783, 2017.

[61] A. Esteban, I. Alia, M. J. Tobin, A. Gil, F. Gordo, I. VALLVERDÚ, L. BLANCH, A. BONET, A. VÁZQUEZ, R. de PABLO, *et al.*, "Effect of spontaneous breathing trial duration on outcome of attempts to discontinue mechanical ventilation",
American journal of respiratory and critical care medicine, vol. 159, no. 2, pp. 512–518, 1999.

[62] S. K. Epstein, "Weaning from ventilatory support",
Current Opinion in Critical Care, vol. 15, no. 1, pp. 36–43, 2009.

[63] A. W. Thille, A. Harrois, F. Schortgen, C. Brun-Buisson, and L. Brochard, "Outcomes of extubation failure in medical intensive care unit patients",
Critical care medicine, vol. 39, no. 12, pp. 2612–2618, 2011.

[64] W. Windisch, D. Dellweg, J. Geiseler, M. Westhoff, M. Pfeifer, S. Suchi, and B. Schönhofer, "Prolonged weaning from mechanical ventilation: Results from specialized weaning centers—a registry-based study from the weannet initiative",
Deutsches Ärzteblatt International, vol. 117, no. 12, p. 197, 2020.

[65] H. Zein, A. Baratloo, A. Negida, and S. Safari, "Ventilator weaning and spontaneous breathing trials; an educational review",
Emergency, vol. 4, no. 2, p. 65, 2016.

[66] N. R. MacIntyre, S. K. Epstein, S. Carson, D. Scheinhorn, K. Christopher, and S. Muldoon,
Management of patients requiring prolonged mechanical ventilation: report of a NAMDRC consensus conference.
2006,
Vol. 130, pp. 1827–1835.

[67] Ó. Peñuelas, A. W. Thille, and A. Esteban, "Discontinuation of ventilatory support: New solutions to old dilemmas",
Current opinion in critical care, vol. 21, no. 1, pp. 74–81, 2015.

[68] G. Hernández, C. Vaquero, P. González, C. Subira, F. Frutos-Vivar, G. Rialp, C. Laborda, L. Colinas, R. Cuena, and R. Fernández, "Effect of postextubation high-flow nasal cannula vs conventional oxygen therapy on reintubation in low-risk patients: A randomized clinical trial",
Jama, vol. 315, no. 13, pp. 1354–1361, 2016.

[69] C. Subirà, G. Hernández, A. Vázquez, R. Rodríguez-García, A. González-Castro, C. García, O. Rubio, L. Ventura, A. López, M.-C. de la Torre, *et al.*, "Effect of pressure support vs T-piece ventilation strategies during spontaneous breathing trials on successful extubation among patients receiving mechanical ventilation: A randomized clinical trial",
Jama, vol. 321, no. 22, pp. 2175–2182, 2019.

[70] J. F. McConville and J. P. Kress, "Weaning patients from the ventilator",
New England Journal of Medicine, vol. 367, no. 23, pp. 2233–2239, 2012.

[71] L. Brochard, F. Rua, H. Lorino, F. Lemaire, and A. Harf, "Inspiratory pressure support compensates for the additional work of breathing caused by the endotracheal tube",
Anesthesiology, vol. 81, no. 3, pp. 721–728, 1994.

[72] A. Esteban, F. Frutos-Vivar, *et al.*, "Evolution of mortality over time in patients receiving mechanical ventilation",
American Journal of Respiratory and Critical Care Medicine, vol. 188, no. 2, pp. 220–230, 2013.

[73] G. Bellani, J. G. Laffey, T. Pham, E. Fan, L. Brochard, A. Esteban, L. Gattinoni, F. Van Haren, A. Larsson, D. F. McAuley, *et al.*, "Epidemiology, patterns of care, and mortality for patients with acute respiratory distress syndrome in intensive care units in 50 countries", *Jama*, vol. 315, no. 8, pp. 788–800, 2016.

[74] A. Esteban, N. D. Ferguson, M. O. Meade, F. Frutos-Vivar, C. Apezteguia, L. Brochard, K. Raymondos, N. Nin, J. Hurtado, V. Tomicic, *et al.*, "Evolution of mechanical ventilation in response to clinical research",
American journal of respiratory and critical care medicine, vol. 177, no. 2, pp. 170–177, 2008.

[75] S. M. Koenig and J. D. Truwit, "Ventilator-associated pneumonia: Diagnosis, treatment, and prevention",
Clinical Microbiology Reviews, vol. 19, no. 4, pp. 637–657, 2006.

[76] J.-L. Vincent, "Nosocomial infections in adult intensive-care units", *The Lancet*, vol. 361, no. 9374, pp. 2068–2077, 2003.

[77] A. W. Thille, J.-C. M. Richard, and L. Brochard, "The decision to extubate in the intensive care unit",
American journal of respiratory and critical care medicine, vol. 187, no. 12, pp. 1294–1302, 2013.

[78] P. Navalesi, P. Frigerio, A. Patzlaff, S. Häußermann, P. Henseke, and M. Kubitschek, "Prolonged weaning: From the intensive care unit to home",
Revista portuguesa de pneumologia, vol. 20, no. 5, pp. 264–272, 2014.

[79] A. S. Slutsky and V. M. Ranieri, "Ventilator-induced lung injury", *New England Journal of Medicine*, vol. 369, no. 22, pp. 2126–2136, 2013.

[80] C. de Haro, J. López-Aguilar, R. Magrans, J. Montanya, S. Fernández-Gonzalo, M. Turon, G. Gomà, E. Chacón, G. M. Albaiceta, R. Fernández, *et al.*, "Double cycling during mechanical ventilation: Frequency, mechanisms, and physiologic implications",
Critical care medicine, vol. 46, no. 9, pp. 1385–1392, 2018.

[81] V. M. Ranieri, G. D. Rubenfeld, B. T. Thompson, N. D. Ferguson, E. Caldwell, E. Fan, L. Camporota, and A. S. Slutsky, "Acute respiratory distress syndrome: The berlin definition",
JAMA, vol. 307, no. 23, pp. 2526–2533, 2012.

[82] D. Chiumello, S. Coppola, S. Froio, and M. Gotti, "What's next after ards: Long-term outcomes",
Respiratory Care, vol. 61, no. 5, pp. 689–699, 2016.

[83] L. Gattinoni, E. Carlesso, P. Cadringher, and F. Valenza, "Physical and biological triggers of ventilator-induced lung injury and its prevention",
European Respiratory Journal Supplement, vol. 47, 15s–25s, 2003.

[84] R. G. Brower, M. A. Matthay, A. Morris, D. Schoenfeld, B. T. Thompson, and A. Wheeler, "Ventilation with lower tidal volumes as compared with traditional tidal volumes for acute lung injury and the acute respiratory distress syndrome",
New England Journal of Medicine, vol. 342, no. 18, pp. 1301–1308, 2000.

[85] M. B. Drakulovic, A. Torres, T. T. Bauer, J. M. Nicolas, S. Nogue, and M. Ferrer, "Supine body position as a risk factor for nosocomial pneumonia in mechanically ventilated patients: A randomised trial",
The Lancet, vol. 354, no. 9193, pp. 1851–1858,

[86] J. P. Kress, A. S. Pohlman, M. F. O'Connor, and J. B. Hall, "Daily interruption of sedative infusions in critically ill patients undergoing mechanical ventilation",
New England Journal of Medicine, vol. 342, no. 20, pp. 1471–1477, 2000.

[87] S. L. Worley, "The extraordinary importance of sleep: The detrimental effects of inadequate sleep on health and public safety drive an explosion of sleep research",
Pharmacy and Therapeutics, vol. 43, no. 12, p. 758, 2018.

[88] S. S. Choudhary and S. R. Choudhary, "Sleep effects on breathing and respiratory diseases",
Lung India, vol. 26, no. 4, pp. 117–122, 2009.

[89] M. L. Alonso-Álvarez, T. Canet, M. Cubell-Alarco, E. Estivill, E. Fernández-Julián, D. Gozal, M. J. Jurado-Luque, M. A. Lluch-Roselló, F. Martínez-Pérez, M. Merino-Andreu, *et al.*, "Documento de consenso del síndrome de apneas-hipopneas durante el sueño en niños (versión completa)",
Archivos de Bronconeumología, vol. 47, pp. 2–18, 2011.

[90] R. B. Berry, R. Budhiraja, D. J. Gottlieb, D. Gozal, C. Iber, V. K. Kapur, C. L. Marcus, R. Mehra, S. Parthasarathy, S. F. Quan, *et al.*, "Rules for scoring respiratory events in sleep: Update of the 2007 aasm manual for the scoring of sleep and associated events: Deliberations of the sleep apnea definitions task force of the american academy of sleep medicine",
Journal of clinical sleep medicine, vol. 8, no. 5, pp. 597–619, 2012.

[91] O. S. Capdevila, L. Kheirandish-Gozal, E. Dayyat, and D. Gozal, "Pediatric obstructive sleep apnea: Complications, management, and long-term outcomes",
Proceedings of the American Thoracic Society, vol. 5, no. 2, pp. 274–282, 2008.

[92] V. Barroso-García,
"Automatic analysis of overnight airflow to help in the diagnosis of pediatric obstructive sleep apnea",
PhD in Information and Telecommunication Technologies,
Ph.D. dissertation, University of Valladolid, 2022.
[Online]. Available: `https://uvadoc.uva.es/handle/10324/55051`.

[93] S. Fouzas, K. N. Priftis, and M. B. Anthracopoulos, "Pulse oximetry in pediatric practice",
Pediatrics, vol. 128, no. 4, pp. 740–752, 2011.

[94] A. Kulkas, B. Duce, T. Leppänen, C. Hukins, and J. Töyräs, "Severity of desaturation events differs between hypopnea and obstructive apnea events and is modulated by their duration in obstructive sleep apnea",
Sleep and Breathing, vol. 21, pp. 829–835, 2017.

[95] C. L. Marcus, R. H. Moore, C. L. Rosen, *et al.*, "A randomized trial of adenotonsillectomy for childhood sleep apnea",
N Engl J Med, vol. 368, no. 25, pp. 2366–2376, 2013.

DOI: 10.1056/NEJMoa1215881.

[96] J. C. Lumeng and R. D. Chervin, "Epidemiology of pediatric obstructive sleep apnea",
Proceedings of the American Thoracic Society, vol. 5, no. 2, pp. 242–252, 2008.

[97] R. Hornero, L. Kheirandish-Gozal, G. C. Gutiérrez-Tobal, M. F. Philby, M. L. Alonso-Álvarez, D. Álvarez, E. A. Dayyat, Z. Xu, Y.-S. Huang, M. Tamae Kakazu, *et al.*, "Nocturnal oximetry–based evaluation of habitually snoring children",
American Journal of Respiratory and Critical Care Medicine, vol. 196, no. 12, pp. 1591–1598, 2017.

[98] C. V. Senaratna, J. L. Perret, C. J. Lodge, A. J. Lowe, B. E. Campbell, M. C. Matheson, G. S. Hamilton, and S. C. Dharmage, "Prevalence of obstructive sleep apnea in the general population: A systematic review",
Sleep medicine reviews, vol. 34, pp. 70–81, 2017.

[99] L. Kheirandish-Gozal, R. Bhattacharjee, and D. Gozal, "Autonomic alterations and endothelial dysfunction in pediatric obstructive sleep apnea",
Sleep medicine, vol. 11, no. 7, pp. 714–720, 2010.

[100] A. M. Katz,
Physiology of the Heart.
Lippincott Williams and Wilkins, 2010.

[101] H.-L. Tan, L. Kheirandish-Gozal, and D. Gozal, "Pediatric home sleep apnea testing: Slowly getting there!",
Chest, vol. 148, no. 6, pp. 1382–1395, 2015.

[102] A. G. Kaditis, M. L. A. Alvarez, A. Boudewyns, E. I. Alexopoulos, R. Ersu, K. Joosten, H. Larramona, S. Miano, I. Narang, H. Trang, *et al.*, "Obstructive sleep disordered breathing in 2-to 18-year-old children: Diagnosis and management",
European Respiratory Journal, vol. 47, no. 1, pp. 69–94, 2016.

[103] F. Del Campo, A. Crespo, A. Cerezo-Hernández, G. C. Gutiérrez-Tobal, R. Hornero, and D. Álvarez, "Oximetry use in obstructive sleep apnea",
Expert review of respiratory medicine, vol. 12, no. 8, pp. 665–681, 2018.

[104] Z. Huang, Y. Wu, K. Huang, P. Chen, J. Chen, and L. Wang, "The nadir oxygen-specific heart rate response in sleep apnea links with the occurrence of acute myocardial infarction",
Frontiers in Cardiovascular Medicine, vol. 9, p. 807 436, 2022.

[105] A. Moffa, V. Rinaldi, A. Costantino, M. Cassano, M. Gelardi, V. Fiore, M. A. Lopez, P. Baptista, P. Campisi, and M. Casale, "Childhood obstructive sleep apnea: From diagnosis to therapy—an update",
Current Sleep Medicine Reports, vol. 6, pp. 157–162, 2020.

[106] R. Arens and H. Muzumdar, "Sleep, sleep disordered breathing, and nocturnal hypoventilation in children with neuromuscular diseases",
Paediatric respiratory reviews, vol. 11, no. 1, pp. 24–30, 2010.

[107] A. S. Jordan, D. G. McSharry, and A. Malhotra, "Adult obstructive sleep apnoea",
The Lancet, vol. 383, no. 9918, pp. 736–747, 2014.

[108] D. Gozal *et al.*, "Chemoreceptors, baroreceptors, and autonomic deregulation in children with obstructive sleep apnea",
Respiratory Physiology and Neurobiology, vol. 185, no. 1, pp. 177–185, 2013.

[109] O. Vitelli *et al.*, "Autonomic imbalance during apneic episodes in pediatric obstructive sleep apnea",
Clinical Neurophysiology, vol. 127, no. 1, pp. 551–555, 2016.

[110] G. Aljadeff *et al.*, "Heart rate variability in children with obstructive sleep apnea",
Sleep, vol. 20, no. 2, pp. 151–157, 1997.
DOI: 10.1093/sleep/20.2.151.

[111] R. B. Shouldice *et al.*, "Detection of obstructive sleep apnea in pediatric subjects using surface lead electrocardiogram features",
Sleep, vol. 27, no. 4, pp. 784–792, 2004.

DOI: 10.1093/sleep/27.4.784.

[112] A. Isaiah, D. Bertoni, K. D. Pereira, M. Diaz-Abad, R. B. Mitchell, and G. Das, "Treatment-related changes in heart rate variability in children with sleep apnea",
Otolaryngol Neck Surg, vol. 162, no. 5, pp. 737–745, 2020.
DOI: 10.1177/0194599820907882.

[113] A. Martín-Montero, P. Armañac-Julián, E. Gil, L. Kheirandish-Gozal, D. Álvarez, J. Lázaro, R. Bailón, D. Gozal, P. Laguna, R. Hornero, *et al.*, "Pediatric sleep apnea: Characterization of apneic events and sleep stages using heart rate variability",
Computers in Biology and Medicine, p. 106 549, 2023.

[114] J. M. Marin, S. J. Carrizo, E. Vicente, and A. G. Agusti, "Long-term cardiovascular outcomes in men with obstructive sleep apnoea-hypopnoea with or without treatment with continuous positive airway pressure: An observational study",
The Lancet, vol. 365, no. 9464, pp. 1046–1053, 2005.

[115] J. M. Marin, A. Agusti, I. Villar, M. Forner, D. Nieto, S. J. Carrizo, F. Barbé, E. Vicente, Y. Wei, F. J. Nieto, *et al.*, "Association between treated and untreated obstructive sleep apnea and risk of hypertension",
Jama, vol. 307, no. 20, pp. 2169–2176, 2012.

[116] M. L. Alonso-Álvarez, T. Canet, M. Cubell-Alarco, E. Estivill, E. Fernández-Julián, D. Gozal, M. J. Jurado-Luque, M. A. Lluch-Roselló, F. Martínez-Pérez, M. Merino-Andreu, *et al.*, "Consensus document on sleep apnea-hypopnea syndrome in children (full version). sociedad española de sueño. el área de sueño de la sociedad española de neumología y cirugía torácica (separ)",
Archivos de bronconeumologia, vol. 47, 2011.

[117] M. Orini, R. Bailón, L. T. Mainardi, P. Laguna, and P. Flandrin, "Characterization of dynamic interactions between cardiovascular signals by time-frequency coherence",
IEEE transactions on biomedical engineering, vol. 59, no. 3, 2011.

[118] P. H. Charlton and V. Marozas,
"Wearable photoplethysmography devices",

In *Photoplethysmography*,
Elsevier, 2022,
Pp. 401–439.

[119] B. Bent, B. A. Goldstein, W. A. Kibbe, and J. P. Dunn, "Investigating sources of inaccuracy in wearable optical heart rate sensors", *npj Digital Medicine*, vol. 3, no. 1, p. 18, 2020.

[120] J. E. Mück, B. Ünal, H. Butt, and A. K. Yetisen, "Market and patent analyses of wearables in medicine", *Trends in Biotechnology*, vol. 37, no. 6, pp. 563–566, Jun. 2019. DOI: 10.1016/j.tibtech.2019.02.001.

[121] Cisco,
Cisco visual networking index (vni) global mobile data traffic forecast update, 2017–2022 white paper,
https://s3.amazonaws.com/media.mediapost.com/uploads/CiscoForecast.pdf,
Accessed: Mar. 15, 2021,
2019.

[122] Gartner,
Gartner forecasts global spending on wearable devices to total 81.5 billion in 2021,
2021.

[123] D. Cajal, M. Posadas-de Miguel, C. de la Cámara, S. Kontaxis, J. Lázaro, and R. Bailón,
"Smartphone ppg validation for a depression assessment protocol",
In *2022 E-Health and Bioengineering Conference (EHB)*,
IEEE,
2022,
Pp. 1–4.

[124] A. Webb, V. P. Wallace, J. John, J. A. Crowe, A. D. Robert, G. Poulter, and J. Amor, "Wavelength selection for optical pulse oximetry", *IEEE Transactions on Biomedical Engineering*, vol. 65, no. 2, pp. 366–373, 2018.

[125] J. Allen, "Photoplethysmography and its application in clinical physiological measurement",

Physiological measurement, vol. 28, no. 3, R1, 2007.

[126] P. H. Charlton, P. Celka, B. Farukh, P. Chowienczyk, and J. Alastruey, "Assessing mental stress from the photoplethysmogram: A numerical study",
Physiological measurement, vol. 39, no. 5, p. 054 001, 2018.

[127] A. Jubran, "Pulse oximetry",
Critical Care, vol. 19, p. 272, 2015.

[128] O. Sayadi, E. H. Weiss, F. M. Merchant, D. Puppala, and A. A. Armoundas, "An optimized method for estimating the tidal volume from intracardiac or body surface electrocardiographic signals: Implications for estimating minute ventilation",
American Journal of Physiology-Heart and Circulatory Physiology, vol. 307, no. 3, H426–H436, 2014.

[129] R. Bailón, L. Sornmo, and P. Laguna, "A robust method for ecg-based estimation of the respiratory frequency during stress testing",
IEEE transactions on biomedical engineering, vol. 53, no. 7, 2006.

[130] J. Lázaro, A. Alcaine, D. Romero, E. Gil, P. Laguna, E. Pueyo, and R. Bailón, "Electrocardiogram derived respiratory rate from qrs slopes and r-wave angle",
Annals of biomedical engineering, vol. 42, pp. 2072–2083, 2014.

[131] J. P. Martínez, R. Almeida, S. Olmos, A. P. Rocha, and P. Laguna, "A wavelet-based ECG delineator: Evaluation on standard databases",
IEEE Transactions on biomedical engineering, vol. 51, no. 4, 2004.

[132] L. Sörnmo, R. Bailón, and P. Laguna, "Spectral analysis of heart rate variability in time-varying conditions and in the presence of confounding factors",
IEEE Reviews in Biomedical Engineering, 2022.

[133] M. Pagani, F. Lombardi, S. Guzzetti, O. Rimoldi, R. Furlan, P. Pizzinelli, G. Sandrone, G. Malfatto, S. Dell'Orto, and E. Piccaluga, "Power spectral analysis of heart rate and arterial pressure variabilities as a marker of sympatho-vagal interaction in man and conscious dog.",
Circulation research, vol. 59, no. 2, pp. 178–193, 1986.

[134] R. Bailón, G. Laouini, C. Grao, M. Orini, P. Laguna, and O. Meste, "The integral pulse frequency modulation model with time-varying threshold: Application to heart rate variability analysis during exercise stress testing",
IEEE transactions on biomedical engineering, vol. 58, no. 3, pp. 642–652, 2010.

[135] J. Mateo and P. Laguna, "Improved heart rate variability signal analysis from the beat occurrence times according to the ipfm model", *IEEE TBME*, vol. 47, no. 8, pp. 985–996, 2000.

[136] J. Mateo and P. Laguna, "Analysis of heart rate variability in the presence of ectopic beats using the heart timing signal",
IEEE Transactions on biomedical engineering, vol. 50, no. 3, 2003.

[137] J. Milagro,
"Noninvasive autonomic nervous system assessment in respiratory disorders and sport sciences applications",
PhD in Biomedical Engineering,
Ph.D. dissertation, University of Zaragoza, 2019.
[Online]. Available: `zaguan.unizar.es/record/89302/`.

[138] J. F. Morales, J. Moeyersons, P. Armañac, M. Orini, L. Faes, S. Overeem, M. Van Gilst, H. van Dijk, S. Van Huffel, R. Bailón, *et al.*, "Model-based evaluation of methods for respiratory sinus arrhythmia estimation.",
IEEE Trans. Biomed. Eng., vol. 68, no. 6, pp. 1882–1893, 2021.

[139] L. Faes, A. Porta, G. Nollo, and M. Javorka, "Information decomposition in multivariate systems: Definitions, implementation and application to cardiovascular networks",
Entropy, vol. 19, no. 1, p. 5, 2017.

[140] M. Elgendi, "Optimal signal quality index for photoplethysmogram signals",
Bioengineering, vol. 3, no. 4, 2016.

[141] P. Armañac-Julián, S. Kontaxis, A. Rapalis, V. Marozas, P. Laguna, R. Bailón, E. Gil, and J. Lázaro, "Reliability of pulse photoplethysmography sensors: Coverage using different setups and body locations",
Frontiers in electronics, vol. 3, 2022.

[142] J. Lázaro, E. Gil, J. M. Vergara, and P. Laguna, "Pulse rate variability analysis for discrimination of sleep-apnea-related decreases in the amplitude fluctuations of pulse photoplethysmographic signal in children",
IEEE journal of biomedical and health informatics, vol. 18, no. 1, pp. 240–246, 2014.

[143] K. Kotzen, P. H. Charlton, A. Landesberg, and J. A. Behar, "Benchmarking photoplethysmography peak detection algorithms using the electrocardiogram signal as a reference",
In *2021 Computing in Cardiology (CinC)*,
IEEE,
Vol. 48, 2021,
Pp. 1–4.

[144] P. H. Charlton, K. Kotzen, E. Mejía-Mejía, P. J. Aston, K. Budidha, J. Mant, C. Pettit, J. A. Behar, and P. A. Kyriacou, "Detecting beats in the photoplethysmogram: Benchmarking open-source algorithms", *Physiological Measurement*, vol. 43, no. 8, p. 085 007, 2022.

[145] J. Moeyersons *et al.*, "R-DECO: An open-source matlab based graphical user interface for the detection and correction of R-peaks", *PeerJ*, 2019.

[146] E. Peralta, J. Lázaro, R. Bailón, V. Marozas, and E. Gil, "Optimal fiducial points for pulse rate variability analysis from forehead and finger photoplethysmographic signals",
Physiological measurement, vol. 40, no. 2, 2019.

[147] L. M. Van Bortel, S. Laurent, P. Boutouyrie, P. Chowienczyk, J. Cruickshank, T. De Backer, J. Filipovsky, S. Huybrechts, F. U. Mattace-Raso, A. D. Protogerou, *et al.*, "Expert consensus document on the measurement of aortic stiffness in daily practice using carotid-femoral pulse wave velocity",
Journal of hypertension, vol. 30, no. 3, 2012.

[148] L. Peter, N. Noury, and M. Cerny, "A review of methods for non-invasive and continuous blood pressure monitoring: Pulse transit time method is promising?",
IRBM, vol. 35, no. 5, 2014.

[149] G. Mancia, R. Fagard, K. Narkiewicz, J. Redon, A. Zanchetti, M. Böhm, T. Christiaens, R. Cifkova, G. De Backer, A. Dominiczak, *et al.*, "2013 esh/esc practice guidelines for the management of arterial hypertension: Esh-esc the task force for the management of arterial hypertension of the european society of hypertension (esh) and of the european society of cardiology (esc)",
Blood pressure, vol. 23, no. 1, 2014.

[150] B. Hametner, S. Wassertheurer, J. Kropf, C. Mayer, B. Eber, and T. Weber, "Oscillometric estimation of aortic pulse wave velocity: Comparison with intra-aortic catheter measurements",
Blood pressure monitoring, vol. 18, no. 3, 2013.

[151] X. Ding and Y.-T. Zhang, "Pulse transit time technique for cuffless unobtrusive blood pressure measurement: From theory to algorithm",
Biomedical engineering letters, vol. 9, 2019.

[152] D. B. Newlin, "Relationships ol pulse transmission times to pre-ejection period and blood pressure",
Psychophysiology, vol. 18, no. 3, 1981.

[153] R. Mukkamala, J.-O. Hahn, O. T. Inan, L. K. Mestha, C.-S. Kim, H. Töreyin, and S. Kyal, "Toward ubiquitous blood pressure monitoring via pulse transit time: Theory and practice",
IEEE Transactions on Biomedical Engineering, vol. 62, no. 8, 2015.

[154] P. Armanac, J. Lázaro, P. Laguna, R. Bailón, E. Gil, *et al.*,
"Cardiovascular changes induced by acute emotional stress estimated from the pulse transit time difference",
In *2019 Computing in Cardiology (CinC)*,
2019.

[155] M. Nitzan, B. Khanokh, and Y. Slovik, "The difference in pulse transit time to the toe and finger measured by photoplethysmography",
Physiological measurement, vol. 23, no. 1, p. 85, 2001.

[156] S. Kontaxis, E. Gil, V. Marozas, J. Lázaro, E. García, M. Posadas-de Miguel, S. Siddi, M. L. Bernal, J. Aguiló, J. M. Haro, *et al.*,
"Photoplethysmographic waveform analysis for autonomic reactivity assessment in depression",

IEEE Transactions on Biomedical Engineering, vol. 68, no. 4, pp. 1273–1281, 2020.

[157] A. Hernando, M. D. Pelaez, M. T. Lozano, M. Aiger, E. Gil, and J. Lázaro,
"Finger and forehead ppg signal comparison for respiratory rate estimation based on pulse amplitude variability",
In *2017 25th European Signal Processing Conference (EUSIPCO)*, IEEE,
2017,
Pp. 2076–2080.

[158] P. Salvi, E. Magnani, F. Valbusa, D. Agnoletti, C. Alecu, L. Joly, and A. Benetos, "Comparative study of methodologies for pulse wave velocity estimation",
Journal of human hypertension, vol. 22, no. 10, 2008.

[159] P. H. Charlton, B. Paliakaitė, K. Pilt, M. Bachler, S. Zanelli, D. Kulin, J. Allen, M. Hallab, E. Bianchini, C. C. Mayer, *et al.*, "Assessing hemodynamics from the photoplethysmogram to gain insights into vascular age: A review from VascAgeNet",
American Journal of Physiology-Heart and Circulatory Physiology, vol. 322, no. 4, 2022.

[160] R. Bailón, L. Sornmo, and P. Laguna, "A robust method for ecg-based estimation of the respiratory frequency during stress testing",
IEEE transactions on biomedical engineering, vol. 53, no. 7, pp. 1273–1285, 2006.

[161] M. T. La Rovere *et al.*, "Baroreflex sensitivity: Measurement and clinical implications",
Ann N.Inv. Electrocard., vol. 13, no. 2, 2008.

[162] J. A. Nowak, A. Ocon, I. Taneja, M. S. Medow, and J. M. Stewart, "Multiresolution wavelet analysis of time-dependent physiological responses in syncopal youths",
American Journal of Physiology-Heart and Circulatory Physiology, vol. 296, no. 1, H171–H179, 2009.

[163] K. Keissar, R. Maestri, G. Pinna, M. La Rovere, and O. Gilad, "Non-invasive baroreflex sensitivity assessment using wavelet transfer function-based time–frequency analysis",
Physiological measurement, vol. 31, no. 7, p. 1021, 2010.

[164] Z. Chen, P. L. Purdon, G. Harrell, E. T. Pierce, J. Walsh, E. N. Brown, and R. Barbieri, "Dynamic assessment of baroreflex control of heart rate during induction of propofol anesthesia using a point process method",
Annals of biomedical engineering, vol. 39, pp. 260–276, 2011.

[165] G. D. Pinna *et al.*, "Different estimation methods of spontaneous baroreflex sensitivity have different predictive value in heart failure patients",
J Hypertension, vol. 35, no. 8, 2017.

[166] M. Di Rienzo, G. Parati, A. Radaelli, and P. Castiglioni, "Baroreflex contribution to blood pressure and heart rate oscillations: Time scales, time-variant characteristics and nonlinearities",
Philosophical Transactions of the Royal Society A: Mathematical, Physical and Engineering Sciences, vol. 367, no. 1892, pp. 1301–1318, 2009.

[167] S. C. G. de Moura-Tonello, A. Porta, A. Marchi, A. de Almeida Fagundes, C. d. O. Francisco, P. Rehder-Santos, J. C. Milan-Mattos, R. P. Simoes, M. d. O. Gois, and A. M. Catai, "Cardiovascular variability analysis and baroreflex estimation in patients with type 2 diabetes in absence of any manifest neuropathy",
PloS one, vol. 11, no. 3, e0148903, 2016.

[168] A. Müller *et al.*, "Bivariate phase-rectified signal averaging for assessment of spontaneous baroreflex sensitivity: Normalization of the results",
J Electrocard., vol. 45, no. 1, 2012.

[169] R. Sassi *et al.*,
"A methodological assessment of phase-rectified signal averaging through simulated beat-to-beat interval time series",
In *CinC*,
2014.

Part II

Cardiovascular Signal Processing in Critical Care Medicine

Chapter 4

Context, Motivation and Data for Part II

4.1 Context

Part II of this thesis is dedicated to leveraging cardiovascular signal processing techniques for enhanced patient monitoring in ICUs, with a particular emphasis on patients undergoing MV. This part underscores the increasing interest of critical care specialists in employing advanced technological solutions, such as signal processing, to refine patient care and monitoring.

A key focus is on the accurate assessment of weaning readiness from MV. The determination of the optimal time to begin weaning is critical, as both premature and delayed weaning carry significant risks (see previous Sec. 2.1.4). Thus, a thorough evaluation of respiratory, cardiac, and cardiovascular function, is essential in guiding these crucial clinical decisions.

After describing the database for weaning readiness assessment in following Sec. 4.2, this part of the thesis comprises two main studies. Chapter 5 presents the first one, focusing on the estimation of BRS by analyzing BP sig-

nals and HRV. This investigation evaluates BRS as a potential ANS marker for predicting successful weaning outcomes, recognizing its diminished control in various cardiac conditions with impaired ANS. The second study, outlined in Chapter 6, expands the scope to include biomarkers from respiration, HRV, and CPC. This comprehensive analysis, which encompasses data from the 24-hour period prior to a SBT, aims to offer a more in-depth evaluation of patient readiness for weaning, employing innovative methods to examine heart-lung interactions and the utility of CPC indices.

4.2 Dataset for Weaning Readiness Assessment

The whole database registered for the assessment of weaning readiness was constructed prospectively in the ICU of two different hospitals in Spain [1], in the *Hospital Universitari Parc Taulí* and the *Fundació Althaia*, using the connectivity platform Better Care (Better Care, Barcelona, Spain. US patent No. 12/538,940).

This database was aimed to establish a new model for the prediction of successful weaning (ClinicalTrial.gov, NCT03451461). The Institutional Review Boards of *Comitè d'Ètica d'Investigació amb medicaments* at the *Corporació Sanitària Parc Taulí* and the *Clinical Research Ethics Committee* of *Fundació Unió Catalana d'Hospitals* approved the database and the study protocol [2]. The requirement for informed consent was waived as part of the study approval, since the current study was an ancillary analysis. Therefore, all the signals were anonymous and encrypted to ensure privacy. The guidelines followed in this study were according to the applicable Spanish regulations (Biomedical Research Law 14/2007).

The original dataset included 60 patients screened at the time of implementing the present studies. Patients with neurological disorder, dementia or focal brain injury at ICU admission were excluded. Patients with arrhythmia, such as atrial fibrillation, were also excluded from the analysis, since HRV cannot be used as an estimate of the ANS function.

4.2.1 Patient Classification and Demographics

After a complete and extensive preliminary analysis, only those patients ventilated with assist/support ventilation modes were included, i.e., excluding

patients that were in controlled ventilation modes in the 24 hours previous to the SBT. This is due to the fact that the RSA mechanism may not be driven by the ANS during controlled ventilation, e.g. VCV mode, but to external systems like MV. Then, the study cohort consists of 22 patients out of the initial 60 available. Patients have heterogeneous clinical pictures, and data during the 24 hours prior to the SBT were registered for analysis.

To classify a patient's weaning outcome, this procedure is followed: when a patient's health improves sufficiently, they are considered ready for weaning, based on criteria outlined in the following subsections. However, these patients must undergo the SBT at this stage. Patients meeting at least one item of the intolerance criteria for a successful SBT (criteria in the following subsections) are deemed not ready for discontinuation, and their weaning is considered a failure. These patients are categorized into the *F-group*. Patients who successfully pass the SBT are categorized into the *S-group*.

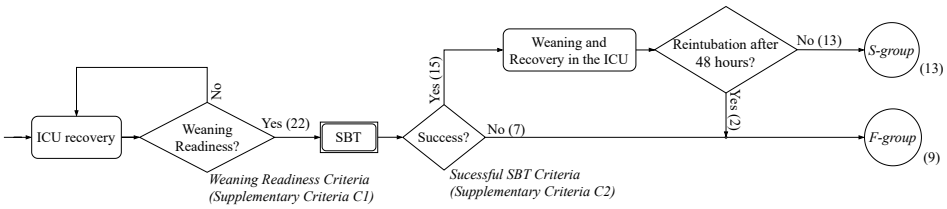

Figure 4.1: General algorithm for the definition of weaning success. Patients are classified into the *S-group* or *F-group* after the Spontaneous Breathing Trial (SBT). The *S-group* stands for the group of patients successfully weaned (successful SBT and no need of reintubation). *F-group* stands for the group of patients with SBT failure and patients with SBT success but with the need of reintubation after 48 hours of weaning.

With all these premises, there are 13 patients in the *S-group* and 9 in the *F-group* available. Note that 2 patients that passed the SBT required orotracheal intubation or reconnection to non-invasive MV within 48 hours after SBT. These 2 patients were reclassified in the *F-group*. See Fig. 4.1 for the patient classification scheme.

The demographics of the 22 patients included for analysis are summarized in Tab. 4.2. The variables available include: age, gender, Acute Physiology and Chronic Health Evaluation II (APACHE II), Sequential Organ Failure Assessment (SOFA), reason for MV, MV duration, ICU length of stay, ICU mortality and in-hospital mortality.

Table 4.2: Demographics. Data are presented as median [IQR 25-75] and percentages.

	S-group	F-group
N	13	9
Age (years)	65 [60-72]	69 [59-72]
Gender (% female)	15%	33%
APACHE II at admission	18 [14-23]	16 [10-20]
SOFA at admission	7 [6-8]	6 [3-10]
Reason for MV		
Acute Respiratory Failure	30.7%	22.2%
Sepsis	38.5%	33.3%
Sepsis + ARDS	7.7%	11.1%
Neurologic	15.4%	11.1%
Cardio-Respiratory Arrest	-	11.1%
Acute Pancreatitis	7.7%	11.1%
MV duration (days)	6 [4-10]	12 [8-16]
ICU length of stay (days)	8 [6-12]	18 [13-23]
ICU mortality	7.69%	22.22%
In-hospital mortality	7.69%	22.22%

Notes: APACHE: Acute Physiology and Chronic Health Evaluation; SOFA: Sequential Organ Failure Assessment; MV: Mechanical Ventilation; ICU: Intensive Care Unit. ARDS: Acute Respiratory Distress Syndrome.

Specific Criteria for Weaning Readiness

As reference, the following criteria is used in the ICU of *Hospital Parc Tauli* in Sabadell, Spain, to determine if a patient is presumably ready to be weaned, i.e., if a patient is ready to perform the SBT [3]–[5]:

1. Medical Assessment
   - Improvement or recovery of the cause for MV
   - Adequate cough
   - Absence of secretion
   - No neuromuscular blocking agents
2. Parametric Measures
   - Time in MV > 24 hours
   - $HR < 140$ bpm
   - $SBP \in [90, 160]$ mmHg
   - Haemoglobin (Hb) ≥ 8g/dL
   - SpO_2 >90%, with $FiO_2 \leq 40\%$

- Tidal Volume (V_T) > 5 mL·kg
- BR < 35 rpm
- pH ≥ 7.30 (no respiratory acidosis)
- Body Temperature (T) ∈ [35,38] ºC
- PEEP < 8 cmH_2O
- Maximal Inspiratory Pressure (MIP) ≤ -25 cmH_2O
- Rapid Shallow Breathing Index (RSBI) < 105
- Richmond Agitation-Sedation Scale (RASS): -1/0
- Glasgow Coma Scale (GCS) >8
- Minimal vasopressors or inotropes < 5 μgr/kg/minute (stable cardiovascular status)

Specific Criteria for successful SBT

As said, once a patient is deemed ready for weaning, they have to perform the SBT. The SBT is carried out by a low-level inspiratory pressure support or by a T-tube test. The following criteria listed below show the indicators used to evaluate the success of the SBT, in order to decide if MV can finally be withdrawn [3]–[5]:

- Good tolerance to the SBT
- BR < 35 rpm
- HR < 140 bpm
- HR < 20% change from baseline
- SpO_2 > 90% or PaO_2 > 60 mmHg on FiO_2 < 40%
- SBP ∈ [80, 180] mmHg
- SBP< 20% change from baseline
- No signs of increased work of breathing or distress

4.2.2 Data Acquisition and Data Analysis

Physiological signals were continuously recorded using the connectivity platform Better Care [2]. The Better Care system (Better Care, Barcelona, Spain. US patent No. 12/538,940), is a proprietary system for data collection designed to interact with output signals from mechanical ventilators and bedside monitors rather than directly with patients. It was firstly developed to interoperate signals from different ventilators and monitors, and subsequently compute algorithms for diagnosing patient-ventilator asynchronies.

Better Care standardizes, synchronizes and stores the signals of all the bedside monitors and ventilators at 200 samples per second, from intubation in the ICU to liberation from MV. Different biomedical signals were recorded, including the three bipolar leads of the electrocardiogram (ECG), as well as the respiratory signals: airflow and airway pressure. In addition, pulse photoplethysmography, blood pressure via invasive catheter, and SpO_2 were also recorded.

The onset of inspiration for each breath was delineated using the algorithms implemented in the Better Care platform. For each respiratory cycle, information on the type of ventilation mode, the trigger of respiration and the appearance or absence of asynchronies, such as ineffective efforts or double cycling, were also given [1], [2]. It is possible that a patient is in PSV mode and the machine automatically triggers a breath, e.g. due to low BR. However, all breathing cycles are delineated by Better Care, considering the characteristic morphologies of the airway pressure and airflow [2]. Then, these automated breathing cycles are labelled as 'controlled' and they are omitted for the analysis of the respiratory signal.

Chapter 5

Baroreflex Sensitivity Evolution in the Hour prior to SBT

5.1 Introduction

This chapter delves into evaluating BRS in the hour preceding the SBT. BRS serves as a key indicator of ANS functionality, crucial in regulating blood pressure. Notably, BRS is often compromised in various cardiac and cardiovascular conditions, and recent studies revealed high incidence of autonomic dysfunction in patients admitted to the ICU, resulting in chronic adrenergic activation and acute respiratory distress syndromes [6]. However, no previous work investigated the role of the BRS in the context of weaning from MV. Moreover, none looked for differences just before the SBT, in

order to improve the predictive value of the weaning indices.

The primary objective is to explore if BRS can enhance the prediction of weaning outcomes, potentially contributing to improved patient management in ICU settings. Given the observed diminished baroreflex control in cardiac conditions, this evaluation is particularly relevant [7], [8]. The study employs two non-invasive techniques for BRS assessment (see previous Section 3.6): Spectral Analysis of HRV and SBP: (a) utilizing the α index to analyze the interplay between HRV and SBP [9], [10]. (b) BPRSA, a novel method for constructing an averaged HRV profile in response to SBP fluctuations [11], [12].

5.2 Materials and Methods

5.2.1 Subset of Weaning Data for BRS analysis

The dataset employed in this chapter has been detailed in the previous section (Sec. 4.2). After SBT, patients were categorized into two groups: those with successful weaning (*S-group*) and those without (*F-group*). Nine patients from the *S-group* and six from the *F-group* were included from the entire database. The reduced number of patients studied is attributed to the limited availability of high-quality invasive blood pressure signals. Specifically, only the last hour preceding the SBT underwent analysis, as the recordings necessitated manual correction of SBP values estimated using automatic algorithms (as described in Sec. 5.2.2).

This study utilizes recordings of lead II from the ECG, the BP signal obtained through an invasive arterial catheter, and the BR signal, denoted as $\hat{f}_r(t)$. The BR, employed for guiding HRV analysis, is derived from the detected inspiration onsets using *BetterCare*®.

5.2.2 BRS Methodologies

SAP Estimation

The delineation of the BP signal utilizes the algorithm described in Sec. 3.5.3, using the envelope-thresholding method for pulse detection. The SAP signal is estimated and interpolated to form an evenly-sampled series, which serves as a basis for calculating BRS indices using spectral analysis (Eq. 3.30).

The PSD used in this analysis are obtained via Cohen's Class Wigner Ville Distribution, as detailed in Section 3.3.4.

BPRSA Analysis

The BPRSA method, an alternative for analyzing BRS, is based on creating an averaged HRV profile in response to SAP increases (refer to [11] for details). Anchor points (APs) in the SAP series are identified using local maxima detection within a specific framework. Subsequently, HRV signal segments around each AP are averaged to form the BPRSA curve. The methodology and its application are illustrated in Fig. 3.24.

The BRS, estimated from the BPRSA curve, is quantified using the capacity term 'C' (Eq. 3.32), which analyzes oscillations in the BPRSA curve relevant to BRS. The selection of the scale parameter 's' is based on the mean BR of each patient, aligning with the guidance in [13].

5.2.3 Statistical Analysis

To assess BRS, the following parameters are included and compared:

- Average heart rate ($\overline{\mathrm{HR}}$)
- Average systolic arterial pressure ($\overline{\mathrm{SAP}}$)
- Average breathing rate ($\overline{\mathrm{BR}}$)
- Standard deviation of NN intervals (SDNN)
- Root mean square of successive differences (RMSSD)
- Averaged alpha indices in low-frequency ($\overline{\alpha_{\mathrm{LF}}}$) and high-frequency ($\overline{\alpha_{\mathrm{HF}}}$) bands
- Normalized low-frequency power ($\overline{\mathrm{P}^n_{\mathrm{LF}}}$)
- Average capacity term ($\overline{C}$)

These parameters are calculated as averages over the entire one-hour recording period, detailed in Tab. 5.1. Additionally, alpha indices (α_{LF}, α_{HF}), normalized low-frequency power ($\mathrm{P}^n_{\mathrm{LF}}$), and the capacity term (C) are also computed as averages over 5-minute intervals. This approach allows for a more detailed analysis, as illustrated in Fig. 5.2.

For statistical testing, we employ the Mann-Whitney U-test to assess differences between the *S-group* (subjects group) and the *F-group* (control group). The objective is to determine whether these parameters exhibit

significant variations between the two groups, considering both the one-hour averages and the 5-minute interval averages. A p-value of 0.05 is established to determine statistical significance.

5.3 Results and Discussion

The results for the scalar variables are in Tab. 5.1. The capacity, $\overline{C}$, obtained from the BPRSA curve, is the only parameter significantly different comparing *S-group* vs *F-group*. No significant differences can be found for SDNN and RMSSD of the HRV, but they are notably higher for the *S-group*. In fact, other works did found significant differences for these between the two groups when comparing values half an hour before the SBT, and half an hour after SBT [6].

Table 5.1: Scalar indices. Inter-subject median (Q_1, Q_3), computed throughout the whole hour before SBT.

	Units	S-group	F-group	p-value
HR	[bpm]	80 (75,89)	84 (81,123)	0.33
SBP	[mmHg]	132 (110,139)	126 (101,141)	0.78
BR	[rpm]	19 (18,23)	22 (18,24)	0.61
SDNN	[ms]	32 (27,53)	22 (15,26)	0.11
RMSSD	[ms]	11 (6,14)	5 (3,8)	0.18
$\boldsymbol{\alpha_{LF}}$	[ms/mmHg]	6.0 (3.5,11.8)	5.1 (2.3,7.1)	0.46
$\boldsymbol{\alpha_{HF}}$	[ms/mmHg]	7.1 (3.1,8.7)	6.7 (1.6,8.6)	0.78
$\mathbf{P^n_{LF}}$		0.56 (0.30,0.65)	0.66 (0.41,0.80)	0.39
Capacity	[ms]	-1.7 (-2.7,-0.8)	0.9 (0.5,1.4)	0.02*

In order to investigate if the absence of differences in the indices was due to the long one hour averaging, which might attenuate short-term variations, the evolution of α_{LF}, α_{HF}, $\mathrm{P}^n_{\mathrm{LF}}$ and C is calculated in 5-minutes averaged-periods, throughout the hour before SBT (Fig. 5.2). Clear statistical significant differences in C are visible comparing the *S-group* vs *F-group* in many 5-minutes periods. Again, no significant differences are found in any period for α_{LF}, α_{HF} or $\mathrm{P}^n_{\mathrm{LF}}$ either. In spite of that, the α_{LF} median values are generally higher for the *S-group* during the whole hour.

Maybe, no strong differences can be found since these patients present strong non-linear dynamics because of the disease severity [7]. This fact

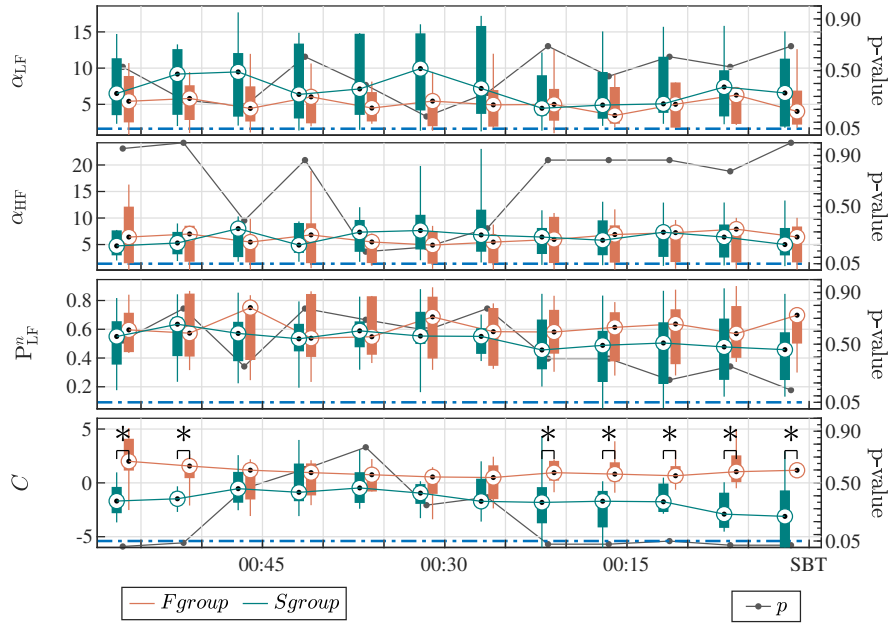

Figure 5.2: Evolution, throughout the hour before SBT, of the BRS with α_{LF} and α_{HF}, in $[1/mmHg]$, $\mathrm{P}^n_{\mathrm{LF}}$ and C are dimensionless. Green and Red boxplots represent the average of each 5-minutes period for the *S-group* and *F-group*, respectively. The *p-value* is represented in the right axis, from 0 to 1, comparing each 5-minutes period and asterisk represents statistical significance.

reflects complex influences of respiration on HR and SAP variability and might limit the ability of α_{LF} and α_{HF} for BRS assessment, even though analysis was guided by respiration.

It is important to remark that C in absolute values, is higher for the *S-group*. This could be because of the effect of the strength of SAP changes in HRV, reflected in the amplitude of the BPRSA curve. Besides, notice that C is negative for the *S-group* but positive for the *F-group*, since sympathetic activity is associated with higher latency shifts in the response of the HRV for the spontaneous increases in BP. In fact, related to this, higher adaptability to changes can be deduced from SDNN and higher parasympathetic activity from RMSSD, for the *S-group*. Note that the scale $s = T$, used for the computation of C, is not distorting the results, since $\overline{\mathrm{BR}}$ is similar for both groups (see Tab. 5.1).

The selection of the AP's for the BPRSA analysis is of relative importance. Using all the increasing samples as AP's [7], [11], produces a reduction in

the amplitude of the average curve, because of the distortion introduced by the average of few-samples-delayed ensembles. This fact compromises the BPRSA curve, and some investigation should be done in order to standardize the selection of AP's.

5.4 Conclusions

In this study, BRS was evaluated in a cohort of critically ill patients undergoing MV using the BPRSA technique. The analysis revealed a stronger and negative capacity of the BRS in patients who were actually ready for weaning. These findings suggest the potential utility of BRS quantification as a predictive measure for weaning outcomes in the ICU. The inclusion of BRS analysis could aid clinicians in more accurately assessing weaning readiness.

Chapter 6

Cardiopulmonary Coupling Indices to Assess Weaning Readiness

6.1 Introduction

This chapter presents the second study, expanding the scope beyond the hour before a spontaneous breathing trial (SBT). Utilizing data from the 24-hour period prior to SBT, it offers a more comprehensive assessment of patient readiness for weaning. The study employs non-invasive biomarkers derived from respiration, HRV, and CPC to evaluate weaning readiness.

The study analyzes HRV and respiratory signals (detailed in Section 3.3.3), focusing on three main methods for CPC quantification (Section 3.4): TFC

(Section 3.4.1) Information Dynamics (ID) for cross entropy estimation (Section 3.4.2) Orthogonal Subspace Projection (OSP) for HRV decomposition (Section 3.4.3)

Given the high incidence ANS dysfunction in ICU patients [14], [15], this study explores the potential of ANS assessment in predicting weaning outcomes. HRV and CPC estimators are hypothesized to provide insights into the multifaceted nature of the weaning process. Previous research has shown the value of HRV in identifying outcomes related to SBT [6], [16], and RSA has been linked to improved pulmonary function and cardiac efficiency [17], [18].

This proof-of-concept study aims to identify novel biomarkers to assist clinicians in predicting weaning readiness. It explores heart-lung interactions and evaluates the utility of CPC indices in a prospective and blinded design relative to the SBT process. The reliability of HRV and CPC estimators as predictors of weaning outcomes is examined, along with the impact of assessment timing in relation to SBT.

6.2 Materials and Methods

6.2.1 Subset of Weaning Data for CPC analysis

The data used in this chapter have been described in previous Sec. 4.2. Then, after SBT, patients were distributed into two groups, those with successful weaning (*S-group*, 13) and those without (*F-group*, 9). For this set of patients under analysis, the most common MV mode was PSV, but also some patients spent some time in Continuous Positive Airway Pressure (CPAP). An example of the respiratory pattern in PSV mode was shown in Fig. 2.3, and Fig. 6.1.

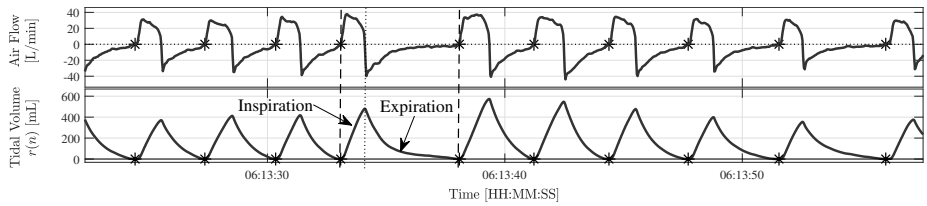

Figure 6.1: Example of respiration in PSV mode. The airflow signal is plotted at (top) and the derived TV signal at (bottom). The onset of inspiration, delineated by Better Care, is marked with asterisks.

6.2.2 CPC Methodologies

Three different techniques are used to compute the CPC indices, with the objective of obtaining an estimate of the RSA. These indices are computed based on TFC, ID and OSP, explained in previous Section 3.4. However, although these three CPC estimates rely on different techniques, the underlying idea is the same: to measure and characterize the RSA function, i.e., respiratory-cardiac interactions, in patients ready for weaning the 24 hours before the SBT. Table 6.2 summarizes all the terms and indices computed in this work.

It is important to remark that the algorithms do not extract the information in the same way, and the indices have different temporal resolution. For this reason, the average value in consecutive 30-minutes periods is considered for each index calculated in this work, in order to be able to compare all the indices through the 24 hours recordings.

Table 6.2: Summary of terms and indices computed.

Term	Description	Framework/Notes
BR	Breathing rate	
HR	Heart Rate	
HRV	Heart Rate Variability	
SDNN	Standard Deviation of NN intervals	
RMSSD	Root-Mean Square of Successive interval Differences	
$\mathbf{P_{VLF}}$	Power in the Very Low Frequency band	
$\mathbf{P_{HF}}$	Power in the High Frequency band, centered to respiration	
$\mathbf{P^{n}_{LF}}$	Normalized LF Power: $P_{LF}/(P_{LF}+P_{HF})$	
CPC	Cardio-Pulmonary Coupling	
$\mathscr{C}^{\mathcal{T}}_{\mathrm{HF}}$	Spectral coherence between HRV and respiration	Time-Frequency Coherence (TFC)
$\mathscr{CE}_{\mathrm{r}\leftrightarrow\mathrm{m}}$	Cross entropy between HRV and respiration	Information Dynamics (ID)
$\mathscr{P}_{\mathrm{mr}}$	Power of the respiratory component in HRV	Orthogonal Subspace Projections (OSP)

6.2.3 Long-term Assessment and Statistical Analysis

Due to the long-term basis of this work, handling missing data is an important issue. First, artifacts, bad detections or ectopic beats appear in the ECG signal. To this end, any NN interval greater than 2.5 seconds is removed from the series, and the corresponding interpolated segment is also suppressed from the $m(t)$ signal. Second, regarding the respiratory signal, support MV modes include a backup frequency, and if the patient falls below, the breath cycle is triggered by the ventilator similarly to controlled ventilation. In the cohort study, breathing cycles were labelled as controlled for the 2,11% of them, and were omitted for the analysis. Then, gaps exist in the estimated signals for the CPC calculations. However, results are analysed in 30-min averaged periods for 24 hours, and these gaps or missing data do not affect the results, since they are omitted for the calculation of the average.

At this point, since SDNN is the state-of-art index for medical stratification of cardiac risk in long-term analysis, the SDNN is calculated for the whole period of 24 hours before the SBT. The Mann-Whitney U-test is also used to compare the value for the *S-group* vs. *F-group*.

After that, the evolution of the common clinical parameters, HRV and CPC indices, through the 24 hours before SBT are analysed, in order to determine if circadian rhythms could be affecting the regulatory mechanisms and the interpretation of the results. However, it must be considered that the SBT's are generally performed in the morning, but not at the same exact time for all patients. For this reason, all the recordings are segmented from 08:00 p.m. to 10:30 a.m. of the SBT day, so that the same time interval is considered for all patients. This means that it is being considered only some part of the circadian rhythm.

The average value in consecutive 30-minutes periods is considered, for the representation of the evolution through the day and for the statistical analysis. Table 6.2 summarizes all the parameters computed to this end. Then, each HRV and CPC indices are calculated separately using different temporal resolutions:

- The parameters BR and HR are unevenly sampled at the inspiration onset and heart beats occurrence, respectively. Therefore, the mean value in each half hour is computed.
- For the computation of $\mathscr{CE}_{\mathrm{r}\leftrightarrow\mathrm{m}}$, $\mathscr{P}_{\mathrm{m_r}}$, and the temporal

HRV parameters –SDNN and RMSSD–, sliding windows of 3-min-length with 75% of overlap are used. For these, there is a sample each 45 seconds and a total of 1920 samples in 24 hours. So, the mean of 40 overlapped windows in each 30-minutes period is computed, for each parameter and for each patient.

- The $\mathscr{C}^{\mathcal{T}}_{\mathrm{HF}}$ and the frequency domain parameters of HRV –$\mathrm{P_{VLF}}$, $\mathrm{P_{HF}}$ and $\mathrm{P^{n}_{LF}}$– are calculated using the TF maps. Therefore, these indices are calculated at the resampling frequency, $F_s = 4$ Hz, and thus the average value of 7200 samples, i.e., 30 minutes, is obtained.

Finally, the averaged values for the *S-group* vs. *F-group* are compared with the non-parametric unpaired Mann-Whitney U-test, for all the parameters. Differences are considered significant for a level of $p \leq 0.05$. The effect size Cohen's d, for an acceptable level of statistical power, was also reported. For data where the assumptions of the parametric tests cannot be satisfied, the non-parametric Cohen's d is recommended [19]:

$$d = \frac{Z}{\sqrt{(n_S + n_F)}}, \tag{6.1}$$

where Z is the standardized U-value, and n_S and n_F are the number of patients of the *S-group* and *F-group*, respectively. A commonly used interpretation is to refer to effect sizes as small ($d = 0.2$), medium ($d = 0.5$) and large ($d = 0.8$).

6.3 Results

Table 6.1 shows the median and quartiles 1 and 3 of the SDNN, calculated in the whole recordings of 24 hours. Higher SDNN is visible for the *S-group* patients, and although the difference is not significant, the *p-value* approaches 0.05. As expected, the SDNN values are higher considering the 24 hours recordings (see Tab. 6.1), than considering the averaged 3-minutes windows (see Figure 6.4), for the same group of patients. The evolution of the patients throughout the day before SBT, from 08:00 p.m. to 10:30 a.m., are illustrated in the Figs. 6.3, 6.4 and 6.5. The commonly-used clinical variables BR and

HR –Figure 6.3–, can be compared to the parameters of HRV –Figure 6.4– and the CPC estimators –Figure 6.5.

Looking at Figure 6.3, both BR and HR rely within the limits of criteria for weaning readiness (Criteria in Sec. 4.2.1) the whole day. In general, patients of the *F-group* have slightly higher HR and BR. The BR is significantly higher only at 9:00, moment when HR differences are larger between both groups. However, no big differences throughout the recordings, during night or day, are appreciable.

Table 6.1: SDNN calculated for the 24 hours recordings. Values shown are the inter-subject median and quartiles $[Q_1, Q_3]$.

	S-group	*F-group*	p
SDNN $[ms]$	57 [46-108]	38 [30-58]	0.07

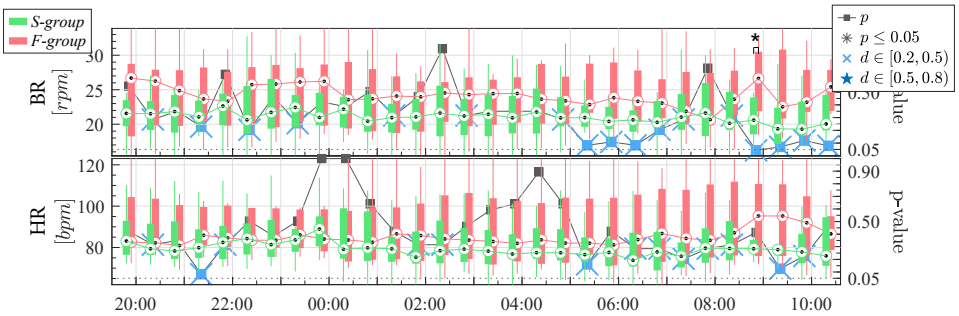

Figure 6.3: Evolution of the common clinical indices for weaning readiness before SBT. The mean BR and mean HR, are represented. Green and Red boxplots represent the patients of the *S-group* and the *F-group*, respectively. The *p-value* comparing each half hour is represented in the right axis, from 0 to 1, and the dotted line represents the $p = 0.05$ threshold. Black asterisks indicate statistical significance with $p \leq 0.05$. Blue stars above *p-values* indicate medium effect size with Cohen's $d \in [0.5, 0.8)$, and blue crosses indicate small effect size with Cohen's $d \in [0.2, 0.5)$.

Figure 6.4 shows the evolution of the HRV parameters. The RMSSD is higher in the *S-group* during the entire recording since midnight, apparently the moment when patients fall asleep. In particular, after waking up, at around 7:00 a.m., significant differences are found. Correspondingly, looking at the $\mathrm{P}^n_{\mathrm{LF}}$, an increment can be seen for the *F-group*, starting at 00:00, compared to the slight decrease for the *S-group*. This increment for the *F-group* can be associated with a sympathetic activation, in view of the sudden increase of the P_{HF} and $\mathrm{P}_{\mathrm{VLF}}$ at the very same time.

Curiously, sudden changes can sometimes be found on the P_{VLF}, especially for the *F-group*. However, much variability exists for the P_{VLF} power, and neither significant differences nor appreciable patterns on the P_{VLF} evolution can be found.

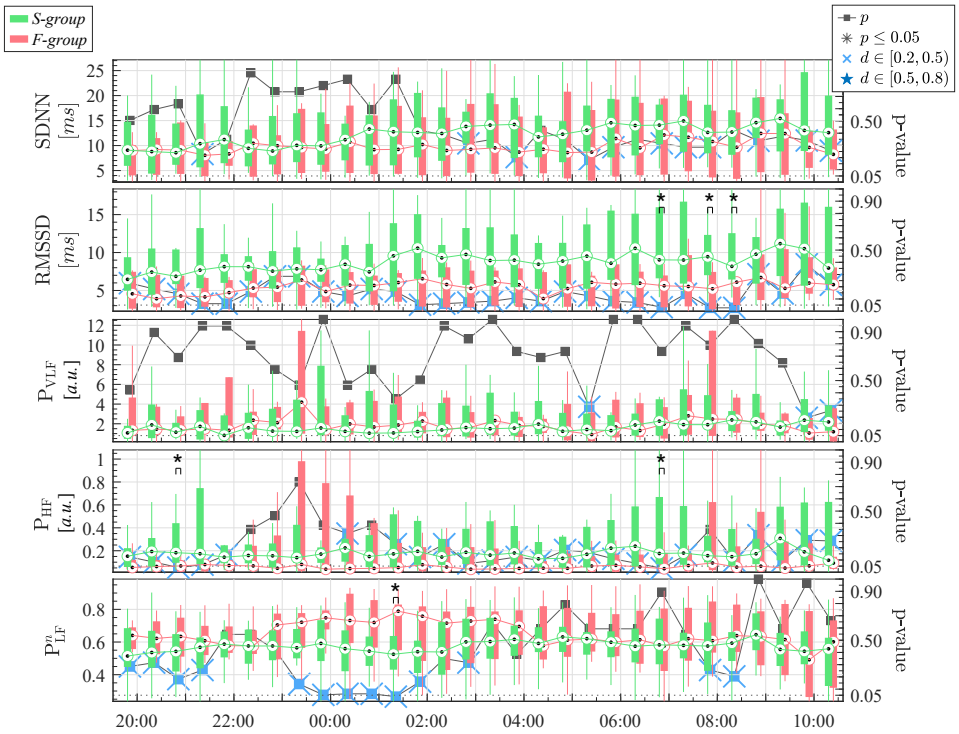

Figure 6.4: Evolution of the HRV indices before SBT. The temporal parameters SDNN and RMSSD, and the frequency parameters, P_{VLF}, P_{HF} and P^n_{LF} are represented. Green and Red boxplots represent the patients of the *S-group* and the *F-group*, respectively. The *p-value* comparing each half hour is represented in the right axis, from 0 to 1, and the dotted line represents the $p = 0.05$ threshold. Black asterisks indicate statistical significance with $p \leq 0.05$. Blue stars above *p-values* indicate medium effect size with Cohen's $d \in [0.5, 0.8)$, and blue crosses indicate small effect size with Cohen's $d \in [0.2, 0.5)$.

The evolution of the CPC estimates is illustrated in Figure 6.5. As said, CPC estimators are computed considering respiration to be the system driving changes in the HRV. Clear differences exist in the CPC mechanism comparing the patients that were successfully weaned, *S-group*, and the patients reintubated or that still needed time in MV, *F-group*.

The $\mathscr{C}^{\mathcal{T}}_{HF}$ index is higher when HRV and respiration have components at the same frequencies, taking into account that these components have

different physiological origin. Differences are significantly higher, particularly at night. The $\mathscr{CE}_{\mathrm{r}\leftrightarrow\mathrm{m}}$ is higher during the night than in the morning before the SBT, especially for the *S-group*. The $\mathscr{P}_{\mathrm{mr}}$ is also higher for the *S-group* than for the *F-group*. Remark that the *p-values* since 9:00 a.m. approximately, right before the SBT, increases abruptly for the three CPC indices. This shows that the differences between the two groups are less substantial at the time right before performing the SBT. Medium effect size ($d = 0.5$) is only present for some comparisons of the CPC parameters (Figure 6.5). For the other parameters (Figures 6.3, 6.4), small effect sizes ($d = 0.2$) or no effect sizes are observed.

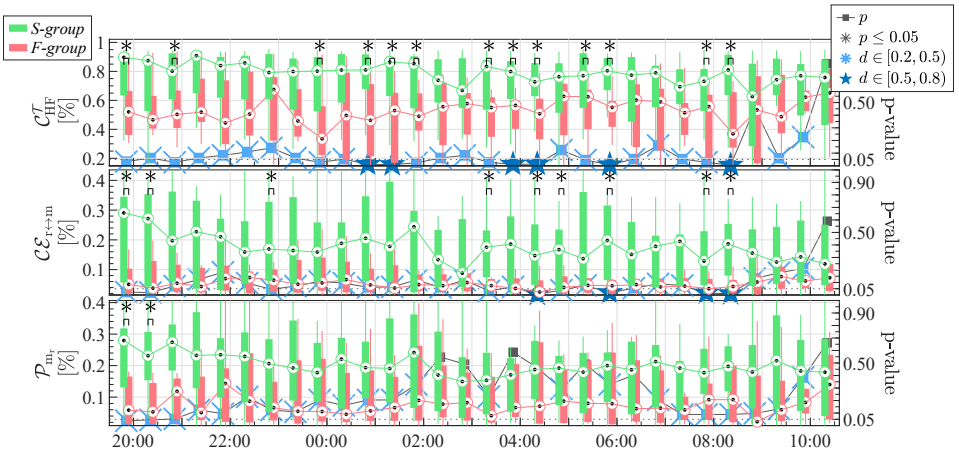

Figure 6.5: Evolution of the CPC estimators before SBT. The CPC parameters $\mathscr{C}^{\mathcal{T}}_{\mathrm{HF}}$,$\mathscr{CE}_{\mathrm{r}\leftrightarrow\mathrm{m}}$ and $\mathscr{P}_{\mathrm{mr}}$, are represented. Green and Red boxplots represent the patients of the *S-group* and the *F-group*, respectively. The *p-value* comparing each half hour is represented in the right axis, from 0 to 1, and the dotted line represents the $p = 0.05$ threshold. Black asterisks indicate statistical significance with $p \leq 0.05$. Blue stars above *p-values* indicate medium effect size with Cohen's $d \in [0.5, 0.8)$, and blue crosses indicate small effect size with Cohen's $d \in [0.2, 0.5)$.

6.4 Discussion

First of all, it should be noted that all patients in the cohort study were deemed ready for weaning. Then, as the SBT determined, some of them were ready, some of them were not, and some of them needed reintubation despite being determined ready by the SBT. Therefore, the prediction of patients ready to undergo SBT has to be improved, in this work for 9 patients: the 2

patients who passed SBT and needed reintubation plus the 7 patients who failed SBT. This suggests that there is some hidden information (e.g., CPC indices) that is not yet taken into account in assessing weaning readiness before SBT.

HRV and CPC have been analysed for a total of 22 patients presumably ready for weaning, in the 24 hours before the SBT. Statistical differences have been found comparing patients who needed reintubation or required more time in MV, the so-called *F-group*, and patients with a successful weaning process, *S-group*. These differences are especially appreciable for the parameters estimating the CPC.

The fact that the CPC changes so much with respect to the *S-group* can be related to a more unstable regulatory system. By monitoring this at night, or continuously, clinicians can obtain additional insight of this stability that can help in making the decision to wean a patient from MV. Then, considering the outcome of the SBT, here it is evaluated if the weaning outcome can be predicted before performing the SBT. Nevertheless, this proposal does not pretend to eliminate the SBT, since SBT is necessary. CPC indices are intended to be used in combination with the current weaning readiness criteria (Criteria in Sec. 4.2.1), to improve the predictive rate of patients ready to undergo the SBT.

Patients of the *S-group* have higher values of SDNN, calculated over 24 hours (see Tab. 6.1). A major component of SDNN is due to a higher variability and day-night difference of the HR. This shows a better adaptability of the heart to changes, for patients actually ready for weaning, *S-group*.

Remark that the SBT is not performed at the same time for all patients. Hence, in order to have all recordings of the patients aligned in time, some segments had to be omitted at the start and end of the recordings for some patients. The average BR, was always above 9 rpm, i.e., 0.15 Hz. However, for some patients, it was above 24 rpm, i.e., 0.4 Hz (see Figure 6.3). The evolution of the currently-used clinical variables, HR and BR, is very similar for both groups. It is clear that these parameters are not giving useful information to predict weaning readiness.

On the contrary, some HRV parameters seem to better discern both groups. The temporal parameter RMSSD has higher values for the *S-group*, in accordance with the fact that this index quantifies parasympathetic

modulation of NN intervals driven by respiration and vagal modulations [20]. These modulations of the vagal activity are also quantified by P_{HF}. Notice that the P_{HF} is much higher for some patients of the *F-group*, around 11 p.m., and around 8:00 a.m. The rest of the time, mainly during sleep at night, P_{HF} is higher for the *S-group*, in agreement with the results of [6]. The time when P_{HF} is higher for the *F-group*, occurs before going to sleep and waking up. However, the P_{VLF} and P^n_{LF} are also higher, so strong vagal modulations are in conflict with strong sympathetic activations.

Nevertheless, Figure 6.4 is striking and summarizes the uncertainty related to the HRV parameters. From these results, the question arises as to what is the validity of HRV indices, since depending on the time of day at which they are measured the results can be totally different. This fact could be attributed to circadian rhythms, having a strong influence on HRV measurements. For example, the P^n_{LF}, commonly used as the standard measure of the sympathovagal balance, is not convenient as a reliable weaning readiness predictor. In fact, it has already been proven that P^n_{LF} is not an appropriate measure of the vagal and sympathetic modulations [21], [22]. On the contrary, and this is favourable, CPC indices seem more appropriate since measurements are quite stable throughout the 24-hour record.

The sudden increase in the P_{HF} for the *F-group*, that could be interpreted as an increase of the vagal activity, is not present in the CPC parameters. These patients are under MV, and for them the frequency content in the HF band may not contain only respiratory information (see Fig. 3.12). These HF components can be a consequence of the non-linear effects of respiration transferred to the HR. These non-linear influences could be mediated by the respiratory pacemaker in the central nervous system [23] through sympathetic modulations [24], and the CPC estimates used in this work are unable to detect them. Further investigation is required using techniques able to take both linear and non-linear effects into account [25], [26].

At this point, results based on the heart-lung interactions, as measured by CPC indices, were encouraging. First, the TFC exhibited illustrative results. The $\mathscr{C}^{\mathcal{T}}_{HF}$, is the CPC estimator which exhibits larger differences between *S-group* and *F-group* patients. These results are also in agreement with those obtained using mutual information, where higher $\mathscr{CE}_{r\leftrightarrow m}$ values were found in the *S-group* than in the *F-group*. Finally, there are also visible

differences looking at the relative power of respiration, $\mathscr{P}_{\mathrm{mr}}$, inserted into the HRV: patients of the *S-group* had a relative power around the 25% of respiration, but those of the *F-group* had it around 5%. Larger effect sizes are obtained for these CPC indices, and most comparisons result in, at least, small effect sizes. These low values of effect size may be associated with the reduced number of patients. Altogether, this illustrates that those patients who are actually ready for weaning, have good levels of CPC and that their ANS is ready to work, in contrast with the patients who did not pass SBT or needed reintubation. Therefore, these CPC estimators are promising as additional indexes to improve the weaning readiness criteria.

Moreover, these differences in the CPC parameters are more evident during sleep than right before the SBT, what could be due to the loop gain. In other words, patients with failed weaning may be experiencing more apnoea events at night, which is directly related to a reduced RSA and higher cardiovascular risk [27], [28]. In fact, the parasympathetic activity is well known to be predominant during sleep at night and, consequently, it is in this moment when the CPC mechanism is stronger.

At this moment, clinicians assess whether patients can perform SBT when they are awake in the morning and conscious. Results suggest that probably, it would be better to check patients' status at night. In fact, less clear differences are found in the morning right before SBT. Maybe, patients generate high levels of stress and anxiety as SBT approaches, and this may alter their biomarkers toward more alert-related values, introducing some physiological bias for interpretation. However, one limitation is that patients in the ICU may not keep similar sleep patterns.

Other works compare the values of the indices obtained right before SBT with the values obtained during and right after SBT and all of them found differences in the respiratory patterns and respiratory variability parameters [29], [30], or in the HRV parameters [6], [16], [31], [32]. Remark that the SBT lasts 30 minutes, a really stressing stage for the patient, when they are proved to spontaneous breathing. This protocol represents a challenge, and some parameters could show greater statistical differences in that situation than in "basal" or "resting" conditions. That is the very important difference of the present study with the state-of-the-art; here, the indices and evolution of the patients are obtained only before the SBT. The

fact that the prediction of weaning readiness can be improved, could only have been revealed by long-term analysis.

From previous data in the literature, variability may be more discriminant when measured during SBT. In fact, it would have been interesting to add values during SBT, although it is a different approach than the proposed. However, the main limitation is that CPC indices cannot be calculated during SBT since patients are disconnected from the ventilator and the respiratory airflow signal is not available. Instead, a surrogate signal such as impedance pneumography, diaphragmatic effort or even an ECG-derived respiratory signal could be used, but this work needs to be developed.

In [33], they stress the importance of the P_{VLF} power in the weaning scenario. The P_{VLF} power, partially related with the circadian rhythms [20], could provide useful information of the neurohumoral regulatory mechanism [34]. On the contrary, here it is illustrated that the P_{VLF} power is not so relevant in the analysis of the 24 hours prior to SBT. Nevertheless, some patients in this MV and ICU context showed strong characteristic VLF oscillations, possibly also related with sleep disorders, that must be further studied. These sudden changes cause non-stationarity, and this is the reason why 3-minute sliding windows and TF analysis are used to calculate the indices.

It should be noted that the estimation of CPC is a new technique, and even less any previous studies have investigated CPC during automated ventilation. Further studies should be performed including controlled MV modes, since this would include the whole amount of patients in MV, and it could be obtained a complete knowledge of the CPC regulation mechanisms. Perhaps, in controlled MV modes, it is the ventilator the one controlling respiration –not the ANS–, and the HRV would be the driving system, since the ventilator would be the one regulating respiration externally. In this work, the CPC is computed to measure and characterize the RSA function. However, the mechanisms responsible for RSA are still a matter of debate, but it is known to be affected by direct parasympathetic modulation, different reflexes such as baroreflex and chemoreflex, as well as mechanical effect of respiration. Then, there is a clear connection between blood volume and RSA and other predictors could also give estimates of the ANS status. Additionally to investigation the role of BRS, as done in Chapter 5, previous

works analysed predictors of fluid responsiveness in mechanically ventilated adults [35], that could also be helpful in this context.

The computational cost for obtaining the CPC indices is low, and it may be obtained in real time in the same way as the standard clinical parameters. Therefore, these algorithms can be implemented in the ICU monitors, and the CPC status could be assessed continuously, together with the well-known clinical variables. Additionally, other CPC estimators were also explored in a preliminary analysis of the study. However, the indices with best performance were the ones also computed here, namely $\mathscr{P}_{\mathrm{mr}}$, $\mathscr{CE}_{\mathrm{r}\leftrightarrow\mathrm{m}}$ and $\mathscr{C}^{\mathcal{T}}_{\mathrm{HF}}$. Interestingly, the study in [36] analyses the best methods for CPC estimation in a simulation study, and concludes that the same three parameters used in this work are the best estimators for CPC assessment.

The clinical utility of this work, and future studies, is that if the CPC is actually proven to predict weaning failure, it might be incorporated as screening guidance of patients ready to undergo SBT. Certainly, there is future work to state how much these CPC indices can improve prediction of weaning readiness. However, this is a preliminary study, which needs to be prospectively validated with a larger cohort. In fact, we still need to report specificity and sensitivity to obtain the thresholds of CPC for which an improvement in accuracy is defined.

In other words, CPC could be assessed before SBT, in a multimodal index combined with current parameters to reinforce the prediction of patients ready to undergo SBT. CPC indices may be of clinical interest since they could help to reduce weaning failure rates and the very adverse effects associated with reintubation, to thereby result in better clinical outcomes.

Finally, it must be kept in mind that patients in the ICU are admitted from very diverse diagnostics. Taking this into account, two patients with the same characteristics and similar evolution may get different outcomes. Hence, sometimes, a patient who does not meet the readiness criteria can be also successfully weaned, and viceversa [37]. This is why clinicians take the criteria for weaning readiness and SBT performance as one among several considerations rather than rigid requirements. In fact, the screening criteria for weaning readiness and SBT are not homogeneous in all sites, and this is a limitation. Such uncertainty can be reduced by implementing new research and technologies to daily clinical practice [38], [39], and this study is other

step forward in the field of predictive precision medicine, that exploits the capabilities of the CPC estimates.

6.5 Conclusions

This second study focused on a 24-hour analysis prior to SBT, evaluating CPC indices to enhance the prediction of weaning readiness. The existing information available to clinicians in the ICU is insufficient for determining weaning readiness, as evidenced by the 15-20% of patients experiencing SBT failure or requiring reintubation. Interestingly, none of the current clinical criteria for weaning readiness showed significant differences between patients who were ready for weaning and those who were not. However, higher CPC values, evaluated through variables $\mathscr{CT}_{\mathrm{HF}}$, $\mathscr{CE}_{\mathrm{r}\leftrightarrow\mathrm{m}}$, and $\mathscr{P}_{\mathrm{mr}}$, were observed in successfully weaned patients, particularly during nighttime.

This study builds on the insights gained from the first study, which identified BRS as a potential predictor for weaning readiness. The findings of the second study underscore the importance of incorporating a broader range of physiological biomarkers, like CPC indices, into the assessment of weaning readiness, and importantly, the use of long-term recordings to monitor the evolution of the biomarkers. By doing so, the predictive accuracy for weaning outcomes could be significantly improved. The combined insights from both studies suggest the need for a multifaceted approach to assess weaning readiness in the ICU, considering signal processing indices, like these based on CPC.

Bibliography of Part II

[1] C. de Haro, J. López-Aguilar, R. Magrans, J. Montanya, S. Fernández-Gonzalo, M. Turon, G. Gomà, E. Chacón, G. M. Albaiceta, R. Fernández, *et al.*, "Double cycling during mechanical ventilation: Frequency, mechanisms, and physiologic implications",
Critical care medicine, vol. 46, no. 9, pp. 1385–1392, 2018.

[2] L. Blanch, B. Sales, J. Montanya, U. Lucangelo, O. Garcia-Esquirol, A. Villagra, E. Chacon, A. Estruga, M. Borelli, M. J. Burgueño, *et al.*, "Validation of the better care® system to detect ineffective efforts during expiration in mechanically ventilated patients: A pilot study",
Intensive care medicine, vol. 38, no. 5, pp. 772–780, 2012.

[3] Ó. Peñuelas, A. W. Thille, and A. Esteban, "Discontinuation of ventilatory support: New solutions to old dilemmas",
Current opinion in critical care, vol. 21, no. 1, pp. 74–81, 2015.

[4] G. Hernández, C. Vaquero, P. González, C. Subira, F. Frutos-Vivar, G. Rialp, C. Laborda, L. Colinas, R. Cuena, and R. Fernández, "Effect of postextubation high-flow nasal cannula vs conventional oxygen therapy on reintubation in low-risk patients: A randomized clinical trial",
Jama, vol. 315, no. 13, pp. 1354–1361, 2016.

[5] C. Subirà, G. Hernández, A. Vázquez, R. Rodríguez-García, A. González-Castro, C. García, O. Rubio, L. Ventura, A. López, M.-C. de la Torre, *et al.*, "Effect of pressure support vs T-piece ventilation strategies during spontaneous breathing trials on successful extubation among patients receiving mechanical ventilation: A randomized clinical trial",
Jama, vol. 321, no. 22, pp. 2175–2182, 2019.

[6] Y.-J. Chen, S.-L. Hwang, C.-R. Li, C.-C. Yang, K.-L. Huang, C.-Y. Lin, and C.-Y. Lee, "Vagal withdrawal and psychological distress during ventilator weaning and the related outcomes",
Journal of Psychosomatic Research, vol. 101, 2017.

[7] G. D. Pinna *et al.*, "Different estimation methods of spontaneous baroreflex sensitivity have different predictive value in heart failure patients",
J Hypertension, vol. 35, no. 8, 2017.

[8] M. T. La Rovere *et al.*, "Baroreflex sensitivity: Measurement and clinical implications",
Ann N.Inv. Electrocard., vol. 13, no. 2, 2008.

[9] M. Orini, R. Bailón, L. T. Mainardi, P. Laguna, and P. Flandrin, "Characterization of dynamic interactions between cardiovascular signals by time-frequency coherence",
IEEE transactions on biomedical engineering, vol. 59, no. 3, 2011.

[10] J. Lázaro, E. Gil, M. Orini, P. Laguna, and R. Bailón, "Baroreflex sensitivity measured by pulse photoplethysmography",
Frontiers in Neuroscience, vol. 13, p. 339, 2019.

[11] A. Müller *et al.*, "Bivariate phase-rectified signal averaging for assessment of spontaneous baroreflex sensitivity: Normalization of the results",
J Electrocard., vol. 45, no. 1, 2012.

[12] A. Y. Schumann, J. W. Kantelhardt, A. Bauer, and G. Schmidt, "Bivariate phase-rectified signal averaging",
Physica A: Statistical Mechanics and its Applications, vol. 387, no. 21, pp. 5091–5100, 2008.

[13] R. Sassi *et al.*,
"A methodological assessment of phase-rectified signal averaging through simulated beat-to-beat interval time series",
In *CinC*,
2014.

[14] H. Schmidt, D. Hoyer, J. Wilhelm, G. Söffker, K. Heinroth, K. Hottenrott, S. M. Said, M. Buerke, U. Müller-Werdan, and K. Werdan, "The alteration of autonomic function in multiple organ dysfunction syndrome",
Critical care clinics, vol. 24, no. 1, pp. 149–163, 2008.

[15] L. Wieske, D. C. P. Yin, C. Verhamme, M. J. Schultz, I. N. van Schaik, and J. Horn, "Autonomic dysfunction in ICU-acquired weakness: A prospective observational pilot study",
Intensive care medicine, vol. 39, no. 9, pp. 1610–1617, 2013.

[16] H.-N. Shen, L.-Y. Lin, K.-Y. Chen, P.-H. Kuo, C.-J. Yu, H.-D. Wu, and P.-C. Yang, "Changes of heart rate variability during ventilator weaning",
Chest, vol. 123, no. 4, 2003.

[17] F. Yasuma and J.-i. Hayano, "Respiratory sinus arrhythmia: Why does the heartbeat synchronize with respiratory rhythm?",
Chest, vol. 125, no. 2, pp. 683–690, 2004.

[18] T. E. Dick, Y.-H. Hsieh, R. R. Dhingra, D. M. Baekey, R. F. Galán, E. Wehrwein, and K. F. Morris,
"Cardiorespiratory coupling: Common rhythms in cardiac, sympathetic, and respiratory activities",
In *Progress in brain research*,
Vol. 209,
Elsevier, 2014,
Pp. 191–205.

[19] M. Tomczak and E. Tomczak, "The need to report effect size estimates revisited. An overview of some recommended measures of effect size.",
Trends in Sport Sciences, vol. 21, no. 1, 2014.

[20] F. Shaffer and J. Ginsberg, "An overview of heart rate variability metrics and norms",
Frontiers in public health, vol. 5, p. 258, 2017.

[21] G. E. Billman, "The LF/HF ratio does not accurately measure cardiac sympatho-vagal balance",
Frontiers in physiology, vol. 4, p. 26, 2013.

[22] C. Varon, J. Lázaro, J. Bolea, A. Hernando, J. Aguiló, E. Gil, S. Van Huffel, and R. Bailón, "Unconstrained estimation of HRV indices after removing respiratory influences from heart rate",
IEEE journal of biomedical and health informatics, vol. 23, no. 6, pp. 2386–2397, 2018.

[23] F. Peña,
"Contribution of pacemaker neurons to respiratory rhythms generation in vitro",
In *Integration in Respiratory Control*,
Springer, 2008,
Pp. 114–118.

[24] J. P. Saul, R. D. Berger, P. Albrecht, S. Stein, M. H. Chen, and R. Cohen, "Transfer function analysis of the circulation: Unique insights into cardiovascular regulation",
American Journal of Physiology-Heart and Circulatory Physiology, vol. 261, no. 4, H1231–H1245, 1991.

[25] S. Kontaxis, J. Lázaro, E. Gil, P. Laguna, and R. Bailón, "Assessment of quadratic nonlinear cardiorespiratory couplings during tilt-table test by means of real wavelet biphase",
IEEE Transactions on Biomedical Engineering, vol. 66, no. 1, pp. 187–198, 2018.

[26] C. Varon, D. Hendrikx, J. Bolea, P. Laguna, and R. Bailón,
"Quantification of linear and nonlinear cardiorespiratory interactions under autonomic nervous system blockade",
In *2019 Computing in Cardiology (CinC)*,
IEEE,
2019,
Page–1.

[27] C. Varon, A. Caicedo, D. Testelmans, B. Buyse, and S. Van Huffel, "A novel algorithm for the automatic detection of sleep apnea from single-lead ECG",
IEEE Transactions on Biomedical Engineering, vol. 62, no. 9, pp. 2269–2278, 2015.

[28] J. Milagro, M. Deviaene, E. Gil, J. Lázaro, B. Buyse, D. Testelmans, P. Borzée, R. Willems, S. Van Huffel, R. Bailón, *et al.*, "Autonomic dysfunction increases cardiovascular risk in the presence of sleep apnea",
Frontiers in Physiology, vol. 10, p. 620, 2019.

[29] K. L. Yang and M. J. Tobin, "A prospective study of indexes predicting the outcome of trials of weaning from mechanical ventilation",
New England Journal of Medicine, vol. 324, no. 21, pp. 1445–1450, 1991.

[30] M.-Y. Bien, S.-S. Hseu, H.-W. Yien, B. I.-T. Kuo, Y.-T. Lin, J.-H. Wang, and Y. R. Kou, "Breathing pattern variability: A weaning predictor in postoperative patients recovering from systemic inflammatory response syndrome",
Intensive care medicine, vol. 30, no. 2, pp. 241–247, 2004.

[31] C.-T. Huang, Y.-J. Tsai, J.-W. Lin, S.-Y. Ruan, H.-D. Wu, and C.-J. Yu, "Application of heart-rate variability in patients undergoing weaning from mechanical ventilation",
Critical care, vol. 18, no. 1, R21, 2014.

[32] A. Arcentales, P. Caminal, I. Diaz, S. Benito, and B. Giraldo, "Classification of patients undergoing weaning from mechanical ventilation using the coherence between heart rate variability and respiratory flow signal",
Physiological measurement, vol. 36, no. 7, p. 1439, 2015.

[33] V. Krasteva, M. Matveev, I. Jekova, and G. Georgiev,
"Heart rate variability analysis during weaning from mechanical ventilation: Models for prediction of the weaning trial outcome",
In *2018 Computing in Cardiology Conference (CinC)*,
IEEE,
Vol. 45, 2018,
Pp. 1–4.

[34] S. K. Frazier, D. K. Moser, R. Schlanger, J. Widener, L. Pender, and K. S. Stone, "Autonomic tone in medical intensive care patients receiving mechanical ventilation and during a CPAP weaning trial",
Biological Research for Nursing, vol. 9, no. 4, pp. 301–310, 2008.

[35] C. Sandroni, F. Cavallaro, C. Marano, C. Falcone, P. De Santis, and M. Antonelli, "Accuracy of plethysmographic indices as predictors of fluid responsiveness in mechanically ventilated adults: A systematic review and meta-analysis",
Intensive care medicine, vol. 38, no. 9, pp. 1429–1437, 2012.

[36] J. F. Morales, J. Moeyersons, P. Armañac, M. Orini, L. Faes, S. Overeem, M. Van Gilst, H. van Dijk, S. Van Huffel, R. Bailón, *et al.*, "Model-based evaluation of methods for respiratory sinus arrhythmia estimation.",
IEEE Trans. Biomed. Eng., vol. 68, no. 6, pp. 1882–1893, 2021.

[37] E. Ely, A. Baker, G. Evans, and E. Haponik, "The prognostic significance of passing a daily screen of weaning parameters",
Intensive care medicine, vol. 25, no. 6, pp. 581–587, 1999.

[38] Y. Marchuk, R. Magrans, B. Sales, J. Montanya, J. López-Aguilar, C. De Haro, G. Gomà, C. Subirà, R. Fernández, R. M. Kacmarek, *et al.*, "Predicting patient-ventilator asynchronies with hidden markov models",
Scientific reports, vol. 8, no. 1, pp. 1–7, 2018.

[39] L. Sarlabous, J. Aquino-Esperanza, R. Magrans, C. de Haro, J. López-Aguilar, C. Subirà, M. Batlle, M. Rué, G. Gomà, A. Ochagavia, *et al.*, "Development and validation of a sample entropy-based method to identify complex patient-ventilator interactions during mechanical ventilation",
Scientific reports, vol. 10, no. 1, pp. 1–12, 2020.

Part III

Cardiovascular Signal Processing in Sleep Apnea Patients

Chapter 7

Context, Motivation and Data for Part III

7.1 Context

Part III of the thesis explores cardiovascular signal processing techniques for the assessment and stratification of pediatric patients with OSA. As mentioned in Part I, despite its prevalence affecting around 5.7% of children, OSA often remains underdiagnosed, impacting a variety of functions ranging from physiological to cognitive. The condition, characterized by respiratory pauses, snoring, and daytime somnolence, can lead to severe cardiovascular and cerebrovascular consequences.

The gold standard for the diagnosis of OSA typically relies on overnight PSG, despite being time-consuming, expensive and requiring specialized personnel. Consequently, many pediatric patients are only diagnosed when their OSA condition has progressed to a severe stage. Given these challenges, there is a clear need for more accessible and convenient diagnostic tools to simplify the process, that help to obtain a prompt diagnosis of OSA.

This part of the thesis is structured into three primary studies, each exploring different methodologies and analytical techniques in cardiovascular

signal processing to improve the understanding, stratification, and severity assessment of OSA, as well as the associated Cardiovascular Risk (CVR) in the pediatric population:

- **Study One**: Chapter 8 investigates HRV during apneic episodes compared to normal breathing periods in pediatric OSA.
- **Study Two**: Chapter 9 explores the application of CPC as a diagnostic and characterization tool in pediatric OSA.
- **Study Three**: Chapter 10 examines the definition of Metabolic Syndrome (MetS) as an index for CVR in children with OSA, and its causal role in the development of OSA. In order to have a reference of CVR to compare with the metrics derived from signal processing analysis, like HRV or CPC, first we need to validate MetS as index of CVR in pediatric patients with OSA, for what we propose the CMA.

Through these studies, this part aims to contribute significantly to the field by introducing innovative methods for assessing and managing pediatric OSA. Utilizing the good quality PSG data from approximately 400 pediatric patients provided by the Childhood Adenotonsillectomy Trial (CHAT) study. This comprehensive dataset not only encompasses biosignals but also includes demographic, clinical, metabolic, and outcome information, providing a basis to test and validate our hypotheses. Detailed description of the study and its utilization in my research will be elaborated in the following sections.

7.2 Sleep Data

The CHAT sleep study was a multicentric prospective randomized trial, designed to evaluate the efficacy of early Adenotonsillectomy (eAT) surgery versus a strategy of Watchful Waiting with Supportive Care (WWSC) for pediatric OSA treatment [1]. The rationale, design, and primary outcomes for the CHAT study have been previously reported [1]. All data are publicly available at `https://sleepdata.org/datasets/chat`.

The study recruited prepubertal children between 5 to 10 years of age with OSA symptoms, who were scheduled for a baseline nocturnal PSG in a clinical laboratory. After allocation to the corresponding treatment strategy, eAT or WWSC, children completed a follow-up PSG 7 months later. The legal caretakers of each patient provided the informed consent, and the

CHAT study was judged ethical and approved by all relevant independent review boards. For more details on the protocol, inclusion-exclusion criteria and ethical considerations, see [1].

Figure 7.1: CHAT Study Protocol. Pediatric patients with OSA underwent a baseline PSG, during which clinical and demographic information was gathered for OSA diagnosis. Participants then received randomized treatment, either eAT or WWSC. Follow-up PSG was conducted 7 months later to assess the outcomes of the treatment.

The study investigators relied on the Apnea-Hypopnea Index (AHI) to establish OSA severity according to the American Academy of Sleep Medicine rules [1]. Children were assigned to one of four common severity groups for pediatric OSA, as follows: no OSA (AHI $<$ 1 events per hour of sleep, e/h), mild OSA (1 $\leq$ AHI $<$ 5 e/h), moderate OSA (5 $\leq$ AHI $<$ 10 e/h), and severe OSA (AHI $\geq$ 10 e/h). Due to the study design, there was no patient with no OSA at baseline.

To evaluate the resolution of OSA in pediatric patients, regardless of the treatment received, two approaches were utilized. Firstly, following the original CHAT study criteria, OSA resolution was considered for subjects who, at follow-up, exhibited an obstructive-AHI $\leq$ 2 e/h and an obstructive-Apnea Index (AI) $\leq$ 1 e/h [1]. Under this criterion, 252 subjects were categorized in the resolution group, while 152 subjects were classified as not having resolved their OSA. Secondly, recognizing the significance of central apneas, a more stringent criterion for disease resolution was applied based on the overall AHI and AI. In this case, children who presented an AHI $\leq$ 2 e/h and an AI $\leq$ 1 e/h at follow-up were considered to have resolved OSA. According to these parameters, 157 subjects were classified in the resolution group, compared to 247 subjects who did not resolve their OSA.

In each of the following Chapter 8, 9, and 10, patient exclusion was based on specific criteria to ensure the reliability and validity of the findings. For the first study, focusing on HRV analysis (Chapter 8), 311 patients were

included, contingent upon the quality of their ECG signal to derive a reliable $m(t)$ signal. Exclusion criteria were:

- ECG signals sampled at rates lower than 250Hz.
- ECG signal coverage less than 75% of the overnight PSG recording.
- Percentage of ectopic beats and miss-detections exceeding 10%.

In the second and third studies (Chapters 9 and 10), patients with reliable HRV and respiratory signals but lacking necessary clinical and demographic information for defining MetS were excluded. This left 255 patients with reliable HRV signals at both baseline and follow-up, possessing all requisite information for defining MetS in both.

Chapter 8

Heart Rate Variability during OSA Episodes in Pediatric Patients

8.1 Introduction

Previous studies using PSG have revealed alterations in the ANS during sleep in patients with moderate or severe OSA compared to healthy control subjects [2]. The physiological response to apnea usually includes a bradycardia-tachycardia pattern (as shown in Fig. 2.10), ending with a significant increase in SNS activity [2]. Persistent HR and respiratory variations due to repeated apneic episodes are linked with a higher risk of cardiovascular morbidity in both adults and children [1]. However, most studies have focused

on sleep stage differences and overlooked the effects of apnea presence or absence on HRV values [3], [4], or have even directly excluded those segments containing apneic episodes for HRV analysis [5]–[7].

In this study, we aim to characterize and compare HRV metrics in pediatric patients with symptoms of OSA, focusing on HRV average values during apneic events, normal sleep breathing, and full night recordings. This approach is designed to discern whether the sympathetic dominance observed in OSA, as reported in previous studies, is merely an episodic response to apneic events or a sustained condition throughout the night, what would be indicative either of an ANS imbalance or cardiovascular disease. Additionally, we explore differences in three newly defined spectral bands of HRV specific to pediatric OSA [8], which have been linked to changes in OSA severity and resolution, providing new insights into the cardiovascular implications of the disorder.

8.2 Materials and Methods

8.2.1 Sleep Data for HRV analysis

In this study, I used the dataset explained in Sec. 7.2. However, this work only includes the data from baseline PSG recordings. The PSG data encompasses the ECG, and thoracic and abdominal respiratory signals [9]. As mentioned in Sec. 7.2, the dataset for this study comprised 311 patients, out of the whole database available, who had a sufficient quality of their ECG signal to derive a reliable $m(t)$ signal. The AHI was employed to determine the severity of OSA [9], categorizing it into mild (N=133), moderate (N=105), and severe (N=76), depending on their AHI.

8.2.2 Time-Frequency Analysis of HRV

The frequency domain parameters are calculated using the TF distribution belonging to the Cohen's class [10], as previously detailed in Sec. 3.3.4. See Fig. 8.1 for a representation of the frequency parameters' evolution derived from HRV, using TF analysis.

As introduced in previous Sec. 1.4.2, due to the higher BR observed in children, sometimes exceeding 24 breaths per minute (0.4 Hz), it is essential

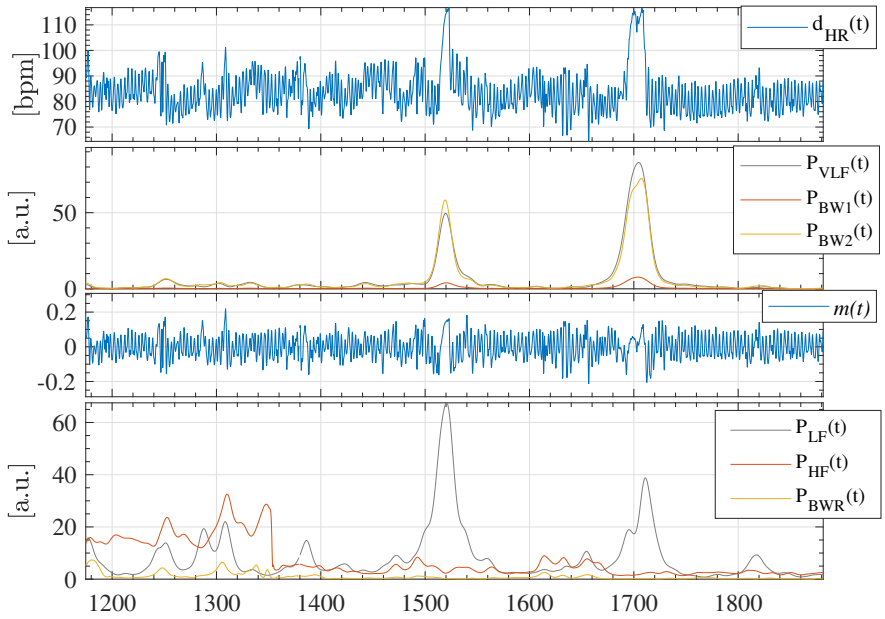

Figure 8.1: TF analysis of a HRV signal, and continuous power signals obtained. Two labeled apnea/hypopnea episodes occur around seconds 1550 and 1700. See Fig. 3.9 for the methodology to compute the power in each spectral band.

to perform a respiratory-guided HRV analysis. To do this, it is necessary to first estimate the instantaneous BR, $\hat{f}_r(n)$. This is obtained from thoracic and abdominal respiratory signals using a signal peak-conditioned spectral averaging method [11], explained in Sec 3.1.2. An illustrative example of this algorithm is shown in Fig. 3.2.

8.2.3 Effects of Apnea on HRV

To analyze the effect of apneas on HRV, each of the annotated apnea and hypopnea segments is identified. As mentioned, the frequency power of each HRV band is continuously obtained at 4 Hz, throughout the overnight recordings. Therefore, from the continuous power signals (see Fig. 8.1), a separate analysis can be easily performed for the segments of normal breathing during sleep and for the apnea episodes. It is worth noting that, for each apneic event, the 5 seconds prior to the start of the apnea and the 15 seconds after its completion are also included, thus encompassing the compensatory/recovery pattern of tachycardia following the apnea episode [8], [12].

8.2.4 Statistical Analysis

For each patient, the median value of each of the HRV metrics is obtained from the complete recordings, during the apnea events, and after excluding them (see Fig. 8.2). Finally, for each patient, a non-parametric rank-sum test is applied to evaluate the observable differences (p-value ¡0.01) between the values obtained in the complete recordings, compared to the values obtained both in the apnea events and in the average nightly recordings after excluding the apnea events.

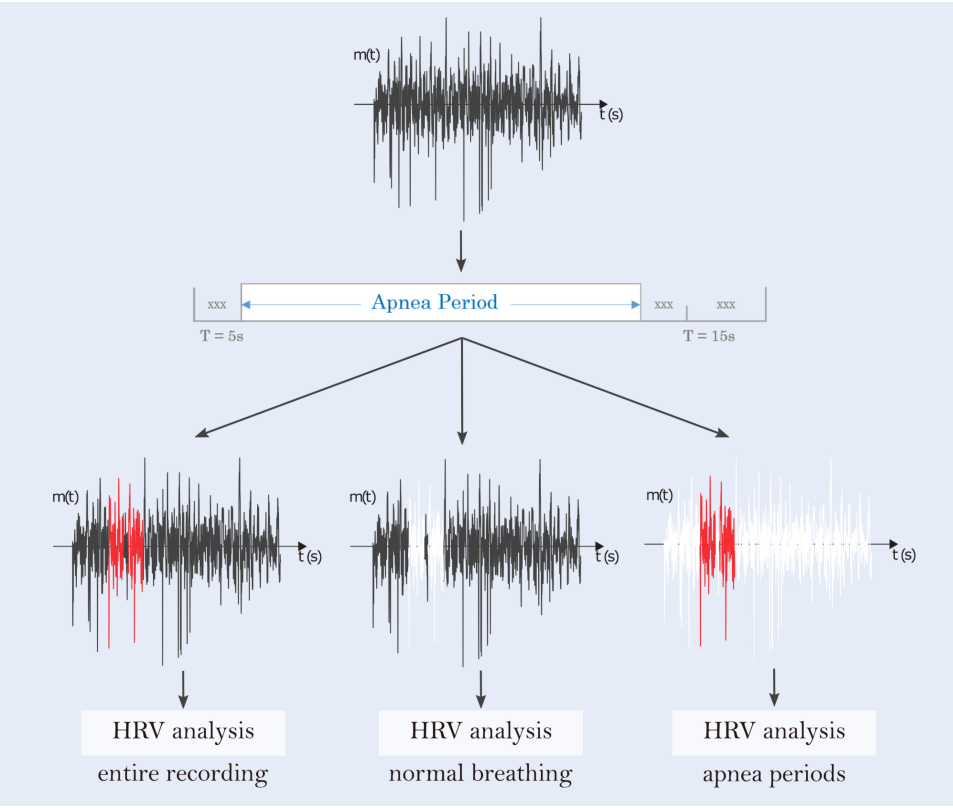

Figure 8.2: Flowchart of the data analysis performed for each patient. The apneic episode are represented in red. Three different HRV analyses were performed: one including the complete recordings, one excluding the apneic episodes (reflecting the HRV status during normal breathing periods), and one including only the apneic episode's periods (reflecting the response of HRV to apneas).

8.3 Results and Discussion

In our study, we assessed the effects of sleep apnea events on HRV by isolating apnea episodes and then separately analyzing normal breathing during sleep. The average values obtained are displayed in Tab. 8.3. Clear significant differences (p-value < 0.01) were observed in all metrics except for RMSSD and P_{HF}. These marked differences, previously unreported, underscore the importance of analyzing apnea events and normal sleep breathing separately. Doing so, ensures accurate physiological interpretation, as the patient experiences acute stress during apnea, while they are relaxed during normal breathing.

Table 8.3: Average median values for HRV metrics of the 311 patients, calculated separately for normal breathing, apnea episodes, and complete records. On the far right, the result of the paired Friedman statistical analysis is shown, with '**' mark in case of significance (p-value ¡ 0.01). Units: 1[b.p.m]; 2[ms]; 3[a.u.].

(N=311)	**Normal Breathing**			**Apnea Episodes**			**Complete Recording**			**p-value**
	mild	moderate	severe	mild	moderate	severe	mild	moderate	severe	Friedman Test
% time	99%	98%	95%	1%	2%	5%	100%	100%	100%	
mHR[1]	87	90	92	89	90	92	87	90	92	**
SDNN[2]	104	108	89	102	96	97	105	109	91	**
RMSSD[2]	77	78	58	60	56	60	76	77	58	.
$P(\Omega_{VLF})^3$	1,81	1,77	1,82	11,92	11,10	11,36	1,89	1,93	2,25	**
$P(\Omega_{LF})^3$	7,70	6,86	6,93	33,63	34,30	36,16	7,90	7,27	8,07	**
$P(\Omega_{HF})^3$	24,78	23,38	25,34	10,64	10,31	13,02	24,56	22,96	24,47	.
$P(\Omega_{B1})^3$	0,17	0,17	0,17	1,11	1,02	1,03	0,18	0,18	0,21	**
$P(\Omega_{B2})^3$	2,00	1,94	2,00	13,31	12,65	13,25	2,08	2,10	2,45	**
$P(\Omega_{BR})^3$	13,49	12,87	13,83	1,32	1,17	1,84	13,17	12,28	12,25	**

One specific finding was that the Ω_{B2} band was closely related to the presence of apnea [8]. The sudden increase of P_{HF}, P_{VLF}, and P_{LF} during apnea can be attributed to the characteristic bradycardia-tachycardia pattern during apnea events. On average, differences may not be noticeable when comparing normal breathing values to complete record values. Yet, a paired statistical analysis was performed, revealing intrinsic differences within each patient.

Notably, P_{HF} and its related RMSSD did not show significant differences. The interpretation of these indices during apneas is debatable. There are both methodological and physiological concerns, especially since these parameters

are tied to breathing and parasympathetic activity, which contrasts with what happens during an apnea event.

Prior research on HRV in pediatric OSA has typically involved whole-night analyses or the exclusion of apneic events [5]–[7], which may not fully represent the autonomic dysregulation occurring during different sleep stages [5], or in response to individual apneic episodes. This study emphasizes the importance of analyzing HRV metrics separately for apneic and normal breathing intervals and considering sleep stage segmentation to capture the episodic nature of SNS activation. This analysis suggests that the increase in SNS activity in OSA patients is primarily a response to individual apneic episodes, not a sustained activity throughout the night. As the amount of apneic episodes rises with OSA severity, so does the overall SNS activity in overnight recordings. This episodic nature of SNS activation highlights the necessity of including apneic events in HRV analyses. Previous studies that excluded these events or averaged HRV over the entire night might miss these crucial, transient changes. These findings are essential for understanding the dynamic autonomic changes in OSA and interpreting HRV metrics accurately in this context.

This study and the work of Martin-Montero et al. in [8] underscore the importance of segmenting HRV data by apneic events. The approach of categorizing 10-minute ECG segments in [8] also revealed significant HRV changes, particularly in Non REM sleep (NREM) stages with increasing apneic events. These findings, combined with our observation of episodic SNS activation, highlight the necessity of detailed HRV analysis for understanding OSA's impact on autonomic function. This collective research advances the precise assessment of disease severity and sleep stage classification in pediatric OSA patients.

8.4 Conclusions

This study analyzing HRV in pediatric patients with OSA reveals significant differences in HRV metrics across complete analyses, during specific apnea episodes with increased sympathetic activity, and during normal breathing in sleep. It appears that power in the HF band and RMSSD may not be reliable indicators during apnea events due to the fluctuating nature of SNS

activity. Besides, the SNS response is typically reactive to apnea episodes rather than consistently elevated.

Chapter 9

Characterization of Cardiopulmonary Coupling in Pediatric Patients with Obstructive Sleep Apnea

9.1 Introduction

In Chapter 9, the research focuses on characterizing CPC in pediatric patients with OSA. The study examines CPC across different sleep stages and in groups categorized by OSA severity. The hypothesis driving this research is that higher CPC levels might indicate better sleep health and overall cardiovascular health in children with OSA.

Previous studies in adults have highlighted CPC's potential as a biomarker

for sleep quality [13]–[15], through spectral coherence analysis, and desaturation severity in OSA [16], yet research in pediatric OSA is limited. In adults with OSA, reduced CPC has been observed compared to healthy individuals, with low-frequency power dominance linked to abnormal sleep-disordered breathing behaviors [13]. Interestingly, previous research has also suggested an increased CPC in sleep apnea, possibly linked to the heightened autonomic stress induced by the disease [13], [15], [17], while high CPC values in the HF band are generally associated with healthy RSA and deep sleep stages [13], [18]. Other studies have shown that aging may lead to a reduced autonomic modulation during wake, S2, and Rapid Eye Movement sleep (REM) sleep in older adults with OSA, when compared to younger individuals [19].

This chapter aims to characterize CPC in children with OSA and explore its diagnostic potential for pediatric OSA. The study hypothesizes that as OSA severity increases, CPC decreases, suggesting an imbalance in autonomic regulation. It is anticipated that reductions in CPC in the high-frequency band will be more pronounced in pediatric OSA patients compared to those who have recovered. This investigation seeks to establish CPC as a non-invasive, effective diagnostic and monitoring tool for pediatric OSA, bridging a gap in current research and offering new insights into this condition.

In this study, CPC is assessed through the analysis of HRV and respiratory signals, commonly recorded during overnight PSG. The methodology for estimating CPC using TFC is an integral part of this thesis and is elaborated in Sec. 3.4.1.

9.2 Materials and Methods

9.2.1 Sleep Data for CPC analysis

This section utilizes the dataset referenced in Section 7.2. The dataset includes data from the PSG recordings, encompassing ECG, and thoracic respiratory signals [1]. In addition for the present study, the sleep stage data is also extracted. These sleep stages were categorized into 30-second epochs by experienced sleep specialists.

The initial focus of this analysis was to establish potential correlations between CPC levels and metabolic biomarkers. Therefore, the subset of pa-

tients chosen for this study were those with comprehensive cardiometabolic data available. As explained in previous chapter 7.2, a total of 255 participants had, at baseline and at followup, reliable HRV data and complete cardiometabolic profiles, which included demographic information (such as age, sex, ethnicity), clinical data (including weight, height, body mass index, systolic and diastolic blood pressure), and metabolic markers (like fasting glucose, HDL, LDL, triglycerides).

The distribution of patients according to OSA severity is shown in Tab. 9.1. OSA resolution was considered for those patients with both AHI $\leq$ 2 e/h and AI $\leq$ 1 e/h at follow-up [8] (103 patients resolved vs. 152 unresolved). Note that this criterion considers both obstructive and central apneas, thus defining stringent rules for disease resolution than the criterion proposed in the original CHAT study [1]. Owing to the study design, all subjects at baseline were diagnosed as suffering from pediatric OSA (Tab. 9.1), such that at baseline none of the subjects could be considered with OSA Resolution (AHI $\leq$ 2 e/h and AI $\leq$ 1 e/h) or No OSA (AHI $\leq$ 1 e/h).

Table 9.1: OSA severity definition and prevalence at baseline and follow-up, including OSA resolution at follow-up.

	OSA severity (e/h)	Baseline (*n*)	Follow-up (*n*)	OSA resolution % (*n*)
No OSA	AHI < 1	-	63	-
Mild OSA	1 < AHI ≤ 5	107	135	48% (52)
Moderate OSA	5 < AHI ≤ 10	90	30	33% (30)
Severe OSA	10 ≤ AHI	58	27	36% (21)
		(255)	(255)	[AHI ≤ 2 and AI ≤ 1] at follow-up[a]

Abbreviations: AHI, apnea–hypopnea index; AI, apnea index; OSA, obstructive sleep apnea.

[a]All subjects at baseline were diagnosed as suffering from pediatric OSA, such that at baseline, none of the subjects could be considered as OSA resolution (AHI ≤ 2 e/h and AI ≤ 1 e/h) or No OSA (AHI ≤ 1 e/h).

9.2.2 Estimation of HRV, CPC and BR

The ECG signal is used to estimate the modulating signal, $m(t)$, with the TVIPFM (as detailed in 3.3). The signal from the abdominal respiratory effort band, $r(t)$, is used to obtain the continuous BR signal, $\hat{f}_r(t)$, which is derived using the spectral peakedness method explained in Eq. 3.2, and shown in Fig. 3.2. The P_{HF} is measured as the power within the BR, $\hat{f}_r(t)$, and time-varying (see Eq. 3.8).

In this study, the influence of respiration on HRV, i.e., CPC, is estimated using TFC 3.12. The CPC biomarker, based on the TFC between HRV and respiration in the HF band, Ω^r_{HF}, is denoted as $\mathscr{C}^{\mathcal{T}}_{\text{HF}}$, and explained in Eq. 3.19, in Sec. 3.4.1. It incorporates both the mean significant coherence averaged over time, and the percentage of time where TFC is significant in that period.

For CPC, by definition, $\mathscr{C}^{\mathcal{T}}_{\text{HF}}$ should be calculated in the Ω^r_{HF} band, but spectral coherence can be also calculated in different spectral bands like LF band, with the TFC in the LF reading as $\mathscr{C}^{\mathcal{T}}_{\text{LF}}$. Methods for estimating HRV and CPC through TFC have been extensively described in previous Sec. 3.4.1.

9.2.3 Statistical Analysis

The CPC biomarkers are derived using 5-min epochs. I conduct a separate analysis of CPC results during the three sleep stages: wake (W), REM, and NREM. For an epoch to be considered in the analysis, it must have at least 90% of its time in the same sleep stage. For each patient, the average CPC in the epochs at the same sleep stage along the overnight recordings is calculated.

The TFC features considered do not fit either normality or homoscedasticity tests, therefore a Kruskal-Wallis test is conducted to compare differences in CPC biomarkers among the four severity groups (no OSA, mild OSA, moderate OSA, and severe OSA). A p-value < 0.05 for the KW test can be considered for statistical significance. Afterwards, a paired signed rank test was employed to compare the differences in TFC values of each patient between sleep stages. A p-value < 0.01 is considered for statistical significance, after correction for multiple comparisons.

9.3 Results and Discussion

Fig. 9.1 exhibits the boxplots of the TFC in the LF and HF bands, comparing the values of the 4 groups of OSA severity for the three sleep stages. The CPC levels in each sleep stage, as measured by TFC in the Ω^r_{HF} band, are significantly lower for increasing OSA severity categories during NREM (KW test, $p = 0.02$), and REM sleep (KW test, $p = 0.03$). On the contrary, the

TFC in the Ω_{LF} band is significantly higher for increasing OSA severity categories, both during NREM (KW test, $p < 0.001$), and REM sleep (KW test, $p < 0.001$), which is consistent with results found in adults [13].

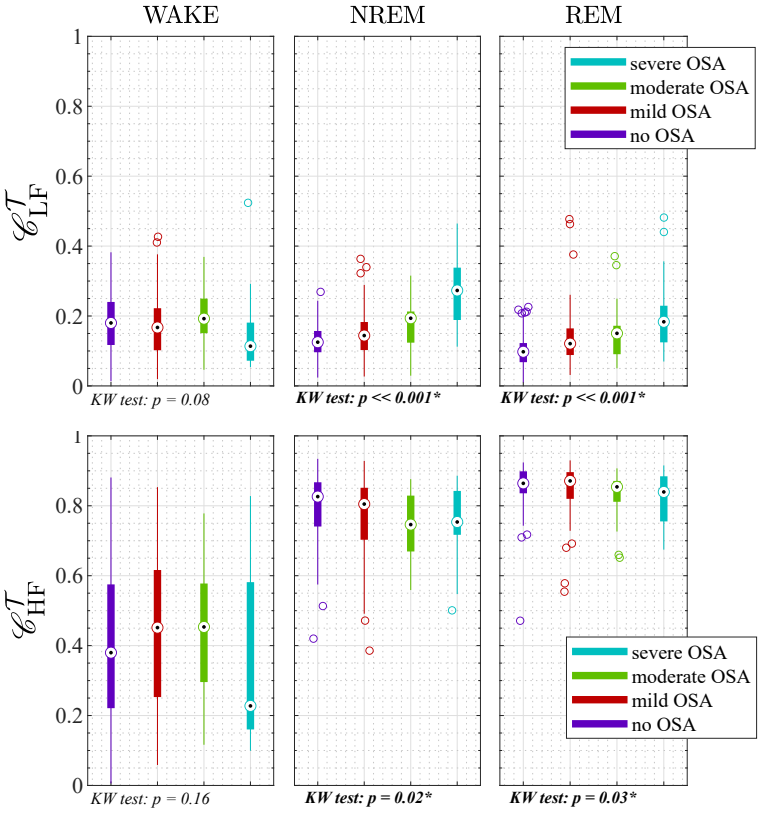

Figure 9.1: Boxplots of the TFC in the LF band (up), $\mathscr{C}^{\mathcal{T}}_{\text{LF}}$, and in the HF band (bottom), $\mathscr{C}^{\mathcal{T}}_{\text{HF}}$, comparing the values of the 4 groups of OSA severity (no, mild, moderate and severe OSA), for the three sleep stages (Wake, NREM and REM). Statistical significant difference between TFC values of the OSA severity groups is obtained using the Kruskal Wallis (KW) test, for each sleep stage.

Tab. 9.2 shows the p-values of the signed rank test, comparing TFC values for the three sleep stages in the Ω_{LF} and $\Omega^{\tau}_{\text{HF}}$ bands, of the different OSA severity levels. The statistical analysis shows that differences exist in CPC (TFC-HF) in all stages, except for the children with severe OSA, stating the fact that a separate analysis in sleep stages is necessary for sleep apnea characterization. No significant differences are found in the LF band in severe OSA patients comparing TFC values in REM and NREM, whereas these differences are clear for no and mild OSA patients. Besides, as

hypothesized, the CPC is also significantly lower during wake compared to NREM and REM in all OSA categories (Tab. 9.2b). According to previous research, processes such as sleep apnea and fibromyalgia, which lead to sleep fragmentation, have been shown to reduce the amount of CPC (TFC-HF) [13]. In addition, higher TFC-LF values have been associated with a higher prevalence of hypertension and stroke in adults [20].

Table 9.2: P-values obtained from the paired signed rank test, comparing the TFC values of each patient between the three sleep stages. The analysis is done in the Ω_{LF} (a), and Ω^{r}_{HF} bands (b), for the different OSA severity levels. Statistical significance is considered for p-values <0.01, to correct for multiple comparisons.

	W-NREM	W-REM	NREM-REM
a) $\mathscr{C}^{\mathcal{T}}_{\mathrm{LF}}$			
No OSA	***<0.01***	***<0.01***	***<0.01***
Mild OSA	0.03	***<0.01***	***<0.01***
Moderate OSA	0.54	0.09	0.03
Severe OSA	***<0.01***	0.05	0.02
b) $\mathscr{C}^{\mathcal{T}}_{\mathrm{HF}}$			
No OSA	***<0.01***	***<0.01***	***<0.01***
Mild OSA	***<0.01***	***<0.01***	***<0.01***
Moderate OSA	***<0.01***	***<0.01***	***<0.01***
Severe OSA	***<0.01***	***<0.01***	0.04

In general, the amount of apnea/hypopnea events are comparable between REM and NREM [8]: approximately 88% of 10-min epochs in REM sleep had less than 5 events per epoch, and 97% of the epochs in NREM sleep had less than 5 apnea/hypopnea events per epoch. The observed increased coupling in the LF band in severe OSA patients could be attributed to the higher prevalence of periodic breathing during REM sleep, as reported in [13], as well as to the pronounced cyclic variations in HRV in response to repeated apnea episodes. However, values of CPC in the Ω^{r}_{HF} band where higher in REM sleep compared to NREM, or at least similar for severe OSA patients, which explains that the significant reduced CPC with increasing severity of OSA may not be due to effects related to apnea events, but rather due to other physiological factors like alterations in the sympathetic activity.

Note that it is necessary the use of a significant coherence threshold. Many existing works studying CPC based on spectral coherence, as biomarker on sleep quality, do not rely on the fact that two white-noise signals will have a baseline level of coherence γ_0, where zero coherence should be reported by definition. Our results show that this methodology might provide additional

phenotypic information to better classify between sleep stages, since wake and REM sleep are sometimes indistinguishable [13].

This study has a limitation in that respiratory signals other than the nasal pressure signal were used. Previous studies have also used alternative respiratory signals [13], [18], such as ECG-Derived respiration. In fact, Varon et al. reported that errors in CPC were significantly greater during apnea events than during normal activity when using EDR signals as surrogate [21]. Owing to chest movements captured by EDR, it may not be related to actual respiration during apnea events, causing an overestimation of CPC. We demonstrated the usefulness of CPC using recordings of respiratory effort bands, but future works should consider using the nasal pressure cannula signal, which would lead to a potential reduction in CPC values in the presence of obstructive respiratory events.

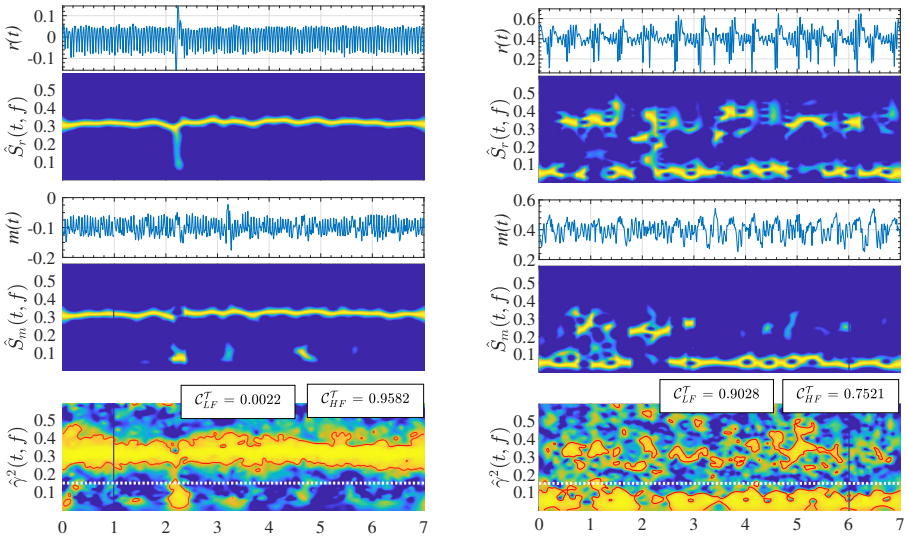

Figure 9.3: Two illustrative examples of TFC from the same patient, at two different moments in the night. (left) High CPC in the HF band, during REM sleep. (right) High TFC in the LF band, during NREM sleep, where a clear pattern of periodic breathing can be seen, and the modulation of HR, accordingly.

The conventional computation of CPC in LF, traditionally associated with an abnormal functioning of the ANS in regulating heart and respiration, is, in fact, indicative of a pathological phenomenon and not a cardiopulmonary

coupling effect. Contrary to its presumed role in ANS regulation, it exhibits a distinctive behavior, where the effect of respiration may significantly impact HR, HRV, and RSA regulation. This behavior directly influences cardiac patterns, manifesting as clear cyclic patterns with implications for cardiovascular health (see Fig. 9.3). Notably, the heart's regulation is not modulated by the ANS but rather by the obstruction resulting from apnea and the recurrent efforts to restore oxygenation in each cyclic inspiratory effort characteristic of Cheyne-Stokes respiration.

9.4 Conclusions

Overall, we can conclude that the TFC in the LF band could be a useful biomarker for assessing the severity of OSA, while CPC as measured by TFC in the HF band could provide additional information about the pathological mechanisms underlying OSA. However, further studies with larger sample sizes are needed to confirm these findings and to investigate the use of respiratory signals in conjunction with HRV analysis.

Chapter 10

Cardiovascular Risk index for Pediatric Patients with OSA

10.1 Introduction

OSA, along with other sleep disorders resulting in fragmented sleep, has emerged as a risk factor for cardiometabolic comorbidities [22], [23]. When persistent over time, particularly when excessive daytime sleepiness is manifest, OSA promotes the risk of Cardiovascular Disease (CVD), such as hypertension or hypercholesterolemia [24]–[27]. In the pediatric population,

OSA is also associated with an increased risk of obesity, insulin resistance and systemic inflammation [28]–[30].

MetS is a cluster of conditions encompassing central obesity, impaired fasting glucose, dyslipidemia, and hypertension [31]. In adults, the criteria and definition of MetS are well established [31]–[33]. Furthermore, MetS is directly associated with CVD risk, insulin resistance, type 2 diabetes mellitus, and overall mortality [27], [34]. In studies that assessed the association of MetS in childhood with adult CVD years later [34], [35], children with MetS were significantly more likely to manifest an increased risk of CVD in adulthood.

Compared to the abundant body of adult data, very few experimental studies examining metabolic sequelae of sleep perturbations have been conducted in children and adolescents [36]–[38]. In general, OSA seems to be associated with increased risk of metabolic dysfunction in overweight and obese children [39], [40]. Metabolic dysfunction is more prevalent in pediatric patients with known insulin resistance and dyslipidemia [41], and in those with one of the individual components of MetS, either the presence of elevated systemic blood pressure or higher blood glucose levels [42], [43]. However, the extant studies have yielded inconsistent findings at times, and the divergence from the findings in adults may be due in part to the several competing definitions of MetS in children, but also to longer lags between disease onset and development of MetS-related sequelae [44]–[47]. From this point of view, an important study (IDEFICS) by Ahrens et al. [48], classified children according to different definitions of MetS in a population-based survey of 18,745 healthy European children, aged 2 to 11 years, which resulted in the proposal of standard specific cut-off values for each of the MetS components according to percentiles in non-obese children.

The hypothesis is that pediatric OSA interacts with MetS, especially in severe cases. Thus, screening for MetS components in children with OSA may be recommended. CMA is a powerful technique that enables determination of mediators affecting a particular disease [49]. Of relevance to the current study, CMA allows for assessing whether a treatment has a measurable effect, while also detecting possible causal pathways through which a treatment influences changes in an outcome. However, CMA has not been systematically employed to study the mediators of OSA and their interactions with MetS

outcomes.

In addition to MetS, Obesity (OB) and C-reactive protein levels (CRP) are also frequently used as biomarkers for CVR. CRP is a well-established marker of systemic inflammation and has been found to be a reliable indicator of cardiovascular morbidity in adults [40], [50]. In addition, OB is also known to be strongly related to the development of OSA and MetS in adults, but different studies disagree on their results in children [36], [40], [51]. Consequently, the main novelty of the study focuses on the evaluation of both the causality of OSA in the development of MetS and the interactions between OSA, MetS, CRP and OB in prepubertal children from CHAT.

10.2 Materials and Methods

The methodological approaches used herein are divided into three stages. First, we conducted analysis of MetS in the cohort of CHAT, based on the IDEFICS cutoff values [48]. Then, we applied CMA to assess the putative causal pathways between pediatric OSA and the development of MetS [52]. Finally, the prevalence of MetS was studied and related to the prevalence of OSA.

10.2.1 Sleep Data for MetS Analysis

As explained in previous Chapter 9, we included 255 subjects from CHAT database, who had all the necessary information to define MetS, both at baseline and follow-up. Among these, 127 subjects were assigned to eAT and 128 were assigned to WWSC. Tab. 10.1 shows the demographic and relevant clinical data for these two groups at baseline. The distribution of patients according to OSA severity and OSA resolution was shown in Tab. 9.1.

10.2.2 Definition of MetS

MetS consists of a cluster of metabolic disorders that are often associated with chronic inflammation or with insulin resistance [53]. The specific criteria for MetS in adults have been defined by the National Cholesterol Education Program (NCEP), the Adult Treatment Panel III, and the World Health Organization [32], [33]. MetS in adults is defined if three or more of the

following risk factors are present: (1) central obesity, (2) hypertension, (3) dyslipidemia and (4) hyperglycemia. However, there are different competing definitions of MetS in children, and each of such proposed criteria has significant limitations. For example, the definition by Cook et al. [44] corresponds to the NCEP criteria, adapted to adolescents, which restricts its applicability in younger children.

In the IDEFICS study, the investigators applied and compared three commonly used definitions of the pediatric MetS, along with a new definition criterion [44]–[46], [48]. Based on the most recent age- and sex-specific percentiles derived from the study, they suggested an updated definition of pediatric MetS [48], which is shown in Tab. 10.2, and summarily consists of percentiles cutoffs based on statistical criteria adapted for age and sex. Using the IDEFICS criteria, a considerable proportion of prepubertal children will be designated as MetS compared to other definitions [48].

Finally, there is also relevance in evaluating the association between OB, OSA and MetS [36], [40], [51], [54]. Therefore, children with body mass index (BMI) z-score values exceeding the 95th percentile were classified as fulfilling the criteria for OB, following the recommendations of the Centers for Disease Control and Prevention (`https://www.cdc.gov/obesity/basics/childhood-defining.html`).

10.2.3 Causal Mediation and Statistical Analysis

The commonly reported total causal effect (TE) of an intervention evaluates whether a treatment modifies the outcome of interest. In this work, we implement a CMA, which further identifies the causal pathways, namely mediators, through which the treatment affects the outcome. A mediator is an intermediate variable that resides within the causal pathway between an independent variable (in this case, OSA treatment), and a dependent variable (outcome of the study, e.g., MetS). It helps to clarify how and why a treatment influences a given outcome. In other words, the mediator is influenced by the independent variable (OSA treatment), which in turn influences the dependent variable (outcome). For example, with a CMA we can evaluate whether variations in MetS are causally attributable to OSA treatment [49], influenced by AHI as mediator/pathway of the disease. Then, CMA allows to split the TE of the OSA treatment into two components (see

Table 10.1: Clinical and demographic characteristics at baseline in CHAT subjects with complete metabolic information. Subjects are separated into two groups considering OSA status at follow-up. Data are shown as mean (σ) or % (n), for each subgroup. Statistically significant differences for the Wilcoxon rank sum test ($p < 0.05$) are marked with asterisks (*), comparing values of patients with OSA resolution against values of patients with persistent OSA at follow.

	Patients who resolved OSA (baseline values)	**Patients with persistent OSA (baseline values)**	**p-value**
Patients (n)	40% (103)	60% (152)	--
Treatment Arm (eAT)	65% (67)	39% (60)	**< 0.001***
Age (years)	6 (1)	7 (1)	0.1908
Sex (females)	57% (59)	50% (76)	0. 2544
Race			0.8455
White	35% (36)	33% (50)	
Black	52% (54)	59% (90)	
Other	13% (13)	8% (12)	
BMIz	0.52 (1.34)	1.03 (1.26)	**0.0019***
WC (cm)	60 (12)	64 (13)	**0.0045***
SBP (mmHg)	96 (8)	98 (9)	0.0805
DBP (mmHg)	62 (7)	64 (8)	**0.0167***
CHOL (mg/dL)	159 (27)	158 (23)	0.6012
HDL (mg/dL)	50 (12)	52 (12)	0.1044
LDL (mg/dL)	95 (22)	92 (21)	0.5922
TRIG (mg/dL)	71 (29)	72 (30)	0.7580
GLUC (mg/dL)	81 (8)	81 (6)	0.3725
HOMA	1.58 (1.77)	1.76 (1.66)	0.0637
CRP (µg/mL)	1.33 (2.21)	2.36 (5.66)	0.0913
AHI (e/h)	6.9 (5.6)	8.0 (5.7)	**0.0114***
AI (e/h)	2.9 (2.5)	3.3 (3.1)	0.2596
HI (e/h)	4.0 (4.0)	4.7 (4.1)	**0.0182***
ODI (e/h)	6.5 (7.0)	7.2 (6.2)	**0.0305***
TAI (e/h)	8.4 (3.1)	8.2 (3.1)	0.6509
Epworth Sleepiness Scale	6.7 (4.8)	7.1 (4.7)	0.4526
Obese (n)	28% (29)	42% (64)	**0.0235***
HR (bpm)	85 (8)	84 (9)	0.5000
Tonsil size, >2+ (n)	78% (80)	70% (107)	0.1986
MetS, ≥ 3 (n)	11% (11)	19% (29)	0.0711
	[AHI ≤ 2 and AI ≤ 1] at follow-up		

Abbreviations: eAT, early adenotonsillectomy; WWSC, watchful waiting with supportive care; BMIz: z-scored Body Mass Index; WC, Waist Circumference; SBP, Systolic Blood Pressure; DBP, Diastolic Blood Pressure; CHOL, Total Cholesterol level; HDL, High-Density Lipoprotein level; LDL, Low-Density Lipoprotein level; TRIG, Triglycerides level; GLUC, Serum Glucose level; HOMA, Homeostatic Model Assessment; CRP, C-Reactive Protein level; AHI, Apnea-Hypopnea Index; AI, Apnea Index; HI, Hypopnea Index; ODI, Oxygen Desaturation Index; TAI, Total Arousal Index; HR, Heart Rate; MetS, Metabolic Syndrome.
OSA resolution, for patients with AHI ≤ 2 e/h and an AI ≤ 1 e/h at follow-up.

Table 10.2: Definition of pediatric MetS [48].

Excess adiposity	Blood pressure	Blood lipids	Blood glucose/insulin
WC ≥ 90th PCT	SBP ≥ 90th PCT	TRIG ≥ 90th PCT	HOMA ≥ 90th PCT
	DBP ≥ 90th PCT	HDL ≤ 10th PCT	GLUC ≥ 90th PCT

Note: All cut-off reference PCT values are dependent on age and sex, but the blood pressure cut-off reference values are also dependent on height. MetS is present if three or more clusters of risk factors are met. If one of two conditions exceeds cut-off criteria, the cluster is considered to be present. PCT reference values were obtained in nonobese healthy children population, which can be found in the IDEFICS study.

Abbreviations: DBP, diastolic blood pressure; GLUC, fasting plasma glucose; HDL, high-density lipoprotein cholesterol; HOMA, homeostatic model assessment, for insulin resistance; PCT, percentile; SBP, systolic blood pressure; TRIG, triglycerides; WC, waist circumference.

Fig. 10.3):

- First, the average causal mediation effect (ACME), represents the indirect effects. ACME measures the changes in the outcome particularly attributable to changes in a given mediator, which changed due to the treatment.
- Second, the average direct effect (ADE), reflects the direct effects of the treatment. ADE measures the changes in the outcome unlinked to the mediator under study.

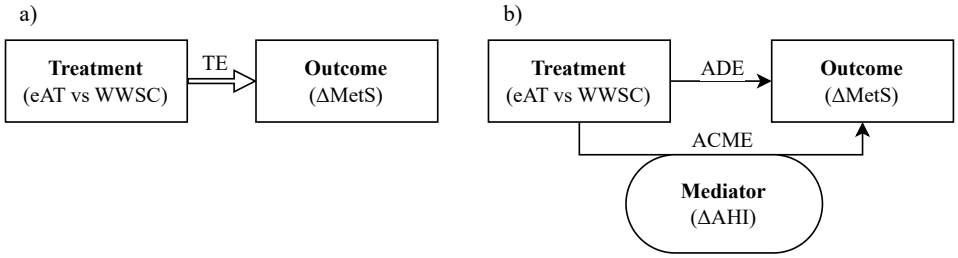

Figure 10.3: (a) Typical estimation of the total causal effect [51] (b) Causal mediation analysis performed in the present study.

On the one hand, ACME evaluates the relationships between the after-treatment variations occurring in the outcome, i.e., the variations of the clinical indicators such as MetS, z-scored BMI (BMIz), SBP, etc., and the variations in the indicators representing the disease severity, i.e., the mediators, such as AHI, oxygen desaturation index (ODI) and so on. The MetS criteria represent an outcome from the disease. On the other hand,

ADE evaluates how treatment affects the outcome through any other (and possibly unknown) factor(s) different from the mediator. ACME and ADE jointly form the TE.

CMA utilizes regression models to estimate the effects and associations between the variables: one model is constructed examining the mediator-outcome relationship, other assessing the treatment-mediator relationship, and a final one exploring the treatment-outcome relationship. One additional model is calculated to conduct the mediation analysis, which combines the estimated coefficients from the previous models to calculate the ACME and the ADE. The software used for the assessment of causal mediation has been extensively validated in R language [55].

In this study, the intervention is represented by one of the treatment arms (either eAT or WWSC). Five different mediators are included:

- AHI, AI, and Hypopnea Index (HI), as measures of the possible different number of apneic events, in e/h.
- ODI: oxygen desaturations with events $\geq 3\%$ desaturation per hour of sleep, related to OSA and intermittent hypoxemia [1].
- Total Arousal Index (TAI), as the measure reflecting sleep disturbance and sleep fragmentation associated with OSA [56].

As outcomes for the analysis, we consider MetS, but also each of the individual variables included in MetS criteria, namely adiposity: waist circumference (WC); blood pressure: SBP and diastolic blood pressure (DBP); blood glucose: homeostatic model assessment (HOMA) and glucose levels (GLUC); blood lipids: triglycerides levels (TRIG) and high-density lipoprotein levels (HDL). In addition, for comparative purposes, BMIz and CRP levels were also included [40], [50].

Finally, to formulate an accurate interpretation of the ACME, all confounders must be controlled based on their potential associations with both the exposure (OSA treatment), and any outcome (MetS, CRP, SBP, etc.). The baseline values of age, race, sex, BMIz, average overnight heart rate, tonsil size, and OSA severity group are included in the statistical adjustment procedures [8], [36], [57]. For example, age, sex, and race -related variations in the metabolic outcomes are incorporated to ensure that any observed effects are not solely driven by demographic factors [48]. In particular, the rationale for including average overnight heart rate is based on previous research

suggesting that increased overnight heart rate is associated with OSA [58], and that it may be also influenced by many other factors such as age, sex, physical condition, etc. [59], ensuring too that any observed effects on causal mediation are not solely attributable to heart rate variations. We additionally computed the Fisher combined probability, which primarily addresses the potential for Type I errors (false positives), in multiple independent testing.

10.3 Results

10.3.1 Baseline Values: Comparing OSA Resolution vs. Persistent OSA

Tab. 10.1 summarizes the baseline data from children included in the CHAT study, comparing the baseline values for subjects whose OSA resolved at follow-up and those with persistent OSA after treatment. Significant differences were found for treatment arm (eAT vs. WWSC), for BMIz, WC, DBP, AHI and OB. No significant differences emerged for all other clinical and demographic parameters, such as age, sex, race, glucose levels, HR, tonsil size, and MetS.

10.3.2 Causality Results

Regarding CMA, statistical significance results of causal mediation are reported in Tab. 10.4. Those p-values that preserved statistical significance after correcting for multiple testing with the combined probability of Fisher are marked in bold with asterisks (*). Mainly, CMA exhibits no significant ACME with the single constitutive criteria for MetS. Nonetheless, there was a significant causal mediation effect on MetS with AHI as mediator. Furthermore, significant ACME was detected for CRP with AHI and ODI as mediators, and for BMIz with TAI as mediator. With TAI as mediator, there was also significant ACME on DPB and WC. Of note, statistically significant differences were found in the change in BMIz from baseline to follow-up (ΔBMIz = BMIz$_{followup}$ – BMIz$_{baseline}$), with TAI as a mediator. However, CMA performed considers BMIz levels at baseline as confounder, thus revealing a robust causal mediation effect of TAI on changes in BMIz, after OSA treatment.

Table 10.4: P values and statistical significance from the CMA, assessing treatment effects on change in clinical variables (follow-up - baseline) through different mediators.

	ΔAHI		ΔAI		ΔHI		ΔODI		ΔTAI	
Mediators	**ACME**	**ADE**	**ACME**	**ADE**	**ACME**	**ADE**	**ACME**	**ADE**	**ACME**	**ADE**
ΔMetS	**0,02**[a]	0,88	0,03	0,91	0,43	0,80	0,41	0,77	0,17	0,88
ΔWC	0,12	0,60	0,83	0,96	0,12	0,86	0,18	0,76	**« 0.01**[a]	0,52
ΔSBP	0,93	0,95	0,35	1,00	0,97	0,44	0,83	0,95	0,20	0,86
ΔDBP	0,41	0,41	0,73	0,83	0,76	0,91	0,75	0,84	**0,02**[a]	0,77
ΔTRIG	0,42	0,28	0,22	0,24	0,97	0,36	0,68	0,23	0,06	0,33
ΔHDL	0,32	0,95	0,77	0,66	0,15	0,60	0,51	0,83	0,41	0,82
ΔHOMA	0,09	0,08	0,40	**0,02**[a]	0,21	0,03	0,14	0,04	0,99	**0,02**[a]
ΔGLUC	0,65	0,36	0,09	0,47	0,85	0,26	**0,02**[a,b]	0,44	0,41	0,22
ΔCRP	**0,02**[a]	0,43	0,13	0,57	0,046	0,56	**0,02**[a]	0,39	0,03	0,40
ΔBMIz	0,10	0,08	0,65	0,046	0.07	**0,02**[a]	0,48	0,06	**0,02**[a]	0,12

Note: Statistically significant effects ($p < .05$) are highlighted with blue and green color for ACME and ADE, respectively.

Abbreviations: ACME, average causal mediation effect; ADE, average direct effect; AHI, apnea–hypopnea index; AI, apnea index; BMIz: z-scored body mass index; CRP, C-reactive protein levels; DBP, diastolic blood pressure; GLUC, serum glucose levels; HDL, high-density lipoprotein levels; HI, hypopnea index; HOMA, homeostasis model assessment; MetS, metabolic syndrome; ODI, oxyhemoglobin desaturation index 3%; SBP, systolic blood pressure; TAI, total arousals index; TRIG, triglycerides levels; WC, waist circumference; WWSC, watchful waiting with supportive care.

[a]Significant effect after correcting for multiple testing with the combined probability of Fisher.

[b]Significant effect only for WWSC arm.

No differences in analytical outcomes were detected when only obstructive apnea and hypopnea events were analyzed with respect to when both central and obstructive events were included. Therefore, the results for AHI, AI and HI are shown considering both central and obstructive events. The significant ADE obtained with different mediators and, e.g., HOMA as outcome, means that OSA treatment significantly affected HOMA through mediators other than those evaluated in the present study.

The original CHAT study found high OSA resolution rates in both treatment arms [1]. These findings have led researchers to analyze CHAT based on OSA resolution rather than relying on treatment arm [8], [57], [58]. However, for CMA, it is mandatory to conduct an initial preliminary analysis, to ascertain if there are interactions between the type of treatment and the outcomes. In general, no significant effects of interactions between treatment types on the outcomes were detected, and therefore the average joint effect (ACME) for the two treatment arms is reported [55]. Only ODI-GLUC results in an interaction effect, and causal mediation effect is provided for the treatment arm for which there is significant effect. Specific values obtained for ACME and ADE can be found in Tab. 10.5.

Table 10.5: Values from the causal mediation analysis assessing treatment effects on change in clinical variables (follow-up - baseline) through different mediators.

Mediators		ΔWC	ΔSBP	ΔDBP	ΔTRIG	ΔHDL	ΔHOMA	ΔGLUC	**ΔMetS**	ΔCRP	ΔzBMI
ΔAHI	ACME	0,2358	0,0384	0,22348	0,9522	-0,264	0,1476	0,128	**0,06842**	**-0,303**	0,01468
	(95% CI)	(-0,0586 to 0,56)	(-0,6581 to 0,8)	(-0,38252 to 1)	(-1,3578 to 3,47)	(-0,9253 to 0,26)	(-0,0206 to 0,41)	(-0,486 to 0,65)	**(0,00768 to 0,14)**	**(-0,636 to -0,04)**	(-0,00311 to 0,04)
	ADE	-0,1439	0,113	0,07915	4,399	-0,0997	0,4999	0,749	-0,0099	0,547	0,07997
	(95% CI)	(-1,168 to 0,66)	(-2,193 to 2,39)	(-2,17651 to 2,07)	(-4,0875 to 12,96)	(-2,2092 to 2,13)	(-0,0611 to 0,96)	(-0,914 to 2,36)	(-0,26074 to 0,23)	(-0,602 to 1,9)	(-0,01259 to 0,17)
ΔAI	ACME	-0,00857	0,1405	0,0445	0,4324	0,0341	0,0303	0,2248	**0,03969**	-0,123	0,00349
	(95% CI)	(-0,09698 to 0,08)	(-0,1339 to 0,53)	(-0,311 to 0,35)	(-0,2751 to 1,36)	(-0,2201 to 0,29)	(-0,0393 to 0,11)	(-0,0315 to 0,57)	**(0,00356 to 0,09)**	(-0,313 to 0,03)	(-0,01041 to 0,02)
	ADE	0,02369	0,0122	0,2322	5,06	-0,4242	**0,5675**	0,5972	0,01846	0,372	**0,09015**
	(95% CI)	(-0,84037 to 0,9)	(-2,3837 to 2,22)	(-1,8609 to 2,25)	(-3,3927 to 13,47)	(-2,496 to 1,8)	**(0,0671 to 1,15)**	(-1,0092 to 2,22)	(-0,22316 to 0,26)	(-0,768 to 1,6)	**(0,00137 to 0,18)**
ΔHI	ACME	0,1152	-0,00285	0,0562	0,01016	-0,243	0,0568	0,0382	0,0125	**-0,131**	0,009523
	(95% CI)	(-0,0322 to 0,32)	(-0,29273 to 0,52)	(-0,2693 to 0,77)	(-1,72017 to 1,18)	(-0,565 to 0,1)	(-0,0269 to 0,24)	(-0,3436 to 0,29)	(-0,0224 to 0,07)	**(-0,399 to 0)**	(-0,000779 to 0,03)
	ADE	-0,0967	0,83829	-0,0386	4,07885	-0,605	**0,5786**	0,9197	-0,0286	0,408	**0,105947**
	(95% CI)	(-0,946 to 0,77)	(-1,53052 to 3,31)	(-2,5482 to 2,24)	(-5,11271 to 13,36)	(-2,884 to 1,56)	**(0,0394 to 1,1)**	(-0,775 to 2,72)	(-0,2874 to 0,22)	(-0,727 to 1,83)	**(0,011208 to 0,19)**
ΔODI	ACME	0,1403	0,0495	0,0764	0,376	-0,154	0,0862	**0,5597 [WWSC]**	0,0246	**-0,281**	0,00635
	(95% CI)	(-0,062 to 0,37)	(-0,4698 to 0,69)	(-0,5275 to 0,66)	(-1,541 to 2,29)	(-0,67 to 0,3)	(-0,0251 to 0,25)	**(0,0903 to 1,12)**	(-0,0367 to 0,09)	**(-0,63 to -0,03)**	(-0,01046 to 0,03)
	ADE	-0,1204	0,0993	0,2118	5,151	-0,249	**0,5182**	0,6597	0,0339	0,525	0,0883
	(95% CI)	(-0,979 to 0,75)	(-2,1723 to 2,34)	(-1,8735 to 2,36)	(-3,453 to 13,55)	(-2,459 to 2,04)	**(0,0143 to 1,07)**	(-0,9598 to 2,3)	(-0,2125 to 0,27)	(-0,62 to 1,85)	(-0,00414 to 0,18)
ΔTAI	ACME	**0,3044**	0,311	**0,5556**	1,4608	-0,0759	-0,000195	-0,138	0,0424	**-0,349**	**0,0202**
	(95% CI)	**(0,1011 to 0,6)**	(-0,135 to 1,12)	**(0,0623 to 1,29)**	(-0,0259 to 3,37)	(-0,5638 to 0,38)	(-0,153824 to 0,12)	(-0,603 to 0,2)	(-0,0146 to 0,12)	**(-0,669 to -0,04)**	**(0,00282 to 0,05)**
	ADE	-0,2846	-0,162	-0,2673	4,0656	-0,3269	**0,604548**	0,963	0,0161	0,593	0,07445
	(95% CI)	(-1,1428 to 0,61)	(-2,542 to 2,11)	(-2,4471 to 1,8)	(-4,3821 to 12,08)	(-2,4188 to 1,83)	**(0,078939 to 1,2)**	(-0,487 to 2,65)	(-0,2213 to 0,27)	(-0,655 to 2)	(-0,01677 to 0,17)

AHI: Apnea-Hypopnea Index; AI: Apnea Index; HI: Hypopnea Index; ODI: Oxyhemoglobin Desaturation Index 3%; TAI: Total Arousals Index.
ACME: Average Causal Mediation Effect; ADE: Average Direct Effect; CI: Confidence Interval.
*Statistically significant effects (p-value <0.05) have been highlighted in green (significant ACME) and blue (significant ADE).*p-value < 0.05.*

10.3.3 Prevalence, Odds Ratio, and Risk Ratio of MetS

In order to further explain the relationship between OSA and MetS, Fig. 10.6 presents a proportion plot with the prevalence and evolution of MetS from baseline to follow-up (data comes from Tab. 10.7 (a)). At first glance, we can see that the number of patients with MetS increased from baseline to follow-up (61 subjects at follow-up with at least 3 cardiovascular risk factors compared to 40 subjects at baseline). However, note that the two categories (MetS vs. no MetS) are not balanced. Upon closer examination, patients with MetS at baseline were more likely to recover at follow-up (32%, 13 patients) as compared to those without MetS at baseline developing MetS at follow-up (16%, 34 patients).

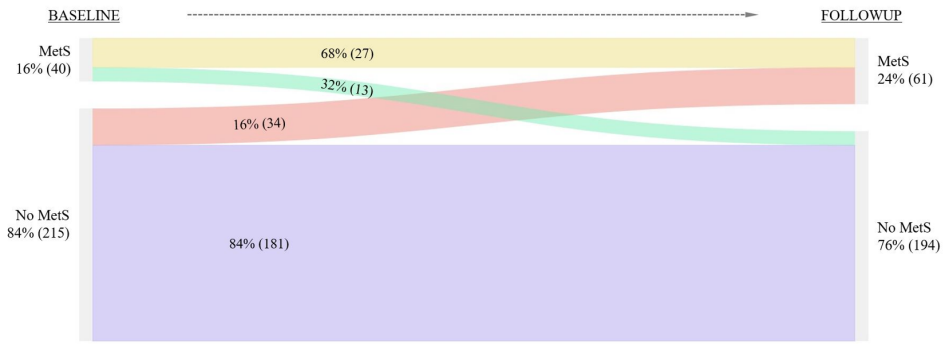

Figure 10.6: Proportion plot showing prevalence and evolution of MetS from baseline to follow-up. Units are % (N). Prevalence is summarized by having or not MetS (number of risk factors ≥ 3).

As shown in Tab. 10.7, there is evidence that among the children who did not recover from MetS after OSA treatment, the number of MetS risk factors decreased. Only 2 out of the 27 patients worsened in terms of the number of risk factors at follow-up, while 17 patients improved.

As such, the odds ratio of changing the health state after OSA treatment from having MetS at baseline to not having MetS at follow-up, with respect to worsening from no MetS to MetS was 2.56 (confidence interval (CI) 95%: 1.2031 - 5.4606); and the risk ratio, was 2.06 (CI95%: 1.1943 - 3.5364). Accordingly, despite the increased total number of subjects with MetS after treatment for OSA (40 vs. 61, respectively), the probability of recovering from MetS was significantly higher (2.06-fold), than the probability of developing

Table 10.7: Prevalence and MetS evolution from baseline to follow-up. Units are % (N). (a) Prevalence summarized by having or not MetS (number of risk factors ≥ 3). (b) Prevalence considering the number of risk factors.

A) FOLLOWUP / BASELINE	METS	NO METS	TOTAL
MetS	68% (27)	**32%** (13)	16% (40)
no MetS	**16%** (34)	84% (181)	84% (215)
Total	24% (61)	76% (194)	(255)

B)	FOLLOWUP / BASELINE	4	3	2	1	0	Total
MetS	4	25% (3)	33% (4)	42% (5)	-	-	5% (12)
	3	7% (2)	64% (18)	29% (8)	-	-	11% (28)
no MetS	2	-	37% (23)	32% (20)	25% (16)	6% (4)	25% (63)
	1	-	12% (7)	17% (10)	39% (23)	32% (19)	23% (59)
	0	-	4% (4)	11% (10)	28% (26)	57% (53)	36% (93)
Total		2% (5)	22% (56)	21% (53)	25% (65)	30% (76)	(255)

MetS. Similarly, the odds of not having MetS after OSA treatment if the patient had MetS at baseline were also significantly higher (2.56-fold), than the odds of having MetS after OSA treatment if the patient did not have MetS at baseline.

10.3.4 MetS and OSA Severity

The prevalence of MetS in our sample is presented in Fig. 10.8 according to OSA severity groups and baseline or follow-up. As mentioned above, a higher MetS presence was found after OSA treatment. However, Fig. 10.8 shows that its prevalence increases with OSA severity: no-OSA (19%), mild-OSA patients (22%), moderate-OSA (27%), and severe-OSA patients (41%), thus suggesting persistent OSA as a risk factor for MetS and gradual relationship with OSA severity.

Further detailed results and analysis, including OSA prevalence, results by treatment strategy, and the proportion of different combinations of MetS, can be found in Tabs. 10.9, and 10.10. In particular, Tab. 10.9 shows the evolution of MetS for children with and without OB at baseline, further illustrating the known impact of obesity on prevalence of MetS over time. Tab. 10.10 exhibits the relationships between OSA severity and the evolution of MetS from baseline to follow-up.

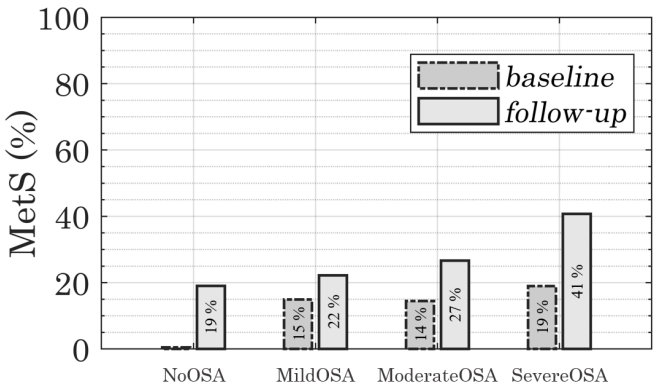

Figure 10.8: Prevalence of Metabolic Syndrome (MetS) according to OSA severity categories based on AHI criteria, at baseline and at follow-up.

Table 10.9: Evolution of MetS by OB status at baseline (BMIz $\geq$ 95th PCT): (a) patients with no OB at baseline, (b) patients with OB at baseline.

BASELINE \ FOLLOW-UP		METS	NO METS	TOTAL
A) NO OB AT BASELINE	*MetS*	100% (4)	0% (0)	2% (4)
	no MetS	8% (12)	92% (146)	98% (158)
	Total	10% (16)	90% (146)	64% (162)
B) OB AT BASELINE	*MetS*	64% (23)	36% (13)	39% (36)
	no MetS	39% (22)	61% (35)	61% (57)
	Total	48% (45)	52% (48)	36% (93)

Table 10.10: Evolution of MetS by severity groups: (a) for patients with mild OSA at baseline, (b) for patients with moderate OSA at baseline, (c) for patients with severe OSA at baseline. In the right column, odds ratio (OR) and risk ratio (RR) are displayed.

BASELINE \ FOLLOW-UP		METS	NO METS		OR AND RR OF CHANGING METS IN FOLLOW-UP
A) MILD OSA AT BASELINE	*MetS*	75% (12)	25% (4)	15% (16)	*RR = 2.19**
	no MetS	13% (12)	87% (79)	85% (91)	*OR = 1.90**
		22% (24)	78% (83)	42% (107)	
B) MODERATE OSA AT BASELINE	*MetS*	69% (9)	31% (4)	14% (13)	*RR = 2.41**
	no MetS	16% (12)	84% (65)	86% (77)	*OR = 1.97**
		23% (21)	77% (69)	35% (90)	
C) SEVERE OSA AT BASELINE	*MetS*	55% (6)	45% (5)	19% (11)	*RR = 3.08**
	no MetS	21% (10)	79% (37)	81% (47)	*OR = 2.14**
		28% (16)	72% (42)	23% (58)	

10.4 Discussion

Using CMA, we assessed and established the putative causal pathways and the contribution of various OSA mediators to the development of MetS in prepubertal children. Furthermore, the present study revealed improvements in MetS as being causally attributable to OSA treatment. In fact, causal mediation was found only for MetS, but not for any of the constitutive elements used to define MetS. In particular, an improvement trend in MetS after OSA treatment can be ascribed to a reduction in the frequency of apnea events during sleep (AI). In addition, a trend of greater presence of systemic inflammation, as illustrated by CRP levels, was causally attributable to the hypopnea index, thereby corroborating previous studies [60]. Furthermore, our findings support the existence of an interrelationship between MetS, OSA, and OB in children, although such associations are less robust than in adults. These novel results may help enhance the putative and unique value of phenotyping pediatric OSA patients with the designated goals of improving patient selection and treatment along with their overall short-term and long-term outcomes.

Fundamentally, CMA revealed that the changes in the number of cardiovascular risk factors of MetS are causally attributable to the changes in the frequency of respiratory events after OSA treatment. Indeed, the causal contribution of OSA to metabolic dysfunction in prepubertal children persisted even after adjusting for confounders. Thus, the association between OSA and MetS is consistent, independent, and not influenced by age, sex, BMIz at baseline, or by other confounders. The mediation results are significant for MetS as outcome when AHI (p=0.02*), is examined as OSA mediator. However, no causal effects emerged for MetS as outcome and ODI as a mediator. Contrary to what has been reported in adults, intermittent hypoxia as reflected by the ODI does not appear to be a causal contributor for MetS in children. This could be due to the relatively minor hypoxic burden frequency found in pediatric OSA when compared to adults with OSA. In contrast, causal mediation effects were found for AHI (p=0.02*), and ODI (p=0.02*) as mediators of CRP levels.

As compared to adults with OSA, prepubertal children with OSA have less pronounced and less severe desaturation profiles likely related to the

decreased collapsibility of their upper airway [61]. These differences may explain why desaturation events do not directly impact on MetS in prepubertal children and may count for children requiring increased OSA treatment duration before they exhibit cardiovascular risk symptoms.

Redline et al. quantified the association between MetS and sleep disordered breathing (SDB, AHI ≥ 5) in adolescents [36]. They found that MetS is significantly more prevalent in subjects with SDB (59% in SDB vs. 16% if no SDB). Our current findings in prepubertal children are closely aligned with the results reported by Redline and colleagues, suggesting the need for MetS screening not only in adults and adolescents but also in children [48]. Of note, the criteria for MetS in children should be implemented using IDEFICS normative reference values to avoid discrepancies across different ages [48].

In Tab. 10.10, we exhibit how OSA and MetS interactions are less prominent in children with persistent OSA at follow-up. However, we should also remark that those children with persistent OSA are more likely to develop MetS, especially when residual OSA remains moderate to severe (Fig. 10.8). As such, it seems likely that although treatment of OSA in these instances did not result in normalization of respiratory parameters, although the latter were improved relative to the baseline disease severity, and as such their impact on MetS may have consequently been mitigated leading to a reduced effect size that nevertheless persists over time and ultimately promotes the emergence of MetS. Notwithstanding, it is suggested that children presenting any of the conditions of MetS, OSA, or OB should be screened and if needed, comprehensively evaluated.

As shown by Redline et al. [36], OB is a strong risk factor for adult OSA, and is also a major risk factor for snoring or OSA in pediatric populations [54], [60], [61]. Accordingly, as illustrated in Tab. 10.1, we found significant differences between the OB prevalence of children with resolved OSA after treatment and those with persistent disease. However, CMA did not uncover a causal mediation effect of OSA over the changes in BMIz.

In the extant literature, there is conflicting evidence about the relationship between OB with OSA and MetS in children [36], [40], [51]. In the current study, OB children were more likely to exhibit MetS at baseline as well as at follow-up (as depicted in Tab. 10.9), further emphasizing the

interdependencies between OB and OSA as causal mediators contributing either additively or synergistically to the risk of MetS. It is also likely that the conflictive findings may be due to the different definitions of MetS. Therefore, we strongly endorse the need for general adoption of the percentile approaches to MetS criteria proposed in the IDEFICS study [48].

As discussed above, one of the important strengths of the current analyses is the utilization of the IDEFICS criteria to define MetS in children [48] along with the implementation of CMA. Another important observation in this study is the fact that isolated components of MetS do not emerge as being causally mediated by OSA and that only when these elements are coalesced into MetS criteria, does the causal mediation then become significant. Thus, MetS appears to be an independent and complementary biomarker of pediatric OSA, which may provide insights into long-term cardiometabolic risk in these children. The major limitation of the present study is that it included sufficient representation of only some ethnic groups, and that no complementary population cohort was available for confirmatory purposes. Therefore, prospective studies similar to CHAT in larger cohorts are needed. In addition, the original study (CHAT) has not been designed for the hypothesis of this reanalysis, therefore different sources of bias cannot be excluded.

10.5 Conclusions

We found that treating OSA in prepubertal children causally reduces the probability of developing MetS and its severity. This effect was independent of age, sex, body mass index and other confounding factors, and was mediated by the decrease in the frequency of respiratory events. Causal mediation effects were not significant for each of the components of MetS and only became apparent when these elements were combined into the definition of MetS, using more epidemiologically robust approaches (i.e., IDEFICS-derived percentiles [48]). Besides, this study is the first one in validating a cardiovascular risk indicator in a pediatric population for OSA treatment assessment, based on clinical and demographic data.

Bibliography of Part III

[1] C. L. Marcus, R. H. Moore, C. L. Rosen, *et al.*, "A randomized trial of adenotonsillectomy for childhood sleep apnea",
N Engl J Med, vol. 368, no. 25, pp. 2366–2376, 2013.
DOI: 10.1056/NEJMoa1215881.

[2] E. Tobaldini, L. Nobili, S. Strada, K. R. Casali, A. Braghiroli, and N. Montano, "Heart rate variability in normal and pathological sleep",
Front. Physiol., vol. 4, no. October, pp. 1–11, 2013.
DOI: 10.3389/fphys.2013.00294.

[3] R. S. C. Horne *et al.*, "The impact of sleep disordered breathing on cardiovascular health in overweight children",
Sleep Med., vol. 41, pp. 58–68, 2018.
DOI: 10.1016/j.sleep.2017.09.012.

[4] Y. Wu *et al.*, "Autonomic nervous function and low-grade inflammation in children with sleep-disordered breathing",
Pediatr. Res., vol. 91, no. 7, pp. 1834–1840, 2022.
DOI: 10.1038/s41390-021-01691-4.

[5] L. C. Nisbet *et al.*, "Nocturnal autonomic function in preschool children with sleep-disordered breathing",
Sleep Med., vol. 14, no. 12, pp. 1310–1316, 2013.
DOI: 10.1016/j.sleep.2013.07.010.

[6] A. Vlahandonis *et al.*, "Long-term changes in heart rate variability in elementary school-aged children with sleep-disordered breathing",
Sleep Med., vol. 15, no. 1, pp. 76–82, 2014.
DOI: 10.1016/j.sleep.2013.06.023.

[7] D. Liao *et al.*, "Sleep-disordered breathing in children is associated with impairment of sleep stage-specific shift of cardiac autonomic modulation",
J. Sleep Res., vol. 19, no. 2, pp. 358–365, 2010.
DOI: 10.1111/j.1365-2869.2009.00807.x.

[8] A. Martín-Montero, P. Armañac-Julián, E. Gil, L. Kheirandish-Gozal, D. Álvarez, J. Lázaro, R. Bailón, D. Gozal, P. Laguna, R. Hornero, *et al.*, "Pediatric sleep apnea: Characterization of apneic events and sleep stages using heart rate variability",
Computers in Biology and Medicine, p. 106 549, 2023.

[9] S. Redline, R. Amin, D. Beebe, R. D. Chervin, S. L. Garetz, B. Giordani, C. L. Marcus, R. H. Moore, C. L. Rosen, R. Arens, *et al.*, "The childhood adenotonsillectomy trial (chat): Rationale, design, and challenges of a randomized controlled trial evaluating a standard surgical procedure in a pediatric population",
Sleep, vol. 34, no. 11, pp. 1509–1517, 2011.

[10] M. Orini, R. Bailón, L. T. Mainardi, P. Laguna, and P. Flandrin, "Characterization of dynamic interactions between cardiovascular signals by time-frequency coherence",
IEEE transactions on biomedical engineering, vol. 59, no. 3, 2011.

[11] S. Kontaxis, J. Lázaro, V. D. Corino, F. Sandberg, R. Bailón, P. Laguna, and L. Sörnmo, "Ecg-derived respiratory rate in atrial fibrillation",
IEEE Transactions on Biomedical Engineering, vol. 67, no. 3, pp. 905–914, 2019.

[12] J. Milagro, M. Deviaene, E. Gil, J. Lázaro, B. Buyse, D. Testelmans, P. Borzée, R. Willems, S. Van Huffel, R. Bailón, *et al.*, "Autonomic dysfunction increases cardiovascular risk in the presence of sleep apnea",
Frontiers in Physiology, vol. 10, p. 620, 2019.

[13] R. J. Thomas, C. Wood, and M. T. Bianchi, "Cardiopulmonary coupling spectrogram as an ambulatory clinical biomarker of sleep stability and quality in health, sleep apnea, and insomnia",
Sleep, vol. 41, no. 2, zsx196, 2018.

[14] J. H. Choi, R. J. Thomas, S. Y. Suh, I. H. Park, T. H. Kim, S. H. Lee, H. M. Lee, C.-H. Yun, and S. H. Lee, "Sleep quality change after upper airway surgery in obstructive sleep apnea: Electrocardiogram-based cardiopulmonary coupling analysis",
The Laryngoscope, vol. 125, no. 7, pp. 1737–1742, 2015.

[15] T. Penzel, J. W. Kantelhardt, R. P. Bartsch, M. Riedl, J. F. Kraemer, N. Wessel, C. Garcia, M. Glos, I. Fietze, and C. Schöbel, "Modulations of heart rate, ecg, and cardio-respiratory coupling observed in polysomnography",
Frontiers in physiology, vol. 7, p. 460, 2016.

[16] S. Hietakoste, P. Armañac-Julián, T. Karhu, R. Bailón, S. Sillanmäki, J. Töyräs, T. Leppänen, S. Myllymaa, and S. Kainulainen, "Acute cardiorespiratory coupling impairment in worsening sleep apnea-related intermittent hypoxemia",
IEEE Transactions on Biomedical Engineering, 2023.

[17] M. Riedl, A. Müller, J. F. Kraemer, T. Penzel, J. Kurths, and N. Wessel, "Cardio-respiratory coordination increases during sleep apnea",
PloS one, vol. 9, no. 4, e93866, 2014.

[18] R. J. Thomas, J. E. Mietus, C.-K. Peng, and A. L. Goldberger, "An electrocardiogram-based technique to assess cardiopulmonary coupling during sleep",
Sleep, vol. 28, no. 9, pp. 1151–1161, 2005.

[19] R. Trimer, R. Cabidu, L. Sampaio, R. Stirbulov, D. Poiares, S. Guizilini, A. M. Bianchi, F. Costa, R. G. Mendes, A. Delfino Jr, *et al.*, "Heart rate variability and cardiorespiratory coupling in obstructive sleep apnea: Elderly compared with young",
Sleep Medicine, vol. 15, no. 11, pp. 1324–1331, 2014.

[20] R. J. Thomas, M. D. Weiss, J. E. Mietus, C.-K. Peng, A. L. Goldberger, and D. J. Gottlieb, "Prevalent hypertension and stroke in the sleep heart health study: Association with an ecg-derived spectrographic marker of cardiopulmonary coupling",
Sleep, vol. 32, no. 7, 897–S2, 2009.

[21] C. Varon, J. Morales, J. Lázaro, M. Orini, M. Deviaene, S. Kontaxis, D. Testelmans, B. Buyse, P. Borzée, L. Sörnmo, *et al.*, "A comparative study of ecg-derived respiration in ambulatory monitoring using the single-lead ecg",
Scientific reports, vol. 10, no. 1, pp. 1–14, 2020.

[22] P. Lévy, M. Kohler, W. McNicholas, *et al.*, "Obstructive sleep apnoea syndrome",
Nat Rev Dis Prim, vol. 1, p. 15 015, 2015.
DOI: 10.1038/nrdp.2015.15.

[23] C. Marcus, L. Brooks, K. Draper, *et al.*, "Diagnosis and management of childhood obstructive sleep apnea syndrome",
Pediatrics, vol. 130, no. 3, e714–55, 2012.
DOI: 10.1542/peds.2012-1672.

[24] F. Cappuccio, D. Cooper, L. D'Elia, P. Strazzullo, and M. Miller, "Sleep duration predicts cardiovascular outcomes: A systematic review and meta-analysis of prospective studies",
Eur Heart J, vol. 32, no. 12, pp. 1484–1492, 2011.
DOI: 10.1093/eurheartj/ehr007.

[25] Z. Shan, H. Ma, M. Xie, *et al.*, "Sleep duration and risk of type 2 diabetes: A meta-analysis of prospective studies",
Diabetes Care, vol. 38, no. 3, pp. 529–537, 2015.
DOI: 10.2337/dc14-2073.

[26] K. Spiegel, K. Knutson, R. Leproult, E. Tasali, and E. Van Cauter, "Sleep loss: A novel risk factor for insulin resistance and type 2 diabetes",
J Appl Physiol, vol. 99, no. 5, pp. 2008–2019, 2005.
DOI: 10.1152/japplphysiol.00660.2005.

[27] J. Jennings, M. Muldoon, M. Hall, D. Buysse, and S. Manuck, "Self-reported sleep quality is associated with the metabolic syndrome",
Sleep, vol. 30, no. 2, pp. 219–223, 2007.
DOI: 10.1093/sleep/30.2.219.

[28] F. Cappuccio, F. Taggart, N. Kandala, *et al.*, "Meta-analysis of short sleep duration and obesity in children and adults",
Sleep, vol. 31, no. 5, pp. 619–626, 2008.

DOI: 10.1093/sleep/31.5.619.

[29] O. Androutsos, G. Moschonis, C. Mavrogianni, *et al.*, "Identification of lifestyle patterns, including sleep deprivation, associated with insulin resistance in children: The healthy growth study",
Eur J Clin Nutr, vol. 68, no. 3, pp. 344–349, 2014.
DOI: 10.1038/ejcn.2013.280.

[30] R. Bhattacharjee, J. Kim, L. Kheirandish-Gozal, and D. Gozal, "Obesity and obstructive sleep apnea syndrome in children: A tale of inflammatory cascades",
Pediatr Pulmonol, vol. 46, no. 4, pp. 313–323, 2011.
DOI: 10.1002/ppul.21370.

[31] R. Eckel, K. Alberti, S. Grundy, and P. Zimmet, "The metabolic syndrome",
Lancet (London, England), vol. 375, no. 9710, pp. 181–183, 2010.
DOI: 10.1016/S0140-6736(09)61794-3.

[32] S. Grundy, J. Cleeman, S. Daniels, *et al.*, "Diagnosis and management of the metabolic syndrome",
Circulation, vol. 112, no. 17, pp. 2735–2752, 2005.
DOI: 10.1161/CIRCULATIONAHA.105.169404.

[33] K. Alberti, P. Zimmet, and J. Shaw, "The metabolic syndrome—a new worldwide definition",
Lancet, vol. 366, no. 9491, pp. 1059–1062, 2005.
DOI: 10.1016/S0140-6736(05)67402-8.

[34] J. Morrison, L. Friedman, and C. Gray-McGuire, "Metabolic syndrome in childhood predicts adult cardiovascular disease 25 years later: The princeton lipid research clinics follow-up study",
Pediatrics, vol. 120, no. 2, pp. 340–345, 2007.
DOI: 10.1542/peds.2006-1699.

[35] C. Magnussen, J. Koskinen, W. Chen, *et al.*, "Pediatric metabolic syndrome predicts adulthood metabolic syndrome, subclinical atherosclerosis, and type 2 diabetes mellitus but is no better than body mass index alone",
Circulation, vol. 122, no. 16, pp. 1604–1611, 2010.
DOI: 10.1161/CIRCULATIONAHA.110.940809.

[36] S. Redline, A. Storfer-Isser, C. Rosen, *et al.*, "Association between metabolic syndrome and sleep-disordered breathing in adolescents", *Am J Respir Crit Care Med*, vol. 176, no. 4, pp. 401–408, 2007. DOI: 10.1164/rccm.200703-375OC.

[37] J. Rey-López, H. de Carvalho, A. de Moraes, *et al.*, "Sleep time and cardiovascular risk factors in adolescents: The helena (healthy lifestyle in europe by nutrition in adolescence) study", *Sleep Med*, vol. 15, no. 1, pp. 104–110, 2014. DOI: 10.1016/j.sleep.2013.07.021.

[38] H. Tan and A. Kaditis, "Phenotypic variance in pediatric obstructive sleep apnea", *Pediatr Pulmonol*, vol. 56, no. 6, pp. 1754–1762, 2021. DOI: 10.1002/ppul.25309.

[39] S. Verhulst, N. Schrauwen, D. Haentjens, *et al.*, "Sleep-disordered breathing and the metabolic syndrome in overweight and obese children and adolescents", *J Pediatr*, vol. 150, no. 6, pp. 608–612, 2007. DOI: 10.1016/j.jpeds.2007.01.051.

[40] D. Gozal, O. Capdevila, L. Kheirandish-Gozal, *et al.*, "Metabolic alterations and systemic inflammation in obstructive sleep apnea among nonobese and obese prepubertal children", *Am J Respir Crit Care Med*, vol. 177, no. 10, pp. 1142–1149, 2008. DOI: 10.1164/rccm.200711-1670OC.

[41] D. Koren, D. Gozal, M. Philby, R. Bhattacharjee, and L. Kheirandish-Gozal, "Impact of obstructive sleep apnoea on insulin resistance in nonobese and obese children", *Eur Respir J*, vol. 47, no. 4, pp. 1152–1161, 2016. DOI: 10.1183/13993003.01430-2015.

[42] S. Javaheri, A. Storfer-Isser, C. Rosen, and S. Redline, "Sleep quality and elevated blood pressure in adolescents", *Circulation*, vol. 118, no. 10, pp. 1034–1040, 2008. DOI: 10.1161/CIRCULATIONAHA.108.766410.

[43] J. Gangwisch, D. Malaspina, L. Babiss, *et al.*, "Short sleep duration as a risk factor for hypercholesterolemia: Analyses of the national longitudinal study of adolescent health",
Sleep, vol. 33, no. 7, pp. 956–961, 2010.
DOI: 10.1093/sleep/33.7.956.

[44] S. Cook, M. Weitzman, P. Auinger, M. Nguyen, and W. Dietz, "Prevalence of a metabolic syndrome phenotype in adolescents",
Arch Pediatr Adolesc Med, vol. 157, no. 8, p. 821, 2003.
DOI: 10.1001/archpedi.157.8.821.

[45] R. Viner, T. Segal, E. Lichtarowicz-Krynska, and P. Hindmarsh, "Prevalence of the insulin resistance syndrome in obesity",
Arch Dis Child, vol. 90, no. 1, pp. 10–14, 2005.
DOI: 10.1136/adc.2003.036467.

[46] P. Zimmet, G. Alberti, F. Kaufman, *et al.*, "The metabolic syndrome in children and adolescents",
Lancet, vol. 369, no. 9579, pp. 2059–2061, 2007.
DOI: 10.1016/S0140-6736(07)60958-1.

[47] H. Mellerio, C. Alberti, C. Druet, *et al.*, "Novel modeling of reference values of cardiovascular risk factors in children aged 7 to 20 years",
Pediatrics, vol. 129, no. 4, e1020–e1029, 2012.
DOI: 10.1542/peds.2011-0449.

[48] W. Ahrens, L. A. Moreno, S. Mårild, *et al.*, "Metabolic syndrome in young children: Definitions and results of the idefics study",
Int J Obes, vol. 38, no. S2, S4–S14, 2014.
DOI: 10.1038/ijo.2014.130.

[49] K. Imai, L. Keele, and D. Tingley, "A general approach to causal mediation analysis",
Psychol Methods, vol. 15, no. 4, pp. 309–334, 2010.
DOI: 10.1037/a0020761.

[50] J. Gaines, A. N. Vgontzas, J. Fernandez-Mendoza, *et al.*, "Inflammation mediates the association between visceral adiposity and obstructive sleep apnea in adolescents",
Am J Physiol Metab, vol. 311, no. 5, E851–E858, 2016.
DOI: 10.1152/ajpendo.00249.2016.

[51] I. Erdim, T. Akcay, R. Yilmazer, O. Erdur, and F. T. Kayhan, "Is metabolic syndrome associated with obstructive sleep apnea in obese adolescents?",
J Clin Sleep Med, vol. 11, no. 12, pp. 1371–1376, 2015.
DOI: 10.5664/jcsm.5266.

[52] D. Gozal, M. Dumin, and D. Koren, "Role of sleep quality in the metabolic syndrome",
Diabetes Metab Syndr Obes, vol. 9, pp. 281–310, 2016.
DOI: 10.2147/DMSO.S95120.

[53] J. S. Yudkin, "Insulin resistance and the metabolic syndrome—or the pitfalls of epidemiology",
Diabetologia, vol. 50, no. 8, pp. 1576–1586, 2007.
DOI: 10.1007/s00125-007-0711-3.

[54] A. Haim, S. Daniel, E. Hershkovitz, A. D. Goldbart, and A. Tarasiuk, "Obstructive sleep apnea and metabolic disorders in morbidly obese adolescents",
Pediatr Pulmonol, vol. 56, no. 12, pp. 3983–3990, 2021.
DOI: 10.1002/ppul.25652.

[55] D. Tingley, T. Yamamoto, K. Hirose, L. Keele, and K. Imai, "Mediation: R package for causal mediation analysis",
J Stat Softw, vol. 59, no. 5, pp. 1–38, 2014.
DOI: 10.18637/jss.v059.i05.

[56] S. Scholle and G. Zwacka, "Arousals and obstructive sleep apnea syndrome in children",
Clin Neurophysiol, vol. 112, no. 6, pp. 984–991, 2001.
DOI: 10.1016/s1388-2457(01)00508-9.

[57] A. Isaiah, D. Bertoni, K. D. Pereira, M. Diaz-Abad, R. B. Mitchell, and G. Das, "Treatment-related changes in heart rate variability in children with sleep apnea",
Otolaryngol Neck Surg, vol. 162, no. 5, pp. 737–745, 2020.
DOI: 10.1177/0194599820907882.

[58] G. Aljadeff, D. Gozal, V. L. Schechtman, B. Burrell, R. M. Harper, and S. L. Davidson Ward, "Heart rate variability in children with obstructive sleep apnea",

Sleep, vol. 20, no. 2, pp. 151–157, 1997.
DOI: 10.1093/sleep/20.2.151.

[59] J. Koenig and J. F. Thayer, "Sex differences in healthy human heart rate variability: A meta-analysis",
Neurosci Biobehav Rev, vol. 64, pp. 288–310, 2016.
DOI: 10.1016/j.neubiorev.2016.03.007.

[60] D. Gozal, L. Kheirandish-Gozal, R. Bhattacharjee, and J. Kim, "C-reactive protein and obstructive sleep apnea syndrome in children",
Front Biosci, vol. E4, no. 7, p. 553, 2012.
DOI: 10.2741/e553.

[61] C. L. Marcus, L. B. Fernandes Do Prado, J. Lutz, *et al.*, "Developmental changes in upper airway dynamics",
J Appl Physiol, vol. 97, no. 1, pp. 98–108, 2004.
DOI: 10.1152/japplphysiol.00462.2003.

Part IV

Cardiovascular Signal Processing Oriented for Wearable Devices

Chapter 11

Context, Motivation and Data for Part IV

11.1 Signal Processing of PPG

Part IV of this thesis explores the analysis of PPG signals, focusing particularly on their application oriented to wearable technology. As yet mentioned in Part I, the intention is to expand our understanding of the parameters wearable devices could capture, especially in real-world scenarios. By moving beyond the typical PR and PRV analysis, we aim to gain deeper cardiovascular insights through novel PPG-derived parameters.

Wearable technologies are gaining traction due to their accessible and cost-effective nature compared to traditional data collection methods [1]. They offer a practical alternative to more cumbersome and expensive setups, such as PSG recordings for diagnosing OSA, or the array of monitoring equipment used in ICUs for patients under mechanical ventilation. However, the reliability of data from wearable PPG devices is often challenged by

motion artifacts. In addition, the physiological background for the biomarkers that can be extracted from PPG signals are still under research [2]. To address these challenges, we explore several methodologies focused on artifact detection, pulse analysis, signal quality improvement, and biomarker extraction under diverse conditions.

Initially, in Section 3.5, I have already provided a comprehensive overview of the preprocessing and analytical methods used for extracting specific biomarkers from PPG signals, used in the following chapters of this Part IV. Subsequent sections are structured around three distinct datasets. The selection of these distinct datasets is justified in each chapter, chosen based on the availability of specific signals, unique requirements, and the particular goals of each individual study.

11.2 Datasets Including PPG signals

Each of the three datasets comprises PPG signals recorded from various body locations, along with ECG signals. These datasets are distinct, featuring unique groups of independent subjects.

To gather these datasets, the researchers implemented three different stress protocols, during which all signals were captured synchronously using commercial recording devices. The specifics of these stress tests, their design, and their relevance to the study are elaborately discussed in prior research [3]–[5]. In the following subsections, we provide a concise overview of each protocol.

The data collection adhered to the ethical standards outlined in the *Declaration of Helsinki*. Detailed inclusion and exclusion criteria for the study participants are available in the corresponding referenced studies [3]–[5]. It is important to note that all participants in these datasets were young, healthy volunteers without any known cardiac or cardiovascular conditions.

11.2.1 Tilt-Table Orthostatic Stress Test Dataset

The first protocol is a Tilt-table stress test (TTT), which consisted of 10 minutes in early resting supine position (R1), followed by 5 minutes tilted up 80^{o} (T), and 5 minutes back to resting supine position (R2). There are

19 subjects available. As mentioned, note that the total time spent in this protocol is around 20 minutes.

During TTT, various biomedical signals were recorded, including ECG lead II, and PPG at two wavelengths, red (660nm, R-PPG) and infrared (940nm, IR-PPG), a transmission-based PPG signal at the finger and a reflection-based PPG signal at the forehead. All these signals were simultaneously recorded by Cardioholter 6.2-8E78 (BMII, Lithuania), using a sampling rate of 500 Hz for the ECG signal and 250 Hz for the PPG signals. Further details can be obtained in [3].

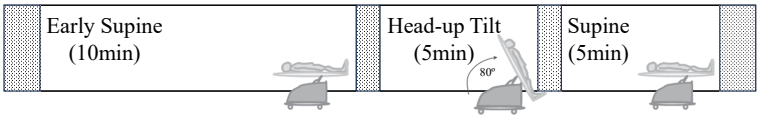

Figure 11.1: The TTT protocol consisted of three phases: 10 min in the early supine position, 5 min head-up tilt, and 5 min back to the supine position.

11.2.2 Acute Mental Stress Test Dataset

This dataset comprises ECG, respiratory, and PPG signals recorded from volunteer students at the Autonomous University of Barcelona (UAB), University of Zaragoza (UZ), and Polytechnic University of Madrid (UPM). The ABP 10 module (Medicom 83 system, MTD Ltd, Russia) facilitated the simultaneous acquisition of PPG signals at the forehead and finger (sampled at 250Hz) and Y orthogonal lead ECG (Frank Lead System) at a 1kHz sampling rate. A total of 120 young healthy participants, free from chronic or psychological diseases, were involved in the stress test. However, forehead PPG data is available for only 41 subjects due to recording issues.

Participants underwent two sessions: a 35-minute Basal Session (BS) involving relaxation and, on a separate day, a Stress Session (SS) induced through a modified Trier Social Stress Test, with an additional arithmetic task [4]. The stress session included the following stages: 1) BL_{S}, Baseline Relaxing stage. 2) ST, Story-Telling stage. 3) MT, Memory Test. 4) SA, Stress Anticipation. 5) VE, Video Exhibition. 6) AT, Arithmetic Task. For detailed protocol information, see [4]. The last five stages of the ES session

are the ones considered stressful. The others are considered relaxing. The protocol stages are illustrated in Figure 11.2.

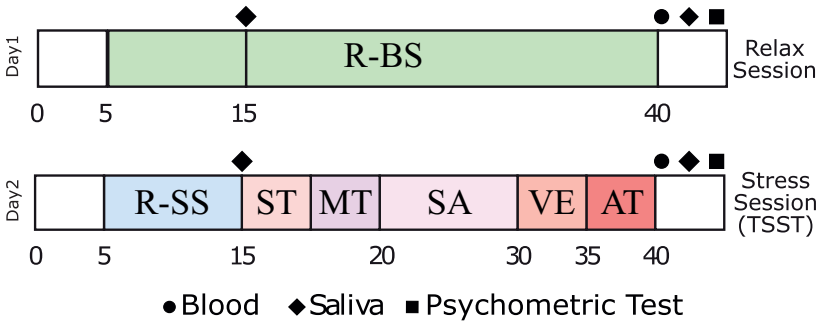

Figure 11.2: Acute Mental Stress Test Protocol. Subjects underwent a basal session (BS) and a stress session (SS) in two different days. The last five stages of the ES session are the ones considered stressful. The others are considered relaxing.

11.2.3 Heat Stress Dataset

The original study aimed to determine whether the exposure to total 36-hr sleep deprivation would suppress the ANS response to whole-body uncompensable passive heat stress in traditional Finnish sauna (air temperature of 80–90°C, relative humidity of 30%). After each sauna session, researchers could assess the impact of evening sauna-induced hyperthermia on nocturnal mental activity, cognitive and neuromuscular system efficiency, and morning stress hormone levels in 15 healthy participants [5].

Each sauna session consists of a heat stress protocol with four repetitive exposures to uncompensable heat in the sauna [5], [6]. Before and after 15-min sauna exposure at 80-90^{o}C, namely stress stages, participants were instructed to rest in semiFowler's position in a neutral temperature environment (25°C), namely rest stages, for around 20-min. The total duration of the heat stress protocol was approximately 2 h and 20 min. The study stages are detailed in Figure 11.3.

Ideally, it is expected to have six sauna recordings for each participant, corresponding to the first and second days of Total Sleep Deprivation [5], the first and second days of Partial Sleep Deprivation (PSD), and the first and second days of the control or normal condition. However, only 51 good quality recordings of biosignals are available from the whole database of 15 different participants.

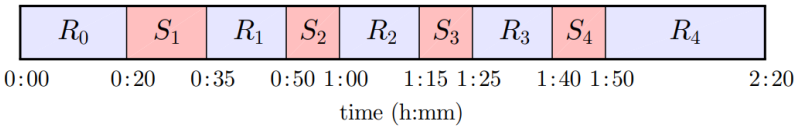

Figure 11.3: Heat stress protocol. Rest stages (R0, R1, R2, R3, R4) and sauna stages (S1, S2, S3, S4) are marked in blue and red, respectively. Refer to [6] for more details.

The biosignals were synchronously recorded at 1000 Hz using the Nautilus1 system (BMII, Lithuania), including the lead-II of the ECG and three PPG signals at red wavelength, with transmission PPG from the middle finger of the right hand (PPG_F), reflection PPG from the forehead above the right eyebrow (PPG_H), and transmission PPG from the right earlobe (PPG_E). Thus, all PPG signals were recorded on the same side of the body. The study was conducted at Lithuanian Sports University, and more information can be found in [5], [6].

Chapter 12

Coverage of PPG Sensors

12.1 Introduction

This study delves into the concept of 'coverage' in PPG signals, specifically exploring the proportion of time during which physiological parameters are reliably estimated by PPG sensors. This concept is crucial, as PPG sensors are notably prone to motion artifacts, significantly affecting signal quality, especially during active daily life periods [7].

Coverage is influenced by various aspects of sensor configuration, including the mode (transmission/reflection), placement on the body, and the stability of sensor-to-skin contact [8]–[10]. While coverage rates for raw PPG signals have been previously studied, this research extends the examination to PPG-derived parameters like PR, PAT, and PAV across different body

locations under various stress conditions [11]–[14]. All methodologies used for estimating these PPG indices are detailed in Sec. 3.5.

PPG, a straightforward and cost-effective technique for garnering cardiovascular insights, is adaptable for placement on diverse body parts, such as the wrist, fingertip, earlobe, or forehead [15]–[21]. Its flexibility makes it a favored technology for wearable devices. However, the signal's vulnerability to motion artifacts and the resultant limitations in data quality during physical activities pose significant challenges [3], [22]–[28].

The prevalence of PPG technology in both clinical settings and wearable devices prompts a need for comprehensive analysis. In clinical practice, fingertip and earlobe sensors are commonly used for heart rate and peripheral oxygen saturation monitoring. Contrastingly, wrist locations are more typical for PPG acquisition in wearable devices [29], [30]. Despite the considerable research on the efficacy of PRV as a surrogate for HRV, studies have not conclusively addressed sensor positioning's impact on coverage [28].

This chapter focuses on quantifying PPG sensor coverage when positioned at various body sites. Three distinct datasets are utilized to study the time percentage during which pulses are detectable across different PPG signals, under varying stress conditions. Additionally, the feasibility of estimating well-known PPG-dependent series such as PAT or PAV is also explored. In summary, this chapter evaluates PPG pulse detection coverage and its reliability in deriving cardiovascular indices such as PR and PAT. While the findings are based on scientific equipment rather than commercial wearables, they provide valuable insights for future wearable-based projects.

12.2 Materials and Methods

In this chapter, all recordings from the three datasets detailed in Sec. 11.2 will be analyzed.

12.2.1 ECG and PPG analysis

As yet extensively explained in Sec. 3.2, R-wave detection employs a wavelet-based method detailed in [31]. Each R-wave occurrence is denoted as n_{R}. Successive R-waves define the RR intervals, from which HR in bpm is calcu-

lated. Correction for ectopic beats and misdetections follows the approach in [32], resulting in the NN interval series for HR derivation.

PPG signals, represented as $x_{\mathrm{PPG}}(n)$, undergo a 0.3 to 15 Hz band-pass filter using a 4-th order Chebyshev type II filter, as per [33]. This filtering, implemented in a forward-backward zero-phase step, preserves signal morphology while removing baseline drift and high-frequency noise.

Prior to PPG delineation, motion artifacts are addressed. An energy-based artifact detection method [34], described in Sec. 3.5.2, is employed to selectively remove segments with significantly higher energy than clean periods.

Cubic spline interpolation is applied to the PPG signals to achieve a finer time resolution (1000 Hz) for FP delineation. The maximum up-slope instants (n_{D}) of each PPG pulse are delineated, based on a low pass differentiator filter and a time-varying threshold [35], as detailed in Sec. 3.5.3. The algorithm also marks the apex (n_{A}) and basal (n_{B}) points of each pulse.

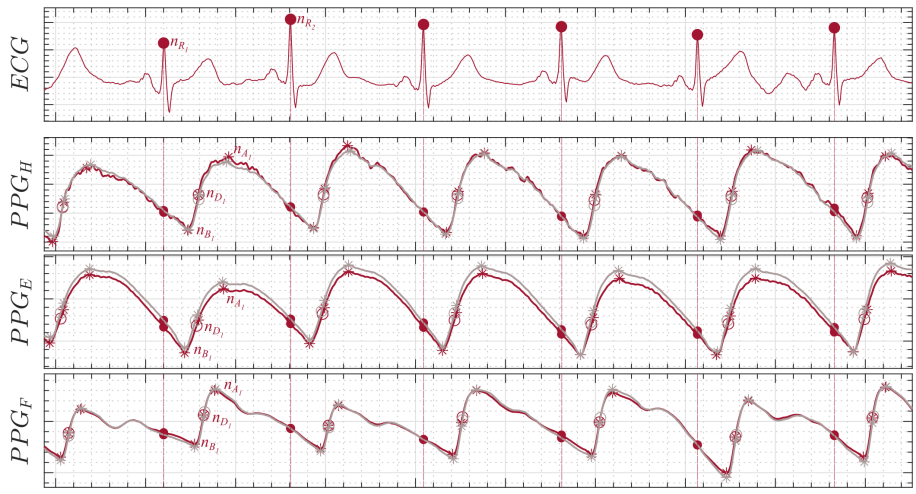

Figure 12.1: ECG and PPG synchronous recording illustration. The three PPG signals are at Forehead ($x_{\mathrm{PPG,H}}(n)$), at Earlobe ($x_{\mathrm{PPG,E}}(n)$) and at Finger ($x_{\mathrm{PPG,F}}(n)$), respectively. The FPs delineated are: n_{R} for the ECG R-wave instant, n_{D} for the PPG maximum up-slope instant, n_{A} for the PPG apex point and n_{B} for the PPG basal point. Both red PPG (R-PPG, in red) and infrared PPG (IR-PPG, in gray) lights, are also illustrated. Refer to [10], [36], for more information on the morphology of PPG in different body locations.

12.2.2 Coverage Measures

Coverage measures are approach in determining the reliability of PPG-based devices compared to ECG, the gold standard for HR monitoring. We assess PR against HR in 10-second non-overlapping segments for each FP in PPG signals. Each segment is classified as either good or bad quality based on pulse detection accuracy. The choice of a 10-second window aligns with findings that this duration suffices for accurate HR estimation [37]. A PPG segment is deemed bad if pulse detections deviate by more than 10% from ECG detections in the same timeframe. An illustrative 70-second example is shown in Table 12.2, highlighting that perfect HR estimation over an average period does not guarantee 100% coverage.

Beyond HR estimation, PPG is valuable for computing cardiovascular indices like PAT and PAV. Accordingly, this study also reports coverage measures based on these parameters. For PAT coverage, the concordance of heartbeat counts in 10-second segments with the number of PAT values is evaluated. Similarly, PAV coverage assesses the segment's validity independently of the ECG. Table 12.2 provides an example for understanding coverage definition in these contexts.

For the calculation of coverage, the reference instants for HR, PR (Eq. (3.24)), PAT (Eq. (3.25)), and PAV (Eq. (3.27)) differ, potentially leading to mismatches in 10-second segments. To mitigate this, the average PAT in the 10-seconds segment is subtracted from the PPG signal before coverage computation. This adjustment is depicted in Fig. 12.3.

As mentioned, three datasets with distinct characteristics are analyzed, each employing different PPG acquisition modes (transmission or reflection), light wavelengths (IR-PPG or R-PPG), and sensor placements (finger, forehead, or earlobe). The results include total average coverage for each dataset for PR, PAT, and PAV, considering ECG as the reference. Additionally, the extent of artifact removal in PPG signals is also quantified.

12.3 Results

Results are shown in three tables for the three different datasets (Tabs. 12.5, 12.6 and 12.7). Each table contains all the coverage information summarized for

Figure 12.2: Illustrative example for the coverage definition. For the PR, good coverage is considered, in a 10-seconds segment, if the estimation error of PPG pulses is lower than 10%, compared to ECG. For PAT-coverage measurement purposes, a 10-seconds segment is considered valid if the number of PAT values differs less than 10% to the number of ECG beats. Note that PAT measures may be omitted either because of being considered out of physiological limits or because the associated PPG pulse is considered spurious. Similarly to PAT, this is done for the PAV-coverage measurement.

Time [secs]	0	10	20	30	40	50	60	
Segment "i"	1	2	3	4	5	6	7	
# ECG beats	9	10	9	10	11	12	11	
HR [bpm]	54	60	54	60	66	72	66	62
# PPG pulses	8	9	9	10	11	14	11	
PR [bpm]	48	54	54	60	66	84	66	62
Coverage, C (10%) # beats - # PPG pulses[1]	X	OK	OK	OK	OK	X	OK	C = 71%
# PAT pulses	8	9	9	9	11	12	11	
# valid PAT pulses	7	9	8	8	10	11	10	
Coverage, C (10%) # beats - # PAT pulses[2]	X	OK	X	X	OK	OK	OK	C = 57%
# PAV Pulses	8	11	9	9	11	12	13	
# valid PAV pulses	8	10	9	9	9	11	11	
Coverage, C (10%) # beats - # PAV pulses[3]	X	OK	OK	OK	X	OK	OK	C = 71%

[1]IF (#PPG-pulses*(i)* ≥ #ECG-beats*(i)**0,9 AND #PPG-pulses*(i)* ≤ #ECG-beats*(i)**1,1), C*(i)*="OK"; else, C*(i)*="X".
[2]IF (#valid PAT-pulses*(i)* ≥ #ECG-beats*(i)* *0,9), C*(i)*="OK"; else, C*(i)*="X".
[3]IF (#valid PAV-pulses*(i)* ≥ #ECG-beats*(i)* *0,9 AND #valid PAV-pulses*(i)* ≤ #ECG-beats*(i)* *1,1), C*(i)*="OK"; else, C*(i)*="X".
With "*i*" being the index for each 10-s segment.

all the PPG signals: body locations, characteristic protocol stages, PPG light emission wavelength and FP's delineated.

First, the percentage of artifacts detected from each PPG signals is displayed in Table 12.4. Note that an artifact is considered only in segments with clearly higher energy than the clean segments. A small percentage of artifacts are suppressed, from 1% to 6% in signals of 20 min and 2h20m, in the Tilt-Table Test and in the Heat Stress Test, respectively. However, the PPG at the Forehead in the Acute Mental Stress Test was low quality and almost 20% of the PPG were artifacts.

12.3.1 Tilt-Table Orthostatic Test Dataset

Coverage results for the TTT are shown in Table 12.5. There is good PPG coverage for estimating PR. Around 80% to 90% of HR can be estimated via PPG with 10% error or less, regardless the FP used. The coverage is similar whether using PPG at finger or at forehead, and for IR-PPG or R-PPG

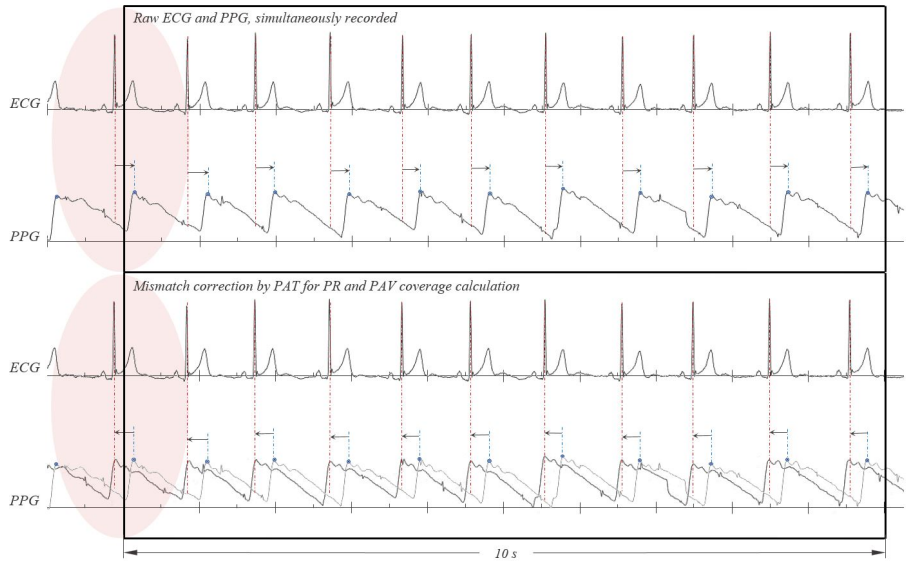

Figure 12.3: Correction of mismatch in the PPG signal for PR and PAV coverage calculation. Prior to assessing coverage for PR or PAV, the average PAT is subtracted to align pulse occurrences (n_{FP_i}) with heartbeat events ($n\mathrm{R}_i$). Failure to do so may result in mismatches, underestimating actual coverage.

Table 12.4: Percentage of artifacts detected for each PPG signal at the three datasets.

C(%)	Finger		Forehead		Earlobe			
	IR-PPG	R-PPG	IR-PPG	R-PPG	IR-PPG	R-PPG	N	Duration
TTT	1%	2%	1%	1%	-	-	19	20min
ES3	6%	-	19%	-	-	-	120	1h10min
Sauna	4%	4%	3%	4%	3%	1%	51	2h20min

lights as well, although slightly better for IR-PPG.

However, it is remarkable that the coverage deteriorates when we try to estimate the PAT. There is an approximate maximum of 75% PAT pulses that can be properly defined, compared to the number of R-waves delineated. Remember that while an R-wave exists, the corresponding PAT can be omitted, either because of a bad definition in time of the FP, or an outlier, or even a PAT defined out of the physiological range. Even more, whereas the n_{A} appears to be a good FP to estimate the PR, now it presents the worst results of coverage in terms of PAT, with an average coverage of 53-56%. The other FPs report a higher coverage, around 70%.

Table 12.5: Coverage results (in %) for the TTT dataset.

C(%)	Finger						Forehead					
	IR-PPG			R-PPG			IR-PPG			R-PPG		
	n_A	n_B	n_D	n_A	n_B	n_D	n_A	n_B	n_D	n_A	n_B	n_D
PR	89	92	89	86	90	89	86	93	92	83	92	90
PAT	56	74	75	57	68	73	53	76	75	53	73	71
PAV	92			91			93			92		

12.3.2 Acute Mental Stress Dataset

Results for the mental stress test are shown in Table 12.6. Again, the coverage of PPG to estimate the PR is notably higher than to estimate the PAT. In addition, it can be seen a sudden decrease in the coverage for the PPG at forehead, compared to the coverage at finger. In fact, looking at the PPG at forehead, the quality of the signal in this dataset is particularly bad. As a result, an average coverage of 30% is found for estimating PR or PAT.

Table 12.6: Coverage results (in %) for the acute mental stress test dataset.

C(%)	Finger			Forehead		
	IR-PPG			IR-PPG		
	n_A	n_B	n_D	n_A	n_B	n_D
PR	73	73	74	34	34	35
PAT	48	59	60	28	25	26
PAV	76			41		

12.3.3 Heat Stress Dataset

Third, results for the heat stress test are shown in Table 12.7. For this dataset, there are available 6 PPG signals for 2h-20min of recordings, including PPG at finger, forehead and at earlobe, both for IR-PPG and R-PPG lights. In general, except for some particular cases, all PPGs have good signal quality.

Coverage for PR estimation is around 70 to 80%. In fact, no big differences are found for the coverage either using IR-PPG or R-PPG lights. Moreover, coverage of PR estimation and of PAT estimation are quite similar. The highest coverage rates are for the PPG at earlobe, using the R-PPG wavelength. Nevertheless, for the PAT estimation using n_{A}, we can see again the smaller coverage rates.

Table 12.7: Coverage results (in %) for the heat stress test dataset.

C(%)	Finger						Forehead						Earlobe					
	IR-PPG			R-PPG			IR-PPG			R-PPG			IR-PPG			R-PPG		
	n_A	n_B	n_D	n_A	n_B	n_D	n_A	n_B	n_D	n_A	n_B	n_D	n_A	n_B	n_D	n_A	n_B	n_D
PR	76	73	76	76	74	77	72	75	78	64	65	69	75	78	79	86	89	90
PAT	70	77	78	72	77	78	58	78	79	51	69	71	68	78	78	75	90	90
PAV	75			76			79			71			76			90		

12.4 Discussion

Coverage for mean PR, PAT, and PAV have been analyzed when using different PPG FPs with signals recorded at different parts of the body and light wavelengths. As mentioned before, the coverage definition differs depending on the physiological parameters to estimate, *i.e.*, PR, PAT or PAV. On the one hand, regarding PR coverage, a segment is considered valid for PR estimation if PPG can estimate this parameter with an error lower than 10% with respect to the HR estimated from the ECG, which is taken as ground truth. On the other hand, a physiological range restriction and an outlier rejection rule are applied to PAT estimation, and only the outlier rejection rule is applied to PAV. A ground truth is not available for these two estimates, since PAT is estimated inside its physiological limits and PAV is a relative measure with arbitrary units. Then, a segment is considered valid if the difference in the number of PAT or PAV estimates determinable in the segment is lower than 10% with respect to the number of heartbeats detected from the ECG. In general, the best results in terms of coverage are obtained for the transmission-PPG at finger, especially using n_{D} or n_{B} as FP. Except for some particular cases, coverage of PPG when estimating the PR, compared to coverage of ECG, is equivalent.

Regarding the placement of the PPG, the obtained coverage for finger and earlobe are higher, whilst the coverage at forehead is usually lower. This is due to the fact that PPG acquisition is very sensitive to artifacts due to either poor contact or minimal motion artifacts, and PPG at forehead is predisposed to these (because of facial expression and setup configuration). Moreover, the device to record PPG at forehead must be dedicated and signal quality must be ensured before recording as well. We show no fundamental differences and no advantage between using IR-PPG or R-PPG light for PPG

recordings. Note that the devices used for the recordings did not include green light, which is the most common wavelength for PPG measurement with wearable devices. An influence of the selected FP in the coverage was observed, specially for PAT and PAV. The end of systole of the PPG pulses are typically smooth, making n_{A} very vulnerable to additive noise, in line with the observations of [38]. Furthermore, the morphology of the apex of PPG at earlobe or at forehead is also usually smoother.

The FP n_{A} might be used for mean PR estimation with a similar performance to that obtained by the other methods. However, results of PAT coverage suggest that the performance weakens for this FP n_{A}. On the contrary, FPs n_{D} and n_{B}, are less prone to this heterogeneity in morphology. In fact, the FP analysis performed in [3] in the TTT dataset, for time domain PRV estimation, reported that n_{B} and n_{D} had the minimum relative errors compared to the HRV estimators based on the ECG, with n_{D} representing the instant of maximum flow velocity for each heartbeat and n_{B} representing the time onset of systole.

In fact, looking at Tabs. 12.5, 12.6 and 12.7, the coverage for estimating PAT, using n_{A} as FP, is lower than using n_{D} or n_{B}. The coverage for PR estimation using n_{A} is also slightly lower than using n_{D} or n_{B}. However, the coverage for estimating PAV is high. Based on that, we can say that the estimation of the maximum point of a PPG pulse, *i.e.*, $x_{\mathrm{PPG}}(n_{\mathrm{A}})$, can be done well. Then, for measurements derived from the amplitude, such as PAV, the coverage is good, but if measurements are based on the time instant of detection, *i.e.*, n_{A}, coverage may worsen both for estimating PR and PAT, the latter getting much worse due to the very small dynamic range intrinsic to PAT. Therefore, the delineation of the FP in time is critical depending on the application of use. In general terms, in order to better suit the smoother shapes of the reflection-based PPG signals, and for a greater robustness under non-stationary conditions such as wearable scenarios, we suggest using n_{D} or n_{B} as FP, to get the best possible coverage rates.

Although many previous works analyzed the feasibility of PRV as a surrogate of HRV, to the best of our knowledge, there are no previous works studying the coverage when deriving other cardiovascular indices such as PR, PAT or PAV estimation. Different coverage is obtained, using the same PPG signal, depending on the PPG pulse fiducial point chosen for delineation.

Additionally, for PRV analysis, the sensor results regarding the position are not conclusive [28]. In this work, some advice and results regarding PPG recording places, delineation or stress protocols are reported. For further studies, each setup should be first analyzed and validated taking the results and guidelines presented in this work into account, to study the feasibility of their recording devices with respect to each specific application.

Finally, some limitations should be noted. Forehead-PPG signal was not of main interest for the purposes of the study for which the Acute Mental Stress Test dataset was recorded. Thus, the choice of the sensor was not optimal. As a consequence, PPG at forehead is very noisy, and very low coverage has been obtained for this dataset. In addition, none of the three datasets analyzed included daily life data from wearables, as in [39], where a greater impact of artifacts is expected. Consequently, the obtained coverage cannot be extrapolated to daily life in absolute terms. However, these datasets allow us to extract interesting conclusions in relative terms between FP and sensor positions.

12.5 Conclusions

Finger- and earlobe-PPG signals obtained the higher coverage rates, with coverage ranging from 70% to 90% for estimating the PR, 50% to 90% for estimating the PAT, and 75% to 90% for estimating the PAV. Lower coverage has been obtained for forehead-PPG signals, probably due to the smoother shapes of the PPG at this location. The results should be read keeping in mind that coverage has been reported using protocolized datasets in controlled environments, and further studies should be performed using data from daily life, for measures of PR, PAT and PAV.

Different coverage is obtained, using the same PPG signal, depending on the PPG pulse FP chosen for delineation. The PPG pulse FP optimal to derive clinically useful measures as PR, PAT or PAV, maximizing the coverage rates are the n_{D}, or alternatively, n_{B}, especially in case of PAT measures.

Chapter 13

PTTD and PAT for Acute Mental Stress Recognition

13.1 Introduction

This chapter 13 delves into the exploration of vascular responses to mental stress, focusing on the PTTD as a viable biomarker. PTTD, an alternative metric to PWV, holds promise due to its independence from PEP variability. This study aims to validate PTTD's efficacy in reflecting stress-induced cardiovascular dynamics, correlating closely with PWV.

PTTD estimation needs precise placement of dual PPG sensors at distinct body locations, artifact removal and appropriate pulse delineation techniques. The theoretical framework for PTTD and its potential as a stress biomarker,

anchored in its association with cardiovascular metrics, has been thoroughly detailed in Sec. 3.5.4.

Stress triggers a complex physiological response regulated by the ANS, which manages the balance between rest-and-digest and fight-or-flight states through vascular changes. To quantify stress-related vascular changes, PTT—the time taken for a pressure wave to travel between arterial sites—is a critical metric [40]. While PAT has been a common surrogate for PTT in non-invasive blood pressure estimation [41], its accuracy is limited due to the inclusion of PEP [42]. PTTD, independent of PEP, theoretically could provide a more reliable assessment of PTT. It is measured as the interval between pulse occurrences in two separate PPG sensors [43], [44]. This chapter focuses on exploring the changes in PTTD under acute mental stress, assessing its effectiveness as a biomarker for stress analysis.

13.2 Materials and Methods

13.2.1 Database

This analysis utilizes data from the acute mental stress test, as detailed in Section 11.2.2. However, due to the inferior quality of forehead PPG signals, only 14 participants' data were deemed suitable for inclusion.

13.2.2 ECG and PPG Analysis

Both ECG and PPG signals underwent a similar processing pipeline as described in earlier chapters. Key steps included band-pass filtering (0.3 to 15 Hz) using a 4th order Chebyshev type II filter and application of an energy-based artifact detector (Sec. 3.5.2).

PAT to the finger ($d^u_{\mathrm{PAT,F}}(n)$) and forehead ($d^u_{\mathrm{PAT,H}}(n)$) was calculated using respective PPG signals and ECG data (Eq. 3.25). PTTD was estimated as the difference in pulse instants between finger and forehead PPG signals, $d^u_{\mathrm{PTTD,HF}}(n)$ (Eq. 3.26). Specific considerations for $d^u_{\mathrm{PTTD,HF}}(n)$ estimation included physiological range limitations, reference instants, and potential negative values, all detailed in Sec. 3.5.4 of Part I.

Outlier detection was applied to $d^u_{\mathrm{PAT,F}}(n)$, $d^u_{\mathrm{PAT,H}}(n)$, and $d_{\mathrm{PTTD,HF}}$ estimates using empirically adjusted parameters [45], explained in Sec. 3.5.4.

Evenly-sampled versions of $d_{\mathrm{PAT,F}}(n)$, $d_{\mathrm{PAT,H}}(n)$, and $d_{\mathrm{PTTD,HF}}(n)$ are obtained through cubic spline interpolation at 4 Hz (see Fig. 3.22), facilitating further analysis (Sec. 3.5.4).

13.2.3 Spectral Estimation of PAT and PTTD

A 300-order-FIR band-pass filter was applied to $d_{\mathrm{PAT,F}}(n)$, $d_{\mathrm{PAT,H}}(n)$ and $d_{\mathrm{PTTD,HF}}(n)$, to obtain its HF power and LF power [46], [47]. The signals were analyzed in a 30-seconds-length running window with a 50%-overlap for spectral analysis.

13.2.4 Statistical Analysis

The features used are the median and standard deviation, σ, calculated with a 1-minute-length sliding window, for each pulse *"i"* of the $d_{\mathrm{PTTD,HF}}(n)$, $d_{\mathrm{PAT,F}}(n)$, and $d_{\mathrm{PAT,H}}(n)$ series. The stages are characterized by the median of the values obtained in each windowed signal.

The Wilcoxon signed-rank test (subject-paired) was performed to study the differences between relax and stress stages. An statistical analysis was applied for finding differences in PTTD-based features between the stress (ST, VE, SA) and relax (BL_{S}) stages of the protocol. In addition, the same features were calculated for the $d^{u}_{\mathrm{PAT,H}}(n)$ and $d^{u}_{\mathrm{PAT,F}}(n)$ signals in order to evaluate their discriminative power differentiating stress and relaxation stages.

The last five stages of the stress session are considered stressful and the psychometric evaluation at the end of the session revealed that subjects responded to the stress stimuli [4]. However, MT and AT phases were excluded from the analysis because subjects were requested to speak during those phases; as PTT has a strong relationship with respiration, changes with respect to basal can be reflecting speaking-induced changes in respiration.

13.3 Results

The subset used was extracted from a larger database, where only 14 volunteers had both PPG signals with sufficient quality to be able to calculate the corresponding PTTD with a detection percentage greater than 70% with

respect to the total number of heartbeats. Surprisingly, there were volunteers who had a negative basal PTTD, which means that the pulse wave was reaching the finger before the forehead in relaxation.

Table 13.1 shows the median and interquartile range (IQR) obtained by comparing the median and σ of the $d^u_{\mathrm{PAT,H}}(n)$, $d^u_{\mathrm{PAT,F}}(n)$ and $d^u_{\mathrm{PTTD,HF}}(n)$ for all the subjects among basal stage and the different stress stages of the protocol. Spectral analysis was also performed in order to compute the frequency indices. Although it could not be done for the whole subset since the duration of the evenly-sampled signals without time gaps were too short to be done, one example is presented in Figure 13.2.

Table 13.1: Median ($IQR_{25\%}$ - $IQR_{75\%}$) for the moving median and σ with a 1 minute-length window for $d_{\mathrm{PTTD,HF}}(n)$, $d_{\mathrm{PAT,H}}(n)$, $d_{\mathrm{PAT,F}}(n)$ in relax and stressful stages. Statistical significance between a stressful stage and BL_{S} is marked with an asterisk.

Parameters [msecs]	BL_S	ST	SA	VE
median ($d^u_{\mathrm{PTTD,HF}}$(n))	26 (16-36)	18 (4-34)	24 (12-40)	21 (0-40)
median ($d^u_{\mathrm{PAT,H}}$(n))	211 (200-245)	192 (162-223)*	208 (185-245)	203 (175-233)*
median ($d^u_{\mathrm{PAT,F}}$(n))	248.5 (235-262)	222 (211.5-227)*	247 (229-261)	235 (221-253)*
σ ($d^u_{\mathrm{PTTD,HF}}$(n))	9.84 (6.7-14)	12 (10.5-17.70)*	14 (7.5-15)	11 (9.6-11.6)
σ ($d^u_{\mathrm{PAT,H}}$(n))	11 (9-20)	11 (8-15)	13 (9-18)	10 (9-19)
σ ($d^u_{\mathrm{PAT,F}}$(n))	6.3 (5.6-7.6)	6.2 (4-7.1)	6.6 (6.3-8)	5.5 (5-6.7)

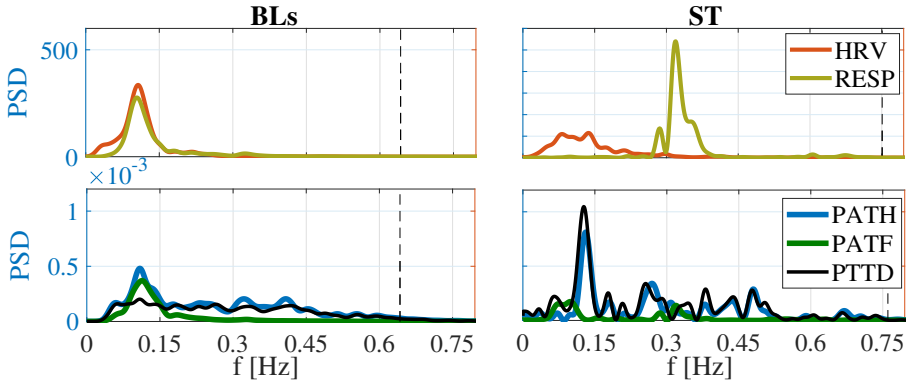

Figure 13.2: PTTD spectral analysis for a subject in BL_{S} and ST stages. HRV (from the ECG) with Respiration (top) and $d_{\mathrm{PTTD,HF}}(n)$, $d_{\mathrm{PAT,F}}(n)$ and $d_{\mathrm{PAT,H}}(n)$ spectral estimation (bottom).

13.4 Discussion

The possibility of quantifying changes in the sympathovagal balance caused by acute mental stress was studied, using non-invasive sensors based on PPG and also without the need of either the ECG or cuff/intra-arterial BP sensors in the case of the PTTD index. As shown in Table 13.1, statistically significant differences for the variance of PTTD were found in the ST when compared to BL_{S}, suggesting that it might be useful to detect states of acute mental stress.

Although there were no statistically significant differences in the median -that could be due to the small number of subjects-, a descending trend may be observed in the stressful stage ST compared to the relax stage BL_{S} suggesting that the $d_{\mathrm{PTTD,HF}}$ decreases with stress. Furthermore, statistically significant reduction in the median of both PATs was seen in ST and VE with respect to BL_{S}. According to the results in [4], ST and VE were also more differentiable than SA because of the specific stressors. With this mechanism, the pulse wave velocity to the limbs is greatly increased with respect to the one to the forehead despite the fact that the volume of blood that reaches to the brain is much greater than to the hands.

Spectral analysis shown in Fig. 13.2 reveals that the $d_{\mathrm{PAT,F}}(n)$ (blue) has less power than the $d_{\mathrm{PAT,H}}(n)$ (green) during stressful stimuli (ST) and, therefore, the power of $d_{\mathrm{PTTD,HF}}$ (orange) is very similar to that of the $d_{\mathrm{PAT,H}}(n)$. On the contrary, PAT spectral power in relaxation (BL_{S}) is similar for both $d_{\mathrm{PAT,F}}(n)$ and $d_{\mathrm{PAT,H}}(n)$, resulting in a lower power of $d_{\mathrm{PTTD,HF}}(n)$. Moreover, in the basal stage, it is clearly seen that there is a component around the BR in both PAT series and $d_{\mathrm{PTTD,HF}}$, related to RSA. However, in the stress stage, the $d_{\mathrm{PAT,F}}(n)$ has two components, one below 0.15 Hz and another around the BR; while almost all the spectral power of $d_{\mathrm{PAT,H}}(n)$ is centered around 0.1 Hz, apparently associated with the Mayer wave which is a resonant effect of vasoconstriction with a period of 10 seconds caused by acute sympathetic activation [46]. This Mayer wave, being very powerful at forehead but not at finger, are reflected in the $d_{\mathrm{PTTD,HF}}$ as a consequence. A similar finding was obtained in [44] for 14 volunteers that performed a tilt-table test. During tilt stage, the power in the LF band at forehead was substantially increased with respect to the one at finger, thus

in the LF power of the $d_{\mathrm{PTTD,HF}}$.

One possible hypothesis to explain that increase of the Mayer wave power in stress stages only in $d_{\mathrm{PAT,H}}(n)$, hence in $d_{\mathrm{PTTD,HF}}$, is the following: During a stressful situation, sympathetic activation causes vasoconstriction in the blood vessels, whose effect is expected to be much greater in the extremities than in the vessels that carry blood to the brain. Then, probably, the rigidity of the peripheral arteries of the extremities under acute sympathetic activation is much greater, thus a lower dynamic range of $d_{\mathrm{PAT,F}}(n)$ relative to that of $d_{\mathrm{PAT,H}}(n)$ might be expected during stress. On the contrary, during relax there is an absence of such strong vasoconstriction and the variations in the PAT that can be observed in the finger and in the forehead are quite similar.

Nevertheless, it's necessary to verify if the existence of all these components is consistent and general in all population. A study involving more subjects is required as the PPG signals registered at forehead in this database were of low quality. Then, only few of them had a reliable spectral estimation from a PTTD signal without time gaps due to the large amount of bad or miss-detections.

This methodology could be embedded in ad-hoc devices for the $d_{\mathrm{PTTD,HF}}$ measurement. It may lead to clinical applications that include not only stress assessment and identification but also non-invasive, continuous and ambulatory monitoring of the arterial tree condition with the need of only two PPG sensors. However, the noise sensitivity of the PPG is a significant aspect to take into account.

13.5 Conclusions

It can be concluded that $d_{\mathrm{PTTD,HF}}$ is able to distinguish between relax and induced mental stress. Local vasoconstriction caused by Mayer waves could explain the significant strong fluctuations in $d_{\mathrm{PTTD,HF}}$. In addition, a descending trend is also observed in the $d_{\mathrm{PTTD,HF}}$ in the case of a sympathetic activation.

Chapter 14

Vascular Reactivity Characterized by PPG-derived Pulse Wave Velocity

14.1 Introduction

The present chapter 14 builds upon the evaluation of PTTD in the acute mental stress trial, by extending the investigation to include a comprehensive analysis of vascular reactivity using PPG-derived PWV biomarkers. This study involves fifteen subjects undergoing a passive heat stress test, a perfect condition to evaluating vascular responses without requiring active mental or physical exercise. The heat stress test used simulates a passive stressor, causing physiological responses including peripheral vasodilation and increased HR, which are expected to influence arterial PWV [48], [49].

Initially focusing on analyzing PTTD, this chapter evolved to include a comprehensive analysis of non-invasive vascular measures such as PAT and PDA. This extended scope is employed to investigate cardiovascular adaptations to heat stress and the effectiveness of PWV surrogates in detecting these changes. Employing the methodologies detailed in Sec. 3.5.1, I analyze PPG signals from healthy participants during the heat stress test to calculate PWV and vascular reactivity surrogates. The study not only compares PWV obtained from PAT-based measurements with those from PTTD and PDA but also aims to provide novel insights into cardiovascular function. This could potentially identify new biomarkers for cardiovascular health assessment that offer an expanded perspective beyond what traditional ECG sensors and HRV indices provide.

14.2 Materials and Methods

14.2.1 Database

The data used in this study comes from one recording for each of the 15 young (26 ± 2 years), healthy male volunteers, as part of a study investigating the impact of sleep deprivation on ANS responses to passive heat stress [5]. The fifteen sauna sessions included in this study comes from the control session, i.e., when the fifteen volunteers had had normal sleep (8h of sleep), before sauna session. All the sauna sessions were collected between 7:00 and 11:00 p.m. The biosignals, including lead-II ECG and PPG signals at different body locations, were captured using the established setup.

14.2.2 Biomarkers from ECG and PPG

From the ECG and PPG signals, all biomarkers described in Sec. 3.5.4 are calculated, including HR, PAT, PTTD and PDA parameters. Outliers are detected and suppressed using a mean absolute deviation method [50], as detailed in Sec. 3.5.4.

14.2.3 Statistical Analysis

In our study, we employed a two-minute moving window strategy with a 50% overlap to compute mean and standard deviation series for each stage of the heat stress protocol. To mitigate transient responses, we excluded the first and last three minutes from all stages. For each stage, we conducted a linear regression analysis on the average values of the two-minute window to track the evolution of the parameters, referred to as slope (see Fig. 14.1).

Key features extracted for each parameter and stage included the initial value, the end-of-stage value, and the slope from the regression analysis. To synthesize the data across all subjects, we averaged these three features for the PAT, PTTD, and PDA measurements from the 15 participants. To compare the average relaxation stages values with the stress ones, we applied a Wilcoxon signed-rank test. This paired statistical test was specifically chosen for its ability to assess differences within the same patient, comparing their average relax values with the corresponding average values observed during stress (as illustrated in Fig 14.2).

Finally, we explored the correlation between the various PWV biomarkers with HR across the different stages. To this end, we first calculated the average HR and PWV values for each patient for the relax stages (1, 3, 5, 7, 9) and stress stages (2, 4, 6, 8) separately. This step was crucial to ensure that the subsequent bootstrap analysis would be based on representative mean values rather than individual stage measurements, which could be subject to transitory fluctuations.

We then employed a bootstrap resampling technique, with 1000 iterations for each PWV biomarker, to estimate the 95% confidence intervals for the mean correlation coefficients of PWV with HR. In each bootstrap iteration, participants' correlation values were resampled with replacement, and the correlation between the averaged HR and PWV values was calculated for

both relax and stress conditions. The bootstrap process thus generated a distribution of mean correlation coefficients, from which we extracted the 2.5th, 50th (median), and 97.5th percentiles, thereby constructing the 95% confidence intervals for the average correlations in both relax and stress states (see Fig. 14.3).

14.3 Results

14.3.1 PWV analysis

Fig. 14.1 presents the evolution of HR, PAT, PTTD and PDA, the latter measured using PPG_F, for one representative volunteer during the heat stress protocol. We can observe that during heat stress, PAT exhibits a highly pronounced linear decrease, parallel to the linear increase trend observed in HR. In contrast, during the relax/recovery stages, the PAT values remain relatively stable, with flat slope. The standard deviation of PAT in each 2-minute window does not show a generalized apparent variability.

Regarding PDA evolution, the patterns observed in the first inner wave width (W_1) and the time interval between the first and second inner waves of PPG_F (T_{12}) have trends similar to PAT. During heat stress, vasoconstriction leads to shorter arrival times, hence higher velocities, resulting in reduced W_1 and T_{12}, as expected by physiology.

The distribution for all participants of inter-stage slope, the initial value, and the end-of-stage values averaged by typology of stress, i.e., at relax vs. stress stages, have been calculated and displayed in boxplots in Fig. 14.2. The arrival times of the pulse wave differ among the PPG measurement sites, with the fingertip PAT presenting the longest absolute values, followed by the forehead and, finally, the earlobe; with median values for all volunteers around 205ms, 155ms and 135ms, respectively, in relax compared to 174ms, 136ms and 123ms during heat stress (absolute reduction around 15% under stress, see Fig. 14.2(b)). On average, PTTD values are also longer during the relax stages compared to the stress stages, as expected. The end-of-stage median values for PTTD in relax compared to stress (Fig. 14.2(b)) are: 47ms vs. 36ms, respectively, for $PTTD_{HF}$; 65ms vs. 48ms for $PTTD_{EF}$; and 20ms vs. 13ms for $PTTD_{EH}$ (an absolute reduction around 30% under stress). As shown in Fig. 14.2(a), the PTTD values did not change during

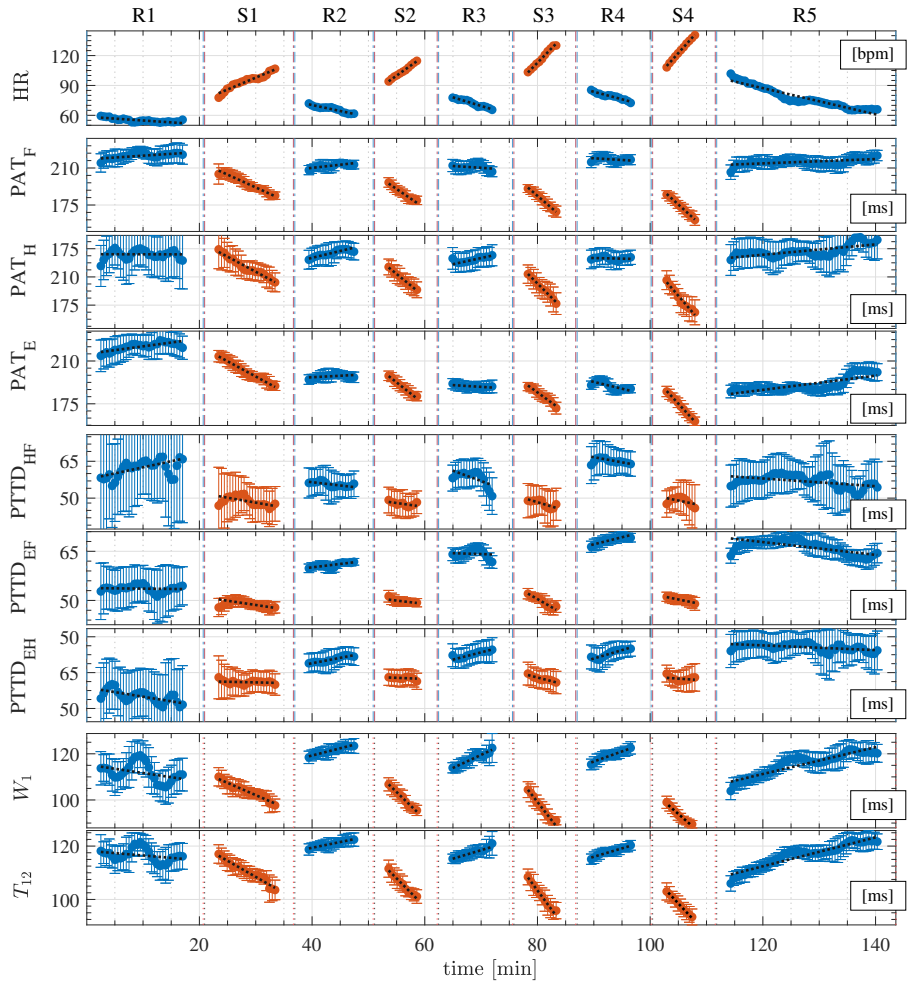

Figure 14.1: HR, PAT, PTTD and PDA evolution for one illustrative volunteer. The black dotted lines represent the first order regression obtained for each metric and stage. Data collected during heat stress exposure within the sauna are represented in red, whereas measurements taken during the basal and recovery phases at normal ambient temperature outside the sauna are indicated in blue. Units: HR: [bpm]; others: [ms].

the corresponding stages, having changes close to 0ms/min, whereas PAT presents a linear decrease $\approx$ 2.5 ms/min, while stress remains.

A notable observation in Fig. 14.1 is that as the protocol progresses, the end-of-stage PWV values in the stress stages gradually become slightly lower, indicating a memory effect. This has been seen for this representative participant in Fig. 14.1, but an exploratory analysis revealed a similar evolution in all subjects included.

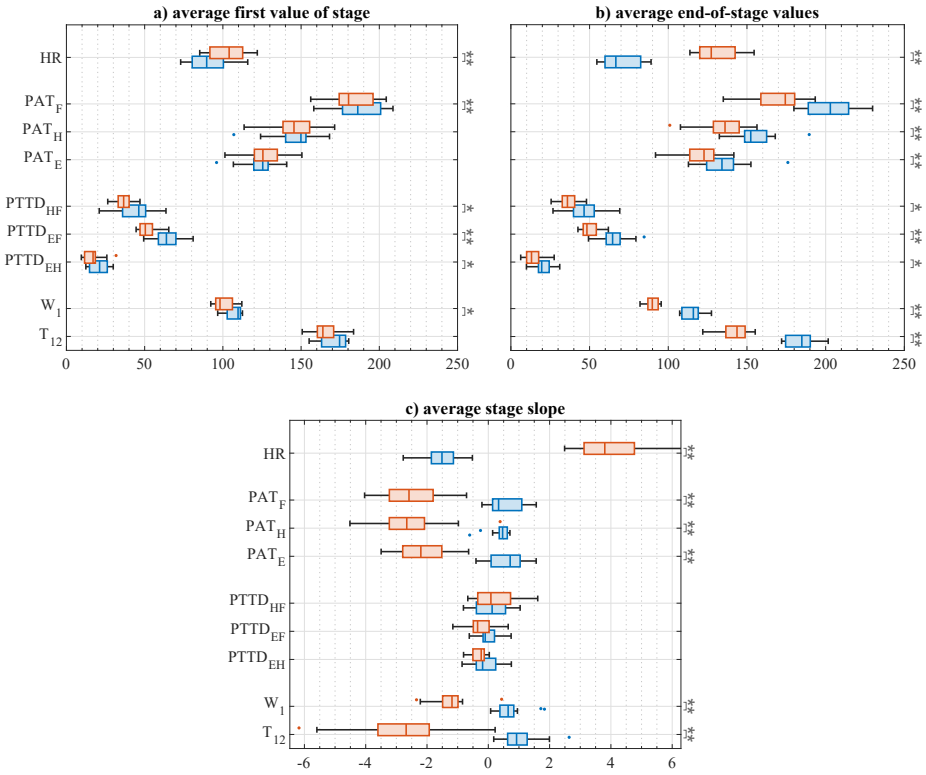

Figure 14.2: Distribution of HR and PWV biomarkers for the 15 subjects, averaged by typology of stress: relax [blue] vs heat stress [red]. (a) represents the average of the first value in the stage, (b) the average end-of-stage PWV values, and (c) the intra-stage change (represented as the slope of a first-order fit). Statistically significant differences comparing relax vs stress values are displayed with asterisks ('+', $p < 0.05$; '*', $p < 0.01$; '**', $p < 0.001$). Units: (a) and (b): HR in [bpm], others in [ms]; (c) HR in [bpm/min], others in [ms/min].

14.3.2 Heart rate correlation with PWV surrogates

Fig. 14.3 displays the 95% confidence intervals for the average correlation coefficient (ρ) between the evolution of HR and PWV biomarkers averaged across the two types of stages: relaxation and stress. A notable correlation is observed between HR and the PWV estimates from PAT_F, PAT_H, PAT_E, W_1, and T_{12} during stress stages, with coefficients significantly deviating from zero and approaching -1, indicating a strong inverse relationship under stress. Conversely, PWV estimates from PTTD exhibit no significant correlation with HR during either relaxation or stress stages, suggesting a lack of association in these measures.

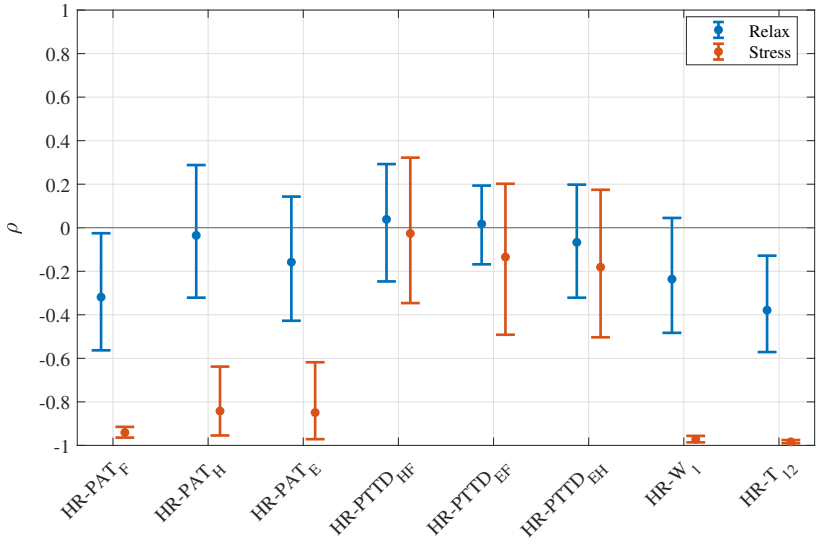

Figure 14.3: Median and 95% confidence intervals for the average correlation, ρ, between HR and the PWV biomarkers of all participants, for Relax and Stress Stages.

14.4 Discussion

The study involved 15 healthy volunteers, and the analysis focused on assessing PWV from PPG at different anatomical locations using PAT, PTTD, and PDA. These surrogate measures offer valuable insights into the relative changes in vasoconstriction, i.e., vascular reactivity. However, it is important to consider the methodological and physiological differences among these metrics, as they can affect the interpretation and usability in various scenarios.

14.4.1 PWV for vascular reactivity assessment

PWV is a crucial indicator of arterial stiffness and overall vascular health. Our study findings, as highlighted in the boxplots of Fig. 14.2, demonstrate that all three PPG-based methods—PAT, PTTD, and PDA—effectively detect changes in PWV and vascular reactivity during heat stress. These methods reveal significant differences in PWV values between relax and stress stages, underscoring their efficacy in capturing vascular dynamics.

Specifically, we observed that the intra-stage slope for PAT and PDA,

as a measure of vascular reactivity, is highly negative during heat stress, as evidenced in Fig. 14.2. This pattern suggests a progressive increase in PWV under these conditions. However, PTTD presents a different response: even as HR undergoes abrupt changes during heat stress stages, the slope of PTTD estimates remains much smaller, especially in $PTTD_{EH}$, while the average level of PTTD does change. This finding implies that PTTD is sensitive to vasoconstriction changes but less so to the progressively increasing changes, which could be partially attributed to PEP.

The distinct behavior of PTTD is further illustrated in Fig. 14.1, which depicts the evolution of these parameters in one representative volunteer. The three PTTDs show a significant and immediate change at the onset of stress exposure, followed by a period of stable values. This immediate response and subsequent stability contrast markedly with the delayed adaptations seen in other biomarkers like HR, PAT, and PDA, which only become evident after a prolonged duration of stress.

This PTTD's unique response highlights its sensitivity and consistency in reflecting swift physiological changes triggered by stress. The key difference lies in the initial PTTD values at the start of stress exposure, which are significant. However, unlike the changes observed in PAT and PDA biomarkers, the alteration in PTTD values during the stress stage itself is not statistically significant, indicating its potential as a stable and sensitive marker of rapid vascular changes.

As found by [51], PEP is a cardiovascular parameter linearly correlated with HR, but the relationship is weaker or stronger under differing circumstances (rest: ρ^2=0.06, physical stress: ρ^2=0.65). This remarks that during stress, PAT provides information about vasoconstriction, but PAT will also exhibit a high component of PEP, since the definition of PAT includes this period. Regarding the correlation obtained in this study of each PWV metric with HR (Fig. 14.3), results suggest that the influence of HR is consistently and highly affecting PAT and PDA specially during heat stress. ρ values of all PAT and PDA estimates are very close to (-1), exhibiting the strong inverse proportionality between HR and these PWV estimates under stress. On the contrary, PTTD has no significant correlation with HR, supporting the hypothesis that the progressive increasing changes observed in PAT and PDA are mainly due to HR variations, mediated through PEP, the ejected

systolic volume, also known as stroke volume, and the other cardiac output (CO) modulators.

PTTD exhibits a similar behavior to HR and PAT during the relax stages. However, during the heat stress stages, unlike PAT, we did not observe the same pronounced trend following the one for HR, which is a novel and interesting finding. Of note, the standard deviation of PTTD is larger than for PAT, as a result of lower precision and/or lower dynamic range.

Therefore, based on these results, PTTD seems to have a superior performance for the evaluation of vasoconstriction reactivity, since PAT and PDA surrogates include additional SNS modulation variables other than vasoconstriction. However, it is important to mention that the standard deviation of PTTD is greater than the one of PAT or PDA measures, which may be indicating a lower signal-to-noise ratio, likely due to the resolution (dependent on the sampling frequency of PPG), and lower dynamic range of PTTD. Besides, PTTD measurements from the fingertip to head (HF) or earlobe (EF) show greater variability than earlobe to head (EH), indicative of the pulse wave's longer travel time. Shorter PTTD travel distances, such as in EH, result in a narrower dynamic range, suggesting that PTTD measurements over longer distances (HF or EF) are more effective for evaluating vascular dynamics and reactivity.

We also performed a complete analysis encompassing frequency domain indices of PAT, PTTD, and PDA, although the details are beyond the scope of the present study. However, it should be highlighted that the significant number of periods where PTTD could not be determined results in a substantial amount of temporal gaps. This limitation arises from the small dynamic range, and the requirements for high sampling rates and high quality of the original PPG signals, which makes frequency analysis of PTTD not feasible. Consequently, future research into PTTD should prioritize studying the evolution of average PTTD absolute values over specific time intervals, such as 2-minute periods, instead of frequency domain analysis.

Our findings are consistent with previous studies that have used PWV measures to assess changes in vascular reactivity during various stressors. For example, several studies have demonstrated that PWV is a sensitive indicator of changes in cardiovascular function under stress [52], [53]. Considering the

methodological differences, PAT values obtained in this work are equivalent to values previously reported [54]. Our study extends these findings by characterizing PWV estimates for monitoring changes in vascular reactivity during heat stress, taking into account the effect of PEP.

14.4.2 Physiological implications and applications

The ability to monitor changes in vascular reactivity, particularly under heat stress, has crucial physiological implications. SNS activity influences BP and HR, essential for thermoregulation during heat exposure [55]. During heat stress, SNS-mediated modulation of the sinus node results in elevated HR and CO.

Arterioles, with their high smooth muscle concentration [56], are central in PWV regulation, differing from larger vessels in their impact on vascular resistance and compliance. While veins primarily support venous return, especially from lower extremities, arterioles are key in modulating vascular dynamics.

SNS activity induces arteriole vasoconstriction that leads to increased preload, as the constriction of the veins enhances venous return, and increased afterload, as the constriction of the arteries and arterioles raises the total peripheral resistance. Concurrently, it enhances myocardial contractility, impacting stroke volume and further elevating BP [57]. Sauna bathing showcases these physiological dynamics. It increases skin blood flow, significantly contributing to CO, while internal organ blood flow decreases [58]. Contrary to assumptions, BP and HR increase during sauna sessions, leading to heightened myocardial oxygen consumption [5], [55]. PWV is influenced by these mechanisms, altering PAT, PTTD, and PDA estimates in different ways. For example, myocardial contractility and vasoconstriction decrease W_1 and T_{12}, while an increase on HR will exhibit a strong linear correlation to an increase on PWV, as in [51].

Vasoconstriction, in response to SNS activation, is a rapid physiological process. Upon exposure to a stimulus, the SNS triggers the release of norepinephrine, initiating vasoconstriction. This response can start within 1-2 seconds, with significant constriction typically occurring within 5-10 seconds [59], [60]. Vasoconstriction responses are immediate, while BP increases require more time due to complex systemic activation to augment CO. PTTD

values change more gradually during stress stages, reflecting SNS modulation, while PAT and PDA estimates rise in tandem with HR during heat stress. These novel findings may be suggesting that PTTD's sensitivity to vasoconstriction has an immediate and consistent response upon stress exposure, a pattern not observed in HR, PAT, and PDA measurements. Based on the physiology, we propose that PTTD may predominantly reflect changes in arterial stiffness and BP linked to vasoconstriction, thus differentiating these specific effects from other physiological influences.

Then, our findings suggest PTTD's unique response to vasoconstriction, with immediate and consistent values during stress stages, unlike HR, PAT, and PDA. PTTD primarily reflects changes in arterial stiffness and BP associated with vasoconstriction, differentiating it from other physiological influences. Unaffected by CO and PEP changes, PTTD correlates well with carotid-femoral PWV, requiring only two PPG sensors [61], [62].

14.4.3 Limitations and future work

This study has two main limitations. The first limitation is the lack of PEP measurements, to compare our PWV estimates with the actual PEP. Although previous studies analyzed the interrelationship between HR and PEP, the absence of this data in these recordings limits the interpretation and capability to draw definitive conclusions. Future studies could benefit from including it to further validate the relationship between PEP and PWV, with respect to variations in HR, too. Furthermore, the incorporation of CO measurements could yield valuable information. One possible approach to address the influence of HR on PEP, PAT, and PDA measures is to compute HR-corrected PWV estimates, as demonstrated in [63]. Therefore, considering the influence of HR on PWV estimation could provide a more accurate reflection of vascular reactivity, unaffected by PEP.

Secondly, it is important to acknowledge that due to the study design, the available data is limited to male participants. Therefore, there is a need to extend the recordings to include data from the female population. This would provide valuable insights into potential gender differences and enhance the generalization of the findings.

In this study, it is essential to clarify that the term 'PWV' refers to measurements derived from transit times rather than directly measured

velocities. Traditional PWV calculations typically require the distance the pulse wave travels, necessitating measurements of vessel length or, by approximation, arm length or participant height. However, for within-subject comparisons where vessel length is constant, transit times can serve as a surrogate for velocity changes, as demonstrated in our results. In contrast, population-based analyses should include normalization against height or arm length to account for inter-individual variability and prevent potential confounding.

14.5 Conclusions

This study underscores the importance of PWV and its surrogate measures, including PAT, PTTD, and PDA, for assessing cardiovascular function under heat stress conditions. The observed patterns and their relationships with HR contribute significantly to our understanding of how the vascular system reacts to different physiological states. Although PAT is a recognized surrogate of PWV and has been extensively used to assess arterial stiffness and blood pressure, less attention has been given to PTTD and PDA. Our study shows that PTTD provides valuable information about vasoconstriction, but its practical use is limited by the need for two synchronized PPG sensors, which is a challenge for wearable technology.

Moreover, it's important to note the lower coverage of PTTD compared to PAT and PDA, mainly due to the challenge of obtaining two high-quality PPG signals at the same time. This difficulty is especially significant for the spectral analysis of PAT and particularly PTTD, as it's hard to achieve enough coverage for a reliable spectrum analysis, an issue that was highlighted in the previous chapter on mental stress analysis (13).

Bibliography of Part IV

[1] P. H. Charlton, P. A. Kyriacou, J. Mant, V. Marozas, P. Chowienczyk, and J. Alastruey, "Wearable photoplethysmography for cardiovascular monitoring",
Proceedings of the IEEE, vol. 110, no. 3, 2022.

[2] P. H. Charlton, J. Allen, R. Bailon, S. Baker, J. A. Behar, F. Chen, G. D. Clifford, D. A. Clifton, H. J. Davies, C. Ding, *et al.*, "The 2023 wearable photoplethysmography roadmap",
Physiological Measurement, 2023.

[3] E. Peralta, J. Lázaro, R. Bailón, V. Marozas, and E. Gil, "Optimal fiducial points for pulse rate variability analysis from forehead and finger photoplethysmographic signals",
Physiological measurement, vol. 40, no. 2, 2019.

[4] A. Hernando, J. Lázaro, E. Gil, A. Arza, J. M. Garzón, R. López-Antón, C. de la Cámara, P. Laguna, J. Aguiló, and R. Bailón, "Inclusion of respiratory frequency information in heart rate variability analysis for stress assessment",
IEEE journal of biomedical and health informatics, vol. 20, no. 4, pp. 1016–1025, 2016.

[5] M. Cernych, A. Satas, A. Rapalis, V. Marozas, L. Malciene, A. Lukosevicius, L. Daniuseviciute, and M. Brazaitis, "Exposure to total 36-hr sleep deprivation reduces physiological and psychological thermal strain to whole-body uncompensable passive heat stress in young adult men",
Journal of Sleep Research, vol. 30, no. 2, e13055, 2021.

[6] S. Kontaxis, R. Bailón, A. Rapalis, M. Brazaitis, M. Cernych, J. Lázaro, P. Laguna, E. Gil, and V. Marozas,
"Autonomic nervous system response to heat stress exposure by means of heart rate variability",
In *2019 Computing in Cardiology (CinC)*,
2019.

[7] S. Ismail, U. Akram, and I. Siddiqi, "Heart rate tracking in photoplethysmography signals affected by motion artifacts: A review",
EURASIP Journal on Advances in Signal Processing, vol. 2021, no. 1, pp. 1–27, 2021.

[8] L. Bernardi, D. Gordin, M. Rosengård-Bärlund, V.-P. Mäkinen, R. Mereu, A. DiToro, and P.-H. Groop, "Arterial function can be obtained by noninvasive finger pressure waveform",
International journal of cardiology, vol. 175, no. 1, pp. 169–171, 2014.

[9] M. Nitzan, A. Babchenko, B. Khanokh, and D. Landau, "The variability of the photoplethysmographic signal-a potential method for the evaluation of the autonomic nervous system",
Physiological measurement, vol. 19, no. 1, p. 93, 1998.

[10] J. Allen, "Photoplethysmography and its application in clinical physiological measurement",
Physiological measurement, vol. 28, no. 3, R1, 2007.

[11] S. K. Bashar, D. Han, S. Hajeb-Mohammadalipour, E. Ding, C. Whitcomb, D. D. McManus, and K. H. Chon, "Atrial fibrillation detection from wrist photoplethysmography signals using smartwatches",
Scientific reports, vol. 9, no. 1, pp. 1–10, 2019.

[12] L. M. Eerikäinen, A. G. Bonomi, F. Schipper, L. R. Dekker, R. Vullings, H. M. de Morree, and R. M. Aarts, "Comparison between electrocardiogram-and photoplethysmogram-derived features for atrial fibrillation detection in free-living conditions",
Physiological measurement, vol. 39, no. 8, p. 084 001, 2018.

[13] A. Tarniceriu, J. Harju, Z. R. Yousefi, A. Vehkaoja, J. Parak, A. Yli-Hankala, and I. Korhonen,
"The accuracy of atrial fibrillation detection from wrist photoplethysmography. a study on post-operative patients",

In *2018 40th Annual International Conference of the IEEE Engineering in Medicine and Biology Society (EMBC)*,
IEEE,
2018,
Pp. 1–4.

[14] A. G. Bonomi, F. Schipper, L. M. Eerikäinen, J. Margarito, R. van Dinther, G. Muesch, H. M. de Morree, R. M. Aarts, S. Babaeizadeh, D. D. McManus, *et al.*, "Atrial fibrillation detection using a novel cardiac ambulatory monitor based on photo-plethysmography at the wrist",
Journal of the American Heart Association, vol. 7, no. 15, e009351, 2018.

[15] G. Lu, F. Yang, J. Taylor, and J. Stein, "A comparison of photoplethysmography and ecg recording to analyse heart rate variability in healthy subjects",
Journal of medical engineering and technology, vol. 33, no. 8, pp. 634–641, 2009.

[16] B. Vescio, M. Salsone, A. Gambardella, and A. Quattrone, "Comparison between electrocardiographic and earlobe pulse photoplethysmographic detection for evaluating heart rate variability in healthy subjects in short-and long-term recordings",
Sensors, vol. 18, no. 3, p. 844, 2018.

[17] S. S. Chreiteh, B. Belhage, K. Hoppe, J. Branebjerg, and E. V. Thomsen,
"Sternal pulse rate variability compared with heart rate variabilit on healthy subjects",
In *2014 36th Annual International Conference of the IEEE Engineering in Medicine and Biology Society*,
IEEE,
2014,
Pp. 3394–3397.

[18] J. Spigulis, "Optical noninvasive monitoring of skin blood pulsations",
Applied optics, vol. 44, no. 10, pp. 1850–1857, 2005.

[19] L. Grajales and I. V. Nicolaescu,

"Wearable multisensor heart rate monitor",
In *International Workshop on Wearable and Implantable Body Sensor Networks (BSN'06)*,
IEEE,
2006,
4–pp.

[20] S. Rhee, B.-H. Yang, and H. H. Asada, "Artifact-resistant power-efficient design of finger-ring plethysmographic sensors",
IEEE transactions on biomedical engineering, vol. 48, no. 7, pp. 795–805, 2001.

[21] L. Wang, B. P. Lo, and G.-Z. Yang, "Multichannel reflective ppg earpiece sensor with passive motion cancellation",
IEEE transactions on biomedical circuits and systems, vol. 1, no. 4, pp. 235–241, 2007.

[22] N. Pinheiro, R. Couceiro, J. Henriques, J. Muehlsteff, I. Quintal, L. Goncalves, and P. Carvalho,
"Can ppg be used for hrv analysis?",
In *2016 38th Annual International Conference of the IEEE Engineering in Medicine and Biology Society (EMBC)*,
IEEE,
2016,
Pp. 2945–2949.

[23] W.-H. Lin, D. Wu, C. Li, H. Zhang, and Y.-T. Zhang,
"Comparison of heart rate variability from ppg with that from ecg",
In *The international conference on health informatics*,
Springer,
2014,
Pp. 213–215.

[24] L. G. G. Porto and L. F. Junqueira Jr, "Comparison of time-domain short-term heart interval variability analysis using a wrist-worn heart rate monitor and the conventional electrocardiogram",
Pacing and Clinical Electrophysiology, vol. 32, no. 1, pp. 43–51, 2009.

[25] K. Charlot, J. Cornolo, J. V. Brugniaux, J.-P. Richalet, and A. Pichon, "Interchangeability between heart rate and photoplethysmography variabilities during sympathetic stimulations",
Physiological measurement, vol. 30, no. 12, p. 1357, 2009.

[26] E. Gil, M. Orini, R. Bailon, J. M. Vergara, L. Mainardi, and P. Laguna, "Photoplethysmography pulse rate variability as a surrogate measurement of heart rate variability during non-stationary conditions",
Physiological measurement, vol. 31, no. 9, p. 1271, 2010.

[27] A. H. Khandoker, C. K. Karmakar, and M. Palaniswami, "Comparison of pulse rate variability with heart rate variability during obstructive sleep apnea",
Medical engineering and physics, vol. 33, no. 2, pp. 204–209, 2011.

[28] A. Schäfer and J. Vagedes, "How accurate is pulse rate variability as an estimate of heart rate variability?: A review on studies comparing photoplethysmographic technology with an electrocardiogram",
International journal of cardiology, vol. 166, no. 1, pp. 15–29, 2013.

[29] T. Tamura, Y. Maeda, M. Sekine, and M. Yoshida, "Wearable photoplethysmographic sensors—past and present",
Electronics, vol. 3, no. 2, pp. 282–302, 2014.

[30] Z. Zhang,
"Heart rate monitoring from wrist-type photoplethysmographic (ppg) signals during intensive physical exercise",
In *2014 IEEE Global Conference on Signal and Information Processing (GlobalSIP)*,
IEEE,
2014,
Pp. 698–702.

[31] J. P. Martínez, R. Almeida, S. Olmos, A. P. Rocha, and P. Laguna, "A wavelet-based ECG delineator: Evaluation on standard databases",
IEEE Transactions on biomedical engineering, vol. 51, no. 4, 2004.

[32] J. Mateo and P. Laguna, "Analysis of heart rate variability in the presence of ectopic beats using the heart timing signal",
IEEE Transactions on biomedical engineering, vol. 50, no. 3, 2003.

[33] M. Elgendi, "Optimal signal quality index for photoplethysmogram signals",
Bioengineering, vol. 3, no. 4, 2016.

[34] P. Armanac, J. Lázaro, P. Laguna, R. Bailón, E. Gil, *et al.*,
"Cardiovascular changes induced by acute emotional stress estimated from the pulse transit time difference",
In *2019 Computing in Cardiology (CinC)*,
2019.

[35] J. Lázaro, E. Gil, J. M. Vergara, and P. Laguna, "Pulse rate variability analysis for discrimination of sleep-apnea-related decreases in the amplitude fluctuations of pulse photoplethysmographic signal in children",
IEEE journal of biomedical and health informatics, vol. 18, no. 1, pp. 240–246, 2014.

[36] P. H. Charlton, P. Celka, B. Farukh, P. Chowienczyk, and J. Alastruey, "Assessing mental stress from the photoplethysmogram: A numerical study",
Physiological measurement, vol. 39, no. 5, p. 054 001, 2018.

[37] C. Orphanidou, T. Bonnici, P. Charlton, D. Clifton, D. Vallance, and L. Tarassenko, "Signal-quality indices for the electrocardiogram and photoplethysmogram: Derivation and applications to wireless monitoring",
IEEE journal of biomedical and health informatics, vol. 19, no. 3, 2014.

[38] S. Rajala, T. Ahmaniemi, H. Lindholm, and T. Taipalus,
"Pulse arrival time (pat) measurement based on arm ecg and finger ppg signals-comparison of ppg feature detection methods for pat calculation",
In *2017 39th Annual International Conference of the IEEE Engineering in Medicine and Biology Society (EMBC)*,
IEEE,
2017,
Pp. 250–253.

[39] P. H. Charlton, P. Kyriacou, J. Mant, and J. Alastruey,

"Acquiring wearable photoplethysmography data in daily life: The ppg diary pilot study",
In *Engineering proceedings*,
Vol. 2, 2020.

[40] R. P. Smith, J. Argod, J.-L. Pépin, and P. A. Lévy, "Pulse transit time: An appraisal of potential clinical applications",
Thorax, vol. 54, no. 5, pp. 452–457, 1999.

[41] X.-R. Ding, Y.-T. Zhang, J. Liu, W.-X. Dai, and H. K. Tsang, "Continuous cuffless blood pressure estimation using pulse transit time and photoplethysmogram intensity ratio",
IEEE Transactions on Biomedical Engineering, vol. 63, no. 5, pp. 964–972, 2016.

[42] D. B. Newlin, "Relationships ol pulse transmission times to preejection period and blood pressure",
Psychophysiology, vol. 18, no. 3, pp. 316–321, 1981.

[43] M. Nitzan, B. Khanokh, and Y. Slovik, "The difference in pulse transit time to the toe and finger measured by photoplethysmography",
Physiological measurement, vol. 23, no. 1, p. 85, 2001.

[44] J. Lázaro, R. Bailón, P. Laguna, V. Marozas, A. Rapalis, and E. Gil, "Difference in pulse arrival time at forehead and at finger as a surrogate of pulse transit time",
In *Computing in Cardiology Conference (CinC), 2016*,
IEEE,
2016,
Pp. 269–272.

[45] R. Bailón, L. Sornmo, and P. Laguna, "A robust method for ecg-based estimation of the respiratory frequency during stress testing",
IEEE transactions on biomedical engineering, vol. 53, no. 7, pp. 1273–1285, 2006.

[46] C. Julien, "The enigma of mayer waves: Facts and models",
Cardiovascular research, vol. 70, no. 1, pp. 12–21, 2006.

[47] C. Chua and C. Heneghan,

"Pulse transit time-derived respiratory parameters and their variability across sleep stages",
In *Engineering in Medicine and Biology Society, 2005. IEEE-EMBS 2005. 27th Annual International Conference of the*,
IEEE,
2006,
Pp. 6153–6156.

[48] C. Crandall and J. Gonzalez-Alonso, "Cardiovascular function in the heat-stressed human",
Acta physiologica, vol. 199, no. 4, 2010.

[49] N. Charkoudian, "Mechanisms and modifiers of reflex induced cutaneous vasodilation and vasoconstriction in humans",
Journal of applied physiology, vol. 109, no. 4, 2010.

[50] R. Bailón, L. Sornmo, and P. Laguna, "A robust method for ecg-based estimation of the respiratory frequency during stress testing",
IEEE transactions on biomedical engineering, vol. 53, no. 7, 2006.

[51] N. Pilz, A. Patzak, and T. L. Bothe, "The pre-ejection period is a highly stress dependent parameter of paramount importance for pulse-wave-velocity based applications",
Frontiers in Cardiovascular Medicine, vol. 10, 2023.

[52] F. Milatz, S. Ketelhut, R. G. Ketelhut, and R. Ketelhut, "Favorable effect of aerobic exercise on arterial pressure and aortic pulse wave velocity during stress testing",
Vasa, vol. 44, no. 4, 2015.

[53] A. Saz-Lara, I. Cavero-Redondo, C. Álvarez-Bueno, B. Notario-Pacheco, M. C. Ruiz-Grao, and V. Martínez-Vizcaíno, "The acute effect of exercise on arterial stiffness in healthy subjects: A meta-analysis",
Journal of Clinical Medicine, vol. 10, no. 2, 2021.

[54] P. Salvi, E. Magnani, F. Valbusa, D. Agnoletti, C. Alecu, L. Joly, and A. Benetos, "Comparative study of methodologies for pulse wave velocity estimation",
Journal of human hypertension, vol. 22, no. 10, 2008.

[55] S. Ketelhut and R. Ketelhut, "The blood pressure and heart rate during sauna bath correspond to cardiac responses during submaximal dynamic exercise",
Complementary Therapies in Medicine, vol. 44, 2019.

[56] L. A. Martinez-Lemus, "The dynamic structure of arterioles",
Basic and clinical pharmacology and toxicology, vol. 110, no. 1, pp. 5–11, 2012.

[57] J. R. Mitchell and J.-J. Wang, "Expanding application of the wiggers diagram to teach cardiovascular physiology",
Advances in physiology education, vol. 38, no. 2, pp. 170–175, 2014.

[58] M. L. Hannuksela and S. Ellahham, "Benefits and risks of sauna bathing",
The American journal of medicine, vol. 110, no. 2, 2001.

[59] J. R. Levick,
Levick's Introduction to Cardiovascular Physiology,
6th.
2018.

[60] A. J. Pappano and W. G. Wier,
Cardiovascular Physiology,
9th.
McGraw-Hill Education., 2018.

[61] Q. Zhong, M.-J. Hu, Y.-J. Cui, L. Liang, M.-M. Zhou, Y.-W. Yang, and F. Huang, "Carotid–femoral pulse wave velocity in the prediction of cardiovascular events and mortality: An updated systematic review and meta-analysis",
Angiology, vol. 69, no. 7, 2018.

[62] B. Williams, G. Mancia, W. Spiering, E. Agabiti Rosei, M. Azizi, M. Burnier, D. L. Clement, A. Coca, G. De Simone, A. Dominiczak, *et al.*, "2018 ESC/ESH guidelines for the management of arterial hypertension: The task force for the management of arterial hypertension of the European society of cardiology (ESC) and the european society of hypertension (ESH)",
European heart journal, vol. 39, no. 33, 2018.

[63] G. Valenza, B. Nackley, B. H. Friedman, and R. Barbieri,
"Validation of sympathetic activity index from heartbeat series: A preliminary study on pre-ejection periods",
In *12th Conference of the European Study Group on Cardiovascular Oscillations (ESGCO)*,
2022.

Part V

Conclusions

Chapter 15

Conclusions and Future Work

15.1 Summary and Final Discussion

The primary aim of this thesis was to enhance cardiovascular health evaluation through noninvasive assessment of ANS activity. This was achieved by analyzing cardiac, respiratory, and PPG signals in both clinical and non-clinical settings, with the use of long-term monitoring. The research targeted several key areas: improving the assessment of weaning readiness from mechanical ventilation, characterizing obstructive sleep apnea in pediatric populations, and identifying potential biomarkers from PPG sensors for integration into wearable technologies. Following an introductory part covering the physiological fundamentals, the targeted disorders, and the

methodologies employed (Part I), the thesis was organized into three principal parts, each addressing specific aspects and applications of noninvasive signal analysis for the improvement of cardiovascular health monitoring.

15.1.1 Weaning Readiness

The first study, in Part II of the thesis, evaluated BRS in critically ill patients undergoing MV, using the BPRSA technique. It revealed a notable negative BRS capacity in patients ready for weaning, suggesting BRS quantification as a potential predictor for weaning outcomes in the ICU.

The second study extended this research by analyzing CPC indices, evaluated using three different techniques, over 24 hours before the SBT. Results exhibited that traditional clinical criteria were insufficient to determine weaning readiness, with 15-20% of patients failing SBT or needing reintubation. However, higher CPC values were observed in successfully weaned patients, especially at night. These studies together highlight the importance of integrating multifaceted physiological biomarkers, such as BRS and CPC indices, for a more accurate assessment of weaning readiness in ICU settings, emphasizing the role of long-term recordings and signal processing techniques.

15.1.2 Obstructive Sleep Apnea

In Part III of the thesis, we explored various aspects of OSA in pediatric patients. The initial study revealed significant differences in HRV metrics during apnea episodes compared to normal breathing, indicating that traditional HRV analysis may not be fully applicable during apnea. The subsequent study highlighted the potential of low-frequency band TFC as a novel biomarker for assessing OSA severity, suggesting a need for future research integrating respiratory signals with HRV.

The third study demonstrated that treating OSA in prepubertal children causally reduces the risk and severity of MetS. This finding was mediated by a decrease in respiratory event frequency, underlining the importance of treating OSA in early childhood to mitigate future cardiometabolic risks. In this study, it is the first time that a cardiovascular risk indicator has been validated for OSA treatment assessment, based on clinical and demographic

data. Collectively, these studies emphasize the complex relationship between OSA and cardiovascular health in children, advocating for more nuanced and comprehensive approaches in pediatric sleep disorder assessments.

15.1.3 PPG Data Analysis

Part IV of the thesis explored the multifaceted potential of PPG in wearable devices. Chapter 12 revealed that coverage rates of PPG sensors vary significantly with sensor location, particularly achieving higher accuracy in finger and earlobe signals for vital metrics estimation. This underlines the importance of sensor placement in wearable design for reliable monitoring. Chapter 13 established the PTTD as a novel biomarker for differentiating stress and relaxation states, highlighting its effectiveness in capturing sympathetic activation and vasoconstriction. Chapter 14 further delves into the use of PPG-derived measures like PAT, PTTD, and PDA for assessing vascular reactivity under heat stress. It demonstrates that while PAT and PDA-based biomarkers offer valuable insights, PTTD provides a more detailed description of vasoconstriction, crucial for understanding cardiovascular responses under stress.

While the PTTD emerged as a superior biomarker of vascular reactivity for assessing stress, its application in wearables is constrained by the necessity of two perfectly synchronized PPG sensors. This requirement complicates its widespread adoption in wearable technology. Conversely, PAT requires both PPG and ECG sensors, adding to its complexity in wearable integration. In contrast, PDA-based biomarkers, needing only a single PPG sensor, offer a more feasible and straightforward approach for wearables.

These findings collectively underscore the versatility and significance of PPG in wearable technology for continuous, non-invasive cardiovascular monitoring, particularly in stress assessment and vascular reactivity analysis.

15.2 Main Conclusion

The integration of cardiovascular health assessment through noninvasive signal processing of cardiac, respiratory, and PPG signals, may serve to enhance clinical decision-making, particularly in weaning ICU patients from mechanical ventilation and in the early detection and management of pe-

diatric obstructive sleep apnea. The findings underscore the importance of CPC as a potential analytical tool for innovative, non-invasive biomarkers that aid clinical decision making.

Additionally, the application of PPG in wearable devices for monitoring cardiovascular reactivity reveals promising avenues for continuous health assessment in real life. This work not only contributes substantially to biomedical engineering but also sets a foundation for future research in personalized healthcare, emphasizing the growing role of long-term signal processing and wearable technologies in health monitoring, and disease prevention and screening.

15.3 Future Work

This thesis has opened several avenues for further research, building upon the findings and methodologies developed herein. The following are potential research directions that could extend and enhance the work presented:

1) Expanding CPC Analysis Across Ventilation Modes: A promising line of investigation involves extending the analysis of CPC to include other modes of ventilation such as assist and controlled ventilation. A particular focus could be on VCV modes. The hypothesis is that including VCV in the CPC analysis might necessitate a distinct analytical approach, given the expected higher CPC in VCV due to the increased ventilatory assistance. This study could explore if variations in CPC levels, particularly sudden changes in the HF and LF bands, can provide insights into cardiovascular health and the occurrence of cardiorespiratory events.

2) Comprehensive Classification and Survival Analysis: After incorporating all mechanical ventilation modes into the analysis, conducting a classification study coupled with survival analysis would be valuable. This research could elucidate the role of CPC in predicting actual SBT success and patient outcomes.

3) Evaluating Sleep Health Prior to Weaning: Assessing sleep health before making decisions on weaning readiness and conducting SBTs presents an innovative approach. This would involve applying the techniques and methodologies detailed in this thesis for HRV and CPC analysis to evaluate sleep quality in mechanically ventilated patients and providing this

information to clinicians.

4) Real-World Application of PPG Biomarkers: Implementing and assessing the practicality of PPG biomarkers in wearable devices and real-life settings, with a focus on coverage and quality, is crucial. The aim is to transition the biomarkers developed for stress assessment in Part IV to clinical applications, such as facilitating OSA diagnosis using wearable technologies.

5) Integrating HRV and CPC with Cardiovascular Risk in OSA: Investigating the relationship between HRV, CPC, and cardiovascular risk, as measured by MetS, in OSA patients, including adult standard metrics of cardiovascular risk and the pediatric MetS validated in this thesis, could provide new insights into the disease's impact on cardiovascular health.

6) Developing PPG-Based OSA Diagnosis and Stratification Tools: The creation of devices utilizing PPG-derived biomarkers for OSA diagnosis and stratification is an exciting possibility. We are already developing a research-based platform using a MAXIM PPG measuring device, which offers a potential pathway for easy and efficient OSA monitoring and diagnosis solutions. However, this system may not be suitable for ICU environments, where comprehensive and continuous monitoring is essential. The adoption of such technologies in clinical settings requires further exploration and validation.

Figure 15.1: Wrist-Based PPG, SpO2, and Accelerometry Health Sensor Platform.

These proposed research directions aim to build upon the current thesis's findings, exploring new methodologies and applications in the fields of mechanical ventilation, sleep health, and wearable sensor technology. The

goal is to further enhance patient care and monitoring in both clinical and non-clinical settings.

15.4 Scientific Contributions

15.4.1 Journal Publications

- **P. Armañac-Julián**, S. Kontaxis, A. Rapalis, V. Marozas, P. Laguna, R. Bailón, E. Gil, J. Lázaro (2023) Vascular Reactivity Characterized by PPG-derived Pulse Wave Velocity. Under Review: Biomedical Signal Processing and Control Journal.
- S. Hietakoste, **P. Armañac-Julián**, T. Karhu, R. Bailón, S. Sillanmäki, J. Töyräs, T. Leppänen, S. Myllymaa, S. Kainulainen (2023) Impaired cardiorespiratory coupling in severe sleep apnea-related hypoxemia. IEEE Trans Biomed Eng.
- **P. Armañac-Julián**, A. Martín-Montero, J. Lázaro, R. Hornero, P. Laguna, L. Kheirandish-Gozal, D. Gozal, E Gil, R. Bailón, G. Gutiérrez-Tobal (2023) Persistent Sleep Disordered Breathing Independently Contributes to Metabolic Syndrome in Prepubertal Children. Pediatric Pulmonology.
- A. Martín-Montero; **P. Armañac-Julián**; E. Gil; L. Kheirandish-Gozal; D. Álvarez; J. Lázaro; R. Bailón; D. Gozal; P. Laguna; R. Hornero; G. C. Gutiérrez-Tobal (2023) Pediatric Sleep Apnea: Characterization of Apneic Events and Sleep Stages Using Heart Rate Variability, Computers in Biology and Medicine, 154, 106549, doi: 10.1016/j.compbiomed.2023.106549.
- **P. Armañac-Julián**, S. Kontaxis, A. Rapalis, V. Marozas, P. Laguna, R. Bailón, E. Gil, J. Lázaro (2022) Reliability of Pulse Photoplethysmography Sensors: Coverage Using Different Setups and Body Locations, Front. Electron. 3:906324. doi: 10.3389/felec.2022.906324
- **P. Armañac-Julián**, D. Hernando, J. Lazaro, C. de Haro, R. Magrans, J. Morales, J. Moeyersons, L. Sarlabous, J. Lopez-Aguilar, C. Subira, R. Fernandez, M. Orini, P. Laguna, C. Varon, E. Gil, R. Bailon, and L. Blanch (2021) Cardiopulmonary Coupling Indices to Assess Weaning Readiness from Mechanical Ventilation. Scientific Reports. 11:16014, doi: 10.1038/s41598-021-95282-2

- JF. MoralesTellez, J. Moeyersons, **P. Armañac-Julián**, M. Orini, L. Faes, S. Overeem, M. Van Gilst, J. Van Dijk, SV. Huffel, R. Bailon, C. Varon (2021) Model-Based Evaluation of Methods for Respiratory Sinus Arrhythmia Estimation. IEEE Trans Biomed Eng. vol. 68, n. 6, doi: 10.1109/TBME.2020.3028204. PMID: 33001798.

15.4.2 Conference Proceedings

- **P. Armañac-Julián**, A. Martín-Montero, J. Lázaro, R. Hornero, P. Laguna, L. Kheirandish-Gozal, D. Gozal, E Gil, R. Bailón, G. Gutiérrez-Tobal (2023) Characterization of the Cardiopulmonary Coupling in pediatric sleep apnea. Computing in Cardiology, Atlanta (Georgia).
- **P. Armañac-Julián**, A. Martín-Montero, J. Lázaro, S. Kontaxis, D. Álvarez, D. Gozal, R. Hornero, P. Laguna, G. Gutiérrez-Tobal, R. Bailón, E Gil (2022) Sleep apnea causally contributes to metabolic syndrome in prepubertal children. CIBER Young Researchers Meeting, Barcelona.
- **P. Armañac-Julián**, A. Martín-Montero, J. Lázaro, S. Kontaxis, D. Álvarez, D. Gozal, R. Hornero, P. Laguna, G. Gutiérrez-Tobal, R. Bailón, E Gil (2022) Caracterización de los Cambios en las Medidas de la HRV durante Episodios de Apnea del Sueño. XL Congreso Anual de la Sociedad Española de Ingeniería Biomédica, Valladolid.
- **P. Armañac-Julián**, A. Martín-Montero, J. Lázaro, S. Kontaxis, D. Álvarez, D. Gozal, R. Hornero, P. Laguna, G. Gutiérrez-Tobal, R. Bailón and E. Gil (2022) Changes in HRV metrics during sleep apnea episodes in children, European Study Group on Cardiovascular Oscillations (ESGCO), Štrbské Pleso (Slovakia). 2nd best poster award
- **P. Armañac-Julián**, D. Hernando, J. Lázaro, C. de Haro, R. Magrans, L. Sarlabous, JF. López-Aguilar, P. Laguna, E. Gil, L. Blanch, R. Bailón (2021). La capacidad del barorreflejo como índice de identificación de los pacientes de UCI preparados para el destete. Jornadas I3A, Zaragoza
- **P. Armañac-Julián**, D. Hernando, J. Lazaro, C. de Haro, R. Magrans, L. Sarlabous, J. López-Aguilar, P. Laguna, E. Gil, L. Blanch, R. Bailón (2020) Baroreflex Sensitivity Evolution before Weaning from Mechanical Ventilation, Proceedings of the XLVII International Conference on Computing in Cardiology. Rimini, Italy, doi:10.22489/CinC.2020.235.

- **P. Armañac-Julián**, S. Kontaxis, J. Lazaro, P. Laguna, R. Bailón, E. Gil (2019) Cardiovascular Changes Induced by Acute Emotional Stress Estimated from the Pulse Transit Time Difference. Proceedings of the XLVI International Conference on Computing in Cardiology. Singapore.
- **P. Armañac-Julián**, S. Kontaxis, J. Lázaro, P. Laguna, R. Bailón, E. Gil (2018) Cambios en la Diferencia del Tiempo de Tránsito del Pulso Sanguíneo en Estados de Estrés Emocional Agudo. XXXVI Congreso Anual de la Sociedad Española de Ingeniería Biomédica, Ciudad Real.

15.5 Supervision of Bachelor/Master Thesis Related to my Ph.D.

Master thesis:

- Zahra-Zidor, F., Implementation of a Pulse Detector in a Wrist Wearable Device (2023), University of Zaragoza

Bachelor thesis:

- Lasala, C., Pulse decomposition analysis as a surrogate of arterial pulse wave velocity (2023), University of Zaragoza
- Barquero, A., Relationship between physical activity and heart rate in patients with depression using wearable wrist devices (Proposal), University of Zaragoza.
- Urbón, J., Algorithms implementation to estimate heart rate in a wearable wristband system (Proposal), University of Zaragoza.

List of Figures

Figure **Page**